

**Device physics of conjugated polymer light
emitting diodes**

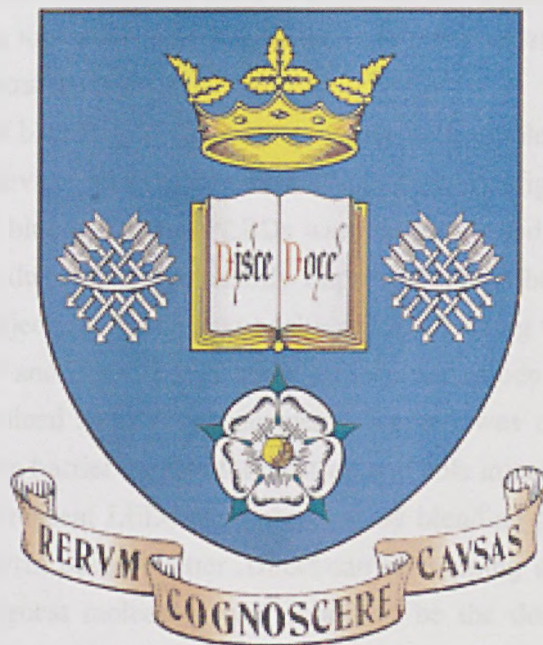
Leonidas Palilis

**A dissertation submitted to the University of
Sheffield for the degree of Doctor of Philosophy**

April 2001

Device physics of conjugated polymer light emitting diodes

Leonidas Palilis



Department of Physics and Astronomy

**A dissertation submitted to the University of
Sheffield for the degree of Doctor of Philosophy**

April 2001

THESIS ABSTRACT

Device physics of conjugated polymer light emitting diodes

Leonidas Palilis

This thesis examines the optical and electrical properties of a series of fluorene-based conjugated polymers and light-emitting devices. It addresses some of the issues related to the performance of polymer light emitting devices based on host-guest systems. The principal aim was to gain insight into the microscopic physics essential to understand device operation and hence optimize device performance.

Emission from exciplex states (formed between a hole from a donor molecule and an electron from an acceptor molecule) in bilayer light-emitting diodes (LEDs) based on hole transport triaryl amines and electron-transport phenylquinoxalines was examined in detail. The emission wavelength and color was found to be determined by the energy difference between the ionization potential of the hole transport material and the electron affinity of the electron transport material.

The concept of blending an emissive polymer with a hole transport material as a means of improving device performance in a single layer configuration was addressed and high performance blue and green PLEDs were demonstrated. Doped LEDs showed enhanced performance due to the significantly improved charge balance factor as a result of the improved hole injection and transport achieved by blending with a hole transporter. The effect of using LiF and PEDOT:PSS at the cathode and anode interface on the device performance was examined and the enhancement observed was mainly attributed to the lowering of the effective barrier heights for electron and hole injection, respectively.

Electrophosphorescent LEDs were prepared by blending polyfluorene with a red phosphorescent porphyrin based emitter. Direct carrier trapping and subsequent exciton recombination on the guest molecules was found to be the dominant EL mechanism whereas Förster energy transfer from the host to the dopant dominated the PL emission.

Small area devices (with an active area of diameter 50 μm) were demonstrated to result in very high brightness LEDs that also sustained very high current densities. Optimized devices reached a peak brightness of 6,500,000 cd/m^2 and sustained peak current densities up to 5,000,000 A/m^2 . The enhanced device performance was attributed to the improved thermal management of the small area devices due to reduced Joule heating. The incorporation of the small area structure in a microcavity allowed the fabrication of novel microcavity LEDs with reduced emission linewidths.

Finally, the issue of energy transfer in a host-guest system was addressed in detail. The large overlap of the host emission spectrum with the guest absorption spectrum gave rise to efficient energy transfer via a Förster-type mechanism and dominated the PL emission. Blend LEDs only exhibited emission from the guest for guest concentrations as low as 0.5% as a result of almost complete excitation energy transfer as well as charge trapping followed by efficient recombination on the guest sites.

Acknowledgements

I am greatly indebted to my supervisor, Donal Bradley, for all his help, advice, support and encouragement. Donal has been an excellent supervisor providing insightful comments and constructive criticisms throughout my PhD (not to mention the opportunity to travel abroad so often). Without his help and guidance it would be impossible to finish my PhD. I will always be grateful for what he has done for me.

I also like to thank David Lidzey for his help, advice and the many fruitful discussions we had. I gratefully acknowledge the help of Chris whom I worked closely with on the project contained in Chapter 7, Stephen for the electroabsorption measurements, Al for the time resolved PL measurements and Michael for the time of flight measurements. Many thanks to Paul Lane for proof reading some of the work contained in Chapter 6 and to Homer Antoniadis for the general advice and help to find a job. I also wish to thank the University of Sheffield for a White Rose studentship.

I also thank Mark Bernius, Ed Woo and all the members of the PLED group at Dow Chemical Company for their hospitality and support during my 3 month stay in Midland and for giving me the opportunity to work there. It has been a very worthwhile experience (including the Greek ouzo drinking contest). A big thanks to my housemate Nathan and also to Ben, Shanna, Neil, Sabiha, Marci, Juliana, George, Eric and Tara for making me feel at home. Special thanks to Melissa for her love and friendship.

The polymer LED group in Sheffield has been a brilliant environment to work in. Many thanks to all the past and present members for their friendship and support and for creating a friendly working atmosphere. Special thanks must go to Tersilla and Joern for always being there. Also Roberto, Marilu', Katie, Stephen, Helen and Juan have been a good laugh. A big thanks to my housemate George for his invaluable support and encouragement during the process of writing up. Thanks to all the technical staff, Phil from the workshop, Roger and Cathy from the office. Special thanks to Rachel for helping me through a difficult period, it was mostly appreciated; also thanks to Sarah.

I would also like to thank everyone in Sheffield who has been part of my life. In particular, I thank Anna, Richard for bearing with my poor sense of humour (and the discussions on Greek philosophy), Raquel, Santiago, Andy, Marc, Marcello and Michela. I also thank Aris for new interesting insights into life, George, Iakovos, Mixalhs, Natia, Mairh, Marios, Evangelia and Thanasis. Special thanks to Maria for her love, friendship and support (and for keeping me up to date with the gossip in Greece).

Finally, I dedicate this thesis to my parents and my brother for all they have done for me, their love, support and encouragement. I am especially grateful to my mother for her encouraging letters. Σας ευχαριστώ από βάθους καρδιάς και σας αγαπώ.

“We are what we repeatedly do. Excellence, then, is not an act, but a habit.”

Aristotle

“I hope nothing, I fear nothing, I am free.”

Nikos Kazantzakis

“Quantum mechanics is very impressive. But an inner voice tells me that it is not yet the real thing. The theory yields a lot, but it hardly brings us any closer to the secret of the Old One. In any case I am convinced that He (God) doesn’t play dice.”

Albert Einstein

...The blood of love has robed me in purple and joys never seen before have covered me in shade. I’ve become corroded in the south wind of humankind Mother far away, my Everlasting Rose.

On the open sea they lay in wait for me, with triple-masted men-of-war they bombarded me. My sin that I too had a love of my own Mother far away, my Everlasting Rose.

Once in July her large eyes half-opened, deep down my entrails, to light up The virgin life for a single moment Mother away, my Everlasting Rose.

And since that day the wrath of ages has turned on me, shouting out the curse: “he who saw you, let him live in blood and stone” Mother far away, my Everlasting Rose.

Once again I took the shape of my native country, I grew and flowered among the stones. And the blood of killers I redeem with light Mother far away, my Everlasting Rose...

From the AXION ESTI, by Odysseus Elytis , Nobel Prize in Literature, 1979.

Contents

Chapter 1: An introduction to conjugated polymers and polymer electroluminescence

1.1 Introduction	1
1.2 Conjugated polymers	2
1.2.1 Introduction	2
1.2.2 Physical properties of conjugated polymers	3
1.2.3 Optical and electronic properties of conjugated polymers	4
1.2.4 The SSH model	7
1.2.5 Excitons in conjugated polymers	9
1.3 Polymer electroluminescence	10
1.4 Principles and theory of operation of polymer LEDs	12
1.4.1 Charge carrier injection	13
1.4.2 Charge carrier transport	17
1.4.3 Charge carrier recombination	18
1.4.4 Luminescence and efficiency	19
1.5 Thesis outline	21
References	27

Chapter 2: Experimental Methods

2.1 Introduction	33
2.2 Preparation of polymer LEDs	34
2.2.1 Indium tin oxide (ITO) coated glass substrates	34

2.2.2 Polymer film deposition	37
2.2.3 Metal cathode evaporation	38
2.3 Optical and electrical characterization of conjugated polymers and LEDs	40
2.3.1 Optical absorption spectra	40
2.3.2 Photoluminescence and electroluminescence spectra	40
2.3.3 Current-voltage-luminance characteristics	42
2.3.4 Thickness measurements	43
2.3.5 Photoluminescence quantum efficiency measurements	43
2.3.6 Electroluminescence quantum efficiency measurements	44
2.4 Electroabsorption measurements	46
2.5 Time of flight measurements	48
2.6 Time resolved photoluminescence measurements	50
References	51

Chapter 3: Exciplex emission in bilayer light-emitting diodes based on hole transport fluorene-triarylamine copolymers and electron transport starburst phenylquinoxalines

3.1 Introduction	53
3.2 Fluorene-triarylamine and fluorene-thiophene copolymers	57
3.3 Starburst tris (phenylquinoxalines)	61
3.4 Absorption and photoluminescence (PL) spectra	63
3.5 Optical spectra from bilayer films of triarylamine and thiophene copolymers with starburst tris (phenylquinoxalines)	65
3.6 EL spectra of single layer triarylamine copolymer LEDs and bilayer LEDs with triarylamine copolymers as HTLs and quionoxalines as ETLs – Exciplex formation at the interface	72
3.7 Electrical characterization of LEDs with hole transport	

triarylamine copolymers and electron transport quinoxalines	80
3.8 Conclusions	93
References	94

Chapter 4: Blue light emitting diodes from blends of polyfluorene (PFO) and hole transporting materials

4.1 Introduction	97
4.2 Experimental details	101
4.3 Optical spectroscopy of individual components and blends	102
4.4 LEDs from PFO/PFM blends with Al/Dow metal cathodes – Current-voltage-luminance characteristics and EL spectra	109
4.5 Time of flight and electroabsorption spectroscopy	122
4.6 Conclusions	138
References	139

Chapter 5: Green light emitting diodes from blends of a benzothiadiazole doped polyfluorene (5BTF8) and triarylamine copolymers

5.1 Introduction	144
5.2 Experimental details	146
5.3 Optical spectroscopy of BFB, 5BTF8 and 5BTF8:BFB blends	147
5.4 LEDs based on 5BTF8 and 5BTF8:BFB blends	154
5.5 Conclusions	176
References	177

Chapter 6: Electrophosphorescence from PtOEP-doped polyfluorene red light-emitting diodes

6.1 Introduction	181
6.2 Experimental details	184
6.3 Optical spectroscopy studies of blends of PtOEP and PFO	186
6.4 Electrical characterization of phosphorescent PLEDs	194
6.5 Utilizing a polymer blend host – Improved efficiency phosphorescent LEDs	210
6.6 Spectroscopic studies of blends of PtOEP and PFO:PFM	210
6.7 Phosphorescent PLEDs from blends of PFO:PFM and PtOEP	213
6.8 Conclusions	218
References	220

Chapter 7: Incorporation of a small area structure in polymer light-emitting diodes and microcavities

7.1 Introduction	224
7.2 Experimental details	227
7.3 Device performance under d.c. and pulsed driving schemes	230
7.4 Small area microcavity LEDs	238
7.4.1 Introduction	238
7.4.2 Theory and experimental details	239
7.4.3 5BTF8 microcavity LEDs	241
7.4.4 PFO microcavity LEDs	244
7.5 Conclusions	250
References	251

Chapter 8: Energy transfer from blue to green in benzothiadiazole-doped polyfluorene based light-emitting diodes

8.1 Introduction	254
8.2 Experimental details	256
8.3 Optical spectroscopy of individual components and blends	257
8.4 Electrical characteristics of LEDs made from F8P:BT blends	266
8.5 Conclusions	275
References	276

Chapter 9: Conclusions and suggestions for future work

9.1 Conclusions	278
9.2 Suggestions for future work	284
References	286

Appendix A: Additional data related to Chapter 4

A.1 Current and luminance vs. electric field	287
A.2 Electroluminescence spectra	288

Appendix B: Additional data related to Chapter 5

B.1 Current and luminance vs. electric field	289
--	-----

Appendix C: Publication list

C.1 List of publications on work prior to this thesis	291
C.2 List of publications on work discussed in this thesis	291

CHAPTER 1

AN INTRODUCTION TO CONJUGATED POLYMERS AND POLYMER ELECTROLUMINESCENCE

1.1 Introduction

Conjugated polymers are a unique class of polymers that exhibit novel optoelectronic properties. They are used to fabricate electronic and photonic devices such as light emitting diodes (LEDs),¹⁻¹⁶ photodiodes,¹⁷⁻¹⁸ electrochemical cells,¹⁹⁻²⁰ photovoltaic cells,²¹⁻²⁴ field effect transistors,²⁵⁻²⁸ microcavities²⁹⁻³¹ and lasers³²⁻³⁴. Research on PLEDs was initiated by the discovery of electroluminescence from poly(p-phenylenevinylene) in 1990.¹ This work stimulated researchers world-wide to investigate polymer EL further. Great progress has been made in the last decade in improving the efficiencies and lifetimes of LEDs. Efficiencies of few % and lifetimes of 10,000 hours have been demonstrated² that are adequate for many display applications.

1.2 Conjugated polymers

1.2.1 Introduction

Conjugated polymers are carbon based materials. Their backbone consists of covalently bonded carbon atoms. Three of the four valence electron atomic orbitals of

the carbon atoms, one s and two p orbitals, are hybridized into three sp^2 orbitals. These orbitals form the σ bonds. The remaining electron is in a p_z atomic orbital which is oriented perpendicular to the σ bonds that form the backbone. The p_z orbitals overlap with their neighbors, forming π bonds between the carbon atoms. The π bonds are oriented perpendicular to the plane of the σ bonds and are delocalised along the backbone forming a delocalised electron system that gives rise to a series of alternating single (σ) and double ($\sigma+\pi$) bonds. Given that each C atom contributes one p_z electron, the lowest energy half of these orbitals (π bonding molecular orbitals in the valence band) is filled whilst the higher energy orbitals (π^* antibonding molecular orbitals in conduction band) are empty. This results in a gap at the Fermi energy that gives the polymer its semiconductor-like band structure. Figure 1.1 shows a schematic diagram of the π -bond formation together with the chemical structure of trans-polyacetylene $[(CH)_n]^{36}$ which is the simplest conjugated polymer [Trans-polyacetylene consists of a chain of C atoms with each C atom bonded to two other C atoms and a hydrogen atom. The σ bonds form the backbone whilst the electrons in the unhybridised p_z orbitals overlap giving an extended π electron system].

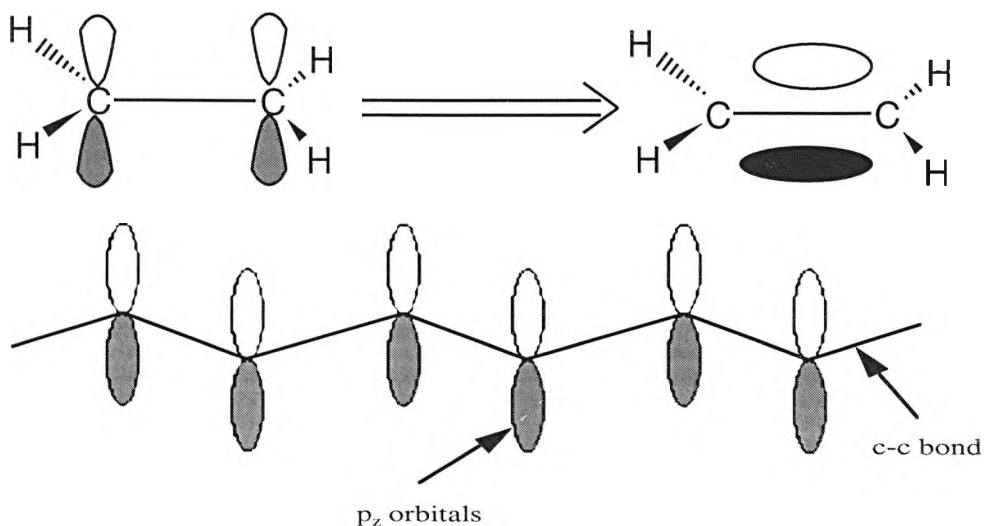


Figure 1.1: Schematic diagram of the π -bond formation in conjugated polymers (top view) - The chemical structure of trans polyacetylene (bottom view).

The gap at the Fermi energy separates the lowest unoccupied antibonding molecular orbital (LUMO) of the conduction band states from the highest occupied bonding molecular orbital (HOMO) of the valence band states. Therefore, conjugated polymers are considered as molecular semiconductors with a band gap between 1.5 and 4 eV and are characterised by their ionization potential and electron affinity. The ionization potential I_P is the energy required to remove an electron from the HOMO level to infinity while the energy gained when adding an electron to the LUMO level from infinity is the electron affinity E_A (both quantities are considered relative to vacuum). If an electron is removed from the HOMO level, the chemical process of oxidation, the molecule will be positively charged, having in conduction terms a hole in the HOMO level. If an electron is added to the LUMO level, the chemical process of reduction, then the molecule will be negatively charged. However, both the I_P and the E_A are different from the HOMO and LUMO, respectively due to electron-electron and electron-lattice interactions (the latter induce a relaxation of the molecular geometry). Therefore, the energy gap, $I_P - E_A$, will not also correspond to the energy difference between HOMO and LUMO. When an electron enters or leaves an orbital, the manner in which the other electrons are distributed and interact with it will influence its own spatial distribution. The addition of a charge to a chain also leads to a lattice deformation and the coupling between the charge and the lattice deformation is called a polaron. This process produces localised energy levels within the energy gap due to a shift in the HOMO and LUMO (one-electron) levels. The picture of a polaron in polythiophene, which is a non-degenerate ground state polymer, is shown in Figure 1.2. Note it consists of a charge carrier and a related relaxation of the molecular geometry.

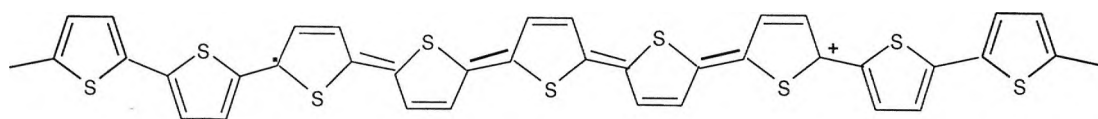


Figure 1.2: The picture (molecular scheme) of a polaron in polythiophene.

To describe the molecular orbitals of conjugated systems, the self-consistent molecular orbital theory has been used. It takes into account electron repulsion that allows all electrons to find the distribution of lowest energy while subject to others' repulsion and allows correctly for the antisymmetrization of the wavefunction.³⁵ This theory improves the 'correlation' of electronic positions compared to Hückel theory which expands a molecular orbital as a linear combination of the available $2p_z$ - π atomic orbitals belonging to the C atoms. This is known as the LCAO approximation which does not include electron repulsion and assumes that the potential of one electron is independent of the position of the other electrons leading to the energy of an electron in a molecular orbital being independent of whether the other molecular orbitals are occupied. Furthermore the wavefunction is not properly antisymmetrized in this case.³⁵

1.2.2 Physical properties of conjugated polymers

The delocalised electron system makes the polymer backbone rigid enough to result in low solubilities and high melting points. Two different approaches have been applied to overcome this problem. The first involves the addition of flexible side groups to the main chain to improve the solubility³⁷⁻³⁸ while the second involves the use of a soluble non conjugated precursor which is converted into its final conjugated form by heat treatment.³⁹⁻⁴⁰ The physical properties are also affected by the packing of the chains relative to one another. The extended conjugation can result in a high degree of crystallinity but the synthetic methods that are used prevent a high degree of order leading to disordered materials.⁴¹ In PPV for example the degree of crystallinity and disorder depend on the type of precursor and the processing conditions.⁴²⁻⁴³ The film morphology is also important when device characteristics are discussed.⁴⁴⁻⁴⁶ The ideal film should be uniform and free from pinholes as defects and impurities affect device performance. Thermal properties such as the stability in air and under light depend on the nature of the side groups. Advanced polymers such as solution-processable PPVs⁴⁷

and polyfluorenes⁴⁸ are less subject to attack from oxygen and water and are stable under illumination. Whether this is a consequence of improved purification and control over defects arising from better controlled synthesis remains an open question.

1.2.3 Optical and electronic properties of conjugated polymers

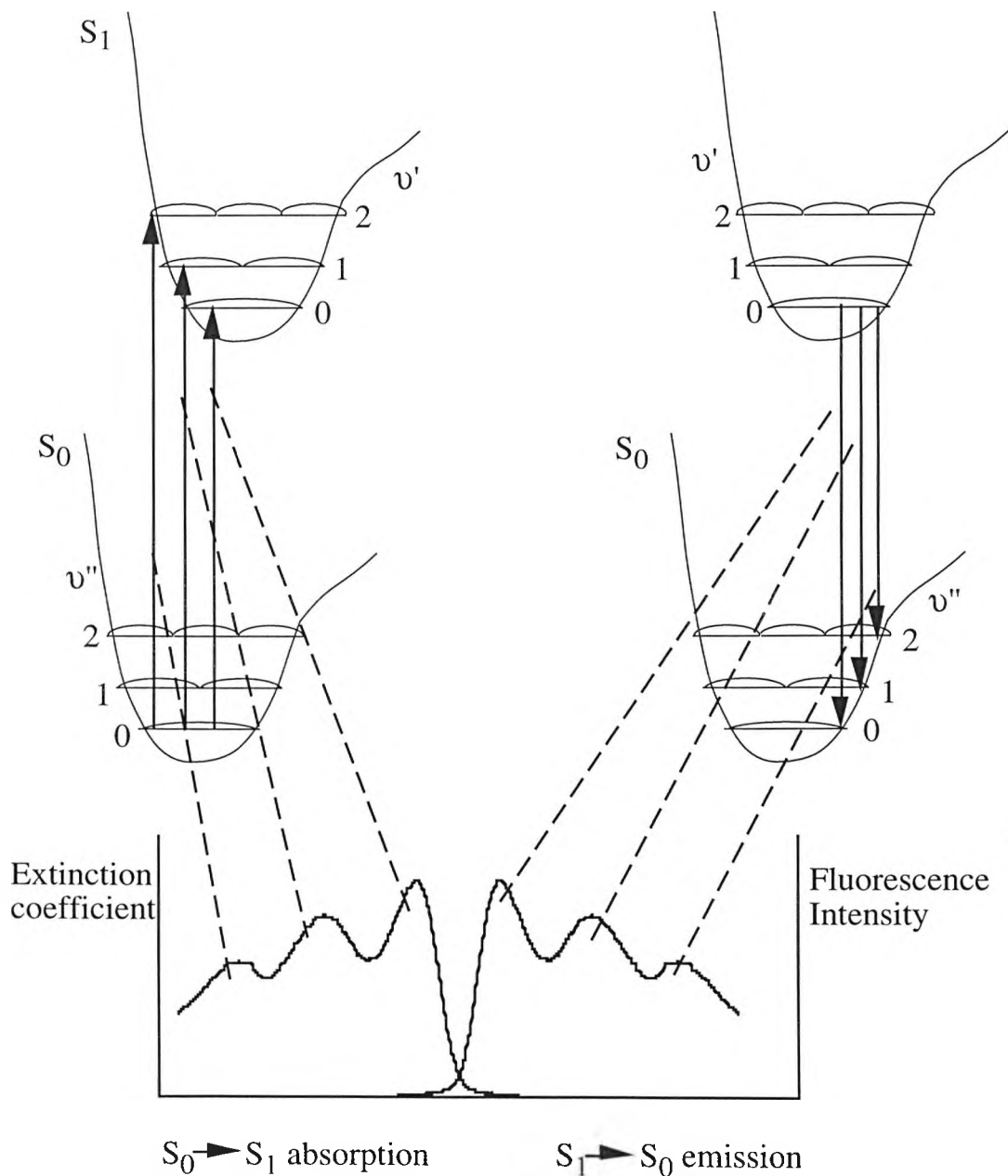


Figure 1.3: A schematic illustration of the absorption and emission spectra of a molecule (figure adapted from Kearwell and Wilkinson⁴⁹) showing the predicted mirror symmetry of the two spectra.

In Figure 1.3, the absorption and emission spectra of a molecule can be seen through the transitions between the different energy levels. The energies of the ground and excited states are shown as a function of a configuration co-ordinate of the system that represents the relative position of the atomic nuclei. The minimum of the potential curve in the excited state is at a different co-ordinate than that of the ground state. As mentioned before, the overlap of the p_z atomic orbitals leads to the formation of π and π^* molecular orbitals associated with different energy levels. Promotion of one electron from the valence to the conduction band leads to a change in the equilibrium geometry of the molecule and is observed experimentally through the coupling of the electronic and vibrational transitions. Both the emission and absorption spectra can be understood in terms of the Franck-Condon principle.⁵⁰ According to this principle, electronic transitions take place much faster than the nuclear motions (10^{-16} sec compared to 10^{-13} sec). That means that the nuclei can be considered as stationary during an electronic transition. The nuclei do not have time to change their configuration co-ordinates during the transition. The ground and excited states have many vibrational and rotational degrees of freedom. Depending on the symmetry of the wavefunction, the excited states will be either singlet or triplet corresponding to a total spin of 0 or 1. The electronic transitions can be considered as vertical transitions and the absorption spectrum shows the vibrational levels of the excited state. During the process of a photon absorption, a transition of the molecule from the lowest energy ground state S_0 to one of the manifold of the excited states in the S_1 band occurs. All these transitions are spin-allowed. The probability of a transition depends on the overlap between the vibrational wavefunctions of the initial and the final state. The transition from the first vibrationally excited state of one level to the vibrational ground state of another level is known as 1-0 transition. A molecule that is in a vibrationally excited state will return to the lowest vibrational state of the excited state within about 0.1 ps (due to phonon-assisted relaxation) and emission will be seen from this lowest state. Relaxation to the ground state occurs either directly (termed fluorescence, if radiative) or through the T_1 band (called phosphorescence).

Intersystem crossing can occur between the singlet S1 and the triplet T1 manifold. The emission mechanism in most organic molecules is fluorescence. Phosphorescence is usually spin-forbidden and if allowed, is inefficient and occurs on a longer timescale than fluorescence.⁵¹⁻⁵² In addition, non-radiative channels that exist between the S1, T1 bands and the ground state reduce the efficiency of the emission. The emission spectrum shows the vibrational levels of the ground state and a mirror symmetry between the two spectra may exist. However, for polymers, the vibronic structure of the emission spectrum is often better resolved than that of the absorption. The reason is that the absorption maps the variety of all conjugation lengths of the material leading to inhomogeneous broadening while the emission occurs only from the lowest energy sites or the longer conjugation segments following migration of the exciton. The difference in the equilibrium configuration co-ordinate between the ground and the excited state relates to the amount of oscillator strength in each of the vibrational peaks. In general, the larger the difference in the configuration co-ordinate, the more widely spread the oscillator strength across each of the vibrational peaks will be. Figure 1.4 shows the Jablonski diagram for photophysical processes in organic materials.

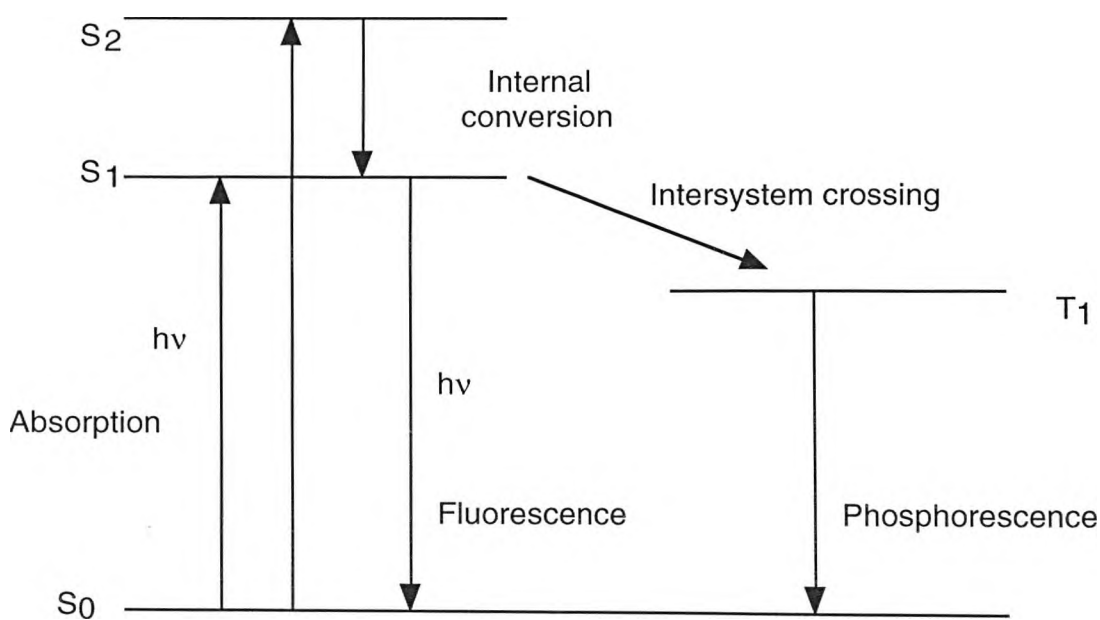


Figure 1.4: The Jablonski diagram for photophysical processes in organic materials.

1.2.4 The SSH Model

Conjugated polymers are thought to have strong intrachain coupling but rather weak interchain (electronic interaction between neighboring chains) coupling and therefore they can be considered as one dimensional materials. It is possible to describe their electronic structure by using the description of the molecular orbitals or by using the band theory as applied to one dimensional chains. The band model and the exciton model have both been applied in the description of the electronic structure of semiconductors. The band model is appropriate for the description of the electronic structure of materials that have a strong inter-site coupling which leads to the formation of free electron-hole pairs. The exciton model is appropriate for the description of the electronic structure of materials that have weak interactions between the sites which leads to the formation of strongly bound localized electron-hole pairs called excitons.

The first band model that was employed by Su, Schrieffer and Heeger (the SSH model)⁵³ to explain the electronic structure of these materials will be briefly discussed below. This model assumes an infinite one dimensional chain but its application to polymers that compose of relatively short conjugated segments separated by defects or impurities is not straightforward. The model takes into account the phonon-electron interactions but not the electron-electron interactions. The effect of the electron-lattice and the electron-electron interactions is to cause localization of the excitations on the chain; these are described as solitons, polarons, bipolarons or excitons depending on the symmetry of the chain and the charge of the excitation. However, an exciton model seems to be more favorable to describe the electronic structure of conjugated polymers after the observation of electron correlation effects (electron-electron and electron-lattice interactions) and bound localized excitons.

In the SSH model, the σ electrons are considered as springs with elastic forces while the π electrons are considered explicitly. The model does not take into account any interchain effects but includes nearest neighbor interactions for the π electrons via a hopping mechanism. The model is described by the following Hamiltonian operator:

$$H = H_{\sigma} + H_{\pi} + H_{\text{core}} \quad (\text{equation 1.1})$$

The different partial Hamiltonian operators are given by the following expressions:

$$H_{\sigma} = k/2 \sum (u_{n+1} - u_n)^2 \quad (\text{equation 1.2})$$

$$H_{\text{core}} = \sum M [d/dt(u_n)]^2 \quad (\text{equation 1.3})$$

$$H_{\pi} = \sum t_{n,n+1} (c_{n+1,s}^{\dagger} c_{n,s} + c_{n+1,s} c_{n,s}^{\dagger}) \quad (\text{equation 1.4})$$

Where H_{core} is a term describing the kinetic energy of the nuclei with mass M and can be neglected when using the Born-Oppenheimer approximation to find the energy levels and the wavefunctions, H_{π} expresses the contribution of π electrons hopping between adjacent sites, u_n is the displacement of a C atom that occupies the site n from its equilibrium position, $c_{n,s}^{\dagger}$ is the creation operator for a π electron at site n and $c_{n,s}$ is the corresponding annihilation operator. The term $t_{n,n+1}$ corresponds to the nearest neighbor transfer integral and can be written as the sum of two terms: t_0 and $a(u_{n+1} - u_n)$ (linear expansion around the equilibrium position) where a is the phonon-electron coupling term between σ and π bonds. H_{σ} expresses the elastic energy contribution due to interaction of the σ bonds and K is the lattice force constant (or spring constant here). One would expect a polymer chain with a metallic behaviour as each atom contributes one free electron leading to a half filled band. However, a one dimensional metal will be energetically unstable to a periodic distortion at the Fermi level of the lattice. This distortion results in the opening of an energy gap with the lowest unoccupied level pushed up in energy and the highest occupied level pulled down in energy. As a result the polymer is characterised by a semiconductor band structure.

1.2.5 Excitons in conjugated polymers

Excitonic effects are particularly important when the exciton binding energy is relatively large as is usually the case for conjugated systems with strong electron-electron interactions. Three different kinds of excitons exist depending on the number of molecular units that they extend over.⁵⁴ An exciton which is considered to be a bound hole-electron pair is classified as a Frenkel exciton if the bound pair is localised on one molecular unit or as a Mott-Wannier exciton if it extends over many units. If it extends only over a few units that are adjacent to each other then is called a charge-transfer exciton (as it involves charge transfer from one unit to the other). Excitons in polymers are considered to be either Frenkel excitons or charge transfer excitons. Optical excitations are believed to extend over the chain that consists of several repeating units so intermediate excitons (between Frenkel and Mott-Wannier excitons) are thought to dominate. Mott-Wannier excitons are considered as hydrogen-like bound states of an electron and a hole. The Mott-Wannier exciton radius which is the exciton case in inorganic semiconductors is much larger than the intermolecular spacing (radius of more than 50 Å has been found). In contrast the radius of a Frenkel exciton is of the order of 5 Å. A more complete description of the exciton has to take into account both coulombic and electron-lattice interactions because the electron-electron interaction results in singlet and triplet states. In PPV the triplet exciton was found to be more localized (not more than one single repeat unit) than the singlet exciton minimising in both cases its energy.⁵⁵ However, polymers that have larger energy bandgaps show poor intrachain delocalization resulting in changes of their optical properties. So interchain interactions leading to the formation of extended excited states that can be described as a mixture of charge transfer and neutral excitons should be considered. Such excitons are classified as excimers⁵⁶ (if the exciton extends over identical molecular units) or as exciplexes⁵⁷ (if the exciton extends over two or more different units). If significant electron-phonon interaction is present then the exciton can be thought of as an excited

state that moves by hopping between adjacent sites. Hopping can occur either by a tunnelling mechanism⁵⁸ that requires an overlap of the wavefunctions of the initial and final state or by a energy transfer process called Förster transfer.⁵⁹ This transfer is moderated as a dipole-dipole interaction and can contribute significantly to the singlet exciton diffusion while triplets can only hop between neighboring sites by tunnelling.

1.3 Polymer Electroluminescence

Electroluminescence from an organic material was first observed by Pope⁶⁰ in 1963. This first EL device used a single crystal of anthracene (shown in Figure 1.5) which was fluorescent in the blue when an external bias above 400 V was applied across the sample. High impurity levels in these first EL materials together with primitive fabrication techniques led to unstable and inefficient devices that required a few hundreds of Volts to be applied in the sample before light emission was observed.

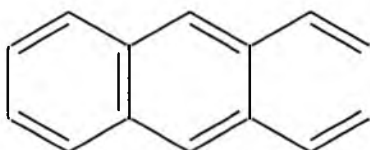


Figure 1.5: Schematic diagram of anthracene, the first organic material found to be electroluminescent. It was used by Pope in 1963.⁶⁰

In the 1970s, Partridge prepared the first organic EL devices with a polymer as an active layer.⁶¹ Polyvinyl carbazole (PVK) doped with perylene was used along with an alkali cathode. Its workfunction closely matched the electron affinity of the polymer and thus it facilitated electron injection. These devices operated at a much lower voltage due to the improved cathode material that was used. Vincett *et al.* reviewed this and other early work in a paper published in 1982.⁶² In 1987 Tang and Van Slyke at Kodak

prepared, for the first time, two-layer EL devices with vacuum-deposited small molecules.⁶³ Their novel structure employed a transparent indium tin oxide (ITO) anode to improve the coupling of light from the device, a hole transport diamine molecule, an electron emitting tris-hydroxyquinoline aluminum (Alq₃) molecule and a low workfunction alloy of magnesium and aluminum to improve electron injection. These devices showed brightnesses of 1000 cd/m² and efficiencies of 1%. The most important breakthrough here was that the LEDs operated below 10 V for the first time.

Then in 1990, a group led by Friend at Cambridge prepared the first polymer EL devices with poly (p-phenylene vinylene) [PPV] (shown in Figure 1.6) as the emitting material in a single layer configuration with an Al₂O₃ anode and an Al cathode.¹ These devices emitted green-yellow light characteristic of PPV that has a π - π^* gap of 2.5 eV.

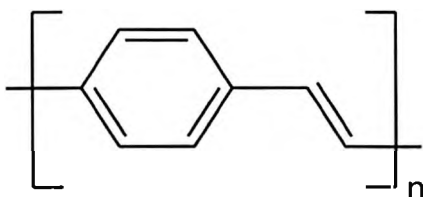


Figure 1.6: Poly(p-phenylene vinylene) [PPV]: The first light-emitting conjugated polymer.

Polymer LEDs differ from inorganic ones in two major ways. The first difference comes from the fact that conjugated polymers can not be doped in a reproducible way to produce p- or n-type molecules and then to form p-n junctions that will not be destroyed by diffusion or other chemical reactions. LEDs are therefore designed to be p-i-n junctions where the emissive layer in which electron-hole recombination takes place is intrinsic (although usually is accidentally doped). The second difference regards the nature of the carrier recombination that produces luminescence with radiative decay. In inorganic semiconductors, charge transport is band-like and the recombination of the oppositely charged carriers results in interband emission. In polymers the charge carriers tend to be polaronic in nature (due to

the excitations generated by electron hole recombination, leading to light emission that escapes out of the device through the transparent anode.

1.4.1 Charge carrier injection

Impurities in organic semiconductors normally act as traps for the carriers rather than as sources of carriers. Thus the concentration of impurities that could give rise to extrinsic p- or n- conduction is small enough not to perturb the electric field distribution in the device. Hence, hole and electron injection from both electrodes is determined by the energy barriers $H_h = I_p - \Phi_A$ and $H_e = \Phi_C - E_A$, respectively, where Φ_A and Φ_C are the workfunctions of the anode and cathode, and I_p and E_A are the ionisation potential and the electron affinity of the molecule. The efficiency of the charge injection that critically depends on the magnitude of the injection barrier will determine if the current that flows through the device is injection-limited or space charge-limited (SCL).^{54, 64}

In order for SCL conduction to occur, at least one of the electrodes must be able to supply more carriers than can be transported through the molecules. Such a contact is usually termed an ohmic contact and it acts as an infinite charge reservoir. The electric field vanishes in the proximity of an ohmic electrode because of electric field screening due to the formation of space charge associated with unipolar current flow. In practise, an electrode can be considered as ohmic if the injection barrier is small enough to ensure that a high charge injection rate can be maintained without any electric field-assisted lowering of this barrier.⁶⁵ Numerical simulations by Malliaras *et. al.*⁶⁶ have shown that a barrier height lower than 0.3 eV is an indispensable condition for an electrode to be considered ohmic. Ohmic conduction for one carrier species is described by the following relation:

$$J = qn\mu V/d \quad \text{(equation 1.5)}$$

where V is the applied voltage and d the sample thickness. The electric field is constant across the device ($=V/d$). Variations in the current density for a given bias will occur if the mobility or the carrier density are temperature dependent. If the mobility is also field dependent, J will depend nonlinearly on V .

In the case of an organic molecule without traps and assuming a charge carrier mobility μ that is independent of the electric field, Child's law gives the SCL current density,

$$J_{\text{SCL}} = (9/8)\epsilon\epsilon_0\mu E^2/d \quad (\text{equation 1.6})$$

Where ϵ is the dielectric constant, ϵ_0 is the dielectric permittivity of free space, E is the electric field ($E=V/d$) and d is the thickness of the material. In the presence of traps,

$$J_{\text{SCL}} = (9/8)\epsilon\epsilon_0\mu\Theta E^2/d \quad (\text{equation 1.7})$$

Where Θ is the fraction of free to trapped charge. Because the injected carriers spend the majority of time in traps, the presence of traps results in an effective mobility $\mu_{\text{eff}}=\mu\Theta$. If only a discrete trap level is present, then the quadratic field dependence of the current will be retained. However if traps are distributed in energy then they will be filled from bottom to top as the field increases in magnitude and the quasi-Fermi level will shift towards the transport states of the molecule. Θ will become a function of E . The point where the conduction switches from equation 1.7 to 1.6 is the trap-filled limit. If an exponential distribution of traps in energy is assumed,

$$n_t(E) = (N_t/KT_c) \exp(-E/KT_c) \quad (\text{equation 1.8})$$

Then it can be calculated that:

$$J_{\text{SCL}} \equiv N_{\text{eff}}\mu(\epsilon\epsilon_0/N_t e)^m E^{m+1}/d^m \quad (\text{equation 1.9})$$

Where N_{eff} is the effective density of the transport states, $m=T_c/T$ (T_c is the characteristic temperature of the trap distribution), k is the Boltzmann's constant, T is the absolute temperature and N_t is the trap concentration. Traps above the Fermi level - by definition the shallow traps - slow down the injected carriers because they have to spend some time there before they can be thermally released. Traps below the Fermi

level - the deep traps - will always be filled and therefore cannot slow down the carriers. As the Fermi level rises with more carriers injected, more traps switch from being shallow to deep and the effective mobility will rise accordingly.

The SCL current is the maximum unipolar current a sample can sustain. In case of LEDs with a ohmic anode and a nonohmic cathode, a transition from SCL conduction to conduction controlled by both bipolar injection and recombination can occur at high electric fields if the barrier for electron injection is small enough to allow for field-assisted injection.⁶⁵ Also if the mobility is electric field dependent as usually happens for molecules where charge hopping occurs,⁶⁷ then a deviation from Child's law is expected. Young *et al.* have presented an analytical solution for arbitrary $\mu(E)$ dependence.⁶⁸ An alternative way to check if SCLC applies is to measure the mobility with TOF and compare the observed current with that calculated from Child's law.

However, usually both electrodes are found to be not ohmic in LEDs and, accordingly, currents will be injection limited. Depending on the oxidation and reduction potential of the molecule and the electrodes used we can have rather symmetric or highly asymmetric barriers. In that case the majority carriers that are determined by the lower injection barrier will govern the current flow. The injection-limited current⁶⁹ can be described in terms of either Richardson-Shottky (RS) thermionic emission⁶⁹ or Fowler-Nordheim (FN) tunnelling.⁶⁴ RS thermionic emission is due to the lowering of the image charge potential by the external voltage applied. Thus the effective injection barrier is given by:

$$H_{\text{eff}} = H - (e^3 E / 4\pi\epsilon\epsilon_0)^{1/2} \quad (\text{equation 1.10})$$

resulting in a square root electric field dependence of the current density. The FN theory considers tunnelling of the charge carriers through a triangular barrier into continuum states of the organic molecule and predicts that the current density j is proportional to:

$E^2 \exp[-4(m_{\text{eff}})^{1/2} H^{3/2} / (h/2\pi)eE]$, where m_{eff} is the effective mass of the carrier, H the barrier height and h the Planck's constant. The RS concept ignores the hopping of the carriers and tunnelling effects while the FN concept ignores coulombic interaction effects. Some studies of charge injection in OLEDs have shown that the FN concept can be readily applied in a variety of systems.^{58,64,70} Parker *et al.*⁶⁴ reported that the $j(E)$ curves follow FN law at high fields with a temperature independence of the j providing further evidence for injection-limited conduction. He also found that the barrier height values estimated on the basis of workfunctions correlate reasonably well with the values calculated from the experiment. However, deviations from the FN law occurred at low fields and these were attributed to a competition between thermionic emission and tunnelling injection at low fields.

The injection mechanism has important implications for the operation of the device. If for example the high barrier at the electrodes is limiting the total amount of charge that can possibly be stored in the device then low workfunction metals are essential as lowering the operating voltage has to take into consideration the band offsets and possible band bending at the organic/contact interface. If on the other hand, the space charge is the limiting factor for the total charge then in order to reduce the operating voltage one has to take into account the carrier mobility in both the emitting layer and the hole/electron transport layers.

1.4.2 Charge carrier transport

Charge transport can be studied with the time of flight technique from where the carrier mobility can be extracted.⁷¹ This technique will be analytically described in the next chapter. The mobility is an important parameter that determines i) the maximum current a device can sustain under SCL conditions and ii) the charge carrier density that can be stored in a device in the absence of trapping. The mobility usually increases with

temperature and electric field because both are expected to accelerate the hopping rate in an energetically disordered system while it decreases with decreasing concentration of the hopping sites. The same picture can apply to a polymer that can be considered an assembly of varying conjugation length units. Optical studies have shown that the transport in PLEDs is polaronic in nature and occurs through carrier hopping in a disorder broadened Gaussian density of states.⁷² However, trapping effects in polymers due to impurities are thought to be more severe than in small molecules.⁷³ The dispersive nature of time of flight signals in many polymeric systems is convincing evidence for this,⁷⁴ although the morphology of thick films fabricated by spin casting may be different from that of thin films and thus caution should be taken when mobilities based on dispersive signals are extracted. Transient EL has also been explored as a means to extract the mobility of majority carriers from real thin film devices.⁷⁵ The idea is that upon application of a voltage pulse, the onset of emission will occur only when both electrons and holes meet each other and recombine. If the electron mobility is much lower than the hole mobility then this will occur at a time identical with the transit time of holes and vice versa. If both mobilities are of the same order of magnitude then their ratio will determine the delay time of EL.⁷⁶

1.4.3 Charge carrier recombination

Electrons and holes move towards each other under the influence of the external field and they can either pass through the sample and get discharged at the counter electrode or they can recombine to form excitons. The spins of the recombining carriers are not correlated and that leads to possible triplet exciton formation whose emission is very weak and red shifted. If however, statistically distributed carrier populations are assumed then 75% of the recombined carriers will lead to triplet formation and only 25% will lead to singlet formation.⁵⁴ Therefore, the maximum internal EL quantum yield of an LED will be only 25% of the PL quantum yield assuming that singlets can

be formed with unit efficiency. In molecular solids where charge transport occurs by hopping among preferentially nearest neighbor sites, recombination is thought to be governed by diffusion and be of Langevin type irrespective of disorder.⁷⁷ In contrast in inorganic LEDs the exciton binding energy is small and only electrons and holes with antiparallel spins will recombine with interband light emission.

Recent results however have put the above argument in question as internal EL quantum efficiencies equal to 35-45% and 50% of the PL quantum yield, respectively have been reported.⁷⁸⁻⁷⁹ Either a small exciton binding energy or a larger cross section for singlet formation have been proposed as possible reasons to explain the experimental results. Even materials that exhibit nearly 100% PL efficiency have been demonstrated⁸⁰ thus making high efficiency PLEDs more attractive for the market.

Other results speculate that the intramolecular excited states are not the only possible products of the bimolecular carrier recombination. Charge-transfer states or complexes like interchain exciplexes⁵⁷ or intrachain excimers⁵⁶ can be formed that mainly decay nonradiatively thus resulting in low efficiencies.

1.4.4 Luminescence and efficiency

Förster energy transfer between molecules⁵⁹ and thermally activated exciton diffusion can be a hindrance to emission. Excitons are quite mobile so it is crucial to limit the inclusion of quenching sites. It has been clearly demonstrated in PPV, that nonexponential PL decay dynamics can be ascribed to oxidation sites within the polymer that effectively quench the excited states nonradiatively.⁸¹ Molecular design has been applied in an effort to eliminate these defects/impurities and produce less "disordered" and more pure materials. Interactions between individual molecules in the form of interchain excitations have also been found to be very important in the

photophysics of PPV.⁸² Also the concentration quenching effect (the phenomenon of the reduction in quantum efficiency when the emitting molecules approach very closely each other),⁸³ is another signature of the fact that the interactions between individual molecules can not be ignored. Different approaches to suppress this effect include doping a suitable host with a small fraction of the emissive dopant⁸⁴ or diluting the emissive polymer via blending with an inert matrix in order to render energy transfer less efficient.⁸⁵ Although by using this approach the efficiency can be increased, the brightness may decrease due to the reduction of the injection rate in the inert matrix.

A major advantage of light-emitting polymers is the ease with which their structures can be altered, thus enabling chemists to tune the properties by modifying their structures. Especially the emission wavelength and color can be adjusted by varying the aromatic rings and the substituents in the polymer backbone. The average conjugation length will determine the energy bandgap. The shorter the conjugation length the wider the energy bandgap and the more shifted to the blue is the emission color. Increasing conjugation length has been shown to reduce the exciton confinement and thus it results in a concomitant red shift of the emission and a lower yield.

The external EL efficiency of an LED (i.e., photons detected per electron injected) is given by the following relation:

$$\eta_{\text{EL}} = \eta_{\text{PL}} r_{\text{st}} \gamma_{\text{cap}} / 2n^2 \quad (\text{equation 1.11})$$

Where η_{EL} is the EL efficiency, η_{PL} is the PL efficiency (fractions of singlet excitons that emit light), r_{st} is the fractions of excitons formed in the singlet state, γ_{cap} is the fraction of opposite charges that meet up to form an exciton, $1/2n^2$ is the fraction of emitted photons that escape out of the device and n is the refractive index of the polymer. The power efficiency is lower than the external EL efficiency by a factor of the energy of the emitted photon divided by the operating voltage. In order thus to achieve high EL efficiency, it is desirable to have a material with a high PL efficiency and also to have

balanced injection of carriers. Carrier trapping can have a positive or a negative effect depending on whether the recombination at the trap will preferentially produce a radiative or a nonradiative state. If trapping enhances the residence time of the majority carriers inside the device and, hence, the probability that they will be encountered by minority carriers of the opposite sign then an enhancement of the device efficiency is expected. The efficiency of the exciton decay will depend on the available decay channels, radiative and non-radiative for singlets and non-radiative for triplets. While it is often assumed that the cross section for triplet and singlet formation is the same and thus that the upper limit to the internal EL efficiency will be 25% of the PL efficiency, recent theoretical studies have indicated that the formation probability of singlets is higher and thus the EL efficiency can be higher than the above limit.⁸⁶

Also the use of multilayer devices will favor the charge accumulation inside the device.⁸⁷⁻⁸⁸ Combining a layer with a low oxidation potential, i.e. low injection barrier for hole injection with a layer with significantly higher oxidation potential, will cause hole accumulation at the heterojunction. This will decrease the number of majority carriers getting discharged at the cathode nonradiatively but simultaneously will result in electric field redistribution inside the device in a way that favors the minority carrier (electron) injection. Hence, the insertion of a hole blocking layer into a hole dominated device improves the electron injection and thus the efficiency but at the expense of the hole injection. A trade-off occurring between charge recombination at the internal interface and leakage of majority (minority) carriers into the electron (hole) transporting layers will further determine the recombination efficiency. However, the electric field screening due to internal space charge is not enough to establish balanced injection and hence the use of low-workfunction cathodes are required. It should be emphasized that any enhancement of the efficiency does not necessarily imply an increase in luminance.

The approach of separating the transport and emission functions within the emissive layer through the use of a dopant in a small concentration to luminesce while the host will be responsible for charge transport has also proved successful.⁸⁹ In that case, the emitter which is doped with a HTL or an ETL must have a lower ionization potential than the HTL and a higher electron affinity than the ETL.

1.5 Thesis Outline

While research in polymer electroluminescence has led to devices that are now approaching commercial standards and soon are expected to be integrated in the first commercial products that will appear in the market,² still much work needs to be done with the aim to further improve the device performance, understand the physics behind the device operation and design new novel structures. This thesis describes some research work that addresses these issues. The approach of blending different materials will be particularly discussed and energy transfer in different host-guest systems will be presented. Emission from charge-transfer as well as triplet excited states will be presented and discussed in detail. A novel device structure and its application in light-emitting diodes and microcavities will also be presented. The structure of each chapter is outlined below along with a summary of some of the main results obtained. A short introduction regarding theoretical aspects and results already presented in the literature relative to the work presented in each chapter accompanied by the motivation for undertaking the specific work will also be presented in the beginning of each chapter. All the work presented here has been carried out in the University of Sheffield over the last three years. Experimental results obtained during a summer placement at the Dow Chemical Company in Midland, USA will not be presented in this thesis.

Chapter 2 describes the experimental methods that are used throughout this thesis. Details of the device fabrication methods including clean room and glove box

techniques that were used at the University of Sheffield are given. Details of the photolithographic patterning of the ITO, the cleaning procedures of the substrates, the preparation of the polymer solutions, the film deposition by spin coating and the cathode evaporation are given in detail. Also the experimental procedures and equipment used in the investigation of PLEDs and the optical and electrical characterisation of conjugated polymers are presented. Examples include measurement of the absorption, photoluminescence and electroluminescence spectra, current-voltage-luminance characteristics, photoluminescence quantum efficiency, electroabsorption spectroscopy, time of flight and time resolved photoluminescence spectroscopy.

Chapter 3 addresses the issue of emission from an exciplex state in bilayer LEDs based on hole transport fluorene-triarylamine copolymers and electron-transport starburst phenylquinoxalines. Exciplex states have attracted considerable interest as emissive states in OLEDs.⁵⁷ An exciplex state is a state formed between a hole from a donor molecule and an electron from an acceptor compound. Emission occurs when relaxation to the ground state takes place. Triarylamine copolymers with low ionization potentials have been examined as HTLs in a bilayer configuration with starburst phenylquinoxalines with high electron affinities as ETLs. Thiophene copolymers with higher ionization potentials have also been employed as HTLs. Emission from an exciplex state was only found to occur in the case of the lower ionization potential HTLs. The emission wavelength was determined by the energy difference between the ionization potential of the hole transporter and the electron affinity of the electron transporter. Differences between the experimental values of the emission wavelength and the theoretically calculated values (based on the difference between the E_{HOMO} of the HTL and the E_{LUMO} of the ETL) have been attributed to either systematic overestimation of the LUMO energy level of the ETL (due to polarization energy effects) or to the formation of an excited state of the HTL prior to the formation of the exciplex state.

Chapter 4 addresses the concept of blending an emissive polymer with hole transport materials as a means of improving the device performance and thus achieving high brightness and efficiency single layer PLEDs. Applying this concept, bright and efficient blue LEDs based on a host-guest system with a blue poly(9,9-dioctylfluorene) (PFO) as a host and a hole-transport triphenylamine copolymer poly(9,9-dioctylfluorene-co-bis-N,N'-(4-methylphenyl)-bis-N,N'-phenyl-1,4 phenylenediamine) (PFM) as a guest are realized. The optimization of device performance in terms of optimum guest concentration and emissive layer thickness is presented in detail. Doped LEDs show significantly improved performance compared to undoped ones due to the significantly improved charge balance factor and despite the fact that the PL efficiency is lower in the blend. Hole trapping is evidenced by transient electroabsorption measurements as well as from the dispersive shape of the time of flight signal in the blend. Weak Förster transfer is demonstrated to occur from PFO to PFM and this is supported by time resolved PL measurements which show a reduction of the PFO PL lifetime in the blend with increasing PFM concentration. The emission wavelength as well as the shape of the EL spectrum changes with the doped layer thickness and this effect is mainly attributed to interference effects. Resemblance of the EL spectra of the doped devices with the PL spectrum of PFM indicates that charge transfer is followed by carrier recombination which occurs preferentially on the PFM molecules.

In chapter 5 the same concept will be applied to produce high brightness and efficiency green single layer PLEDs. The host, termed 5BTF8, is a blend of poly(9,9-dioctylfluorene-co-benzothiadiazole) (BT) and PFO in a 5:95 ratio. The guest is a hole transport copolymer poly(9,9-dioctylfluorene-co-bis-N,N'-(4-butylphenyl)-bis-N,N'-phenylbenzidine) (BFB). Förster transfer occurs from PFO to BT and the improvement of the charge balance factor in the blend increases the device brightness and efficiency by an order of magnitude compared with the undoped device. LEDs with a peak emission wavelength at 535 nm that exhibit brightness up to 36,500 cd/m² at 10 V were

realized. The effect of a LiF/Al cathode on device performance was examined and the improved device performance was attributed to enhanced electron injection due to a lowering of the electron injection barrier as evidenced by EA measurements. A similar decrease of the hole injection barrier was found on LEDs where an ITO/PEDOT anode was used. These results are consistent with results reported in the literature.⁹⁰

Chapter 6 is concerned with electrophosphorescence with the aim to utilize both singlet and triplet states to produce high efficiency PLEDs. In an LED both triplets and singlets are formed with a ratio of 3:1. Thus the performance is limited by the fact that triplets do not contribute to EL and the maximum efficiency can not exceed 25% of the PL efficiency of the emitter. However, in some molecules the incorporation of a heavy metal atom makes the transition from the triplet to the ground state weakly allowed. Thus emission from both singlets and triplets is possible and the efficiency can reach 100% of the PLQE. In this chapter we employ the red phosphorescent emitter 2,3,7,8,12,13,17,18-octaethyl-21H,23H-porphyrin platinum (II), (PtOEP) as a dopant in a PFO host. Saturated red emission centred at 646 nm was obtained and doped LEDs with external EL efficiencies up to 1% at low brightness were realized. By decreasing the ITO workfunction, efficiencies up to 3% were reached due to the improved carrier balance. We also attribute these high efficiencies to the trapping of holes and electrons and the subsequent formation of excitons on PtOEP. We also doped PFO with PFM and used this blend as a host with a PtOEP guest. The efficiency increased by a factor of 3 and reached 3% for a high workfunction ITO anode. For a low workfunction ITO, an external EL efficiency of 5.8% was obtained at low brightness. The improved performance of the blend LEDs is attributed to more efficient energy transfer from the host to PtOEP as well as to improved charge balance due to hole trapping on PFM.

Chapter 7 shows how novel small area devices can result in very high brightness LEDs that can sustain significantly higher current densities than normal LEDs and can

also be highly efficient. A small area device structure (with an active area of a diameter down to 50 μm) is employed here. A photolithographically patterned silicon nitride layer is deposited on top of ITO in order to define active areas with diameters of 500, 100 and 50 μm , respectively. A significant improvement of the maximum brightness and current density is achieved in these small area devices and optimized green LEDs were found to emit light with a brightness of 155,000 cd/m^2 in DC mode. In AC mode these devices reached a brightness of 6,500,000 cd/m^2 and sustained current densities up to 5,000,000 A/m^2 . These improvements are attributed to an improved thermal management of the small area devices due to the reduced Joule heating effect. However, full color displays require materials with narrow emission spectra. Polymers usually have broad emission spectra due to inhomogeneous broadening and coupling to vibronic modes. Microcavities narrow the emission linewidth significantly²⁹ and they have been extensively used to overcome this problem.³⁰⁻³¹ Incorporation of the small area structure in a microcavity and results from electrically pumped small area cavity LEDs will be presented in the context of efforts towards electrically pumped polymer lasing.

Chapter 8 is concerned with energy transfer in a host-guest system where the host is a blue conjugated polymer based on poly(9,9-dioctylfluorene), namely F8P and the guest is the green emitter poly(9,9-dioctylfluorene-co-benzothiadiazole), BT. Absorption, photoluminescence, electroluminescence, PL quantum efficiency as well as time resolved PL measurements of varying guest concentration blends are presented. Optimized devices exhibit brightnesses up to 15,000 cd/m^2 and efficiencies up to 7 cd/A while the incorporation of a BFB hole transport material in the above blends increases the maximum brightness by a factor of 1.6 and reduces the operating voltage (for a brightness of 100 cd/m^2) to below 3 V without significantly affecting the EL efficiency.

Finally, chapter 9 draws together all the results and concludes the thesis. The issues addressed by this work are summarised and some suggestions for future work are

given. Appendix A provides some additional data related to the work presented in chapter 4 while Appendix B provides additional data related to the work presented in chapter 5. Finally, Appendix C lists all the journal publications and conference proceedings that have arisen from this work and are presented in this thesis.

References

1. Burroughes, J.H., Bradley, D.D.C., Brown, A.R., Marks, R.N., Mackay, K., Friend, R.H., Burns, P.L. & Holmes, A.B. *Nature* **347**, 539 (1990).
2. See CDT web page at <http://www.CDTLtd.co.uk> for latest results.
3. Fukuda, Y., Watanabe, T., Wakimoto, T., Miyagushi, S. & Tsuchida, M. *Synthetic Metals* **111**, 1 (2000).
4. Ho, P.K.H., Kim, J.S., Burroughes, J.H., Becker, H., Li, S.F.Y., Brown, T.M., Cacialli, F. & Friend, R.H. *Nature* **404**, 481 (2000).
5. Cao, Y., Yu, G., Parker, I.D. & Heeger, A.J. *Journal of Applied Physics* **88**, 18 (2000).
6. Cao, Y., Yu, G. & Heeger, A.J. *Advanced Materials* **10**, 917 (1998).
7. Yu, W.L., Cao, Y., Pei, J.A., Huang, W. & Heeger, A.J. *Applied Physics Letters* **75**, 3270 (1999).
8. Grice, A.W., Bradley, D.D.C., Bernius, M.T., Inbasekaran, M., Wu, W.W. & Woo, E.P. *Applied Physics Letters* **73**, 629 (1999).
9. Spreitzer, H., Becker, H., Kluge, E., Kreuder, W., Schenk, H., Demandt, R. & Schoo, H. *Advanced Materials* **10**, 1340 (1998).
10. Steubel, F., Staudigel, J., Stossel, M., Simmerer, J., Winnacker, A., Spreitzer, H., Weissortel, F. & Salbeck, J. *Advanced Materials* **12**, 133 (2000).
11. Tessler, N., Harrison, N.T. & Friend, R.H. *Advanced Materials* **10**, 64 (1998).
12. Shaheen, S.E., Jabbour, G.E., Kippelen, B., Peyghambarian, N., Anderson, J.D.,

Marder, S.R., Armstrong, N.R., Bellmann, E. & Grubbs, R.H., *Applied Physics Letters* **74**, 3212 (1999).

13. Fletcher, R.B., Lidzey, D.G., Bradley, D.D.C., Walker, S., Inbasekaran, M. & Woo, E.P. *Synthetic Metals* **111**, 153 (2000).

14. Jiang, X.Z., Liu, S., Ma, H. & Jen, A.K.Y. *Applied Physics Letters* **76**, 1813 (2000).

15. Yang, Y., Pei, Q. & Heeger, A.J. *Journal of Applied Physics* **79**, 934 (1996).

16. Stoessel, M., Wittmann, G., Staudigel, J., Steuber, F., Blassing, J., Roth, W., Klausmann, H., Rogler, W. Simmerer, J., Winnacker, A., Inbasekaran, M. & Woo, E.P. *Journal of Applied Physics* **87**, 4467 (2000).

17. Halls, J.J.M., Walsh, C.A., Greenham, N.C., Marseglia, E.A., Friend, R.H., Moratti, S.C. & Holmes, A.B. *Nature* **376**, 498 (1995).

18. Halls, J.J.M., Arias, A.C., MacKenzie, J.D., Wu, W.S., Inbasekaran, M., Woo, E.P. & Friend, R.H. *Advanced Materials* **12**, 498 (2000).

19. Pei, Q.B., Yu, G., Zhang, C., Yang, Y. & Heeger, A.J. *Science* **269**, 1086 (1995).

20. Gao, J., Heeger, A.J., Campbell, I.H. & Smith, D.L. *Physical Review B* **59**, R2482 (1999).

21. Yu, G., Gao, J., Hummelen, J.C., Wudl, F. & Heeger, A.J. *Science* **270**, 1789 (1995).

22. Yu, G., Srdanov, G., Wang, J., Wang, H., Cao, Y. & Heeger, A.J. *Synthetic Metals* **111**, 133 (2000).

23. Chen, L.C., Godovsky, D., Inganas, O., Hummelen, J.C., Janssens, R.A.J., Svensson, M. & Andersson, M.R. *Advanced Materials* **12**, 1367 (2000).

24. Dittmer, J.J., Marseglia, E.A. & Friend, R.H. *Advanced Materials* **12**, 1270 (2000).

25. Brown, A.R., Romp, A., Hart, C.M. & Deleeuw, D.M., *Science* **270**, 972 (1995).

26. Dodabalapur, A., Laquindanum, J, Katz, H.E. & Bao, Z. *Applied Physics Letters* **69**, 4227 (1996).
27. Dimitrakopoulos, C.D., Purushothaman, S., Kymissis, J., Callegari, A. & Shaw, J.M. *Science* **283**, 822 (1999).
28. Crone, B., Dodabalapur, A., Lin, Y.Y., Filas, R.W., Bao, Z., LaDuca, A., Sarpeshkar, R., Katz, H.E. & Li, W. *Nature* **403**, 521 (2000).
29. Tessler, N., Denton, G.J. & Friend, R.H. *Nature* **382**, 695 (1996).
30. Virgili, T., Lidzey, D.G., Bradley, D.D.C., Cerullo, G., Stagira, S. & De Silvestri, S. *Applied Physics Letters* **74**, 2767 (1999).
31. Frolov, S.V., Shkunov, M., Fujii, A., Yoshino, K. & Vardeny, Z.V. *IEEE Journal of Quantum Electronics* **36**, 2 (2000).
32. Kozlov, V.G., Bulovic, V. & Forrest, S.R. *Applied Physics Letters* **71**, 2575 (1997).
33. Dodabalapur, A., Berggren, M., Slusher, R.E., Bao, Z., Timko, A., Schiortino, P., Laskowski, E., Katz, H.E. & Nalamasu, O. *IEEE Journal of Selected Topics in Quantum Electronics* **4**, 67 (1998).
34. McGehee, M.D. & Heeger, A.J. *Advanced Materials* **12**, 1655 (2000).
35. Salem, L. *The molecular orbital theory of conjugated systems* (W.A.Benjamin, Inc., New York – Amsterdam, 1966).
36. Chiang, C.K., Fincher, C.R., Park, Y.W., Heeger, A.J., Shirakawa, H., Louis, E.J., Gau, S.C. & MacDiarmid, A.G. *Physical Review Letters* **39**, 1098 (1977).
37. Cacialli, F., Friend, R.H., Haylett, N., Daik, R., Feast, W.J., dosSantos, D.A. & Bredas, J.L. *Applied Physics Letters* **69**, 3794 (1996).
38. Braun, D. & Heeger, A.J. *Applied Physics Letters* **58**, 1982 (1991).
39. Brown, A.R., Bradley, D.D.C., Burroughes, J.H., Friend, R.H., Greenham, N.C., Burn, P.L., Holmes, A.B. & Kraft, A. *Applied Physics Letters* **61**, 2793 (1992).
40. Garten, F., Hilberer, A., Cacialli, F., Esselink, E., vanDam, Y., Schlattmann, B., Friend, R.H., Klapwijk, T.M. & Hadziioannou, G. *Advanced Materials* **9**, 127 (1997).

41. Sirringhaus, H., Tessler, N. & Friend, R.H. *Science* **280**, 1741 (1998).
42. Papadimitrakopoulos, F., Yan, M., Rothberg, L.J., Katz, H.E., Chandross, E.A. & Galvin, M.E. *Molecular Crystals Liquid Crystals* **256**, 663 (1994).
43. Kraft, A., Grimsdale, A.C. & Holmes, A.B. *Angew. Chem. Int. Ed.* **37**, 402 (1998).
44. Rasmusson, J.R., Broms, P., Birgerson, J., Erlandsson, R. & Salaneck, W.R. *Synthetic Metals* **79**, 75 (1996).
45. Shi, Y., Liu, J. & Yang, Y. *Journal of Applied Physics* **87**, 4254 (2000).
46. Liu, J., Shi, Y.J., Ma, L.P. & Yang, Y. *Journal of Applied Physics* **88**, 605 (2000).
47. Chung, S.J., Jin, J.I., Lee, C.H. & Lee, C.E. *Advanced Materials* **10**, 684 (1998).
48. Yu, W.L., Pei, J., Huang, W. & Heeger, A.J. *Advanced Materials* **12**, 828 (2000).
49. Kearwell, A. & Wilkinson, F. *Transfer and Storage of Energy by Molecules* (Wiley, New York, 1969).
50. Schiff, L.I. *Quantum mechanics*, McGraw Hill.
51. Thompson, M.E., Burrows, P.E. & Forrest, S.R. *Current Opinion in Solid State & Materials Science* **4**, 369 (1999).
52. Klessinger, M. & Michi, J. *Excited States and Photochemistry of Organic Molecules*, VCH, New York (1995).
53. Su, W.-P., Schrieffer, J.R. & Heeger, A.J. *Physical Review Letters* **42**, 1698 (1979).
54. Pope, M. & Swenberg, C.E. *Electronic Processes in Organic Crystals and Polymers*, 2nd Edition, Oxford University Press, Oxford (1999).
55. Vardeny, Z.V. & Wei, X. *Synthetic Metals* **55**, 255 (1993).
56. Bliznyuk, V.N., Carter, S.A., Scott, H.C., Klaerner, G., Miller, R.D. & Miller, D.C. *Macromolecules* **32**, 361 (1999).
57. Wang, J.F., Kawabe, Y., Shaheen, S.E., Morrell, M.M., Jabbour, G.E., Lee,

- P.A., Anderson, J., Armstrong, N.R., Kippelen, B., Mash, E.A. & Peyghambarian, N. *Advanced Materials* **10**, 230 (1998).
58. Heeger, A.J., Parker, I.D. & Yang, Y. *Synthetic Metals* **67**, 23 (1994).
59. Förster, T. *Annalen der Physik* **2**, 55 (1948).
60. Pope, M., Kallman, H. & Magnante, P. *Journal of Chemical Physics* **38**, 2042 (1963).
61. Partridge, R.H. *Polymer* **24**, 733 (1983).
62. Vincett, P., Barlow, W., Hann, R. & Roberts, G. *Thin Solid Films* **94**, 171 (1982).
63. Tang, C.W. & Van Slyke, S.A. *Applied Physics Letters* **51**, 913 (1987).
64. Parker, I.D. *Journal of Applied Physics* **75**, 1656 (1994).
65. Arkhipov, V.I., Emeljarova, E.V., Tak, Y.H. & Bässler, H. *Journal of Applied Physics* **84**, 848 (1998).
66. Malliaras, G.G. & Scott, J.C. *Journal of Applied Physics* **85**, 7426 (1999).
67. Bässler, H. *Physica Status Solidi B* **175**, 15 (1993).
68. Young, R. *Philosophical Magazine Letters* **70**, 331 (1994).
69. Barth, S., Wolf, U., Bässler, H., Muller, P., Riel, H., Vestweber, H., Seidler, P.F. & Riess, W. *Physical Review B* **60**, 8791 (1999).
70. Vestweber, H., Pommerehne, J., Sander, R., Marht, R.F., Greiner, A., Heitz, W. & Bässler, H. *Synthetic Metals* **68**, 263 (1995).
71. Redecker, M., Bradley, D.D.C., Inbasekaran, M. & Woo, E.P. *Applied Physics Letters* **73**, 1565 (1998).
72. Campbell, A.J., Bradley, D.D.C. & Lidzey, D.G. *Journal of Applied Physics* **82**, 6326 (1997).
73. Graupner, W., Leditzky, G., Leising, G. & Scherf, U. *Physical Review B* **54**, 7610 (1996).
74. Meyer, H., Haarer, D., Naarmann, H. & Hörhold, H.H. *Physical Review B* **52**, 2587 (1995).

75. Pinner, D.J., Friend, R.H. & Tessler, N. *Journal of Applied Physics* **86**, 5116 (1999).
76. Pommerehne, J., Vestweber, H., Tak, Y.H. & Bäessler, H. *Synthetic Metals* **76**, 67 (1996).
77. Albrecht, U. & Bäessler, H. *Physica Status Solidi B* **191**, 455 (1995).
78. Kim, J.S., Ho, P.K.H., Greenham, N.C. & Friend, R.H. *Journal of Applied Physics* **88**, 1073 (2000).
79. Cao, Y., Parker, I.D., Yu, G., Zhang, C. & Heeger, A.J. *Nature* **397**, 414 (1999).
80. Mattoussi, H., Murata, H., Merritt, C.D., Iizumi, Y., Kido, J. & Kafafi, Z.H. *Journal Of Applied Physics* **86**, 2641 (1999).
81. Yan, M, Rothberg, L.J., Papadimitrakopoulos, F., Galvin, M.E. & Miller, T.M. *Physical Review Letters* **73**, 744 (1994).
82. Yan, M., Rothberg, L.J., Kwock, E.W. & Miller, T.M. *Physical Review Letters* **75**, 1995 (1992).
83. Dodabalapur, A. *Solid State Communications* **102**, 259 (1997).
84. Virgili, T., Lidzey, D.G. & Bradley, D.D.C. *Advanced Materials* **12**, 58 (2000).
85. Tasch, S., List, E.J.W., Ekstrom, O., Graupner, W., Leising, G., Schlichting, P., Rohr, U., Geerts, Y., Scherf, U. & Mullen, K. *Applied Physics Letters* **71**, 2883 (1997).
86. Shuai, Z., Beljonne, D., Silbey, R.J. & Bredas, J.L. *Physical Review Letters* **84**, 131 (2000).
87. Brown, A.R., Burroughes, J.H., Greenham, N.C., Friend, R.H., Bradley, D.D.C., Burn, P.L., Kraft, A. & Holmes, A.B. *Applied Physics Letters* **61**, 2703 (1992).
88. Staudigel, J., Stossel, M., Steuber, F. & Simmerer, J. *Journal of Applied Physics* **86**, 3895 (1999).
89. Tasch, S., List, E.J.W., Hochfilzer, C., Leising, G., Schlichting, P., Rohr, U., Geerts, Y., Scherf, U. & Mullen, K. *Physical Review B* **56**, 4479 (1997).
90. Brown, T.M., Kim, J.S., Friend, R.H., Cacialli, F., Daik, R. & Feast, W.J. *Applied Physics Letters* **75**, 1679 (1999).

CHAPTER 2

EXPERIMENTAL METHODS

2.1 Introduction

This chapter outlines the fabrication methods for producing polymer light-emitting diodes and the different experimental techniques employed during the course of this thesis in order to optically and electrically characterize conjugated polymers and devices. All these techniques have been employed in the last three years in the Department of Physics of the University of Sheffield. Rather different techniques were employed during a summer industrial placement at the Dow Chemical Company in Midland, Michigan, USA but they will not be reported in this thesis.

Section 2.2 describes the device fabrication methods including clean room and glove box techniques. Details of the photolithographic patterning of indium tin oxide, the cleaning of the substrates, the deposition of the polymer films by spin-coating techniques and the evaporation of the top cathode metal are presented in detail. Section 2.3 discusses the experimental techniques used in order to optically and electrically characterize conjugated polymers and devices. Absorption, photoluminescence, electroluminescence spectra, photoluminescence quantum efficiency measurements as well as current-voltage-luminance characteristics are described. In section 2.4 electroabsorption spectroscopy is presented in detail while in section 2.5 the time of

flight technique is analyzed. Finally in section 2.6, details of photoluminescence time resolved spectroscopy will be presented.

2.2 Preparation of Polymer LEDs

Polymer light emitting diodes are fabricated in a clean room environment and a typical PLED has the following structure: glass substrate / positive electrode (ITO) / polymer layer / negative electrode¹⁻². Figure 2.1 and 2.2 show schematic diagrams of an LED configuration based on the Sheffield geometry from two different angles.

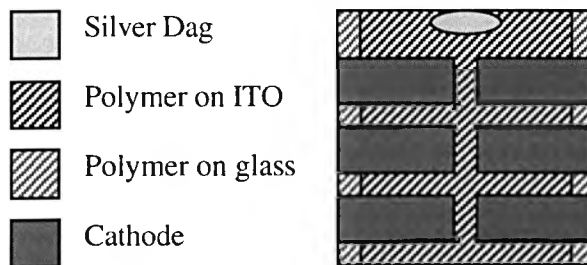


Figure 2.1: Schematic diagram illustrating a typical LED substrate with six pixels. The active device area is defined by the spatial overlap between the polymer on ITO (dark striped region) and the cathode (dark grey shaded area). Silver dag (light grey shaded area) is used to contact the ITO through the polymer.

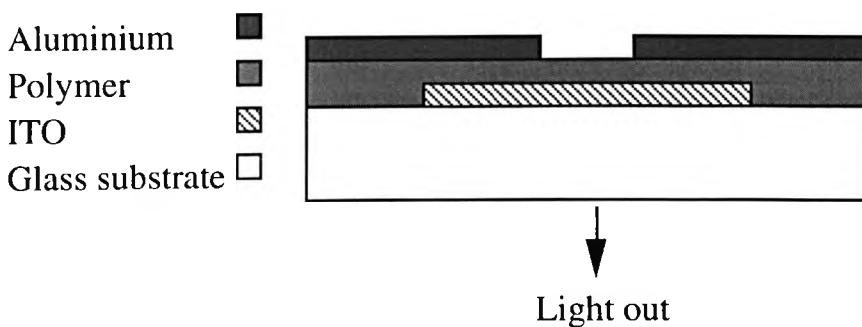


Figure 2.2: A schematic diagram of a typical electroluminescent device used at Sheffield University with an aluminum cathode.

2.2.1 Indium tin oxide (ITO) coated glass substrates

A glass substrate covered with a SiO₂ diffusion blocking layer and coated on one side with indium tin oxide (ITO) is used as the substrate for devices fabricated in Sheffield. ITO is used as the hole injecting contact because a) is highly transparent in the whole range of the visible spectrum (transmittance of 85% at 550 nm) and thus light can escape out of the device b) is readily available from many different companies and thus easy and cheap to purchase and c) has a high workfunction (between 4.3 and 4.8 eV depending on the supplier³⁻⁴) and thus it matches closely the HOMO level of most conjugated polymers. However, it has been widely shown that the ITO workfunction is highly dependent on its chemical composition near the surface⁵ and the cleaning procedure used⁶⁻⁷. The estimated workfunction has also been found to vary with the measurement technique used⁸. The ITO has to be etched and a photoresist is used for this purpose. We have used ITO purchased from two different suppliers, namely Balzers and Applied Thin Films. Their workfunctions are not precisely known. However other research groups have used ITO coated glass substrates from the above suppliers and have also measured their workfunction using the Kelvin probe technique³⁻⁴. According to these reports, the Balzers ITO has a workfunction of approximately 4.7 eV³ while the Applied Films ITO has a workfunction of approximately 4.3 eV⁴. We will use these values from the literature as reference values throughout this thesis although we should point out that differences can occur between different batches even from the same supplier. The thickness of the ITO is approximately 150 nm and the sheet resistance is 20 Ω per square. The dimensions of the substrates are 12x12 mm.

The ITO has to be etched along the two sides to prevent short circuits when contact is made between the ITO and the cathode and an external bias is applied. Standard photolithographic patterning was used and the etching procedure is outlined below and shown in Figure 2.3.

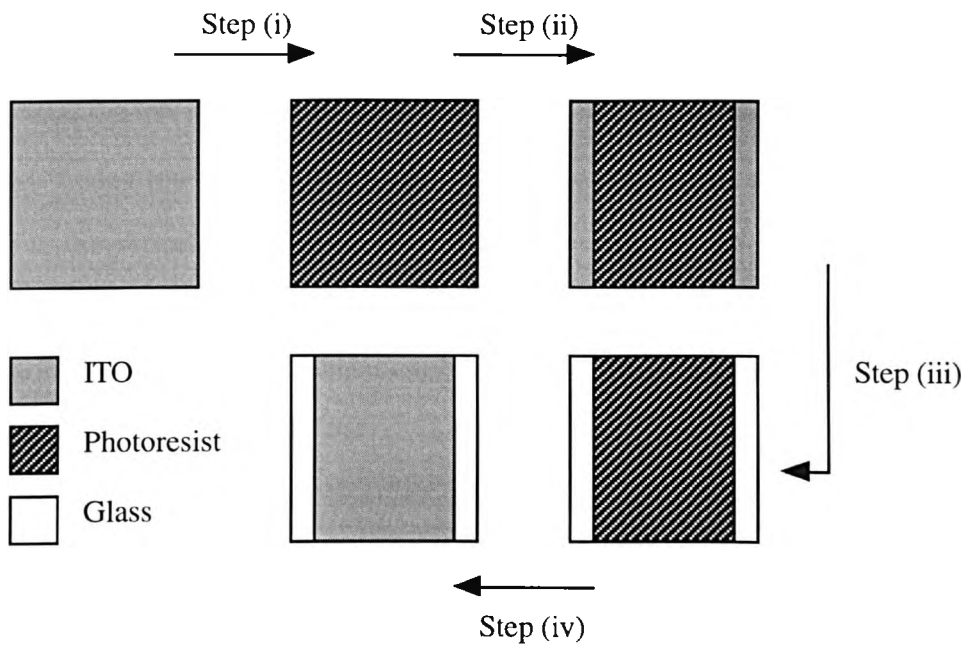


Figure 2.3: A diagram of the etching procedure used to pattern the ITO electrode. Moving from step (i) to step (iv): "positive" photoresist is spin coated onto the ITO substrate, step (ii): unmasked regions of the photoresist are exposed to UV light, step (iii) the substrate is then placed in developer solution and the regions exposed to the UV light are washed away in deionized water, and step (iv) the substrate is then placed in a dilute HCl solution to etch off the ITO and the photoresist is finally removed by rinsing in acetone to leave a patterned ITO electrode.

A few drops of photoresist are placed on the glass/ITO substrate and the layer is then spin-coated at a speed of 4000 rpm for about 30 seconds. The photoresist layer is then baked for 1 min on the hot plate at 100°C in air to remove any residual solvent (step i). The substrate is then placed in a shadow mask that exposes an area of 12×2 mm on both sides and covers the rest of the substrate. The mask is placed to an ultraviolet (UV) light source for about 2 min in order for the appropriate area of the substrate covered with photoresist to be exposed (step ii). The substrate is then placed in a developer (diluted with deionised water in a ratio of 1:3) for approximately 1 min and the regions exposed to the UV light are developed (step iii). The substrate is then rinsed with deionized water and the exposed regions are washed away (step iv). After the substrate is placed in a hot solution of 10% diluted HCl (in deionized water) and left

there for a few minutes to etch the exposed ITO region. The substrate is removed only when the exposed ITO has been washed away. The acid is washed away from the substrate by rinsing it with deionised water. Finally, the substrate is rinsed with acetone in order for the remaining photoresist to be removed from the ITO surface. The photoresist is removed very easily and the ITO is now fully etched (step v). The substrate is then placed in a ultrasonic bath that contains propanol for about 15 minutes and then left to dry prior to further use.

After the ITO is etched, a final cleaning procedure is applied before the deposition of the polymer layer by spin coating. The procedure is as follows: The substrate is placed in a 5% Decon 90 surfactant solution (a mixture of 5% Decon 90 surfactant and 95% deionized water). Its surface is gently wiped with a cotton bud in order to remove any dust from the ITO side. After this the ITO is rinsed in flowing deionized water for 10 minutes and finally it is rinsed in methanol for 5 minutes. It is then dried with a filtered air gun and immediately afterwards the ITO is ready to be used for the film deposition process.

2.2.2 Polymer film deposition

Most of the polymers used in this work have been synthesised at the Dow Chemical Company in Midland, Michigan, USA. The only exceptions are two electron transport starburst phenylquinoxalines that were synthesised at the University of Bayreuth in Germany and a PtOEP dye that was commercially purchased. A spin coating process is used for the deposition of the polymers from their solutions in organic solvents. This is a relatively cheap and reliable technique to deposit a homogeneous polymer film from its solution. Although we have used a range of different solvents for dissolving the polymers, we chose to use solvents with high boiling point such as xylene and toluene whenever possible as they tend to form more homogeneous films compared to solvents with low boiling point such as tetrahydrofuran

(THF)⁹. It is also important to note that the polymer solution has to be as clear as possible before spin casting. That happens only when the polymer is fully dissolved in the solvent that has been used. For this purpose the solution was always heated gently for a while at a temperature below the boiling point of the solvent used and it was then passed through a 0.2 or a 0.45 μm glass fibre acrodisc filter. Typical solution concentrations were between 5 and 30 mg/mL. The substrate was then placed on top of the spin coater chuck and held down by a weak vacuum from a rotary pump during the spinning process. Different speeds can be applied ranging from 800 to 8000 rpm and the spinning speed will determine the thickness of the polymer film (the higher the spinning speed the thinner the polymer film). A few drops of the polymer solution are carefully dropped onto the substrate so as to cover the whole area and then spun for about 40 sec. The following relation is used to give an estimate of the film thickness¹⁰:

$$\text{Thickness} \propto [(\text{concentration} \cdot \text{viscosity}) / (\text{spin speed})^{1/2}] \quad (\text{equation 2.1})$$

For 2 layer devices, extra care should be taken as most polymers are soluble in the same range of solvents. In that case, a good interface between the two layers can only be formed when the solvent that is used for the second layer does not dissolve the first layer. Also the first layer should be baked for a few hours at a temperature close to the boiling point of the solvent used in order to remove any residual solvent before the deposition of the second layer.

2.2.3 Metal cathode evaporation

The final stage in the preparation of an LED is the deposition of the negative electrode (electron injecting electrode) on top of the polymer film. This procedure is carried out in the evaporator of the clean room when air stable metals like aluminum (Al) are used. If air reactive metals like calcium (Ca) or magnesium (Mg) are used then the evaporation has to be done in the evaporator of a nitrogen filled glove box where very few parts of oxygen and water exist (typically a few parts per million). The

evaporation is being carried out under a vacuum of approximately 3×10^{-6} mbar and the rate of the evaporation is typically 0.3-0.5 A/sec for the first 20 nm and 3-6 A/sec for the rest of the deposited metal. A low rate is used for the first few nm to prevent metal diffusion in the polymer film. The metal is evaporated using a resistive heating element and the rate is controlled by the current that flows through this element. The thickness of the metal is measured by a sensitive quartz crystal and typical thicknesses used are between 150 and 300 nm. Al has been widely used as the negative contact because it has a relatively low workfunction (~ 4.3 eV) providing a moderate barrier for electron injection and is also very stable in air. In contrast, Ca and Mg have much lower workfunctions (2.9 and 3.7 eV, respectively) thus providing a small barrier for electron injection but are very reactive in the presence of water and oxygen and therefore very unstable in air requiring encapsulation techniques to be applied in the device. Figure 2.4 shows a digital photograph of typical blue, green and red LEDs based on Dow Chemical materials fabricated and tested at Sheffield.

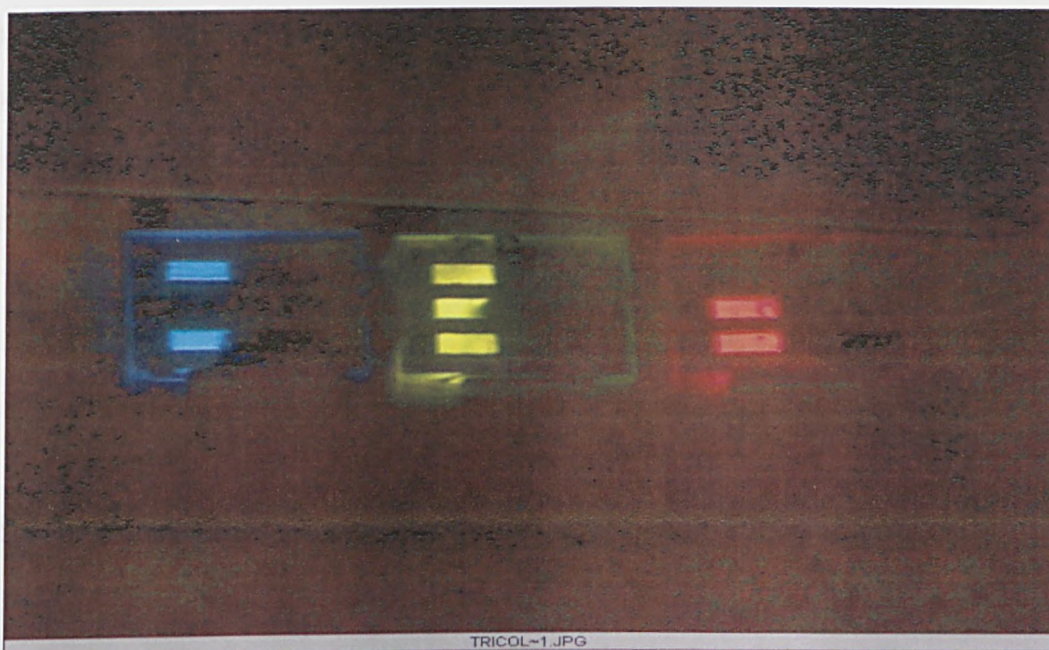


Figure 2.4: A digital photograph of blue, green and red polymer LEDs fabricated and tested at Sheffield using materials from The Dow Chemical Company. The devices were connected in parallel and placed in a nitrogen filled glove box; they emitted simultaneously with an external bias of 8 V.

2.3 Optical and electrical characterisation of conjugated polymers and LEDs

Light emitting diodes and conjugated polymers are characterised optically (by means of optical absorption, photoluminescence spectra and photoluminescence quantum yield measurements) and electrically (by means of electroluminescence spectra, current-voltage and luminance-voltage characteristics). Thickness measurements of the polymer thin films that are used in the fabrication of LEDs are also performed. An analytical description of these experimental techniques is given below.

2.3.1 Optical absorption spectra

In order for optical absorption spectra to be taken, spectrosil B quartz substrates are used that are transparent at all wavelengths over 200 nm with the polymer solution to be spun on top of these substrates. A Unicam UV/Vis spectrophotometer that is able to scan all wavelengths between 200 and 900 nm is used for optical absorption measurements. The measurement is not corrected for scattered or reflected light from the surface of the sample. When the transmission spectrum is recorded the absorption coefficient a can be calculated using the following relation:

$$I = I_0 \exp(-ad) \quad \text{(equation 2.2)}$$

with d being the film thickness, a the absorption coefficient, I and I_0 the light intensity measured with and without a film on the quartz substrate.

2.3.2 Photoluminescence and electroluminescence spectra

The photoluminescence spectra are recorded in the solid state. The same quartz substrates are used as in the case of the absorption spectra. The sample can be optically excited from a series of different optical sources. A GaN blue LED can be used with three different filters available that provide three different excitation wavelengths

(narrow lines at 419, 450 and 481 nm). A monochromator with a tungsten or a xenon lamp as a light source can also be used. In that case all the range of wavelengths between 350 and 750 nm can be achieved and used to excite the sample. The signal when collected must be corrected for the background and also the detection response of the CCD camera. The CCD detects poorly in the blue with vastly enhanced performance after 500 nm. The detection response of the CCD can be seen in figure 2.5.

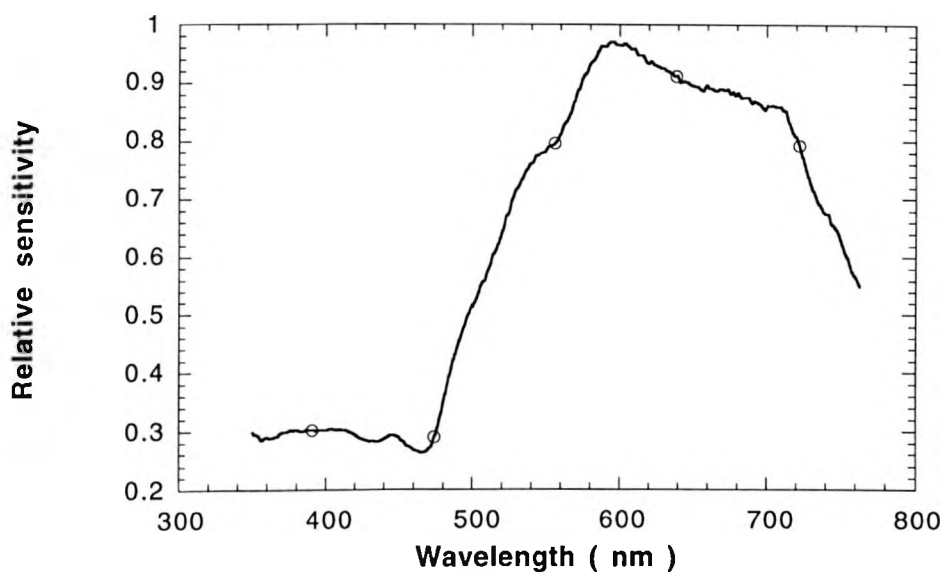


Figure 2.5: Calibration Curve for the Oriel CCD Spectrograph.

The choice of the appropriate wavelength depends on the absorption spectrum maximum. In order for a strong photoluminescence spectrum to be recorded, the polymer has to be excited as close as possible to its absorption maximum because in that case the polymer will absorb almost all the light and will give a strong photoluminescent signal shifted to the red according to the Stokes shift. However, if the spectrum is not very strong the sample can be excited for a longer time to get a stronger spectrum and is preferably taken in reflection and not in transmission. The optical fiber is placed at an angle relative to the sample and all the light that is collected is sent to the CCD camera (Instaspec IV spectrometer). Samples can also be excited by the 354 nm

line of a He:Cd laser with light being collected by a spectrometer through an optical fiber and with a photomultiplier being used as the detector.

The electroluminescence spectrum is recorded from devices (LEDs) under operation (emission) conditions. The device is being driven from an external voltage source and when the emitted light is visible in a dark environment and strong enough to be recorded, the same optical fibre as above is placed exactly in front of the device and collects all the light which is then transferred to the CCD camera.

2.3.3 Current-voltage-luminance characteristics

The current-voltage characteristics are measured either by using a Keithley 237 model source unit which measures at the same time both the applied voltage and the current that flows through the device or by using a Keithley 230 programmable voltage source and a Blackstar 4503 intelligent multimeter that measure voltage and current, respectively. The luminance (brightness) of the device is measured with a multimeter that measures the voltage across a photodiode which is proportional to the light emitted from the device. The absolute brightness of the device in cd/m^2 is measured with a Topcon luminance meter. Its sensitivity is 1 cd/m^2 . A current amplifier connected to the photodiode is used to increase the sensitivity of the light output measurements. Under forward bias the positive voltage is applied to the ITO contact and the negative voltage is applied to the negative contact. The device is placed into a sample chamber that can allow device measurements to be performed in the air, under a rotary pump vacuum of 10^{-2} mbar or in a nitrogen filled glove box. Each substrate has six devices on it and they can all be tested subsequently by changing the device that is connected each time to the circuit. In each case an external voltage is applied and both the current and the luminance are measured and recorded by using Labview software. The current density is calculated by dividing the current that flows through the device with the active surface of the device which is about 4.5 mm^2 . The external electric field is given if the

external voltage that is applied across the two electrodes is divided by the thickness of the device. The maximum current that can pass through the device is limited to 100 mA and is set as the current compliance.

2.3.4 Thickness measurements

Thickness measurements are carried out by using a Dektak surface profilometer. The polymer film is first scratched with a needle and then placed below the tip of the profilometer which exerts a very light constant force to the sample when moved across the sample. The tip is then moved across the scratch and the vertical position of the tip is monitored. The thickness of the sample is determined as the average value of a few different measured thicknesses of the sample in different positions on the surface of the polymer film. This is necessary as thickness variations of the order of 10 - 30 nm exist for the same polymer film in most cases. Uniformity of the film is not always easy to be achieved due to different amounts of polymer solution dropping onto different areas of the substrate leading to inhomogeneities of the film at a nm scale.

2.3.5 Photoluminescence Quantum Efficiency measurements

The photoluminescence quantum efficiency of a sample defines the number of photons emitted per photon absorbed and as such is an important parameter used to characterise the relative efficiency of radiative decay of a singlet exciton in a material. Theoretically it can be as high as unity and values above 0.9 have been recently reported¹¹. PL quantum efficiency measurements were performed within a calibrated integrating sphere coupled via a fiber-optic link to a scanning monochromator with a photomultiplier as a detector. The samples were mounted in the centre of an integrating sphere. The inner surface of the sphere was covered with a highly reflective coating. The sample was optically excited using the 354 nm line of a He:Cd laser. Light from the He:Cd laser was incident onto the sample through a small aperture hole in the sphere

wall. A typical laser power density was $\approx 0.1 \text{ mW/cm}^2$. Photoluminescence was collected through a small exit port in the sphere and is assumed to be proportional to the total amount of light emitted within the sphere. A baffle was used to prevent any light reaching the exit port directly from the sample. The collected light was coupled to a Spex 270M spectrometer via an optical fibre.

Solid state PL efficiencies were measured utilising a technique similar to the one proposed by Greenham *et al.*¹² and de Mello *et al.*¹³ The spectrometer has been calibrated with reference to a standard. The use of a monochromator to measure the light field within the sphere allows the relative contribution of the emission and the excitation to be separated. So we determine the relative number of photons inside the sphere after excitation with the sample absent, and then we measure the relative number of photons absorbed by the sample with the sample present. This is compared to the number of the photons emitted by the sample when excited to give the absolute PL quantum efficiency. Measurements were taken with and without the sample present. The spectra were corrected for the total response of the system (i.e. response of sphere and spectrometer). The PL efficiency was then calculated using the following relation:

$$\eta_{PL} = \left(\frac{P_h}{L_a - L_h} \right) \quad (\text{equation 2.3})$$

where P_h and L_h are the PL and laser signals respectively measured with the sample present and L_a is the laser signal measured without the sample present. The relative absorbance (A) of the sample may also be calculated by:

$$A = 1 - (L_h/L_a) \quad (\text{equation 2.4})$$

Typically a few different samples from the same material were prepared and measured under the same conditions and a average value was calculated. All measurements were made under a nitrogen atmosphere to avoid photooxidation of the samples by the laser beam during optical excitation.

2.3.6 Electroluminescence quantum efficiency calculations

The external EL quantum efficiency of an LED is defined as the number of photons produced within the emissive layer and emitted in the forward direction per charge carrier flowing in the external circuit. It is calculated from a standard expression involving the measured ratio of forward directed light and device current density, taking into account the EL spectral distribution and the photopic efficacy spectrum¹⁴ :

$$\eta_{ext} = \frac{\pi e}{K_m hc} \frac{L}{j} \frac{\int F(\lambda) d\lambda}{\int \frac{F(\lambda) \cdot y(\lambda) d\lambda}{\lambda}} \quad (\text{equation 2.5})$$

where η_{ext} is the external quantum efficiency, L is the luminance in cd/m^2 , J is the current density in mA/cm^2 , K_M is the maximum luminous efficacy (namely 680 lm/W), $y(\lambda)$ the normalised photopic spectral response function (see figure 2.6), $F(\lambda)$ the electroluminescence emission spectrum of the device and λ is the wavelength in nm.

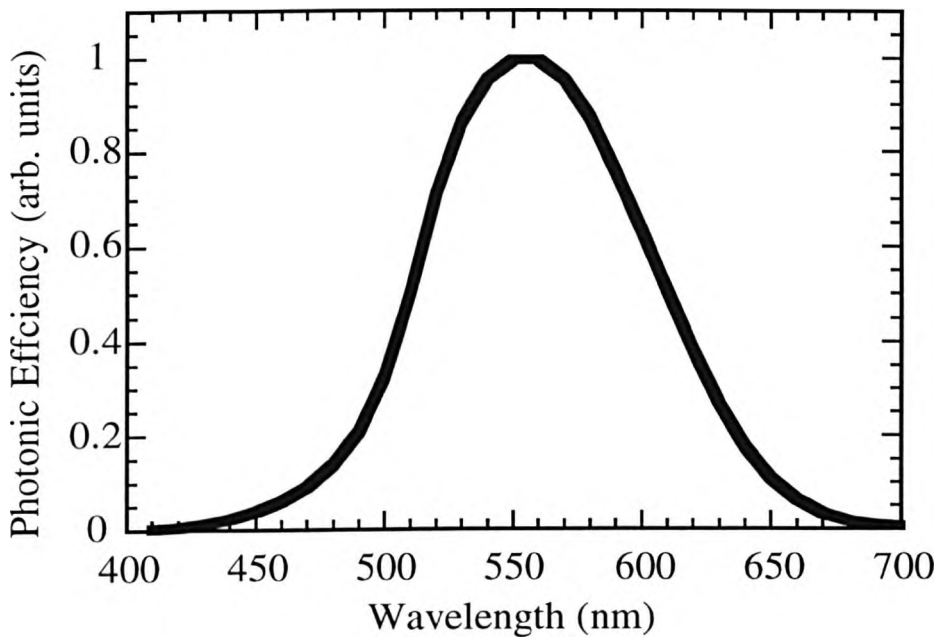


Figure 2.6: A plot of the photopic efficacy curve. This plots the response of the human eye to different wavelengths. The peak response is 680 lm/W at a wavelength of 555 nm . This curve is used for the estimation of the luminous efficiency and the calculation of the external quantum efficiency.

Internal quantum efficiencies η_{int} are estimated from the relationship proposed by Greenham *et al.*¹⁵:

$$n_{\text{int}} = n_{\text{ext}} 2n^2 \quad (\text{equation (2.6)})$$

where n is the refractive index of the polymer, generally in the region of 1.5~2. The power efficiencies quoted in this thesis are determined by the following relation:

$$\text{Power efficiency (lm/W)} = (3.14 * L) / (10 * J * V) \quad (\text{equation 2.7})$$

Where the current density J is expressed in mA/cm^2 , the luminance in cd/m^2 and the operating voltage in V . The operating voltage is the voltage at which the current density and luminance which were used in the calculation of the external quantum efficiency were measured.

2.4 Electroabsorption measurements

Electroabsorption (EA) spectroscopy is an experimental technique in which the absorption of a material is modulated by an electric field and it has been widely used to study the electronic structure of molecular semiconductors¹⁶. The EA spectrum of most organic materials exhibits a significant feature due to the Stark effect: a shift of the first optically allowed excitonic state or in other words the shift of the electronic states' energy and absorption by the applied external electric field. Therefore the EA spectrum is closely related to the absorption spectrum of the material.

The electroabsorption signal depends on the square of the electric field F and is given by:

$$\frac{\Delta T}{T} \propto F^2 \quad (\text{equation (2.8)})$$

where $\frac{\Delta T}{T}$ represents the change in transmission of light normalised to the total transmission T . This is equal to the change in the absorbance of the sample as given by:

$$\Delta T/T = \Delta \alpha d \quad (\text{equation 2.9})$$

where α is the extinction coefficient and d is the sample thickness.

Substituting the electric field term F by the sum of the AC and the DC field,

$$F = F_{DC} + F_{AC} \cos(\omega t) \quad \text{equation (2.10)}$$

where ω is the modulation frequency of the electric field, leads to

$$\frac{\Delta T}{T} = \text{const.} \left(F_{DC}^2 + 2F_{DC}F_{AC} \cos(\omega t) + \frac{F_{AC}^2}{2} + \frac{F_{AC}^2}{2} \cos(2\omega t) \right) \quad \text{(equation 2.11)}$$

The lock-in technique used in this experiment allows selective detection of signals that oscillate with a certain frequency ω . Thus, the pure DC and AC signals in equation 2.11 are not detectable. However, there are two contributions according to equation 2.11 which are detectable. One term containing only the F_{AC} signal which oscillates with 2ω and a second term containing both, the F_{AC} and the F_{DC} part of the electric field which oscillates with ω . We refer to the EA spectrum measured with a lock-in amplifier referenced to the modulation frequency as the EA(1f) spectrum and to that with the lock-in amplifier referenced to the second harmonic as the EA(2f) spectrum. The experimental apparatus used to detect electroabsorption signals is displayed in figure 2.7.

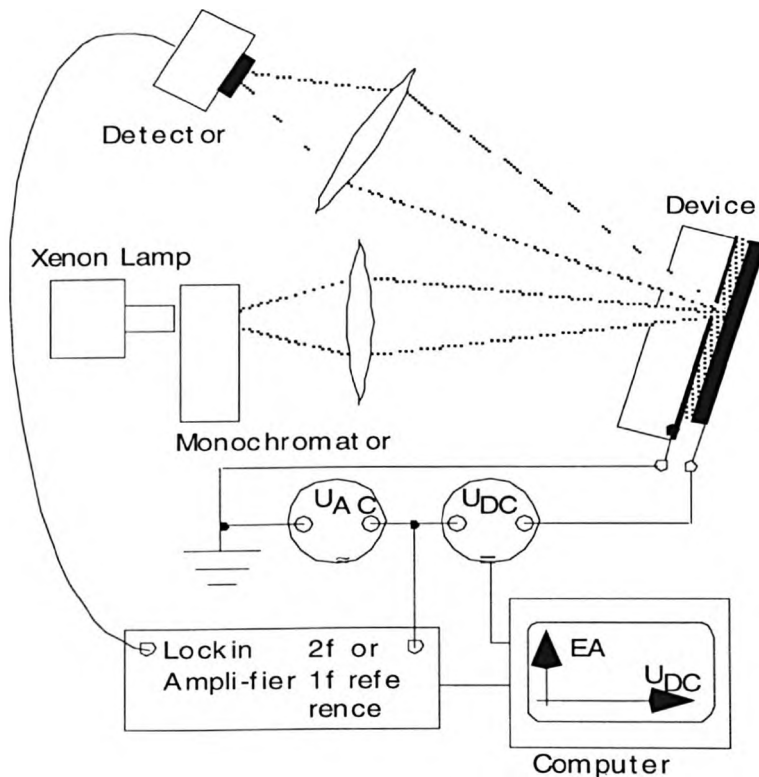


Figure 2.7: A schematic diagram of the electroabsorption experiment.

Light from a Xenon lamp is passed through a monochromator and is focused onto the device, which was placed in a sample chamber and held under a rotary pump vacuum of 10^{-1} mbar. The monochromatic light excites the sample at an angle of approximately 45° . The light passes through the ITO and the polymer film and is then reflected at the cathode electrode. The reflected light is focused onto a photodiode and all measurements were done in reflection geometry. The signal from the photodiode is preamplified with an amplifier and the EA signal is detected by the lock-in amplifier. An electric field consisting of an AC and a DC component is applied to the sample with both AC and DC biases to be added together by a mixer. The DC bias is supplied by a DC power supply. The AC source consists of a sinusoidally varying voltage while the AC modulation frequency is used as the reference frequency for the lock-in amplifier that supplies the AC bias. Usually the AC bias is kept below 2 V to minimise any distortion on the EA signal due to light emitted from the device.

This technique can also be used as a probe of the workfunction of an electrode, providing the workfunction of the counter electrode is known. In this case, we have examined the effect on the cathode workfunction by inserting a thin layer of LiF and the effect on the anode (ITO) workfunction by inserting a PEDOT:PSS buffer layer. Furthermore it can also be used as an optical probe of the electric fields in PLEDs thus providing information about the internal field distribution¹⁷ and trapped charges within a device¹⁸. More details about the induced electric field in PLEDs and the information one can obtain from these measurements will be given in chapter 4.

2.5 Time of Flight measurements

A well-known technique to study carrier transport and investigate charge carrier mobilities in amorphous semiconductors is the time-of-flight (TOF) technique¹⁹. This experiment involves photogeneration of a packet of charge carriers by illumination of a sample sandwiched between two electrodes. Optical excitation of the charge carrier

packet is achieved using 10 ns light pulses from a frequency-tripled Nd:YAG laser at 355 nm. The illumination of the sample occurs through a semitransparent (35 nm) Au electrode that is used as a cathode in that case. Thick polymer films are cast onto ITO coated glass substrates from toluene solutions with concentrations in the range of 60-120 mg/mL using the spin-coating technique. The polymer films were typically dried for a few hours at 60 °C under vacuum to remove any residual solvent. Typical film thicknesses were in the range 1.5-3 μm. Under application of an external voltage, the charge carriers drift towards the collecting electrode and this results in a time dependent current that can be monitored across an external load resistor. The transient current is measured across variable series resistors using a Tektronix digital storage oscilloscope.

The experimental set-up of the TOF experiment is depicted in figure 2.8.

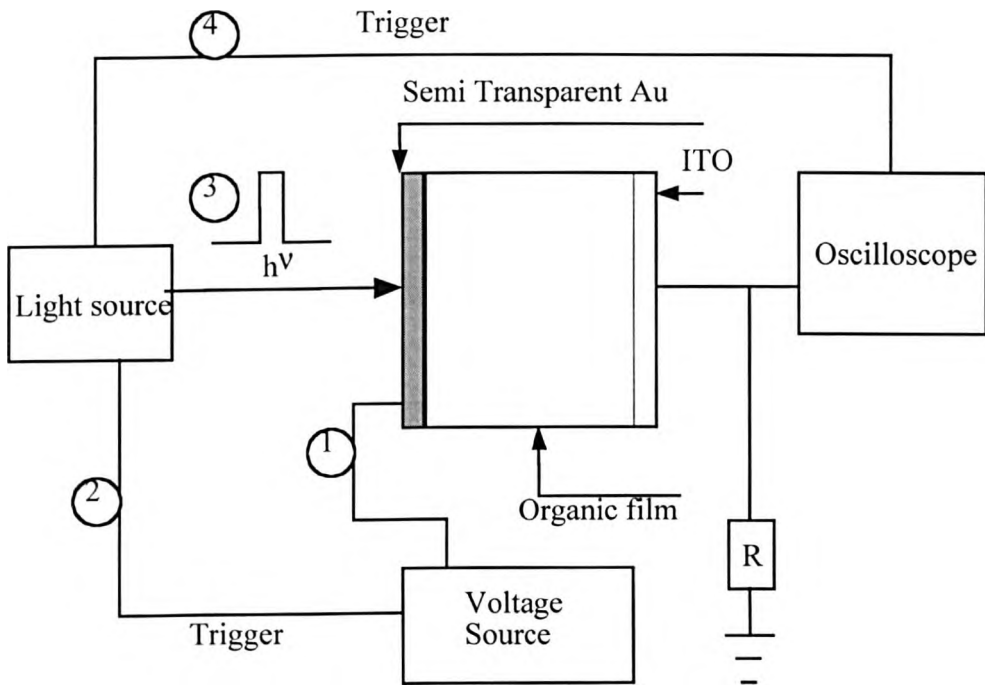


Figure 2.8: A schematic view of the experimental set-up for the time of flight measurement

The transit time, t_{tr} , for the arrival of the carrier packet is given by:

$$\mu = d / t_{tr}E, \quad (\text{equation 2.12})$$

Where μ is the carrier mobility, d is the film thickness and $E (=V/d)$ is the applied electric field. The large value of the absorption coefficient (typically $\sim 10^5 \text{ cm}^{-1}$) for most conjugated polymers ensures that the excitation pulse will be absorbed within a distance of the order of 100 nm from the illuminated electrode and thus, that the photogenerated packet will be extended in a similar distance. This has the direct consequence that a separate charge generation layer is not necessary to be used as is typically the case for mobilities measurements of inorganic semiconductors because a 100 nm extension of the carrier packet in a film of 1 μm thickness will not affect significantly the resolution of the carrier transit time. The light intensity was chosen such as that the photogenerated charges were around 10 % of the maximum capacity charge of the devices to avoid space charge effects within the device. By changing the polarity of the applied bias, we can select if electrons or holes will drift in the bulk of the film and thus which mobilities will be measured. All measurements were performed under vacuum of 10^{-4} mbar and at room temperature. By varying the magnitude of the external bias, different electric fields can be applied in the sample. The RC constant of the experimental set-up is controlled by a variable resistance R .

2.6 Time resolved photoluminescence measurements

Time resolved photoluminescence measurements were performed using a DRS Hadland synchroscan streak camera and a Spectra Physics Tsunami mode-locked Ti:Sapphire laser. The samples are optically excited in a 2mm diameter spot with femtosecond pulses provided by the Ti:Sapphire laser, which is photopumped by a CW Nd:YAG laser. The duration of the pulses is 80 fs. Pulses are generated at a rate of 80 MHz and the energy of each pulse is 1 nJ. The laser beam is frequency doubled and tunability of the excitation wavelength between 350 and 450 nm can be achieved. The Streak camera records the photoluminescence emitted by the excited sample which is previously focused and collected with a set of lenses and is then dispersed to a subtractive double monochromator. The monochromator allows the spectral filtering of

the different emission wavelengths. Placing attenuation filters across the optical path of the beam can reduce the intensity of the 2nd harmonic of the laser that is used to excite the sample. The temporal resolution of the system is estimated to be around 5 ps²⁰.

References

1. Burroughes, J.H., Bradley, D.D.C., Brown, A.R., Marks, R.N., Mackay, K., Friend, R.H., Burns, P.L., Holmes, A.B. *Nature* **347**, 539 (1990).
2. Friend, R.H., Gymer, R.W., Holmes, A.B., Burroughes, J.H., Marks, R.N., Taliani, C., Bradley, D.D.C., Dos Santos, D.A., Bredas, J.L., Logdlund, M. & Salaneck, W.R., *Nature* **397**, 121 (1999).
3. Sheats, J.R., Antoniadis, H., Hueschen, M., Leonard, W., Miller, J., Moon, R., Roitman, D. & Stocking, A. *Science* **273**, 884 (1996).
4. Mason, M.G., Hung, L.S., Tang, C.W., Lee, S.T., Wong, K.W. & Wang, M. *Journal of Applied Physics* **86**, 1688 (1999).
5. Wu, C.C., Wu, C.I., Sturm, J.C. & Kahn, A. *Applied Physics Letters* **70**, 1348 (1997).
6. Hung, L.S., Tang, C.W. & Mason, M.G. *Applied Physics Letters* **70**, 152 (1997).
7. Park, Y., Choong, V., Gao, Y., Hsieh, B.R. & Tang, C.W. *Applied Physics Letters* **68**, 2699 (1996).
8. Kim, J.S., Granstrom, M., Friend, R.H., Johansson, N., Salaneck, W.R., Daik, R., Feast, W.J. & Cacialli, F. *Journal of Applied Physics* **84**, 6859 (1998).
9. Grice, A.W. *Device physics of conjugated Polymer LEDs* (Sheffield University, 1998).
10. Greenham, N.C. & Friend, R.H. *Semiconductor Device Physics of Conjugated Polymers* **49**, Solid State Physics, Academic Press (1995).
11. Mattoussi, H., Murata, H., Merritt, C.D., Iizumi, Y., Kido, J. & Kafafi, Z.H. *Journal Of Applied Physics* **86**, 2641 (1999).
12. Greenham, N.C., Samuel, I.D.W., Hayes, G.R., Phillips, R.T., Kesseser,

- Y.A.R.R., Moratti, S.C., Holmes, A.B. & Friend, R.H., *Chemical Physics Letters* **241**, 89 (1995).
13. de Mello, J.C., Wittmann, F. & Friend, R.H. *Advanced Materials* **9**, 230 (1997).
 14. O'Brien, D. *Conjugated Polymer Electroluminescence* (Sheffield University), (1997).
 15. Greenham, N.C., Friend, R.H. & Bradley, D.D.C. *Advanced Materials* **6**, 491 (1994).
 16. Campbell, I.H., Hagler, T.W., Smith, D.L. & Ferraris, J.P. *Physical Review Letters* **76**, 1900 (1996).
 17. Rohlfing, F., Yamada, T. & Tsutsui, T. *Journal of Applied Physics* **86**, 4978 (1999).
 18. Giebeler, C., Whitelegg, S.A., Campbell, A.J., Liess, M., Martin, S.J., Lane, P.A., Bradley, D.D.C., Webster, G. & Burn, P.L. *Applied Physics Letters* **74**, 3714 (1999).
 19. Redecker, M., Bradley, D.D.C., Inbasekaran, M. & Woo, E.P. *Applied Physics Letters* **73**, 1565 (1998).
 20. Buckley, A.R., Rahn, M.D., Hill, J., Cabanillas-Gonzalez, J., Fox, A.M. & Bradley, D.D.C. *Chemical Physics Letters* (in press).

CHAPTER 3

EXCIPLEX EMISSION IN BILAYER LIGHT-EMITTING DIODES BASED ON HOLE TRANSPORT FLUORENE-TRIARYLAMINE COPOLYMERS AND ELECTRON TRANSPORT STARBURST PHENYLQUINOXALINES

3.1 Introduction

One of the key advantages of organic and polymeric materials for light emitting diode (LED) design is the possibility to choose the emission color by tailoring the chemical structure of the emitter material. Electroluminescence (EL) emission from the infrared¹ to the near UV region² has been reported in the literature. All these devices operate on the basis of charge injection through metallic or semiconductor contacts, with subsequent recombination of charge carriers of opposite sign to form an excited, emissive state.

Almost all the work published to date reports on emission from excited singlet states.³ Since only about a quarter of all recombination events leads to the formation of singlet states while three quarters yield excited triplet states which will not lead to light

Chapter 3: Exciplex emission in bilayer light-emitting diodes based on hole transport fluorene-triarylamine copolymers and electron transport starburst phenylquinoxalines

emission in most materials, the maximum internal theoretical quantum yield is limited to 25%. This motivated the search for suitable triplet emitters. Compounds containing heavy transition metals have been taken into especial consideration.⁴⁻⁵

All these approaches rely on light emission from the excited state of a discrete molecule or molecular entity. However, a new mechanism for LED operation has been recently reported in the literature, namely the emission of light from a charge-transfer state namely an exciplex state.⁶ Intermolecular charge transfer can occur between different compounds to form new electronic states. When the charge transfer occurs in the ground state of the system, then the formation of a charge-transfer complex takes place. In order for a charge transfer complex to be identified as an exciplex state, one of the molecules (the donor) has to be in the excited state and the other (the acceptor) has to be in the ground state. Usually there are no direct transitions between the exciplex state and the ground state of the system, sometimes however the exciplex states can emit fluorescence. In order to facilitate exciplex formation, usually one of the molecules should have a low ionization potential so that it can donate an electron to the second molecule, while the second molecule should have a large electron affinity so that it can accept an electron from the first molecule. The emission wavelength of the exciplex will be then mainly determined by the energy difference between the highest occupied molecular orbital (HOMO) of the donor molecule and the lowest unoccupied molecular orbital (LUMO) of the acceptor molecule although additional relaxation effects may also play a role. The formation of an exciplex will be facilitated by a decrease of the energy difference between the ionization potential of the donor and the electron affinity of the acceptor and this will lead to a shift of the emission maximum to longer wavelengths.

In general, emission from charge-transfer states is known to be rather weak^{7,9} resulting in poor performance light emitting devices.¹¹ Intramolecular exciplex formation in

Chapter 3: Exciplex emission in bilayer light-emitting diodes based on hole transport fluorene-triarylamine copolymers and electron transport starburst phenylquinoxalines

photoluminescence (PL) experiments is a well known phenomenon.¹⁰ Osaheni and Jenekhe⁷⁻⁸ have reported photoluminescence emission due to exciplex formation in bilayers of poly(p-phenylene benzobisoxazole) (PBO) and tris(p-tolyl)amine, but they did not report electroluminescence emission, although they suggest that exciplexes may be important in light-emitting devices. Emission from an exciplex state has been regarded as rather inefficient, though, since the transition dipole moment is generally lower than for the very efficient transition from the excited singlet to the singlet ground state. Nonradiative decay pathways are therefore important and the role of impurities and other chemical defects as possible quenching sites becomes dominant. In layered polymer LEDs, there is a possibility that exciplex emission takes place at the heterojunction interface between the hole transport layer and the electron transport-emitting layer for certain combinations of charge transport and emitting materials which alters the emission wavelength and the color of the device. Photoluminescence and electroluminescence exciplex emission from blends of poly(vinyl carbazole) (PVK) and a conjugated/non conjugated multiblock copolymer has also been reported¹², but emission from a bilayer device was not studied. Yang *et. al.*¹³ also reported intermolecular exciplex emission in PL and EL from a blend of a p-type polymer, poly[9-(3,6,9-trioxadecyl)-carbazole-3,6-diyl] (TOD-PC) and a n-type polymer poly[2,3-di(p-tolyl)-quinoxaline-5,8-diyl] (DT-PQX) in a light-emitting electrochemical cell configuration but emission from separate layers was not studied.

However, recent studies on enhanced emission from an exciplex state in a polymeric system by optical excitation have suggested the possibility of using these charge-transfer states as emission sources in LEDs. Recent publications report on organic LEDs that operate on the basis of emission from an exciplex state. The group led by Professor A. Epstein at Ohio State University has published a number of papers regarding exciplex emission in bilayer organic LEDs with PVK as a hole transport layer and pyridine based conjugated

Chapter 3: Exciplex emission in bilayer light-emitting diodes based on hole transport fluorene-triarylamine copolymers and electron transport starburst phenylquinoxalines

copolymers as electron transport layers.^{6,11,14-16} They have reported photoluminescence quantum efficiencies in the range of 20% for exciplex emission from the bilayer system PVK / Poly(pyridine-co-dialkoxyphenylenevinylene). This approaches the PL efficiency of the well-known polymer Poly(p-phenylene vinylene) (PPV).¹⁷ They also reported electroluminescence from the exciplex state, with external efficiencies achieved exceeding 0.02%. These efficiencies were almost three orders of magnitude higher than that of the corresponding single layer devices with a Poly(pyridine-co-dialkoxyphenylenevinylene) emissive layer and they attributed this effect to the exciplex formation as well as to the elimination of exciton formation near the quenching cathode electrode.

Itano *et al.*¹⁸ have reported exciplex formation at the interface between tris(8-quinolinolato)aluminum (Alq₃), which is widely used as a green-emitting material with electron transport properties, and hole transport materials with low ionization potentials, namely 1,3,5-tris(3-methylphenylphenylamino)triphenylamine (m-MTDATA) and 4,4',4''-tris[bis(4-tert-butylbiphenyl-4-yl)amino]triphenylamine (t-Bu-TBATA). Chao *et al.*¹⁹ have also reported exciplex formation at the interface between poly(N-vinylcarbazole) (PVK) and poly(2-dodecyl-p-phenylene) (C12O-PPP). Their devices emitted white light originating from an exciplex state only when a solvent that could dissolve both polymers was used. Otherwise blue emission from the second layer, C12O-PPP, was dominant. They attributed this effect to mixing of the two polymers at the interface upon use of a cosolvent. This allows the formation of an exciplex between an electron in the lowest unoccupied molecular orbital (LUMO) of C12O-PPP and a hole in the highest occupied molecular orbital (HOMO) of PVK. Giro *et al.*²⁰ have also reported exciplex emission under electrical excitation from bilayer organic LEDs with a TPD hole transport layer and a PBD electron transport layer, both incorporated in a polycarbonate (PC) matrix. Appropriate choice of the two components that form the exciplex upon excitation can lead to a large variety of possible emission colors.

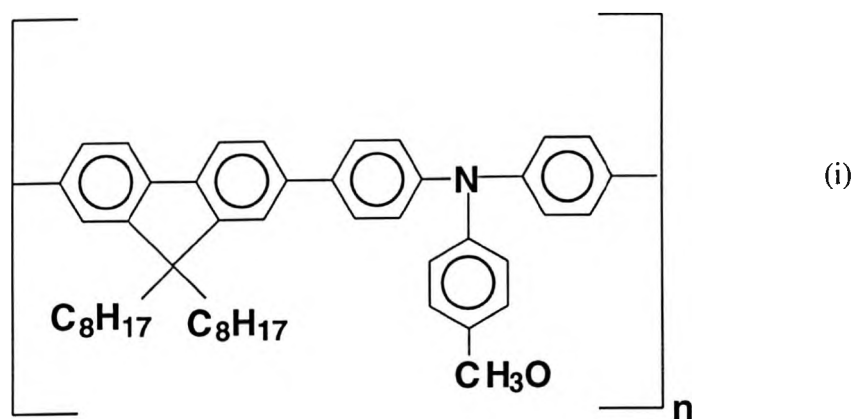
Chapter 3: Exciplex emission in bilayer light-emitting diodes based on hole transport fluorene-triarylamine copolymers and electron transport starburst phenylquinoxalines

This method can thus provide an alternative way to tune the emission color of OLEDs. This has in fact been observed for bilayer LEDs comprising PVK and TPD (N,N'-Diphenyl-N,N'-di(3-methyl-phenyl)) as hole transporters and two quinoxalines as electron transporters.²¹ In these studies, both spincoating and vapor deposition were used to combine the materials into bilayer devices. These hybrid devices showed unstructured, broad emission peaks centered between wavelengths of 575 nm and 600 nm, relatively high brightnesses ($\sim 300 \text{ cd/m}^2$) and external quantum EL efficiencies reaching 0.65 %.

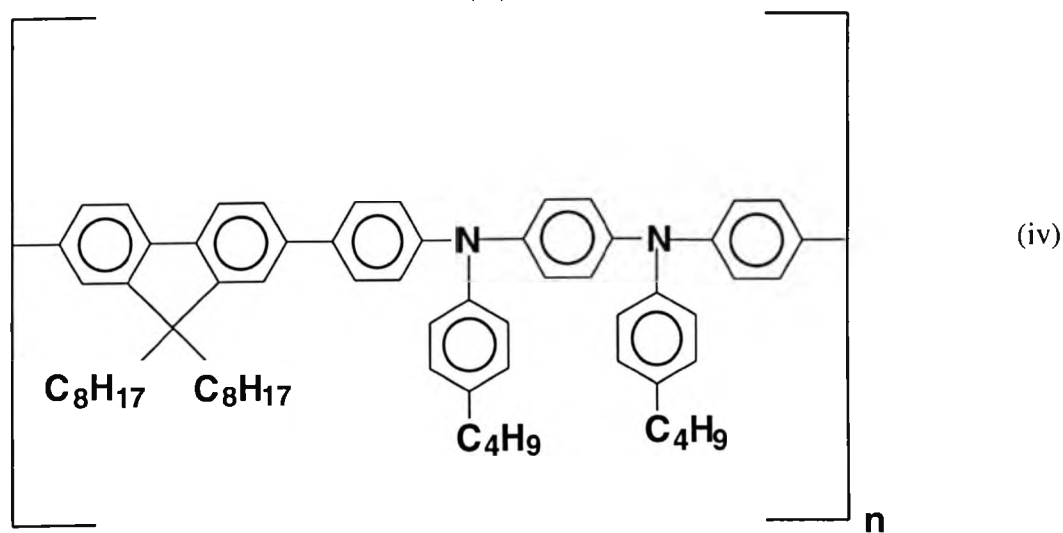
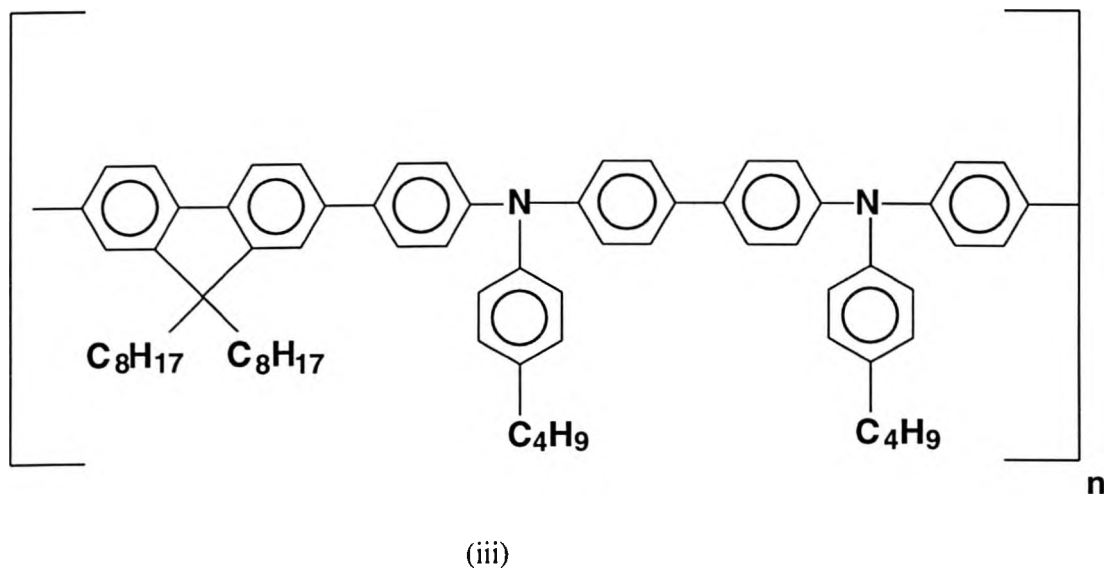
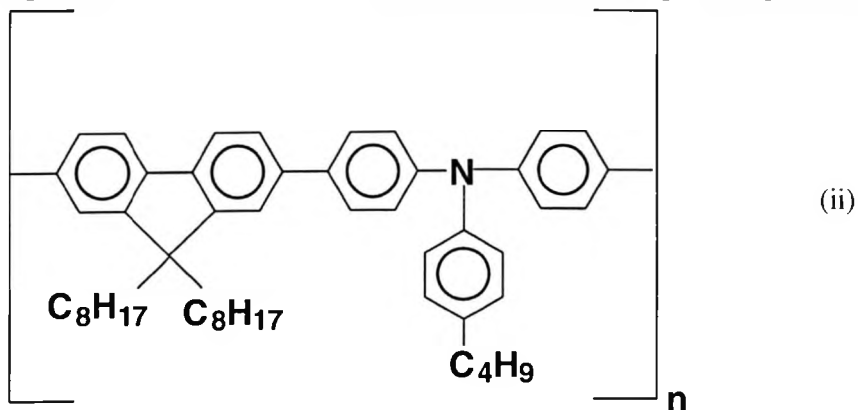
In this chapter we will show that it is possible to prepare exciplex emission LEDs by spincoating subsequent polymer layers onto ITO substrates, prior to the deposition of a cathode metal. The emission color is tuned by the choice of the ionization potential of the hole transport layer.

3.2 Fluorene-triarylamine and fluorene-thiophene copolymers

The chemical structures of the hole transport fluorene triarylamine copolymers used in this work are shown in Figure 3.1.



Chapter 3: Exciplex emission in bilayer light-emitting diodes based on hole transport fluorene-triarylamine copolymers and electron transport starburst phenylquinoxalines



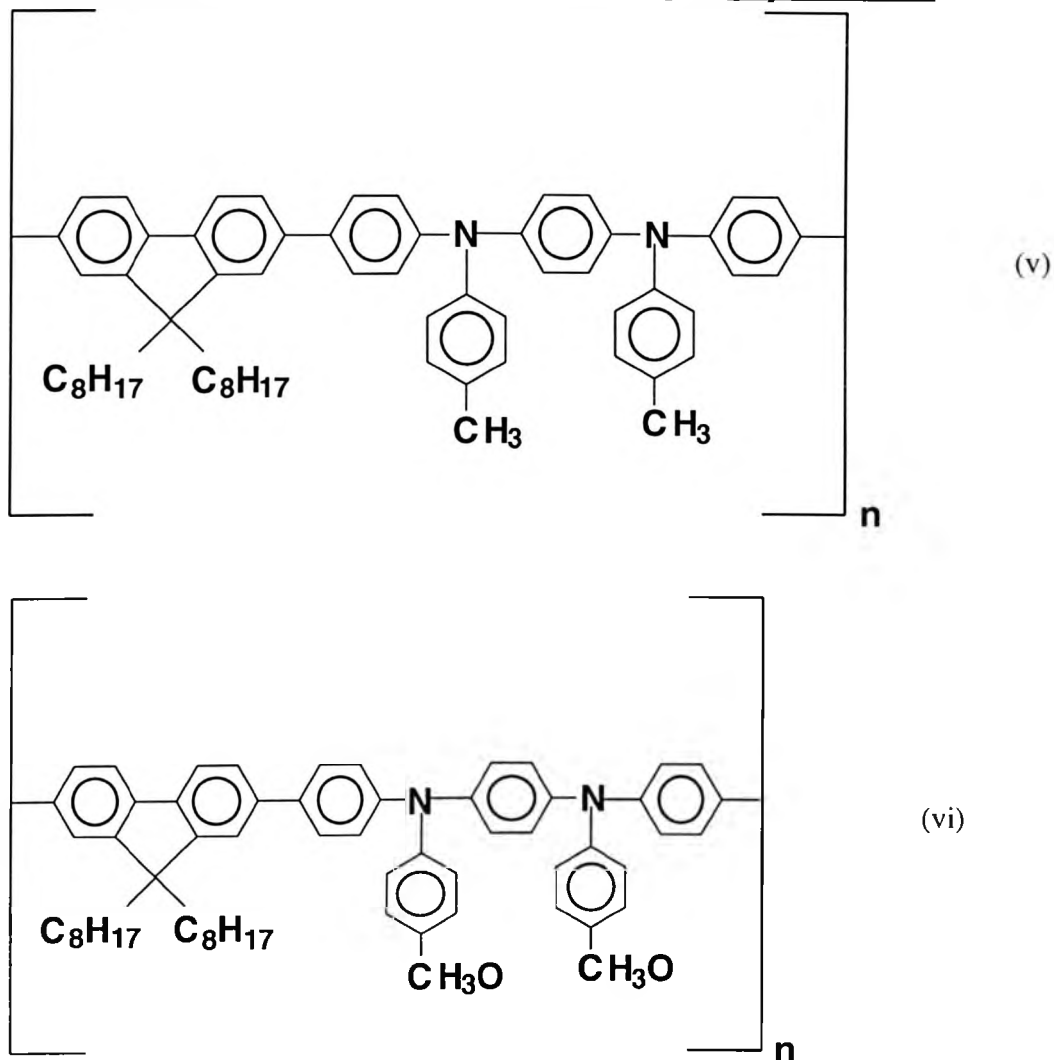


Figure 3.1: Chemical structures of fluorene triarylamine copolymers: (i) TFMO, (ii) TFB, (iii) BFB, (iv) PFB, (v) PFM and (vi) PFMO.

They are identified by their abbreviated names: TFB is poly(9,9'-dioctylfluorene-co-N-(4-butylphenyl) diphenylamine), TFMO is poly(9,9'-dioctylfluorene-co-N-(4-methoxyphenyl)diphenylamine), BFB is poly(9,9'-dioctylfluorene-co-bis-N,N'-(4-butylphenyl)-bis-N,N'-phenylbenzidine), PFB is poly(9,9'-dioctylfluorene-co-bis-N,N'-(4-butylphenyl)-bis-N,N'-phenyl-1,4-phenylenediamine), PFM is poly(9,9'-dioctylfluorene-co-bis-N,N'-(4-methylphenyl)-bis-N,N'-phenyl-1,4-phenylenediamine) and PFMO is

Chapter 3: Exciplex emission in bilayer light-emitting diodes based on hole transport fluorene-triarylamine copolymers and electron transport starburst phenylquinoxalines

poly(9,9'-dioctylfluorene-co-bis-N,N'-(4-methoxyphenyl)-bis-N,N'-phenyl-1,4 phenylenediamine). They were all synthesized via a Suzuki coupling reaction²² and they have molecular weights M_w in the range between 10000 and 30000. From differential scanning calorimetry (DSC) measurements, their glass transition temperatures have been found to range between 75 °C for PFM (lowest T_g) and 140 °C for BFB (highest T_g). The aryamine donor functionality further leads to a significant reduction in the ionization potential, I_p , from the 5.8 eV value for the polyfluorene homopolymer, PFO²³. From cyclic voltammetry measurements, the ionization potentials have been calculated to fall in the range between 5.0 and 5.3 eV²⁴ and thus they match relatively well with the workfunction of ITO [-4.7 eV] offering the possibility of an ohmic contact, at least for PFMO, as identified by the 0.3 eV barrier height which has been proposed by Malliaras *et al.*²⁵ as a criterion for an ohmic contact. Their exact values are listed in Table 1 along with the weight percentage (wt.-%) of the triarylamine component in each compound.

Copolymer	Triarylamine [wt.-%]	Ionization potential [eV]
TFB	44	5.30
TFMO	42	5.20
BFB	61	5.26
PFB	57	5.09
PFM	53	5.04
PFMO	55	4.98

Table 1: Weight percentage (wt.-%) of the triarylamine component in the fluorene-triarylamine copolymers and their ionization potentials.

Triarylamines have already attracted considerable interest as hole transport materials in multilayer OLEDs²⁶⁻²⁷ due to their high hole mobilities and their low ionization potentials

Chapter 3: Exciplex emission in bilayer light-emitting diodes based on hole transport fluorene-triarylamine copolymers and electron transport starburst phenylquinoxalines

which allow for efficient hole injection from an indium tin oxide anode and excellent hole transport in the bulk of the device with reduced probability for trapping. TFB, TFMO, BFB, PFB, PFMO and PFM have been well-characterized in terms of their hole mobilities at room temperature, in the range $2 \cdot 10^{-4}$ - $8 \cdot 10^{-4}$ cm^2/Vsec ,²⁸ which are some of the higher values reported to date for conjugated polymers. Thus they offer the desirable high mobilities required for low operating voltage PLEDs along with the ease of processability of polymers.

F1226T1 and F8T2, namely poly(9,9-dioctylfluorene-co-thiophene) and poly(9,9-dioctylfluorene-co-dithiophene), respectively consist of fluorene-thiophene copolymers. They are also synthesized via a Suzuki coupling reaction that leads to alternating fluorene-thiophene moieties. Compared to the fluorene-triarylamine copolymers, they possess higher ionization potentials, 5.8 and 5.5 eV respectively. Their chemical structures are shown below.

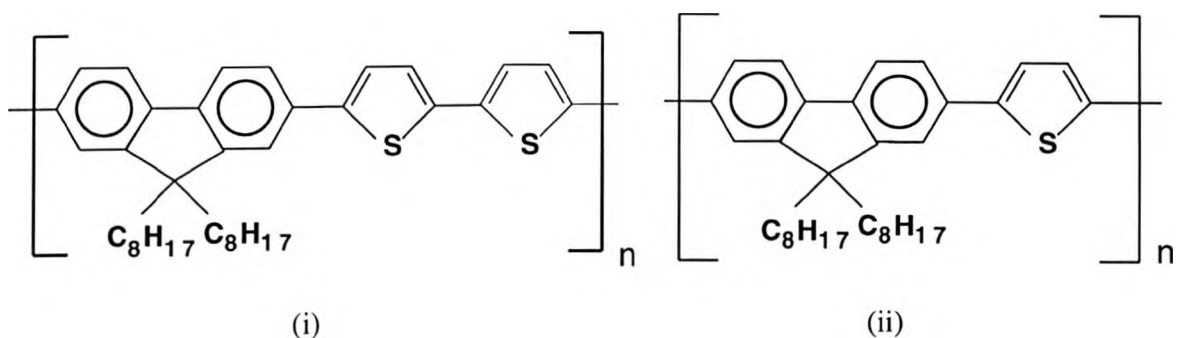


Figure 3.2: Chemical structures of the polyfluorene thiophene copolymers: (i) F8T2 and (ii) F1226T1.

3.3 Starburst tris(phenylquinoxalines)

As electron transport materials we used two starburst tris(phenylquinoxalines) (TPQs) that were synthesized at the University of Bayreuth in Germany by M. Jandke and P. Strohriegl. More details about the synthetic methods used for their preparation have been

Chapter 3: Exciplex emission in bilayer light-emitting diodes based on hole transport fluorene-triarylamine copolymers and electron transport starburst phenylquinoxalines

reported elsewhere.²⁹⁻³⁰ They are soluble in chlorinated hydrocarbons and they form good quality films. Due to their strongly branched structure and high glass transition temperatures (~150 °C), both TPQs can be spin coated from solution to form stable and fully amorphous low molar mass glassy films.³¹⁻³² No recrystallization of the TPQs has been observed after annealing above their glass transition temperature. As revealed by cyclic voltammetry measurements, they both have low-lying lowest unoccupied molecular orbital levels at about -3.6 eV below vacuum that makes them attractive for use as electron transport materials in bilayer light-emitting diodes. From time of flight measurements room temperature electron mobilities in the range 10^{-5} cm²/Vs to 10^{-4} cm²/Vs have been deduced.³³ This further suggests that triphenylquinoxalines will be well suited for use as electron transport materials in light-emitting diodes. The chemical structures of TPQ15f and TPQ15c, namely 1,3,5-tris[3-(4-tert.-butylphenyl)-6-trifluoromethyl]quinoxaline-2-yl]benzene and 1,3,5-tris[3-(4-tert.-butylphenyl)-6-trifluoromethyl]quinoxaline-2-yl]benzene, respectively are shown in Figure 3.3.

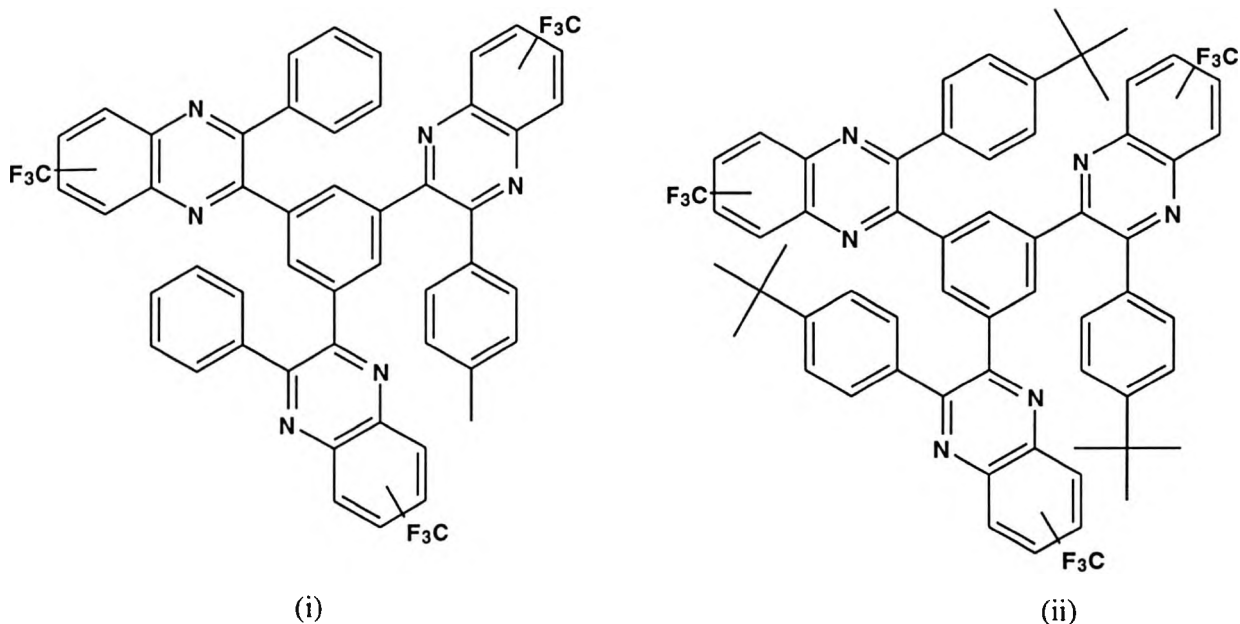


Figure 3.3: Chemical structures of the starburst quinoxalines (i) TPQ15c and (ii) TPQ15f.

3.4 Absorption and photoluminescence (PL) spectra

Figure 3.4 shows the absorption and PL spectra of a TPQ15f thin film. Films were prepared by spin casting TPQ15f from solution (2%) in butanone at a spin rate of 2000 rpm.

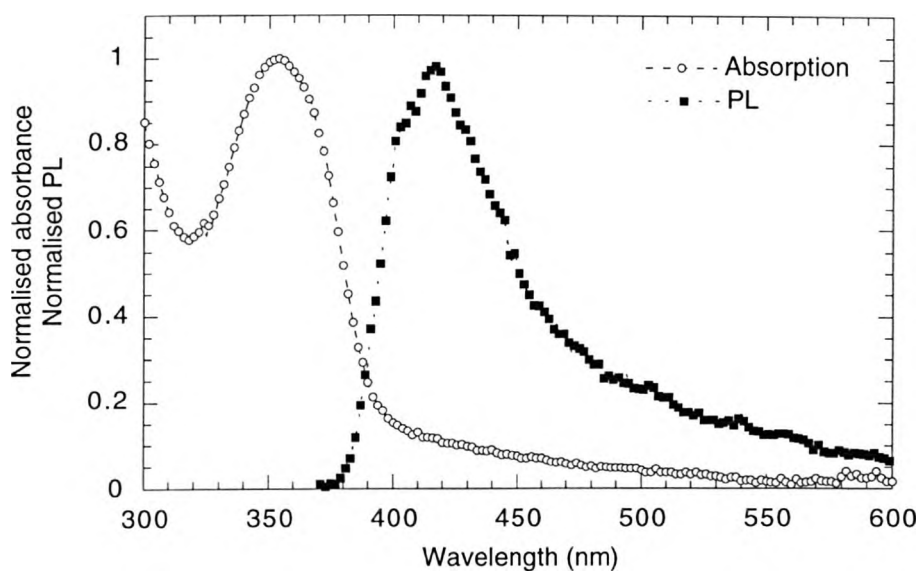


Figure 3.4: Absorption (open circles) and photoluminescence (filled squares) spectra of TPQ15f.

The absorption has an onset at 400 nm and peaks at 355 nm (The absorption spectrum of TPQ15c is not shown here but it is almost identical to that of TPQ15f). By considering an optical gap of 3.2 eV (derived from the absorption spectra) and a LUMO energy level of -3.6 eV below vacuum, we can estimate the HOMO level to be at 6.8 eV below vacuum. TPQ15f also shows weak blue fluorescence that peaks at 415 nm with a long tail stretching into the red portion of the visible spectrum. Its photoluminescence quantum efficiency was measured to be approximately 4% which suggests that nonradiative decay channels are dominant in this class of electron transport materials. TPQ15c also shows weak

Chapter 3: Exciplex emission in bilayer light-emitting diodes based on hole transport fluorene-triarylamine copolymers and electron transport starburst phenylquinoxalines

blue fluorescence in the 400 nm range but shows a second emission band around 500 nm that exceeds the former in intensity (not shown here). The total emission quantum efficiency is about 8%. This second band in the blue-green area of the spectrum is attributed to excimer fluorescence. Jandke *et. al.*³² have proposed that sterically demanding groups such as tert-butyl that are present in TPQ15f prevent molecules from stacking one on top of the other thus suppressing the tendency for excimer formation.

Figure 3.5 shows the absorption spectra of the hole transport fluorene-triarylamine copolymers used in this study.

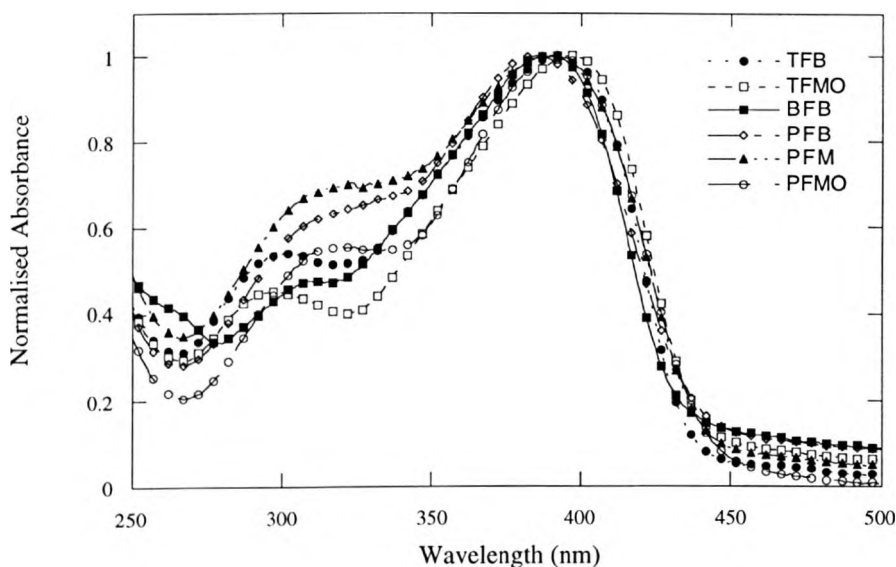


Figure 3.5: Absorption spectra of triarylamine copolymers. Absorption of TFB (filled circles), TFMO (open squares), BFB (filled squares), PFB (open diamonds), PFM (filled triangles) and PFMO (open circles).

All the fluorene copolymers show rather broad featureless absorption spectra with an onset in the range between 430 and 440 nm and a peak maximum around 380 to 390 nm. This is attributed to the π - π^* transition from the ground state to the first excited state. The

Chapter 3: Exciplex emission in bilayer light-emitting diodes based on hole transport fluorene-triarylamine copolymers and electron transport starburst phenylquinoxalines

spectral positions of the absorption maxima for all the copolymers do not depend to any significant degree on the solvent that is used so we do not expect charge-transfer states to be formed in their electronic ground state. In Table 2, the peak absorption wavelengths for all the fluorene-triarylamine copolymers are listed along with the corresponding photoluminescence maxima. The absorption spectra of F1226T1 and F8T2 are broad and featureless, the former shows a peak maximum at 436 nm while the latter has a peak maximum at 458 nm (not shown here).

Copolymer	Absorption peak wavelength (nm)	Photoluminescence peak wavelength (nm)
TFB	392	433
TFMO	397	438
BFB	386	435
PFB	385	457
PFM	390	451
PFMO	392	474

Table 2: Absorption and photoluminescence peak wavelengths of the fluorene-triarylamine copolymers.

3.5 Optical spectra from bilayer films of triarylamine and thiophene copolymers with starburst tris (phenylquinoxalines)

We then prepared bilayer (HTL/ETL) structures and the details of fabrication are given below. The hole transport layer was fabricated by spin coating a solution of 25 mg/ml of PFM, PFMO, TFMO, TFB, BFB, PFB, F1226T1 or F8T2 in toluene onto quartz glass substrates. The samples were then baked for 2 hours at a temperature of 75° C in vacuum (10^{-4} mbar) to remove any residual solvent remaining in the film after spin casting

and finally left to cool down to room temperature. The electron transport layer was then subsequently spincoated from a solution of 25 mg/ml TPQ15f or TPQ15c in 2-Butanone on top of the hole transport layer. We used 2-Butanone as a solvent for the second layer because we found that PFM, PFMO, TFMO, TFB, BFB, PFB, F1226T1 and F8T2 are either insoluble or have very low solubility in this solvent. Thus by using mutually incompatible solvents we can expect that the ETL won't dissolve the HTL upon spin coating and thus a good interface will be formed between them with only a little degree of mixing occurring. Figure 3.6 shows the absorption spectra of the bilayer (HTL/TPQ15f) films.

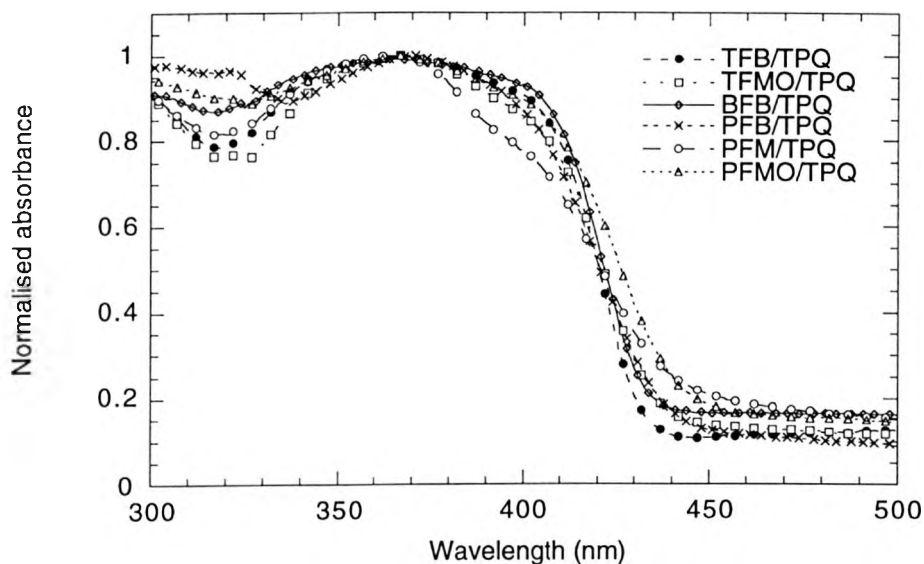


Figure 3.6: Absorption spectra of bilayer films. TFB/TPQ (filled circles), TFMO/TPQ (open squares), BFB/TPQ (open diamonds), PFB/TPQ (crosses), PFM/TPQ (open circles) and PFMO/TPQ (open triangles).

The absorption of the bilayer systems is a superposition of the absorption spectra of the individual components with no new features appearing. This is as expected if no significant ground state interaction between the two materials occurs. The same behavior is

Chapter 3: Exciplex emission in bilayer light-emitting diodes based on hole transport fluorene-triarylamine copolymers and electron transport starburst phenylquinoxalines

also characteristic for the absorption spectra of the bilayer systems with either F8T2 or F1226T1 as hole transport layers and TPQs as electron transport layers. The same observation stands also for blends of individual materials that were also employed in this study (irrespective of the material which is chosen as the hole transport layer and the one chosen as the electron transport layer). All features in the bilayer systems are thus attributed to one of the two component materials. The lack of any new absorption features in the films of the bilayer systems implies that the new emission species that gives rise to a new emission feature in the bilayer system is not accessible from the ground state of either of the two individual components. In other words, no charge transfer ground state complexes are formed in the bilayer systems we have employed here. Figure 3.7 shows the PL spectra of PFMO, PFB, PFMO/TPQ15c and PFB/TPQ15c.

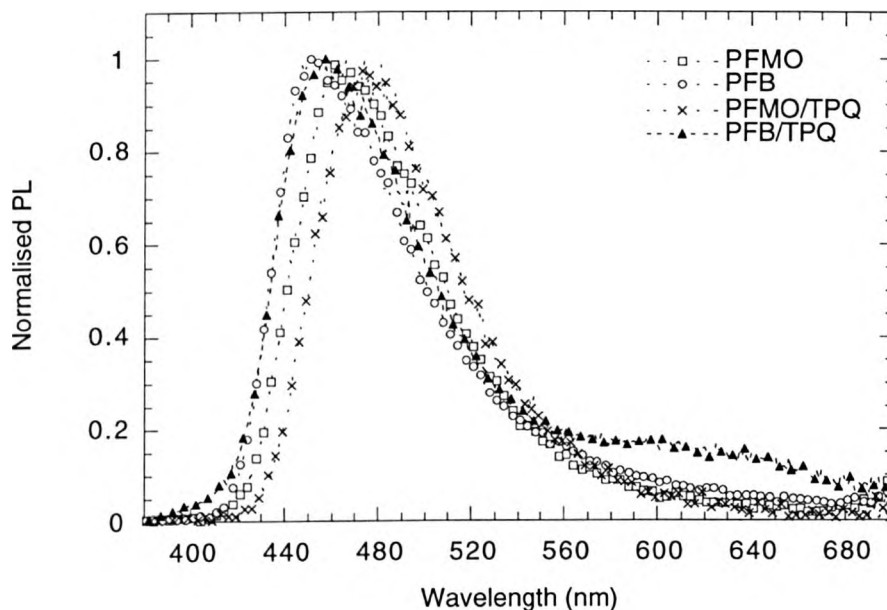


Figure 3.7: PL spectra of PFMO (open squares), PFB (open circles), PFMO/TPQ15c (crosses) and PFB/TPQ15c (filled triangles).

Chapter 3: Exciplex emission in bilayer light-emitting diodes based on hole transport fluorene-triarylamine copolymers and electron transport starburst phenylquinoxalines

The single layer as well as the bilayer films were excited at 354 nm which is equivalent to the excitation wavelength for a single TPQ15c layer and where all the low I_p hole transport materials used in this study show significant absorption (F1226T1 and F8T2 on the other hand show smaller absorption at this wavelength). On each bilayer film the photoluminescence was measured twice. In the first case, the exciting light was entering the sample from the HTL side and the PL was recorded from the HTL side. In the second case, the exciting light was incident on the ETL side and the PL emission was measured from the ETL side. All the PL spectra of bilayer films shown in this figure are collected after excitation through the TPQ side first. The PL spectra for PFMO and PFB single layer films show a broad featureless emission peak at 480 nm and 460 nm respectively which is considerably red-shifted due to aggregation effects from the solution PL (not shown here). The PL spectrum of the PFMO/TPQ15c bilayer film is only slightly red shifted compared to the PL spectrum of PFMO regardless of which side of the sample the exciting light is incident on. This suggests that even when the light excites the TPQ first, emission mainly arises from a PFMO singlet excited state. We can't rule out the possibility of exciton formation on the TPQ sites followed by energy transfer to PFMO due to the larger energy bandgap of TPQ. The situation is somewhat different for PFB/TPQ15c bilayer films. The bilayer film shows identical emission to the PFB when excited through the PFB side but it shows a very low intensity tail on the low energy side of the spectrum with a shoulder around 600 nm when excited through the TPQ side. This tail might be due to the formation of a new species, which we identify as an exciplex. As we will see below, the formation of a new exciplex emission species is much more pronounced in some other combinations of HTLs and TPQ15c.

We must also note that the exciplex formation is not restricted only to the TPQ15c. The results are nearly identical when TPQ15f is used as an electron transport material, combined with the same hole transport materials. However, in the case where the exciplex

emission is present in the PL spectrum the relative intensities of the two emission bands that are associated with the singlet excited and the exciplex state are different for the two electron transporters. When TPQ15c is used, the relative intensity of the exciplex emission band is larger than that of the singlet emission band. Instead when TPQ15f is used, the dominant contribution to the PL spectrum is from the singlet state emission band. This indicates that the formation of the exciplex species under photo excitation is more favorable when TPQ15c is used which might be related to the higher efficiency of radiative recombination for this material compared to the TPQ15f as evidenced from the PL efficiency measurements.

Figure 3.8 shows the PL spectra of TFMO, TFB, TFMO/TPQ15c and TFB/TPQ15c.

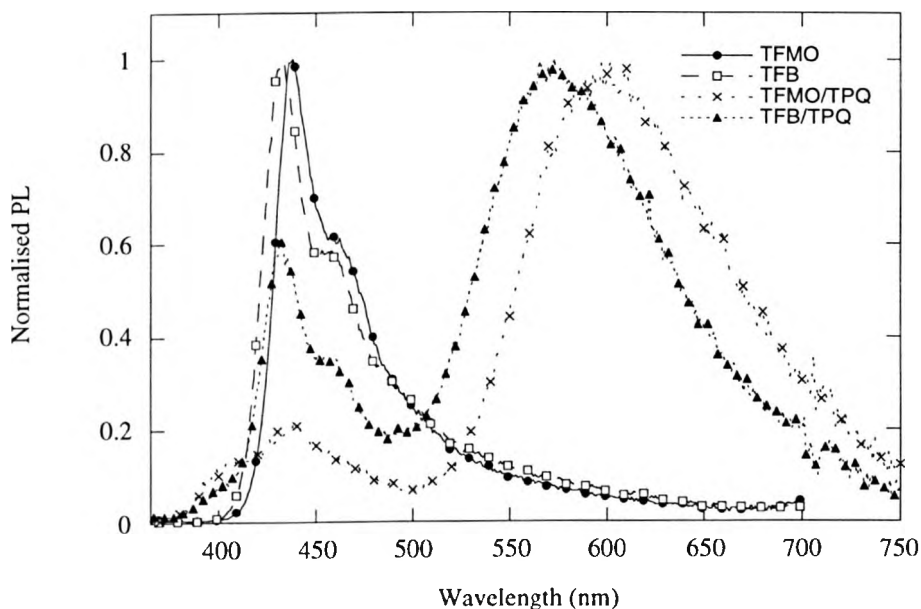


Figure 3.8: PL spectra of TFMO (open squares), TFB (open circles), TFMO/TPQ15c (crosses) and TFB/TPQ15c (filled triangles).

The PL spectra of TFB and TFMO show blue structured emission with a main peak at 430 and 440 nm, respectively, and a shoulder at 460 nm. Bilayers of TFMO/TPQ15c and

Chapter 3: Exciplex emission in bilayer light-emitting diodes based on hole transport fluorene-triarylamine copolymers and electron transport starburst phenylquinoxalines

TFB/TPQ15c show identical emission to that of the single layer films when excited through the HTL side while they show contributions from TFB, TFMO as well as from a completely new species which we have previously identified as an exciplex when excited through the ETL side. The emission band from the exciplex state is broad and featureless and peaks around 570 nm for the TFB based bilayer film and around 590 nm for the TFMO based one. Figure 3.9 shows the PL spectra of PFM, BFB, PFM/TPQ15c and BFB/TPQ15c.

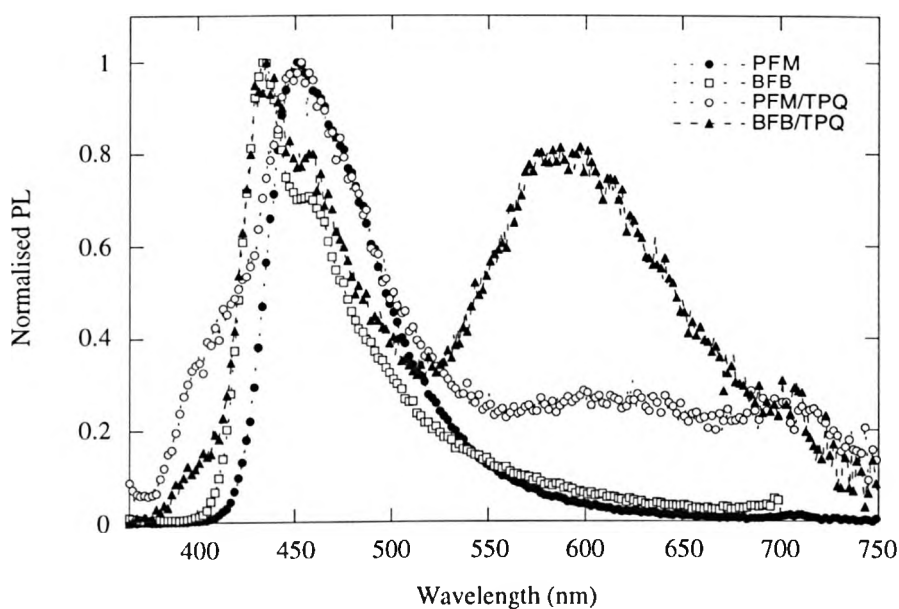


Figure 3.9: Photoluminescence spectra of PFM (filled circles), BFB (open squares), PFM/TPQ15c (open circles) and BFB/TPQ15c (filled triangles).

PFM shows a PL spectrum that peaks at 455 nm with no vibronic structure while BFB shows vibronic structure with the main peak at 430 nm and a shoulder at 455 nm. Bilayers of BFB/TPQ15c show a new broad exciplex band appearing around 580 nm only when the light is incident on the ETL side. For PFM/TPQ15c films the exciplex band is much weaker and appears as a weak shoulder around 610 nm. As we notice the peak

wavelength of the emission from the exciplex state in PL shifts to the red as the ionization potential of the hole transport material decreases. The emission from this state becomes less pronounced as the ionization potential of the HTL decreases and for the case of PFMO which has the lowest HOMO no emission band associated with an exciplex is present in the PL. Figure 3.10 shows the PL spectra of F1226T1 and F8T2, respectively.

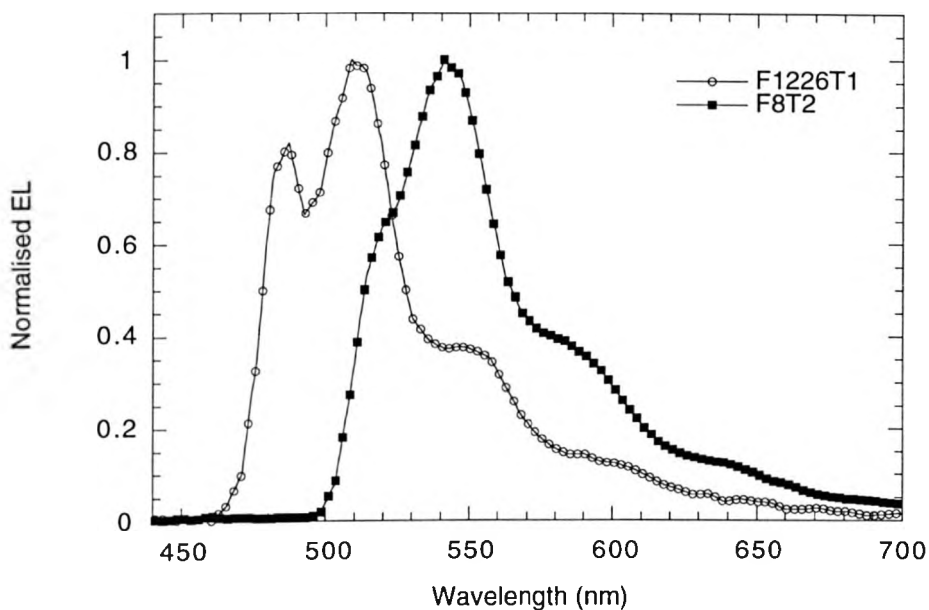


Figure 3.10: PL spectra of F1226T1 (open circles) and F8T2 (filled squares).

The PL of F1226T1 shows vibronic structure with two main peaks at 480 and 510 nm and a shoulder at 545 nm while emission from F8T2 peaks at 550 nm with two shoulders appearing at 525 and 580 nm respectively. In this case, no exciplex emission is observed from bilayer films with TPQs. The PL emission of the bilayer films is nearly identical to the emission of the hole transport component with confirms that radiative recombination and emission occur in the low bandgap fluorene-thiophene copolymers. When F8T2 is used as

the HTL, an extremely weak shoulder appears around 415 nm which can be attributed to very weak emission from the TPQ excited state.

We also fabricated blends of the lower ionization potential hole transporters and TPQs in order to see if exciplex emission occurs on a blend film apart from the bilayer films. We did not observe any exciplex emission in PL, which implies that exciplexes are formed strictly at the interface. The increased probability for exciplex formation when the light is incident on the ETL side first implies that due to the low PL efficiency of TPQs a significant fraction of excitons will diffuse through the ETL to the interface where they can form exciplex states with HTL molecules that will either decay radiatively with light emission or undergo nonradiative decay. The PL efficiency of the exciplex emission was very low (~ 2-5 %) which indicates that it is an inefficient process. When light first enters the bilayer film from the HTL side, the possibility of exciplex formation at the interface is greatly reduced because the light will be mainly absorbed in the HTL resulting in exciton formation in the bulk of the HTL which are much more likely to undergo radiative decay in the HTL (due to the higher PLQE) rather than diffuse to the HTL/TPQ interface and form exciplex states with TPQ molecules.

3.6 EL spectra of single layer triarylamine copolymer LEDs and bilayer LEDs with triarylamine copolymers as HTLs and quinoxalines as ETLs - Exciplex formation at the interface

To examine the possibility of exciplex formation in LEDs, we fabricated bilayer LEDs with an ITO anode, a fluorene-triarylamine copolymer as the hole transport layer, TPQ15f or TPQ15c as the electron transport layer and Dow metal as the cathode. The ITO was routinely cleaned following the procedure we describe in chapter 2. The bilayer films were prepared

Chapter 3: Exciplex emission in bilayer light-emitting diodes based on hole transport fluorene-triarylamine copolymers and electron transport starburst phenylquinoxalines

using the process we followed to prepare the films for the absorption/PL spectral measurements in order to obtain good interfaces between the corresponding HTL and ETL as they are of high importance in order to obtain good device performance. Dow metal is a proprietary product of the Dow Chemical Company and was thermally deposited at a high evaporation rate (typically 5-10 nm/sec after the first few nm) at a pressure of 3×10^{-6} mbar through a shadow mask to form the cathode (typical thickness of 200 nm) with an active device area of 4.5 mm^2 . This alloy comprises magnesium (Mg) and aluminum (Al) with traces of Zn. It has the work function of Mg (3.7 eV) but unlike Mg, it is very stable in air. The approximate ratio of the component metals in the alloy is 95% Al, 4% Mg and 1% Zn. The fact that it's already a stable alloy allows the use of one evaporation source. All device measurements were carried out under a vacuum of 10^{-1} mbar. The electroluminescence emission spectra of bilayer LEDs with a fluorene-triarylamine copolymer as HTL and TPQ15f as ETL are displayed in Figure 3.11.

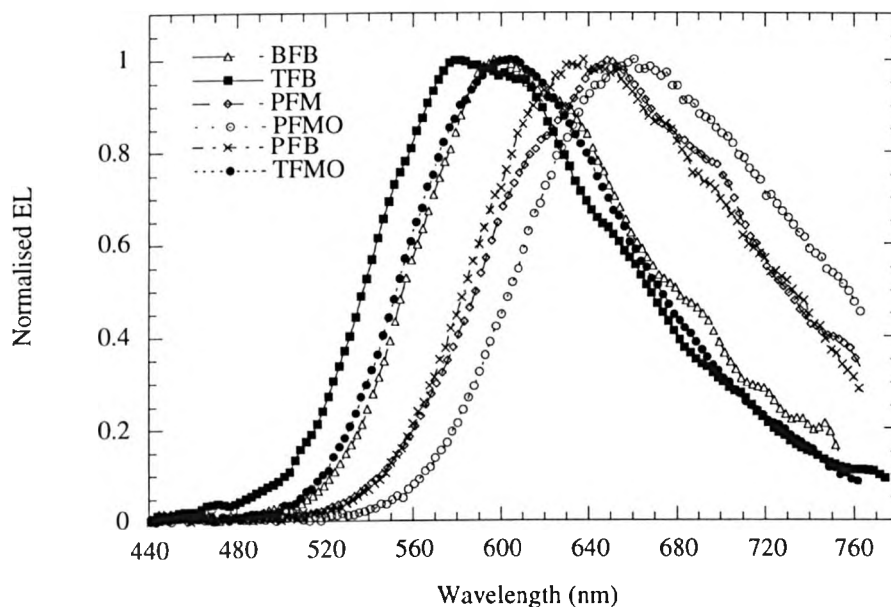


Figure 3.11. EL spectra of ITO/HTL/TPQ15f/Dow metal LEDs with a triarylamine copolymer as the HTL.

Chapter 3: Exciplex emission in bilayer light-emitting diodes based on hole transport fluorene-triarylamine copolymers and electron transport starburst phenylquinoxalines

The EL emission spectra of single layer devices comprising one of the hole transporters and an aluminium cathode are shown in Figure 3.12.

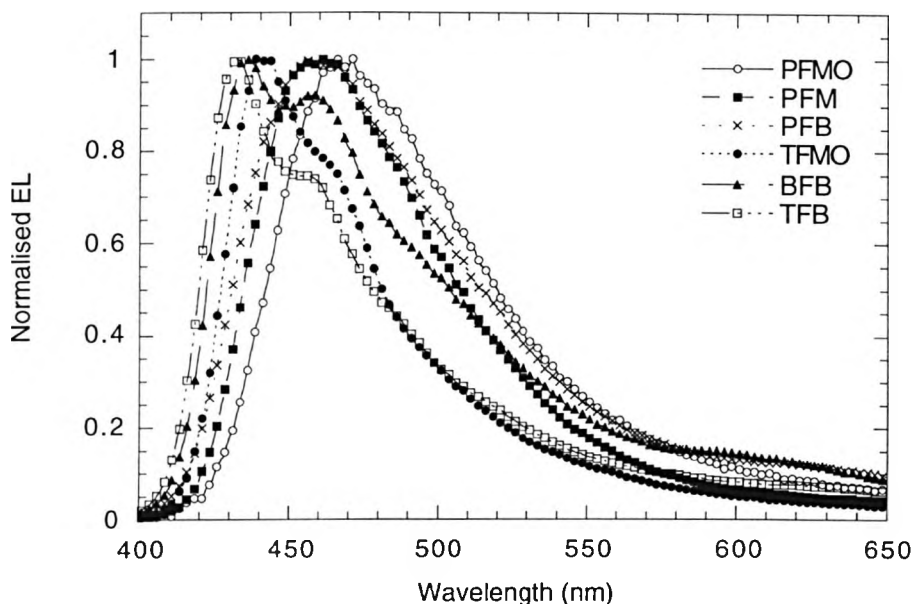


Figure 3.12. EL spectra of ITO/HTL/Al devices with a triarylamine copolymer as the emissive layer.

The similarity between the PL of most of the bilayer (HTL/ETL) films and the EL of all the bilayer LEDs demonstrates that the exciplex is responsible for the EL emission. The emission mechanism for BFB/ETL LEDs can be described as follows: By taking into consideration that the HOMO level of BFB is at 5.26 eV and that of TPQ is at 6.6 eV below vacuum, holes injected from ITO into the valence band of BFB will have to cross an energetic barrier of approximately 1.34 eV at the HTL/ETL interface in order to enter the ETL. Similarly electrons injected from the Dow metal cathode into the conduction band of TPQ will have to cross a barrier of 1-1.1 eV in order to enter the HTL (the LUMO levels of BFB and TPQ are 2.4 eV and 3.4-3.5 eV below vacuum). Due to the energetics of the HTL/ETL interface that imposes very high internal barriers for both carriers to cross the

Chapter 3: Exciplex emission in bilayer light-emitting diodes based on hole transport fluorene-triarylamine copolymers and electron transport starburst phenylquinoxalines

interface and enter the other layer, we expect that very significant accumulation of electron and hole space charge will take place at the interface as more charge carriers will be confined in this region. The carrier confinement at the interface not only enhances the recombination probability but also makes the recombination current almost equal to the device current as few carriers will reach the opposite electrodes. Hence, the blocking of electrons and holes at the interface of the two materials results in an increased probability for radiative recombination at the interface with very few holes or electrons crossing the barrier and entering the second layer. A schematic energy level diagram of the HOMO levels of the HTLs and the LUMO level of TPQ obtained from cyclic voltammetry is summarized in Figure 3.13 below.

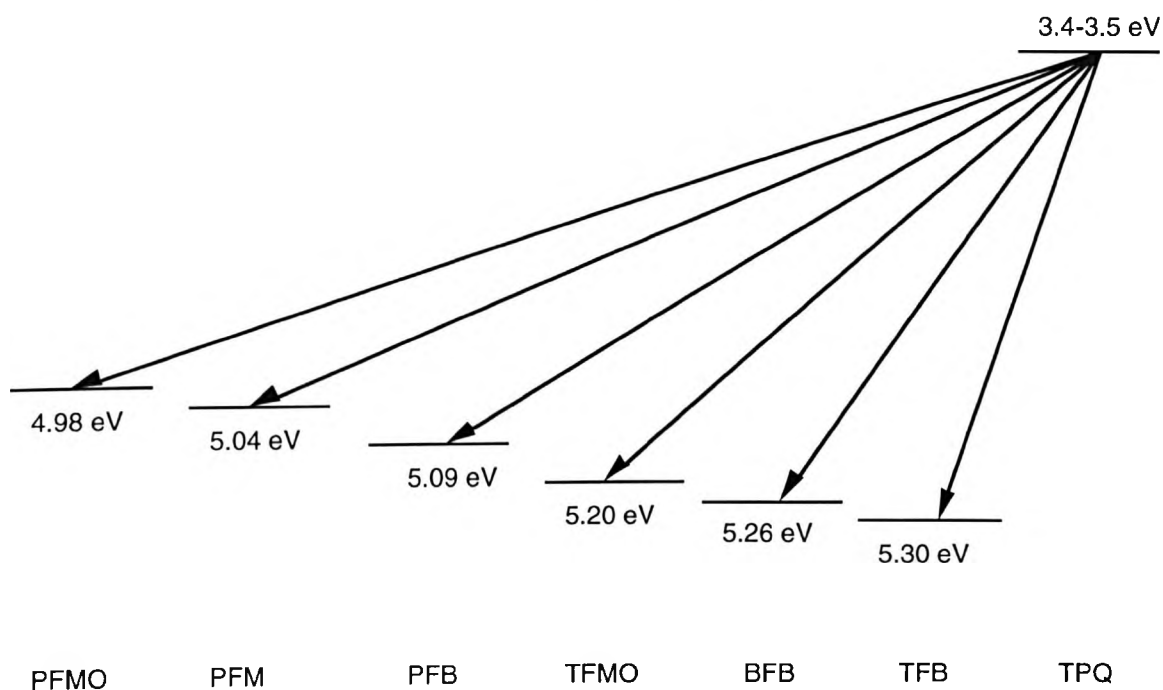


Figure 3.13: Schematic energy level diagram of the HOMO levels of the HTLs and the LUMO level of TPQ obtained from cyclic voltammetry.

Exciplex formation will be favored as a result of the large difference between the ionization potential of the HTL and the electron affinity of the ETL. Furthermore, the

Chapter 3: Exciplex emission in bilayer light-emitting diodes based on hole transport fluorene-triarylamine copolymers and electron transport starburst phenylquinoxalines

difficulty of hole tunneling from the HTL to the ETL and electron tunneling from the ETL to the HTL will also favor their indirect recombination at the interface. Emission from this charge transfer complex state will then occur by relaxation of this excited state to the ground state of the system. The formation of exciplexes at the interface may however provide non-radiative decay channels that result in low efficiencies as we generally observe from these devices. The low efficiencies can also be attributed to the inefficient generation of excitons at the interface, since the energetic barriers for charge carrier interface crossing are very high.

For the double-layer devices, the peak wavelength of the emitted light shifts to the red with decreasing ionization potential of the hole transporter. The emission bands are highly symmetric and featureless. No variation of the emission color was observed with increasing applied voltage, which further supports the argument that the recombination zone with consequent formation of an exciplex state is restricted at a narrow region at the heterojunction interface between TPQ and the HTLs.

In contrast, the emission from the LEDs fabricated from the hole transport materials as single emitting layers is very different in that it shows emission in the blue-green part of the visible spectrum. TFMO, TFB and BFB show structured blue EL emission with vibronic features similar to that of the homopolymer polyfluorene (PFO).^{23,34} PFB, PFM and PFMO show featureless blue-green emission with no vibronic structure. All the EL emission spectra of these single layer LEDs are in good agreement with the corresponding PL spectra although they are slightly red shifted and with a more pronounced tail in the red portion of the visible spectrum which can probably be attributed to charge carrier trapping and radiative recombination at neighboring sites. The main features in the EL spectra, however, are attributed to the optical transition from the excited singlet state to the singlet ground state.

Chapter 3: Exciplex emission in bilayer light-emitting diodes based on hole transport fluorene-triarylamine copolymers and electron transport starburst phenylquinoxalines

No exciplex emission is seen from F1226T1/TPQ and F8T2/TPQ devices in agreement with the PL spectra. The complete suppression of the exciplex formation in these devices can be rationalized in terms of the much higher ionization potential of these thiophene copolymers compared to the triarylamine copolymers. This suggests that the energy barrier for the electron injection from the ETL into the HTL is lower than that for the hole injection from the HTL into the ETL. So it is easier for electrons to be injected into the HTL than holes to be injected into the ETL because of the smaller barrier for electron transport at the interface. Charge carrier recombination and thus emission will then occur in the HTL.

Judging from more detailed PL results on PFMO both as a film and dissolved in different solvents,³⁵ the situation is more complicated for this material. Upon excitation in a polar environment, PFMO forms an intramolecular charge transfer state with subsequent featureless emission in the green range of the visible spectrum. The wavelength of this emission as well as the lifetime of the excited state depends on the dielectric constant of the environment, e.g. the solvent. The PL emission as we noted above from the polymer film itself is centered at a wavelength of 490 nm while a solution of PFMO in toluene yields emission peaks at 450 nm and 480 nm. Even without the addition of an acceptor compound like TPQ, the PL emission in the PFMO film is therefore already partly due to a charge transfer state. This is evident from the EL spectra of PFMO devices (Figure 3.12) which yield blue-green, featureless EL emission. We note however that there is no final conclusion yet about the detailed structure of these intrachain states although it is possible that those polymers that contain a phenylenediamine group as the donor functionality, namely PFM and PFB could also be susceptible to the formation of intrachain charge transfer states.

However, the stronger redshift observed with the bilayer devices suggests that the interaction with TPQ overrides the tendency to form intrachain charge transfer states. Those

Chapter 3: Exciplex emission in bilayer light-emitting diodes based on hole transport fluorene-triarylamine copolymers and electron transport starburst phenylquinoxalines

new emission features are much more clearly correlated with the corresponding energy levels of PFMO, PFM, PFB, TFMO, BFB, TFB and TPQ. If we assume that the emission is due to a transition of an electron from the LUMO of TPQ to the HOMO of one of the hole transporters, the emission energy would simply be given by the corresponding difference between the electron affinity of the acceptor compound and the ionization potential of the donor compound. The electron affinity for TPQ has been determined both by cyclic voltammetry^{30,32} and by photoelectron spectroscopy³¹ to be in the range of 3.4-3.5 eV. The ionization potentials for the hole transporters, as determined by cyclic voltammetry, have already been mentioned above. The observed photon energies at the EL emission peaks are compared to the (theoretical) energy differences ΔE in table 3 for LEDs with TPQ15f as an ETL (An electron affinity of 3.4 eV is used for the calculations). Also the Commission Internationale de l'Eclairage (CIE) (1931) coordinates are given for the emission spectra.

Device structure	Wavelength of emission peak [nm]	CIE (1931) coordinates (X,Y)	Energy of the emission peak [eV]	ΔE [eV]
PFMO/TPQ	661	(0.600, 0.387)	1.88	1.58
PFM/TPQ	649	(0.591, 0.406)	1.91	1.64
PFB/TPQ	638	(0.555, 0.442)	1.94	1.69
TFMO/TPQ	607	(0.539, 0.450)	2.04	1.80
BFB/TPQ	596	(0.534, 0.429)	2.08	1.86
TFB/TPQ	581	(0.497, 0.479)	2.13	1.90

Table 3. EL emission peak wavelengths, corresponding photon energies and theoretical energy level differences [$E_{\text{HOMO}}(\text{HTL}) - E_{\text{LUMO}}(\text{ETL})$] for a series of LEDs with a fluorene-triarylamine copolymer as HTL and TPQ15f as ETL. Also the Commission Internationale de l'Eclairage (CIE) (1931) coordinates are given.

Chapter 3: Exciplex emission in bilayer light-emitting diodes based on hole transport fluorene-triarylamine copolymers and electron transport starburst phenylquinoxalines

A decrease in ΔE is accompanied by a similar decrease in photon energy. However, the overall values as observed in the experiment are systematically higher than ΔE . The deviation amounts to approximately 0.25 eV if the peak emission wavelengths are considered. Using the high-energy onset of exciplex emission instead of the peak value would result in even larger discrepancies, with a maximum photon energy of approximately 2.25 eV for the device PFMO/TPQ, being 0.65 eV larger than ΔE . This demonstrates that the interpretation of exciplex emission in our bilayer devices in terms of the energy difference between the HOMO level of the donor and the LUMO level of the acceptor is oversimplified.

As a consequence, it is likely that recombination does not primarily yield the exciplex state but the formation of the latter is a secondary step. The primary step is then the formation of an excited singlet state of the hole transporter. This is likely to happen very close to the donor-acceptor interface since the flow of carriers will not be limited by their mobility but rather by the substantial interfacial barriers for holes entering the acceptor, and for electrons entering the donor layer. The exciplex will then be formed by the interaction between the excited singlet-state of the hole transport material, generated by radiative recombination of electrons and holes in the HTL, and the electron transport material in the ground state. A small probability for recombination of charge carriers in the acceptor layer cannot also be ruled out but, due to the larger optical bandgap of TPQ, subsequent energy transfer to the donor is very likely. Another explanation for the above deviation could be based on the fact that usually the values of the electron affinities are overestimated due to the existence of a small polarization energy in solution (~ 0.2 eV) and to the relative difficulty in determining accurately the reduction potential by applying cyclic voltammetry. An electron affinity of 3.2 eV (reduced by 0.2 eV compared to the value we used) would result in a very good agreement between the photon energies at the emission peaks and the theoretical energy differences based on the energy levels of these materials.

Chapter 3: Exciplex emission in bilayer light-emitting diodes based on hole transport fluorene-triarylamine copolymers and electron transport starburst phenylquinoxalines

We note that this interpretation is somewhat different from that of Wang *et. al.*²¹ who claim that the difference between the oxidation potential of the donor TPD and the reduction potential of the quinoxaline acceptor matches very well with the observed exciplex emission energy. This means that even the absolute values of the photon energies agree with the HOMO (donor)-LUMO (acceptor) gap in contrast to the case we examine here.

3.7 Electrical characterization of LEDs with hole transport triarylamine copolymers and electron transport quinoxalines

The current-field and the luminance-field characteristics of PFMO/TPQ, PFM/TPQ, TFMO/TPQ, PFB/TPQ, BFB/TPQ and TFB/TPQ LEDs with an ITO anode and a Dow metal cathode are shown in Figures 3.14 and 3.15 respectively (TPQ15f is used as ETL).

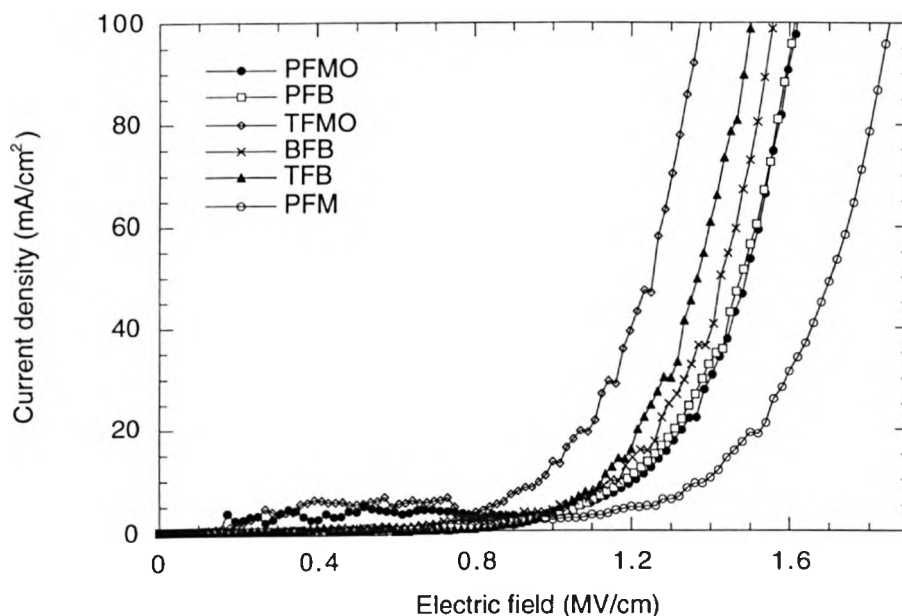


Figure 3.14: Current density vs. field characteristics of two layer devices with a HTL fluorene-triarylamine copolymer and a TPQ15f ETL. ITO and Dow metal were used as anode and cathode, respectively.

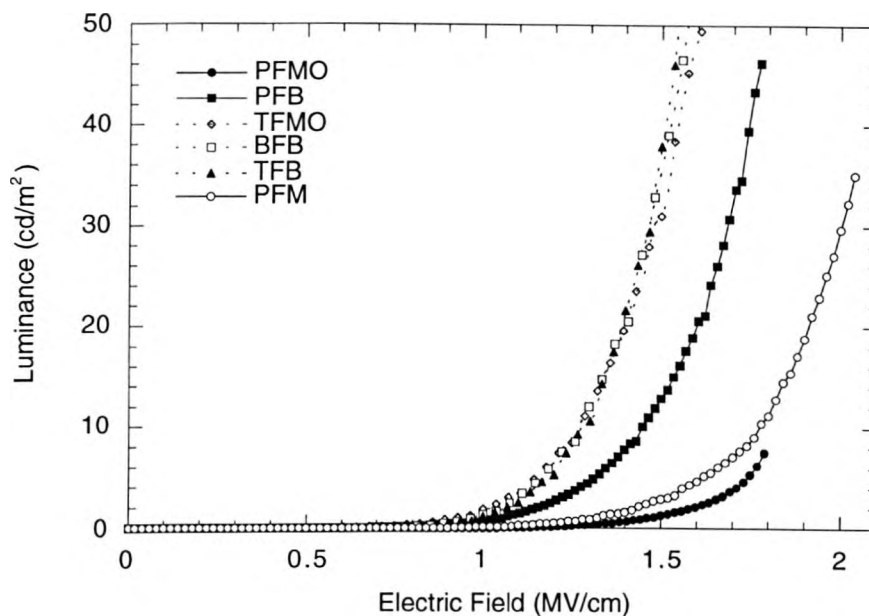


Figure 3.15: Luminance vs. electric field characteristics of two layer devices with a HTL fluorene-triarylamine copolymer and a TPQ15f ETL. ITO and Dow metal were used as anode and cathode, respectively.

The average electric field across the device E is calculated as the ratio of the external voltage applied V to the total device thickness d , irrespective of any possible differences in the strength of the electric field in the two layers due to internal electric field redistribution. When Al is used as a cathode material, the performance of the devices is very poor with much lower efficiencies. The emission is barely seen in a lit room and the current density is a few orders of magnitude lower. This indicates that the electron injection is the limiting factor in the overall performance of these devices. The Fermi level of the Dow metal cathode matches quite well with the LUMO of the TPQs which allows electrons to be injected over a relatively small barrier. The use of Ca as a cathode proved unsuccessful as the device characteristics were not improved. Efficiencies were even lower than the corresponding devices with a Dow metal cathode and the maximum brightness and current did not exceed the values already

attained with Dow metal. As the device characteristics with Dow metal were drastically improved compared to the ones with Al, we might expect a further improvement to occur when we replaced Dow metal with Ca. The poor performance of devices with a Ca cathode indicates that the interface between Ca and the TPQ films is not a "clean" interface. Interfacial dipole formation through interaction of Ca atoms with either the aromatic carbon atoms or the nitrogen atoms of TPQ that break the carbon bonds³⁶ or another undesirable interfacial reaction such as Ca diffusion into TPQ³⁷ can be identified as possible reasons for the poor performance of devices with a Ca cathode as has been already suggested in the literature. We also examined the effect of the thickness of the individual layers on the performance of the LEDs for a certain combination of HTL and ETL. We thus prepared devices with BFB as HTL and TPQ15f as ETL. We first kept the thickness of the ETL constant (50 nm) and varied the thickness of the HTL. The current-field and the luminance-field characteristics of the corresponding devices are shown in Figures 3.16 and 3.17.

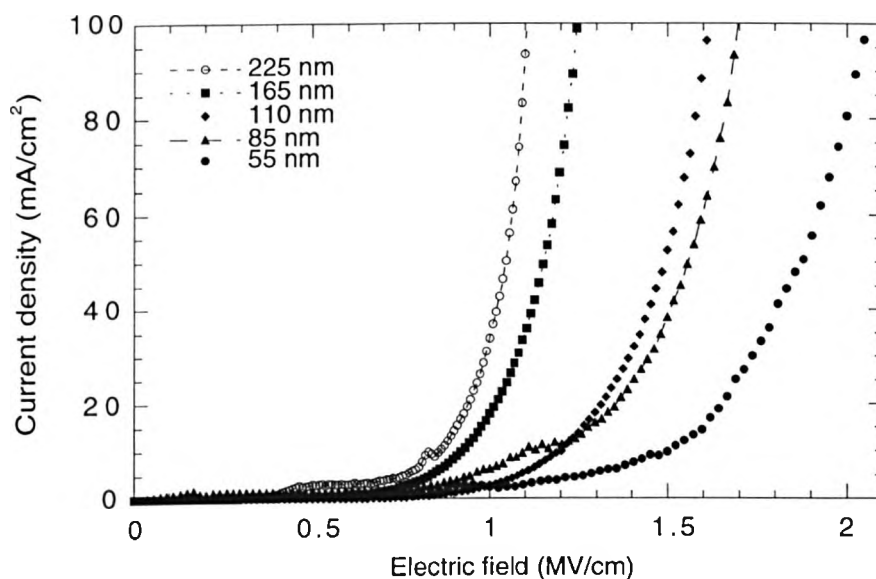


Figure 3.16: Current density vs. electric field characteristics of two layer devices ITO/BFB/TPQ15f (50 nm)/Dow metal with varying thickness of BFB.

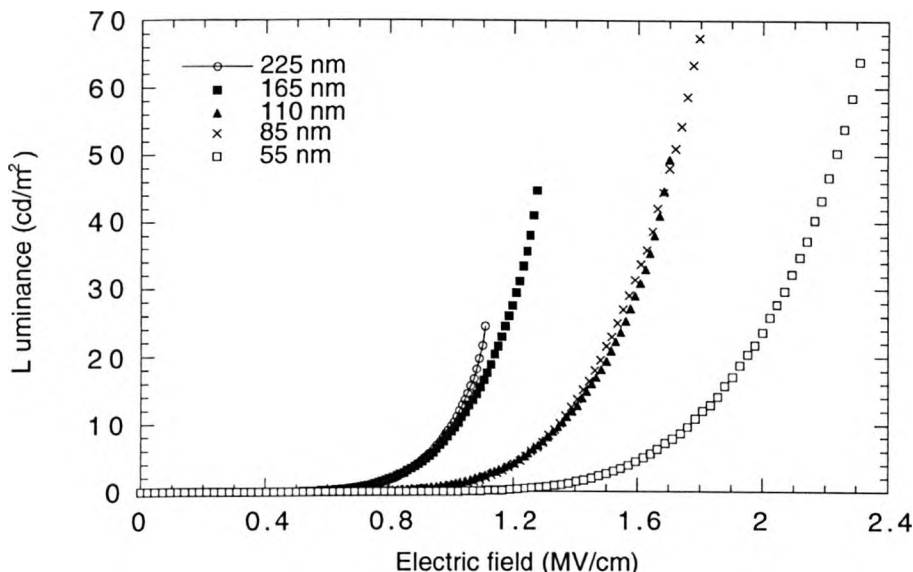


Figure 3.17: Luminance vs. electric field characteristics of two layer devices ITO/BFB/TPQ15f (50 nm)/Dow metal with varying thickness of BFB.

The J-E and L-E characteristics are strongly dependent on the thickness of the HTL. Apart from any leakage current that is observed at low electric fields in some cases, the devices with a thicker HTL are able to generate a substantially larger current density as well as EL output at the same electric field compared to the devices with a thinner HTL. This is somewhat surprising as one would expect that an increase of the device thickness would result in a decrease of the current density due to the lower total electric field that leads to a reduced injection of charge carriers as well as reduced transport through the bulk of the device. In order to understand the above behavior, we should consider the following: In a double layer LED the electric field distribution in the two layers is not known *a priori* and in combination with the existence of internal barriers at the heterojunction it can significantly affect the current. In our LEDs, the energetics of the HTL/ETL interface is expected to impose very high energetic barriers for both carriers to enter the second layer resulting in

Chapter 3: Exciplex emission in bilayer light-emitting diodes based on hole transport fluorene-triarylamine copolymers and electron transport starburst phenylquinoxalines

significant interfacial charge accumulation densities. The presence of the high energetic barriers is expected to make the recombination current almost equal to the device current as very few electrons and holes are expected to cross the interface and enter the HTL and the ETL, respectively with most of them eventually recombining at the interface forming donor-acceptor (exciplex) states. Although holes are more mobile than electrons (as evidenced by the higher hole mobilities in BFB²⁸ compared to the electron mobilities in TPQ15f³³) and they face a higher barrier at the interface, hole accumulation on the HTL side of the interface is not expected to be larger than electron accumulation on the other side as both barriers are very high for carriers to be able to cross the interface. However, from the energetics of the ITO/HTL and the Dow metal/TPQ interface, the barrier for hole injection (~0.6 eV) is higher than the barrier for electron injection (~0.1-0.3 eV), thus electrons are expected to be the majority carriers in the device assuming no band bending occurring at either the ITO/HTL or the cathode/ETL interface. Hence, most of the applied voltage and subsequently the electric field will be dropped across the HTL and thus a field enhancement for hole injection will occur at the anode resulting in an increased hole density in the BFB layer near the interface. This trend will be enhanced with increasing thickness of BFB and thus it will finally result in increased carrier recombination at the interface with increased device current at a certain field with increasing HTL thickness. Although the LED current is usually governed by the injection of the majority carriers, here it is equally affected by the injection of both carriers as we explained above. Also the enhancement of the minority (hole) carrier injection with increasing thickness of BFB will increase the recombination current and thus the light output, which is governed by the minority carrier injection.

Figure 3.18 shows the EL quantum efficiency versus electric field characteristics for ITO/BFB/TPQ15f (50nm)/Dow metal LEDs with varying thickness of BFB.

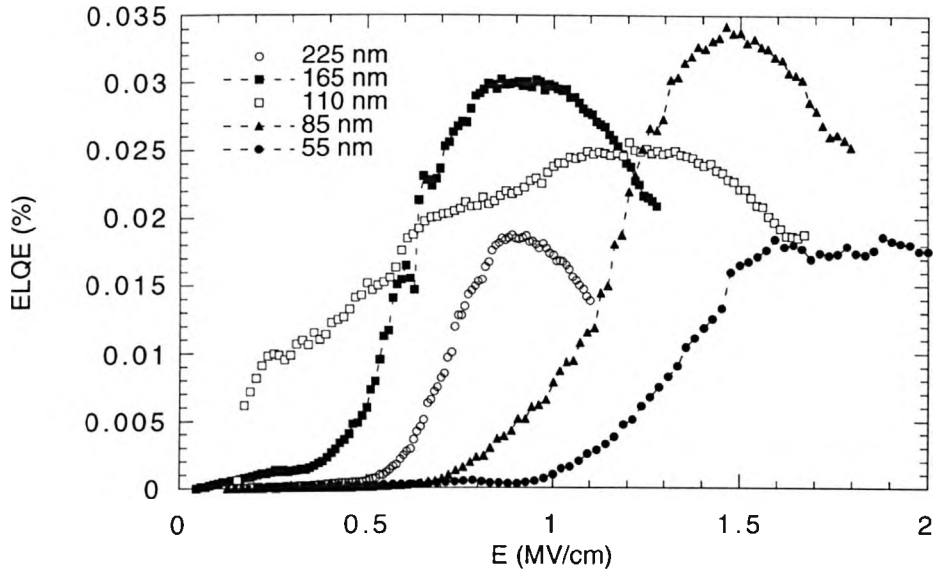


Figure 3.18: The EL quantum efficiency versus electric field characteristics for ITO/BFB/TPQ15f (50nm)/Dow metal LEDs with varying thickness of BFB.

The efficiency reaches a maximum of 0.035 cd/A for a 85 nm thick layer of BFB but it does not show a clear trend with varying BFB thickness. An oscillation of the efficiency is observed to occur with the thickness of BFB, which suggests that the electric field redistribution affects both the optimum balance of carriers and the recombination efficiency at the interface. The efficiency is lower in the low voltage regime and reaches the maximum at high voltage; this is attributed to the charge carrier imbalance at low voltages. For thicker devices, the maximum efficiencies are achieved at lower electric fields due to the enhanced hole injection that results in an overall more balanced hole and electron injection at lower voltages. LEDs with an 85 thick BFB layer showed the maximum luminance and efficiency and therefore we chose to use this HTL thickness to fabricate a series of LEDs with a varying ETL thickness. The J versus E and L versus E characteristics of the corresponding double layer devices are shown in Figures 3.19 and 3.20, respectively.

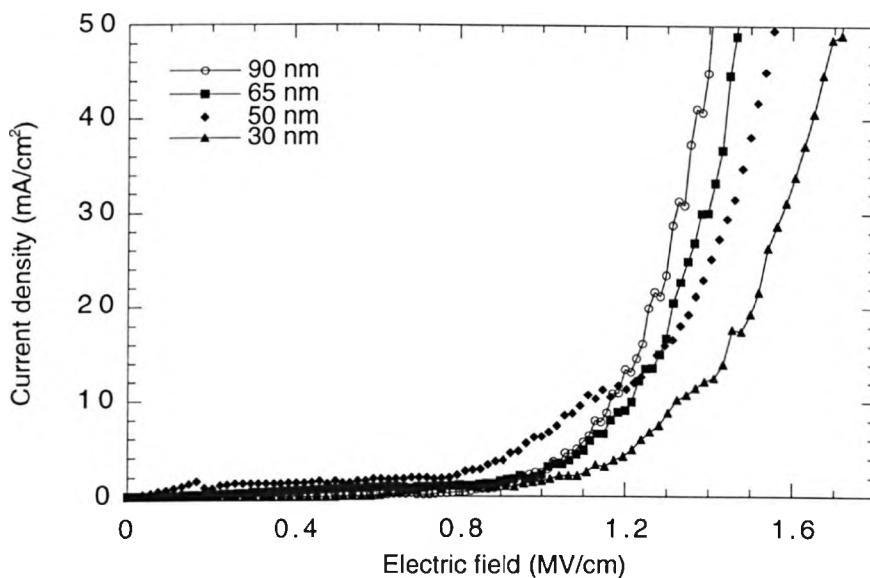


Figure 3.19: Current density vs. electric field characteristics of two layer devices ITO/BFB (85 nm)/TPQ15f/Dow metal with varying thickness of TPQ15f.

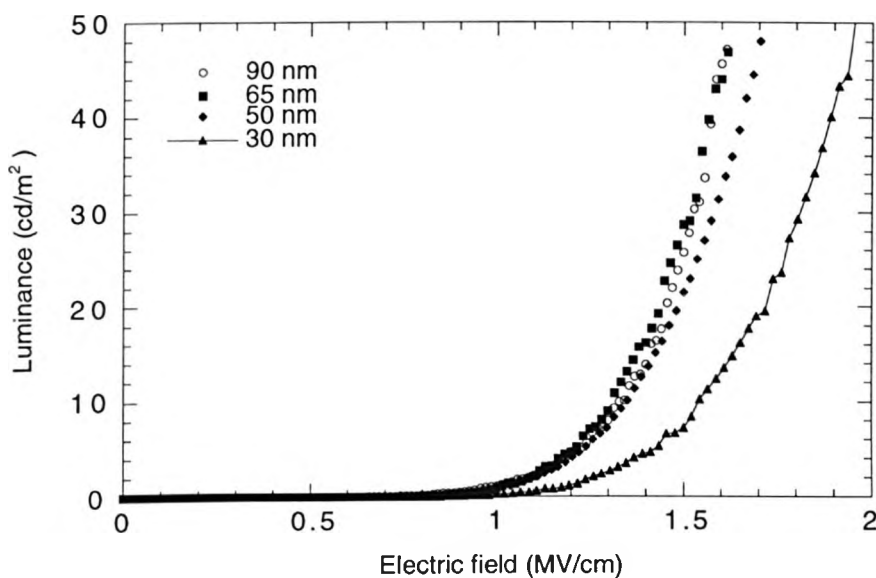


Figure 3.20: Luminance vs. electric field characteristics of two layer devices ITO/BFB (85 nm)/TPQ15f/Dow metal with varying thickness of TPQ15f.

Chapter 3: Exciplex emission in bilayer light-emitting diodes based on hole transport fluorene-triarylamine copolymers and electron transport starburst phenylquinoxalines

The current and light output also increase with increasing thickness of the ETL at a certain electric field following the same dependence as when the thickness of the HTL was increased. However, the effect of the varying ETL thickness on the J-E-L characteristics is not as pronounced. This is somewhat expected as the thickness of the layer that transports the minority carriers is kept constant and thus the electric field redistribution will not be as significant as before.

We further examined the effect of the ETL on the performance of the bilayer LEDs. For this reason, we fabricated devices with a triarylamine copolymer as the HTL and TPQ15c as the ETL instead of TPQ15f. The current and luminance-electric field characteristics of the corresponding devices are shown in Figures 3.21 and 3.22, respectively.

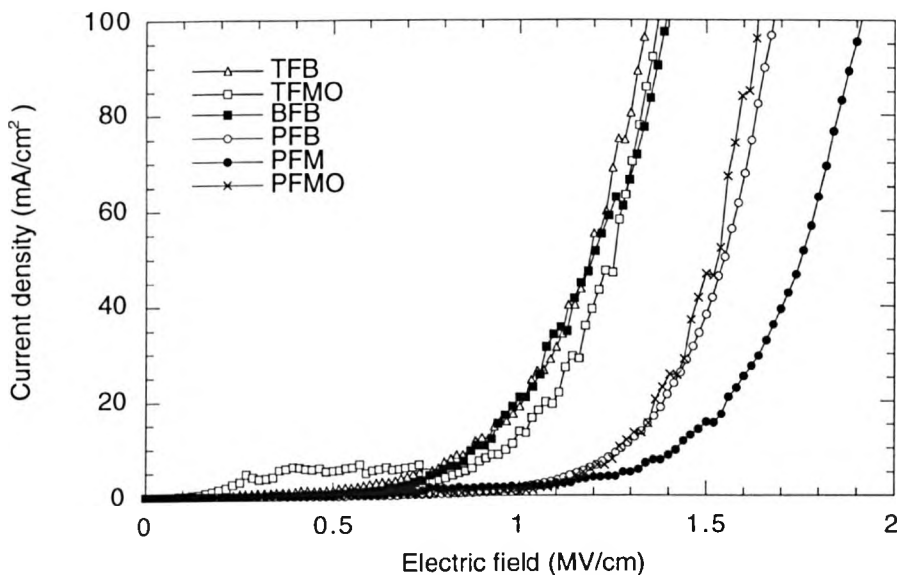


Figure 3.21: Current density vs. electric field characteristics of two layer devices with a HTL fluorene-triarylamine copolymer and a TPQ15c ETL. ITO and Dow metal were used as anode and cathode, respectively.

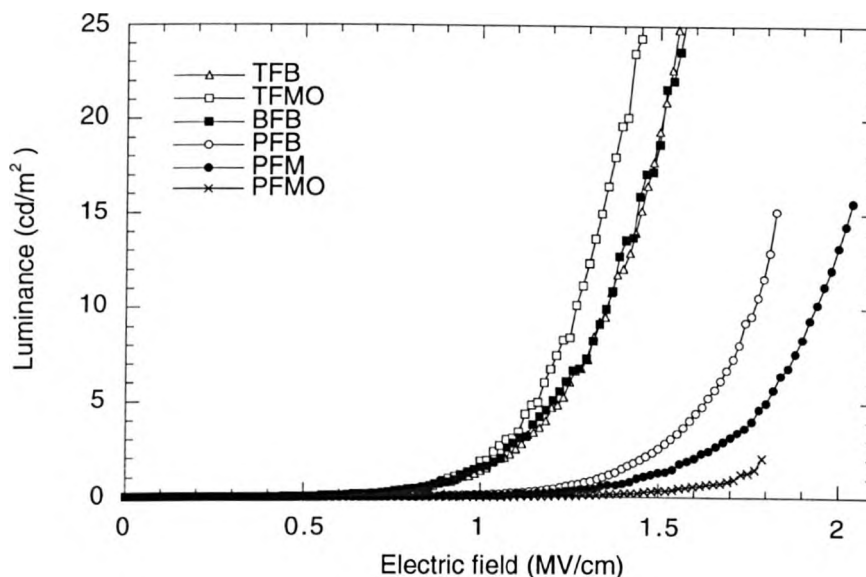


Figure 3.22: Luminance vs. electric field characteristics of the same series of bilayer HTL/TPQ15c LEDs.

The turn-on field for the devices with TPQ15f and TPQ15c as the ETL (defined as the field at which a current density of 10 mA/cm^2 is achieved) is listed in Table 4 (the device structures are listed in ascending order of the ionization potential of the hole transport material).

Device structure	Onset field [MV/cm]	Onset field [MV/cm]
	(TPQ15c)	(TPQ15f)
PFMO/TPQ	1.25	1.2
PFM/TPQ	1.4	1.35
PFB/TPQ	1.25	1.15
TFMO/TPQ	0.95	0.95
BFB/TPQ	0.85	1.15
TFB/TPQ	0.85	1.1

Table 4. Onset field for LEDs comprising of a triarylamine HTL and TPQ15f or TPQ15c as the ETL.

Chapter 3: Exciplex emission in bilayer light-emitting diodes based on hole transport fluorene-triarylamine copolymers and electron transport starburst phenylquinoxalines

The lowest onset field is observed for TFMO when TPQ15f is used as ETL and for BFB and TFB when TPQ15c is used as ETL. PFM requires the highest onset field regardless of the ETL used. If we had assumed that the onset electric field, for a certain ETL, will be determined by the hole injection and we take into consideration the HOMO energy level of the HTLs, we would expect that the injection barrier for holes and consequently the onset field will increase in the order that the ionization potential of the HTL increases (this happens in the order PFMO-PFM-PFB-TFMO-BFB-TFB, the values that are inferred from oxidation potentials measured by cyclic voltammetry are 4.98, 5.04, 5.09, 5.2, 5.26 and 5.30 eV respectively). However there seems to be no clear correlation between the onset electric field and the barrier for hole injection as inferred from the difference between the Fermi level of the ITO and the HOMO energy level of the HTL for these double layer structures. This indicates that a simple picture of hole injection based on a simple energy level scheme is not always enough to account for the experimental results and other factors like interfacial surface dipoles and the adhesion properties of different polymers on ITO may play a role in determining the energy barrier associated with this interface and thus affecting significantly the hole injection. We also note that devices made with TPQ15c instead of TPQ15f generally exhibit a lower performance in terms of efficiency and maximum brightness for the same thickness of the ETL. This indicates that not only the injection but also the transport of electrons to the interface is of high importance in order to achieve efficient exciplex emission.

An improved device performance was achieved when a 50 nm PEDOT:PSS, a mix of poly(3,4-ethylenedioxythiophene) [Baytron-P] and poly(styrenesulfonic acid), is used as a hole injection layer spun between the ITO and the HTL. PEDOT:PSS was obtained from Bayer. It has been widely used as a hole-injecting layer in LEDs³⁸⁻³⁹ as it has major advantages: it is highly transparent, highly conductive resulting in negligible electric field drop at the ITO interface and it smoothes the ITO surface when deposited on top. It was spun

Chapter 3: Exciplex emission in bilayer light-emitting diodes based on hole transport fluorene-triarylamine copolymers and electron transport starburst phenylquinoxalines

at 2000 rpm and then it was baked for 15 minutes at 150 °C in air to render it insoluble. The chemical structures of Baytron P and poly(styrenesulfonic acid) are shown in Figure 3.23.

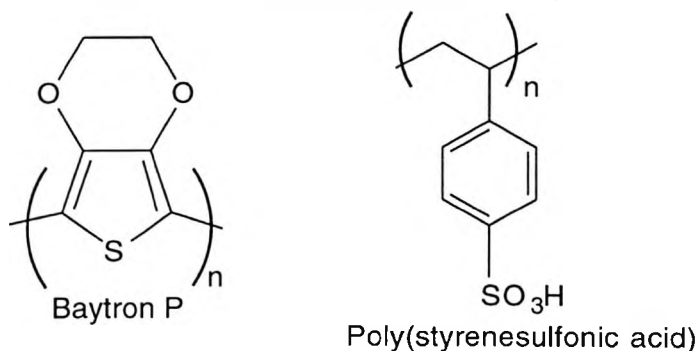


Figure 3.23: Chemical formulae of Baytron P and poly(styrenesulfonic acid).

The J vs. E, L vs. E and cd/A vs. E characteristics of these LEDs are shown in Figures 3.24, 3.25 and 3.26 together with data for annealed LEDs.

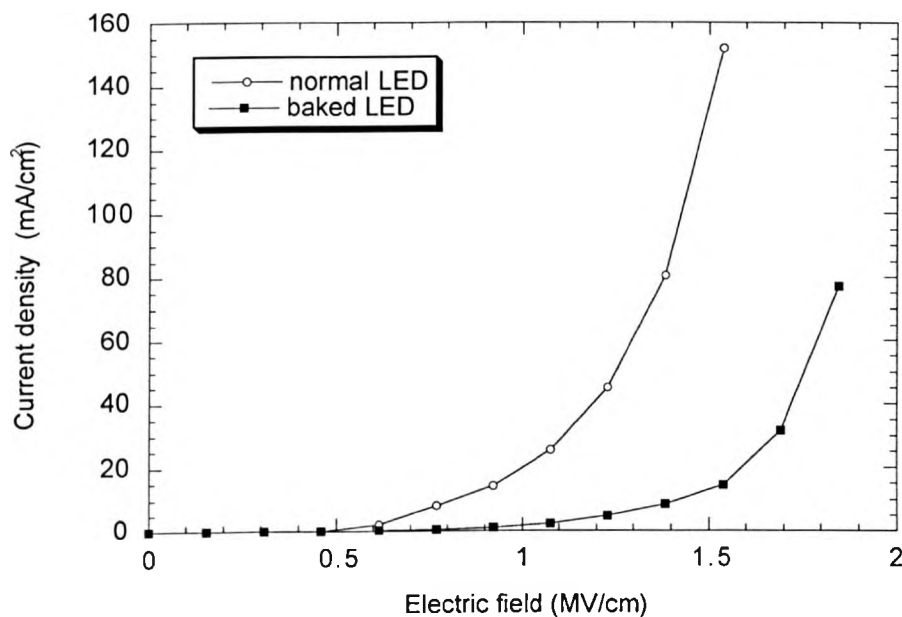


Figure 3.24: J vs. E characteristics of a PEDOT/BFB/TPQ15f/Dow metal LED before (open circles) and after annealing (filled squares) (130 °C, 30 minutes, after film deposition but prior to cathode evaporation).

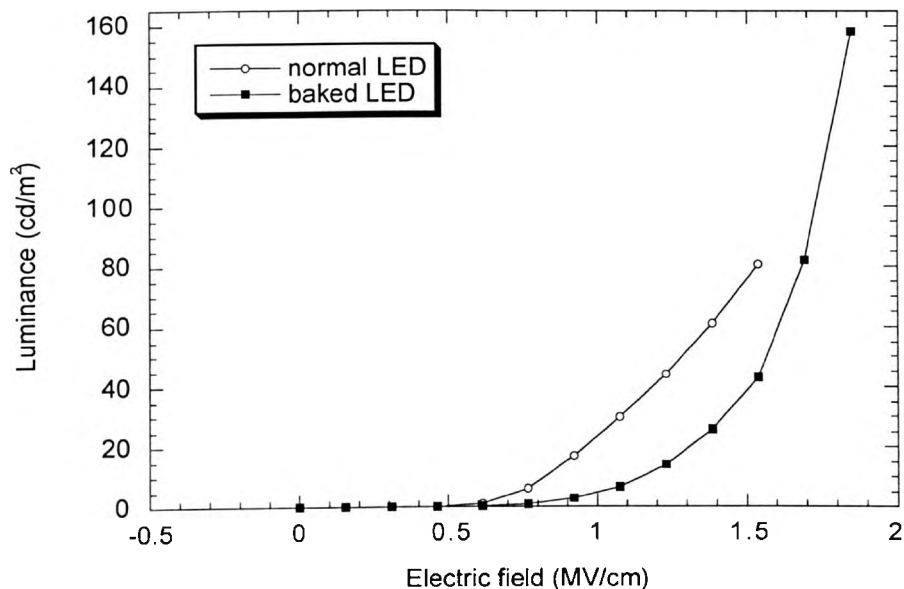


Figure 3.25: L vs. E characteristics of a PEDOT/BFB/TPQ15f/Dow metal LED before (open circles) and after annealing (filled squares) (130 °C, 30 minutes, after film deposition but prior to cathode evaporation).

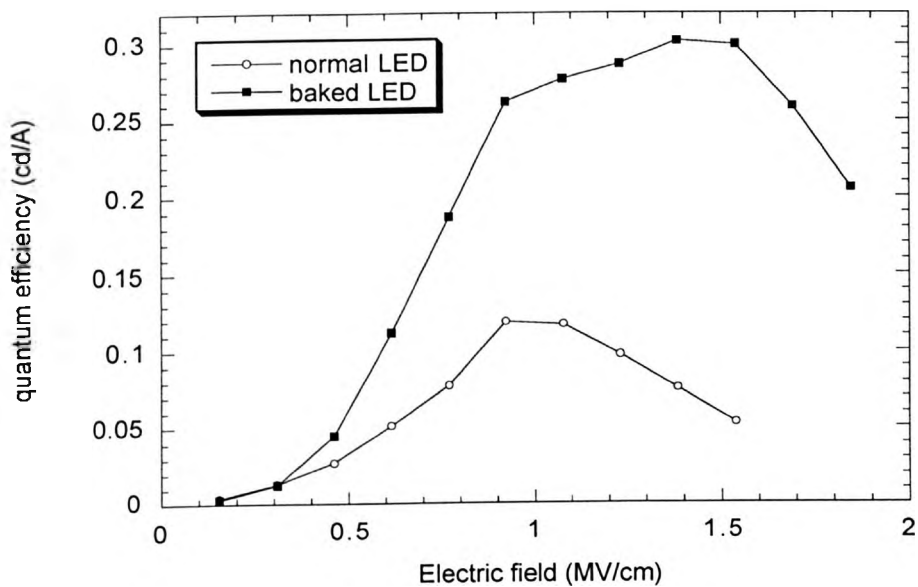


Figure 3.26: cd/A vs. E characteristics of a PEDOT/BFB/TPQ15f/Dow metal LED before (open circles) and after annealing (filled squares) (130°C, 30 minutes, after film deposition but prior to cathode evaporation).

Chapter 3: Exciplex emission in bilayer light-emitting diodes based on hole transport fluorene-triarylamine copolymers and electron transport starburst phenylquinoxalines

A PEDOT (50 nm)/BFB (85 nm)/TPQ15f (50 nm) LED has an onset field of 0.6 MV/cm (for $J = 5 \text{ mA/cm}^2$), it reaches a brightness of 80 cd/m^2 at 18 V and a maximum efficiency of 0.06 % or 0.1 cd/A. Thermal annealing was carried out to remove the residual solvent after HTL casting and to examine its effect on the device performance. The process included annealing after deposition of both films (before cathode deposition) at 130 °C in air for 0.5 hr. This temperature was chosen as it is slightly below the glass transition temperature of BFB. The effect of the annealing on the device performance is as follows: The maximum EL quantum yield increases by a factor 3 and the maximum brightness also increases by a factor of 2 compared to non annealed devices. The maximum current density decreases by a factor of 2 while the turn on as well as the operating voltage slightly increase. Improvement of the device performance due to thermal treatment of the polymer layer has been reported in the literature in single layer LEDs⁴⁰⁻⁴¹ and it was attributed to increased thermal endurance due to changes of the polymer morphology that enhance the chain packing of the film. In this case, as the annealing temperature is slightly below the glass transition temperature of the HTL, no significant change of the morphological properties of the HTL should be expected. However, a change on the HTL/ETL interfacial properties together with a more balanced hole and electron injection in the annealed device could account for the enhanced performance. The reduced current density can probably be attributed to reduced hole injection after annealing. A possible change of the interfacial properties after baking that could enhance the brightness and the efficiency by increasing the probability for radiative recombination between electrons and holes at the interface is the increased diffusion of molecules from the HTL towards the interface where they could meet up with ETL molecules and form excited states. Enhanced interfacial adhesion after annealing is another possible change of the interfacial properties that would increase the contact area for the carriers and hence could increase the recombination efficiency. Also the improved thermal stability of the film after annealing could also account for the increased light output at high fields. Also we

note that no change of the emission color was observed after annealing thus verifying that the exciplex emission mechanism is predominant in these bilayer devices.

3.8 Conclusions

In this chapter, we have addressed the issue of emission from charge-transfer states, specifically the emission from an exciplex state in bilayer LEDs based on hole transport triarylamine copolymers and electron-transport starburst quinoxalines. The fabrication and characterization of bilayer LEDs that operate on the basis of exciplex emission has been presented in detail. The use of hole transport materials with a low ionization potential leads to the formation of the exciplex with TPQs, as evidenced by the measurement of PL and EL spectra, whereas no exciplex formation takes place for hole transport materials with higher ionization potentials. The emission wavelength and color was determined by the energy difference between the ionization potential of the hole transport material and the electron affinity of the electron transport material. Because the exciplex formation takes place only at the interface, the emission color can be tuned by varying the ionization potential of the hole transporter. Our data show that, although the change in I_p correlates with the change in photon energy, the absolute energies are higher than expected on the basis of a simple consideration of the energies of the participating frontier orbitals. We attribute the differences between the experimental values of the peak emission wavelength and the theoretically calculated values (based on the difference between the E_{HOMO} of the HTL and the E_{LUMO} of the ETL) to either systematic overestimation of the energy of the LUMO level of the ETL (due to polarization energy effects) or to the formation of an excited singlet state of the hole transporter prior to the formation of the exciplex state. However, the character of the exciplex state as a new excited state is predominant in our LEDs and offers a simple, alternative way of tuning the emission color.

References

1. Andersson, M.R., Berggren, M., Inganäs, O., Gustafsson, G., Gustafsson-Carlberg, J.C., Selse, D., Hjertberg, T. & Wennerström, O. *Macromolecules* **28**, 7525 (1995).
2. Berggren, M., Granström, M., Inganäs, O. & Andersson, M. *Advanced Materials* **7**, 900 (1995).
3. Burroughes, J.H, Bradley, D.D.C., Brown, A.R, Marks, R.N, Mackay, K., Friend, R.H, Burn, P.L. & Holmes, A.B. *Nature* **347**, 539 (1990).
4. Wittmann, H.F, Fuhrmann, K., Friend, R.H., Khan, M.S. & Lewis, J. *Synthetic Metals* **55-57**, 56 (1993).
5. Baldo, M.A., O'Brien, D.F., You, Y., Shoustikov, A., Silbley, S., Thompson, M.E. & Forrest, S.R. *Nature* **395**, 151 (1998).
6. Gebler, D.D., Wang, Y.Z., Blatchford, J.W., Jessen, S.W., Fu, D.K., Swager, T.M., MacDiarmid, A.G. & Epstein, A.J. *Applied Physics Letters* **70**, 1644 (1997).
7. Jenekhe, S.A. & Osaheni, J.A. *Science* **265**, 765 (1994).
8. Jenekhe, S.A. *Advanced Materials* **7**, 309 (1995).
9. Osaheni, J.A. & Jenekhe, S.A. *Macromolecules* **27**, 739 (1994).
10. Okada, T, Kobayashi, Y., Yamasa, H. & Mataga, N. *Chemical Physics Letters* **128**, 583 (1986).
11. Gebler, D.D., Wang, Y.Z., Fu, D.-K., Swager, T.M. & Epstein, A.J. *Journal of Chemical Physics* **108**, 7842 (1998).
12. Hu, B., Yang, Z. & Karasz, F.E. *Journal of Applied Physics* **76**, 2419 (1994).
13. Yang, Y. & Pei, Q.B. *Applied Physics Letters* **70**, 1926 (1997).
14. Wang, Y.Z., Gebler, D.D., Fu, D.K., Swager, T.M., MacDiarmid, A.G. & Epstein, A.J. *Synthetic Metals* **85**, 1179 (1997).

Chapter 3: Exciplex emission in bilayer light-emitting diodes based on hole transport fluorene-triarylamine copolymers and electron transport starburst phenylquinoxalines

15. Wang, Y.Z., Gebler, D.D., Spry, D.J., Fu, D.K., Swager, T.M., MacDiarmid, A.G. & Epstein, A.J. *IEEE Transactions on Electron Devices* **44**, 1263 (1997).
16. Gebler, D.D., Wang, Y.Z., Jessen, S.W., Blatchford, J.W., MacDiarmid, A.G., Swager, T.M., Fu, D.K. & Epstein, A.J. *Synthetic Metals* **85**, 1205 (1997).
17. Greenham, N.C., Samuel, I.D.W., Hayes, G.R., Phillips, R.T., Kessener, Y.A.R.R., Moratti, S.C., Holmes, A.B. & Friend, R.H. *Chemical Physics Letters* **241**, 89 (1995).
18. Itano, K., Ogawa, H. & Shirota, Y. *Applied Physics Letters* **72**, 636 (1998).
19. Chao, C.-I & Chen, S.-A. *Applied Physics Letters* **73**, 426 (1998).
20. Giro, G., Cocchi, M., Kalinowski, J., Di Marco, P. & Fattori, V. *Chemical Physics Letters* **318**, 137 (2000).
21. Wang, J.F., Kawabe, Y., Shaheen, S.E., Morrell, M.M., Jabbour, G.E., Lee, P.A., Anderson, J., Armstrong, N.R., Kippelen, B., Mash, E.A. & Peyghambarian, N. *Advanced Materials* **10**, 230 (1998).
22. Miyaura, N. & Suzuki, A. *Chemical Reviews* **95**, 2457 (1995).
23. Grice, A.W., Bradley, D.D.C., Bernius, M.T., Inbasekaran, M., Wu, W.W. & Woo, E.P., *Applied Physics Letters* **73**, 629 (1998).
24. Bernius, M., Inbasekaran, M., Woo, E., Wu, W. & Wujkowski, L. *Journal of Materials Science: Materials in Electronics* **11**, 111 (2000).
25. Malliaras, G.G. & Scott, J.C. *Journal of Applied Physics* **85**, 7426 (1999).
26. Tang, C.W. *Applied Physics Letters* **48**, 183 (1986).
27. Giebeler, C., Antoniadis, H., Bradley, D.D.C. & Shirota, Y. *Applied Physics Letters* **72**, 2448 (1998).
28. Redecker, M., Bradley, D.D.C., Inbasekaran, M., Wu, W.W. & Woo, E.P. *Advanced Materials* **11** 241 (1999).
29. Bettenhausen, J., Greczmiel, M., Jandke, M. & Strohmriegl, P. *Synthetic Metals* **91**,

Chapter 3: Exciplex emission in bilayer light-emitting diodes based on hole transport fluorene-triarylamine copolymers and electron transport starburst phenylquinoxalines

223 (1997).

30. Hohle, C., Jandke, M., Schloter, S., Koch, N., Resel, R., Haarer, D. & Strohriegl, P. *Synthetic Metals* **102**, 1535 (1999).
31. Schürmann, H., Koch, N., Imperia, P., Schrader, S., Jandke, M., Strohriegl, P., Schulz, B., Leising, G. & Brehmer, L., *Synthetic Metals* **102**, 1069 (1999).
32. Jandke, M., Strohriegl, P., Berleb, S., Werner, E. & Brütting, W., *Macromolecules* **31**, 6434 (1998).
33. Redecker, M., Bradley, D.D.C., Jandke, M. & Strohriegl, P. *Applied Physics Letters* **75**, 109 (1999).
34. Grell, M., Bradley, D.D.C., Inbasekaran, M. & Woo, E.P. *Advanced Materials* **9**, 798 (1997).
35. Redecker, M., Bradley, D.D.C., Baldwin, K.J., Smith, D.A., Inbasekaran, M., Wu, W.W., Woo, E.P., *Journal of Materials Chemistry* **9**, 2151 (1999).
36. Rajagopal, A., Koch, N., Ghijsen, J., Johnson, R.L., Kaeriyama, K., Leising, G. & Pireaux, J.J. *Journal of Applied Physics* **87**, 1331 (2000).
37. Stoessel, M., Wittmann, G., Staudigel, J., Steuber, F., Blässing, J., Roth, W., Klausmann, H., Rogler, W. & Simmerer, J. *Journal of Applied Physics* **87**, 4467 (2000).
38. Sainova, D., Miteva, T., Nothofer, H.G., Scherf, U., Glowacki, I., Ulanski, J., Fujikawa, H. & Neher, D. *Applied Physics Letters* **76**, 1810 (2000).
39. Spreitzer, H., Becker, H., Kluge, E., Kreuder, W., Schenk, H., Demandt, R. & Schöo, H. *Advanced Materials* **10**, 1340 (1998).
40. Lee, T.-W. & Park, O.O. *Advanced Materials* **12**, 801 (2000).
41. Lee, T.-W. & Park, O.O. *Applied Physics Letters* **77**, 3334 (2000).

CHAPTER 4

BLUE LIGHT EMITTING DIODES FROM BLENDS OF POLYFLUORENE (PFO) AND HOLE TRANSPORTING MATERIALS

4.1 Introduction

Since the discovery of polymer electroluminescence by the group at Cambridge University in 1990,¹ polymer light emitting diodes (PLEDs) that show high brightness, high quantum efficiency and low operating voltage have been of considerable interest due to their high potential for application in full color displays. Bright and efficient polymer LEDs emitting red, green and white color that approach the high standards required from industry for commercial applications have already been demonstrated by many different academic and industrial research groups.²⁻¹¹ High performance blue PLEDs with sufficient efficiencies and operating lifetimes are more difficult to fabricate due to the large band gap energy. This generally results in large barriers for charge injection from either one or both electrodes.

The first demonstration of a blue PLED was done in 1992 using poly(para-phenylene) (PPP) as the emissive polymer.¹² Using a ladder-type poly(para-phenylene) (LPPP) the

Chapter 4: Blue light emitting diodes from blends of polyfluorene (PFO) and hole transporting materials

group at Graz demonstrated blue single layer LEDs with an Al cathode that reached a maximum efficiency of 0.1%.¹³ The group at Uniax subsequently synthesized and used other PPP derivatives to fabricate blue LEDs. Two layer LEDs with a poly(N-vinylcarbazole) (PVK) hole transport layer, a PPP derivative as an emissive layer and a Ca cathode exhibited a maximum external efficiency of 3% and a brightness of 500 cd/m² at 30 V.¹⁴ Small molecules and other conjugated polymers have also been employed to fabricate organic and polymer LEDs that emit blue color. Some examples include amino-oxadiazole-fluorenes (AODFs)¹⁵, dipyrzolopyridine derivatives¹⁶, bicarbazyle derivates¹⁷, amorphous materials such as bis(2,2-diphenylvinyl)biphenyl derivatives¹⁸⁻¹⁹ and 5,5'-bis(dimesitylboryl)-2,2'-bithiophene²⁰, organometallic complexes like lithium tetra-(8-hydroxy-quinolino) boron (LiBq₄)²¹, triazole derivatives²² and binaphthalene derivatives²³.

More recently, 9,9-disubstituted polyfluorenes have attracted significant interest as new blue emissive materials for polymer LEDs. A family of 9,9-dialkylfluorene homopolymers and copolymers was first developed at Dow Chemical Company in the early 1990s.²⁴ The main characteristics of these polymers were the high molecular weight, the low polydispersity and the high purity. Efficient blue light emission (under photoexcitation as well as in a LED configuration) from poly(9,9-dioctylfluorene) (PFO) was first demonstrated from the group at Sheffield University in 1997.²⁵⁻²⁷ Optimized two layer devices emitted blue light with a peak wavelength at 436 nm and with a maximum brightness of 600 cd/m² corresponding to a maximum external efficiency of 0.25 cd/A or 0.25%.

Since then, many other fluorene-based conjugated polymers have been reported as efficient blue emitters and employed in the fabrication of bright and efficient blue polymer LEDs by various academic and industrial research groups.²⁸⁻³⁹ In particular, the group at IBM has synthesized a portfolio of high molecular weight poly(alkylfluorene)

copolymers.²⁹⁻³³ Statistically random copolymers of substituted fluorenes with other aryl moieties were found to form excimers upon annealing or electrical excitation and depending on the polymer composition and the film morphology. The introduction of small amounts of anthracene into the polyfluorene main chain results in a strong twisting of the plane of the anthracene units relative to those of the neighboring planar dihexylfluorene units and a complete suppression of the excimer emission band was achieved even after long term annealing at high temperatures. Other copolymers based on dialkylfluorenes incorporating low bandgap chromophores such as perylene or α -cyanostilbene also do not show any excimer emission due to efficient exciton migration and trapping on the low bandgap chromophoric segments which are populated by rapid energy transfer and serve as efficient excitonic energy traps upon excitation of the main chain fluorene chromophores. Optimized triple layer LEDs with an ITO anode, a thermally cross-linkable hole transporting polyarylamine, a blue emissive polyfluorene, an electron transporting oxadiazole trimer and a Ca cathode show maximum external quantum efficiency in excess of 1% and maximum brightness in excess of 1500 cd/m^2 . Two layer devices with a crosslinked hole transporting triphenylamine and a tri-block emissive copolymer exhibit maximum external quantum efficiencies of 0.5%. The tri-block copolymer contains a 9,9-di-n-hexylfluorene-co-anthracene emitting unit along with a triphenylamine containing hole transporting unit and an oxadiazole containing electron transporting unit. The group at Santa Barbara has also synthesized new spiro-functionalized polyfluorene derivatives and para-phenylene containing polyfluorenes.^{28,34} The spiro-functionalized fluorene derivatives exhibit narrower emission spectra (with a smaller tail at longer wavelengths) compared with conventional polyfluorenes and this was attributed to the weak interchain interactions in the solid state as a result of the steric-hindrance of the spiro-structure. They also show improved spectral stability due to their higher glass transition temperatures. The para-phenylene containing poly(9,9-dihexylfluorenes) show high PL quantum efficiencies of approximately 40%, a peak

Chapter 4: Blue light emitting diodes from blends of polyfluorene (PFO) and hole transporting materials

emission wavelength at 420 nm, maximum external efficiencies of 0.5% and maximum luminances of 700 cd/m^2 in bilayer LEDs with CuPc/PVK hole transporting layers and Ca cathodes. Other promising fluorene-based polymers for LEDs include a poly-p-phenylene (PPP) derivative, namely poly-2,8-indenofluorene³⁷, 2,7-poly(9-fluorenone)³⁸, a binaphthyl polyfluorene³⁵ and fluorene-oxadiazole compounds.³⁹

In most cases, however, multilayer structures, usually comprising a hole transport layer and an emissive layer have been employed. In this case, the different layers will be deposited by consecutive spin coating of polymer solutions. This approach is not always straightforward with polymers. Many conjugated polymers are soluble in a wide range of common organic solvents and unless a system of mutually incompatible solvents is used in order to exclude the dissolution and swelling of the first layer by the second solvent, a significant interpenetration between the different layers is expected that results in poor interface quality and can prove detrimental to the device performance. The incorporation of the functions of the different materials into a single film in the form of a blend⁴⁰⁻⁴² can be used to overcome the above problem. Despite the fact that there is no longer a multilayer structure, where separate optimization of the injection and transport of each carrier type and the introduction of energy offsets at the interface takes place, the properties of each of the different materials may be maintained in the blend so that an improved charge balance factor can be achieved with a consequent improvement in the device performance.

In this chapter, the fabrication and the performance of single layer blue light emitting diodes that use a blend of conjugated polymers as the emissive layer will be presented in detail. The blend consists of a blue light-emitting poly(9,9-dioctylfluorene), PFO as host with a hole transport fluorene/triarylamine copolymer as guest. The doping of the emissive polymer with a material that has hole-accepting properties allows for a simpler device

structure with the removal of the separate hole transport layer. LEDs employing this blend as the active layer show a significantly enhanced quantum and power efficiency, reach a higher brightness, sustain higher current densities and exhibit a lower turn on as well as operating voltage compared with undoped devices and results obtained using different optical spectroscopy and electrical characterization techniques will be presented.

4.2 Experimental details

Two types of device have been fabricated and compared. The first have a single layer of the emissive polyfluorene between the electrodes. In the second type, an amount of the hole transport material is added to form a blend. Different concentrations of the guest were employed for optical and electrical characterization measurements. Indium tin oxide (ITO) coated glass was used as the substrate for device fabrication and cleaned following the procedure described in Chapter 2. The LED structures consist of an ITO anode, a single layer of the polymer or the blend and a top evaporated metal cathode. Occasionally, a PEDOT:PSS layer was used as a hole injection layer on top of ITO. It was spun from a methanol solution at 5000 rpm to form a 15 nm thick layer on top of ITO and it was then baked at 120 °C for 10 minutes in air to render it insoluble. The polymer films were typically spin coated from a 20 mg/ml toluene solution. Al, Dow metal or Ca were thermally deposited under a vacuum of 3×10^{-6} mbar to form the cathode electrode. A typical cathode thickness was about 200 nm. The blend was spin coated at various spin speeds (1000 to 8000 rpm) to give uniform and pinhole-free films, with thicknesses ranging from 50 to 250 nm. All measurements were carried out either under a dynamic vacuum (10^{-1} mbar) or in a nitrogen filled glove box. Films of the PFO/PFM blend were prepared by spin-coating onto quartz substrates. Films of PFO and PFM were also prepared as control samples. The 354 nm line of a HeCd laser was used as excitation source for PL and PL efficiency measurements.

4.3 Optical spectroscopy of individual components and blends

Figure 4.1 shows the chemical structures of the polymers used in this chapter.

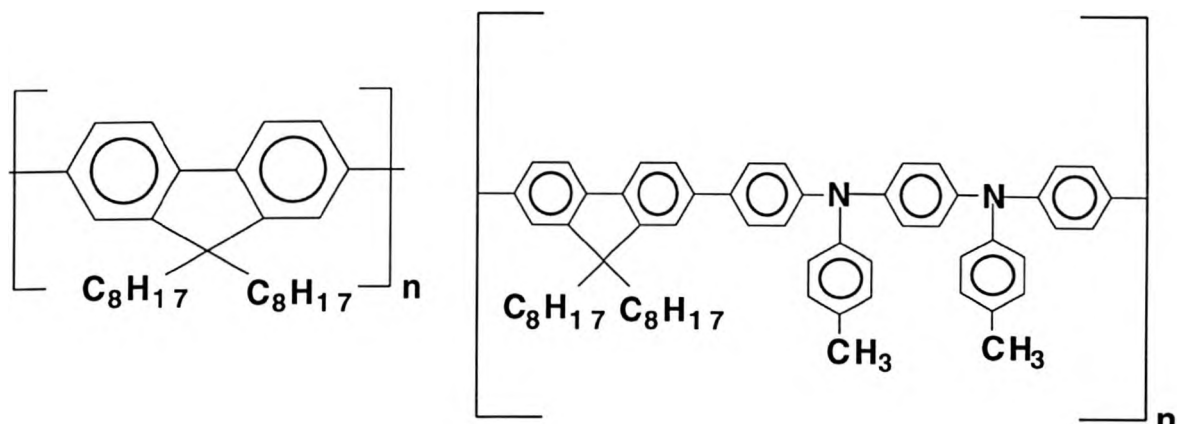


Figure 4.1: Chemical structures of the homopolymer polyfluorene PFO (on the left) and the hole transport triarylamine/fluorene copolymer PFM (on the right).

The blue emitting conjugated polymer poly(9,9-dioctylfluorene) (PFO) is used as the host material in the blend. It possesses a large room temperature hole mobility of order 10^{-4} to $10^{-3} \text{ cm}^2\text{V}^{-1}\text{s}^{-1}$ with rather weak field dependence.⁴³ It displays intense blue fluorescence with a high photoluminescence quantum efficiency of $55 \pm 5 \%$ in the solid state. The guest material in the blend was a hole transporting triarylamine copolymer namely poly(9,9-dioctylfluorene-co-bis-N,N'-(4-methylphenyl)-bis-N,N'-phenyl-1,4-phenylenediamine) (PFM). PFM also possesses a high hole mobility of order $7 \times 10^{-4} \text{ cm}^2\text{V}^{-1}\text{s}^{-1}$ with weak field dependence⁴⁴ and emits blue light with a fluorescence quantum efficiency of $27 \pm 2 \%$. Both polymers were synthesized via a modified Suzuki coupling polymerization reaction⁴⁵ and were carefully purified to remove ionic impurities and catalyst residues. The arylamine donor functionality in the copolymer leads to a significant reduction in the ionization potential from the 5.8 eV value deduced from cyclic voltammetry measurements for the polyfluorene

polymer. PFM has an ionization potential of 5.04 eV³ allowing for more efficient hole injection from ITO (which has a workfunction of 4.7 eV) due to the lower injection barrier.

Blends containing three different concentrations of the PFM guest (by weight) have been examined via photoluminescence, namely 5%, 20% and 33%. Typical absorption and photoluminescence spectra of the PFO polymer are presented in Figure 4.2 below. The absorption spectrum exhibits a very strong featureless maximum at 385 nm. The photoluminescence spectrum peaks at 422 nm (corresponding to the 0-0 electronic transition) with a well-defined vibronic feature at 447 nm (corresponding to the 0-1 transition) and a shoulder at 473 nm. The electroluminescence spectrum of PFO (not shown) very closely resembles the PL spectrum.²⁶ Photoluminescence and absorption spectra of the hole transport material PFM are also shown in Figure 4.2.

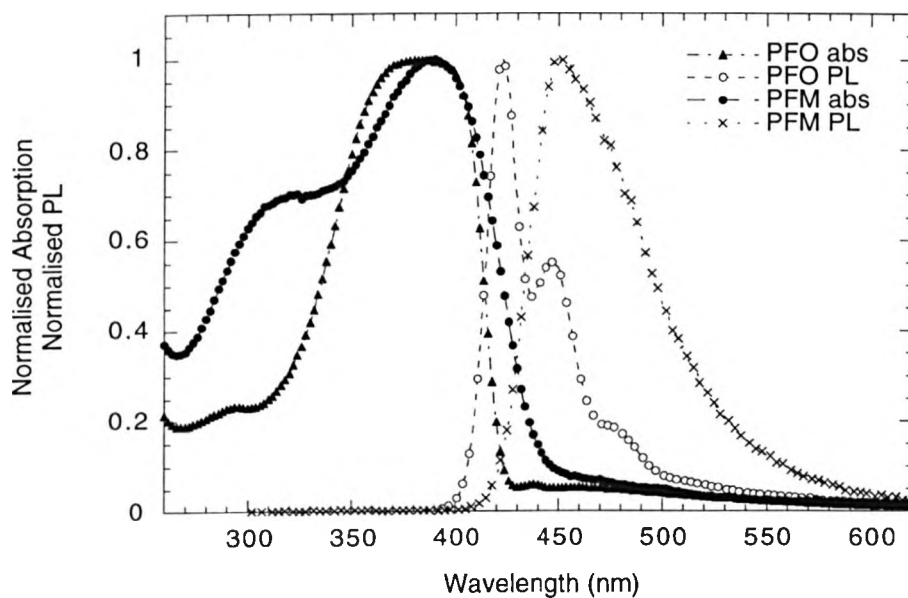


Figure 4.2: Absorption and photoluminescence spectra of PFO and PFM films [PFO absorption (filled triangles), PFO PL (open circles), PFM absorption (filled circles) and PFM PL (crosses)].

The absorption spectrum shows a peak at 390 nm and a featureless band dominates the PL spectrum with a peak at 450 nm that shows no vibronic features. The PL spectra of PFM do not vary with concentration (for concentrations ranging from 2mg/ml to 25mg/ml). For different solvents, only small solvatochromic changes were observed in the red emission tail of the spectra without significantly affecting the emission color. The absorption spectra of the blends (not shown here) are a linear superposition of the absorption spectra of the individual components and thus dominated by the PFO absorption. The absolute absorption coefficients for PFO and PFM (at the corresponding maxima) are $a = 2.7 \times 10^5 \text{ cm}^{-1}$ and $a = 1.1 \times 10^5 \text{ cm}^{-1}$, respectively. Photons are therefore absorbed with a factor of 2.5 higher probability in PFO compared to PFM. Films of the PFO_{(100-x)%}: PFM_{(x)%} blends with $x=5\%$, 20% and 33% were optically excited at 354 nm where the absorbance of both materials is high and the PL spectra of these blends are shown in Figure 4.3 below.

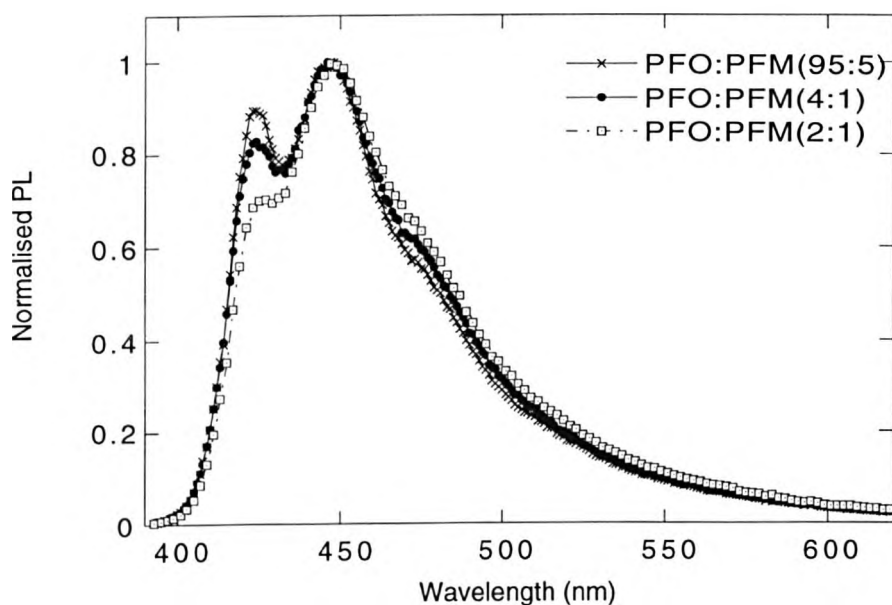


Figure 4.3: Fluorescence spectra of PFO:PFM polymer blends with different PFM wt. % concentrations [PFO:PFM(95:5) (crosses), PFO:PFM(4:1) (filled circles) and PFO:PFM(2:1) (open squares)].

Chapter 4: Blue light emitting diodes from blends of polyfluorene (PFO) and hole transporting materials

Most of the excitation light is absorbed by PFO due to the higher PFO concentration in the blend as well as the larger absorption coefficient of PFO. Due to the overlap between the PL spectrum of PFO and the absorption spectrum of PFM, singlet excitons in the host can transfer their energy to the guest. This occurs via a Förster transfer mechanism due to dipole-dipole coupling.⁴⁶ The PL spectra of the blends appear to be a composite of the PL spectra of PFO and PFM and they can be accurately deconvoluted as a non-linear superposition of the spectra of the two components. If a and b are the relative weights of the contribution of the PFO PL and the PFM PL to the PL of the blends then the deconvolution results can be summarized as follows: For 95% PFO, $a=0.58$ and $b=0.42$, for 80% PFO, $a=0.53$ and $b=0.47$ and for 67% PFO, $a=0.44$ and $b=0.56$, respectively. PFM can thus be excited either directly or via Förster transfer. However, even for 33% PFM, the energy transfer is still not complete. This is attributed to the weak overlap between the donor emission and the acceptor absorption spectrum. However, the relative contribution of the 447 nm peak (the peak of the PFM PL) in the blend PL increases as the PFM concentration increases.

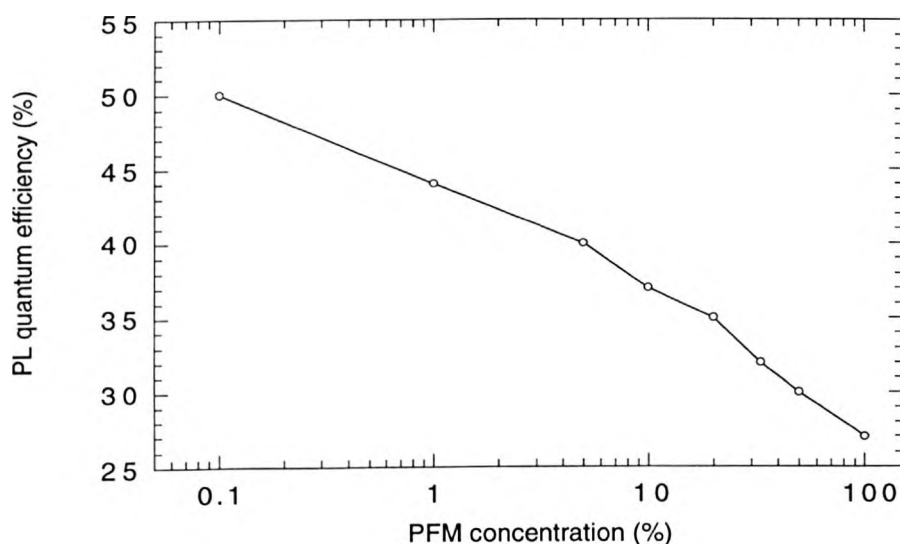


Figure 4.4: PL quantum efficiency of the blend as a function of the PFM concentration.

In Figures 4.4 (above) and 4.5 (below), the PL efficiency of the blend as a function of PFM concentration and the PL decays of both PFO and PFM emission are shown.

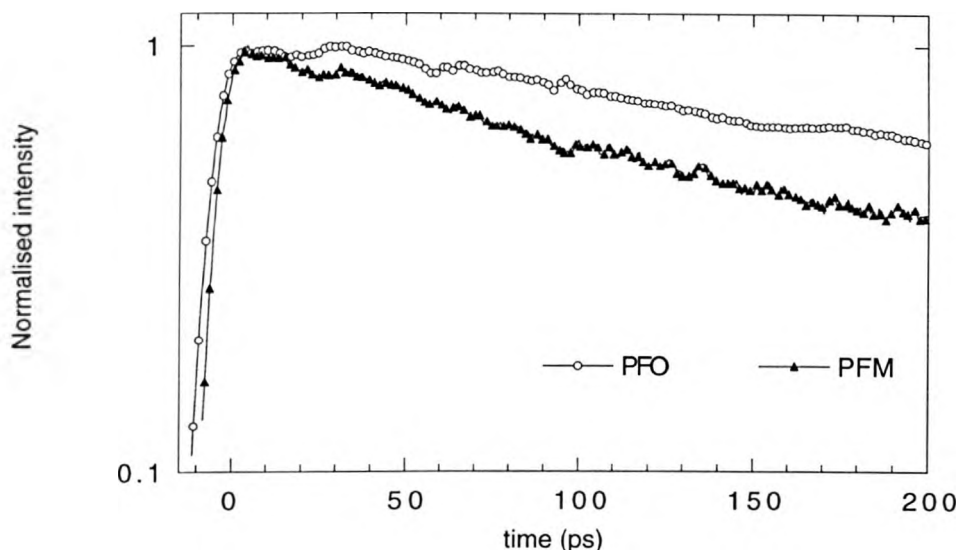


Figure 4.5: Fluorescence decay of the PFO (open circles) and the PFM emission (filled triangles).

A significant decrease of the PL efficiency of the blend with respect to that of pure PFO is observed as the guest concentration increases. For 5, 20 and 33% PFM the PL quantum efficiency falls to 40, 35 and 32 %, respectively. This suggests that transfer of singlet excitons formed in the host to the guest is taking place since the guest has a lower PL quantum efficiency than the host. The fluorescence decay of the emission from the two individual components is recorded with time resolved photoluminescence spectroscopy. The time-resolved PL is detected at the peaks of PFO (422 nm) and PFM (447 nm) emission while both components are excited at the peaks of their absorption spectra, respectively. The data from the fluorescence decay of the PFO emission can be fitted accurately with a single component exponential decay. An emission lifetime of 350 ps is extracted for PFO. The data for PFM can be fitted accurately with a double component exponential decay. Two different

fluorescence lifetimes are found; a fast component with a fitted lifetime value of 180 ps and a slower component with a fitted lifetime value of 230 ps. The relative weights of the two components in the decay are 60% and 40%, respectively. Figure 4.6 shows typical PL decay curves of the PFO emission from PFO/PFM blends with different PFM concentrations.

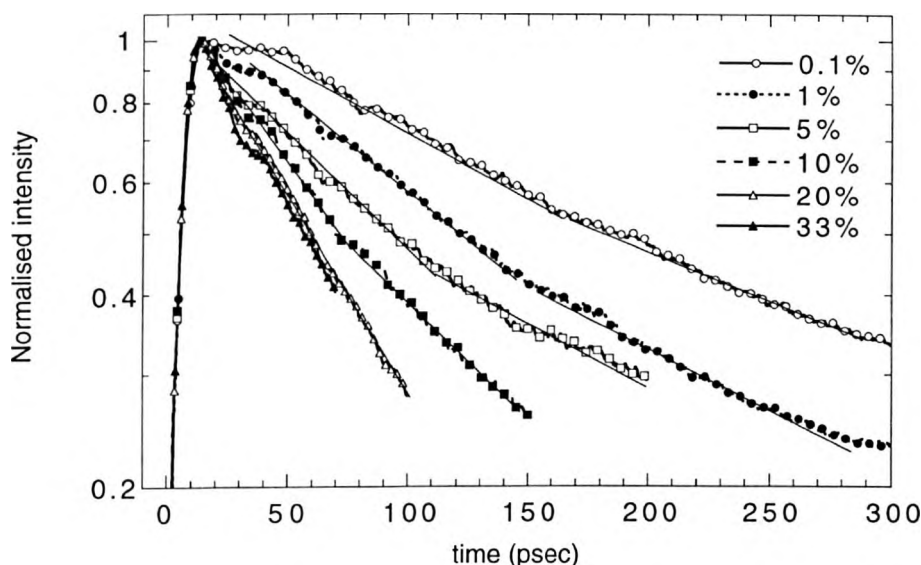


Figure 4.6: PL decay curves of PFO emission from PFO/PFM blends with different PFM concentrations [0.1%(open circles), 1%(filled circles), 5%(open squares), 10%(filled squares), 20%(open triangles) and 33%(filled triangles)].

The data from the low concentration samples (PFM fraction < 20%) could be fitted accurately with a double exponential decay while the higher concentration samples needed only a single exponential component. A decrease of the lifetime of the PFO fluorescence is observed with increasing concentration of PFM. This indicates that the energy transfer becomes more efficient as the concentration of PFM increases in the blend. For low PFM concentrations (PFM fraction $\leq 20\%$), the relative weighting of the fast component compared to that of the slower component is larger and it continues to increase as the PFM

concentration increases. As the concentration of PFM is increased above 20%, the faster component becomes dominant and the energy transfer probability increases as the interchain distance between the donor and the acceptor chains is reduced and the chains more closely interact with each other. The fast component can be associated with exciton migration from PFO to PFM sites via a Förster transfer mechanism while the longer component can be associated with a two step mechanism; intrachain or interchain excitation migration on PFO sites (either from the shorter to the longer conjugation segments or between nearest neighbor sites) followed by exciton migration to the lower energy PFM chain segments. Similar conclusions have been drawn for other polymer-polymer blends.⁴⁷⁻⁴⁸ In Figure 4.7 the PL lifetime of PFO emission (values are extracted from the exponential fits by considering the relative weightings of the two lifetime components) is plotted versus the PFM concentration.

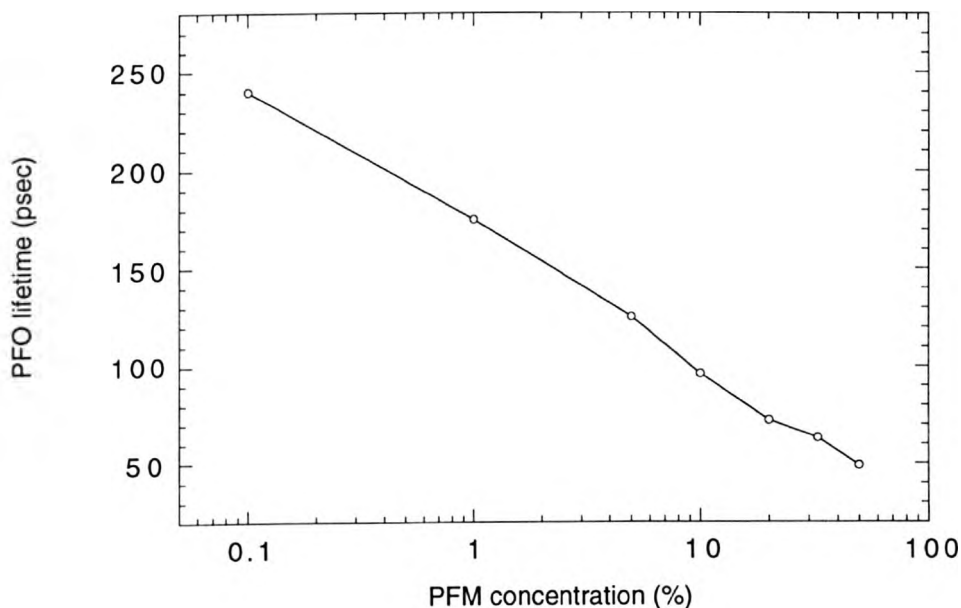


Figure 4.7: Fluorescence lifetime of the PFO emission versus PFM concentration in PFO/PFM blends.

Chapter 4: Blue light emitting diodes from blends of polyfluorene (PFO) and hole transporting materials

Table 1 summarizes the data from PLQE and time resolved PL measurements.

PFM concentration (%)	PLQE of PFO/PFM blends (%)	PFO lifetime (ps) (fast component)	PFO lifetime (ps) (slow component)	Relative weighting of fast (%)	Relative weighting of slow (%)
0.1	50	210	265	60	40
1	44	150	215	65	35
5	40	125	200	70	30
10	37	90	165	75	25
20	35	70	140	85	15
33	32	60	115	90	10
50	30	45	85	95	5

Table 1: Summary of data from PLQE and time resolved PL measurements for PFO/PFM blends.

The decrease of the lifetime of PFO emission together with the increased weighting of the shorter lifetime component of PFO in the biexponential decay of PFO provides unambiguous evidence for the increased exciton transfer efficiency from PFO to PFM with increasing PFM concentration.

4.4 LEDs from PFO/PFM blends with Al/Dow metal cathodes - Current-voltage-luminance characteristics and EL spectra

Pure PFO single layer devices with either an Al or a Dow metal cathode sustain low current densities and show almost no emission. This is a direct consequence of the very large injection barriers for both holes and electrons at the ITO/PFO and the PFO/cathode interfaces. The HOMO energy level of PFO lies at around 5.8 eV below vacuum and if the ITO Fermi

level is assumed to lie at around 4.7 eV below vacuum then the barrier for hole injection will be as high as 1.1 eV. On the other hand, the Fermi level of Al is at 4.2 eV and that of Dow metal at 3.7 eV below vacuum. The LUMO energy level of PFO is estimated to be at 2.8 eV (electrochemical measurements have shown that the LUMO energy is as low as 2.12 eV⁴⁹) thus resulting in electron injection barriers of 0.9 and 1.4 eV for Dow metal and Al respectively. It is expected that the charge carrier injection from both electrodes will be low even at high fields. This will result in low current densities and consequently in a low exciton formation and recombination probability. In the case of the blend PFO:PFM LEDs, significant changes in the device properties are observed. Emission occurs at low voltages and significantly higher current densities can be sustained compared to pure PFO LEDs. Figure 4.8 shows current density and luminance vs. field characteristics for PFO:PFM LEDs with Al or Dow metal (PFM concentration was 33% and the blend thickness was 100 nm).

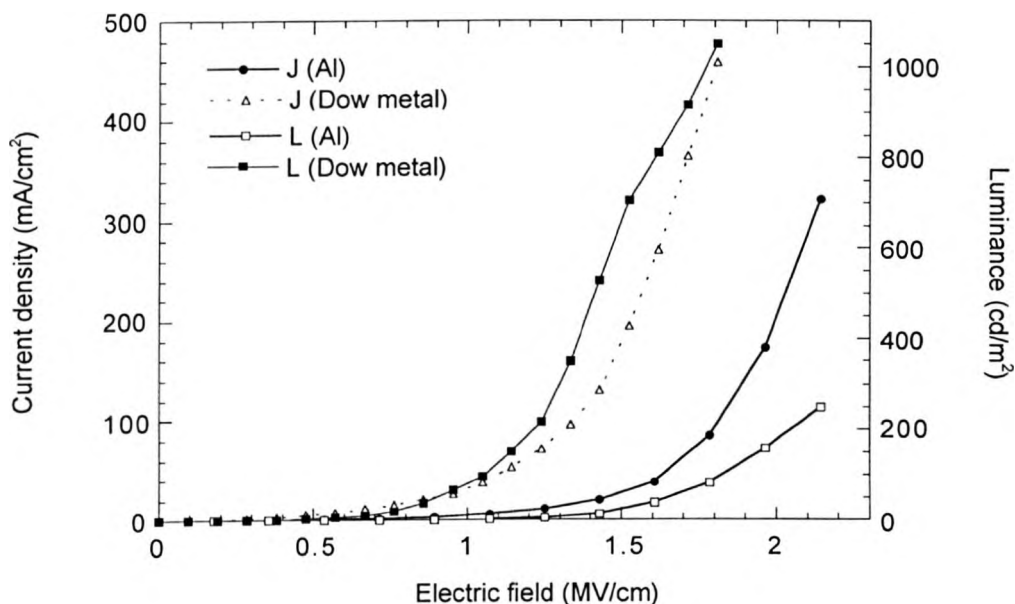


Figure 4.8: J vs. E and L vs. E characteristics of ITO/PFO:PFM/Al or Dow metal LEDs. [J(Al) (filled circles), L(Al) (open squares), J(Dow metal) (open triangles), L(Dow metal) (filled squares)].

The device with Dow metal reaches a maximum luminance of 1050 cd/m^2 at a corresponding current density of 460 mA/cm^2 . For Al, the maximum luminance is 250 cd/m^2 and the corresponding current density is 320 mA/cm^2 . The turn on electric fields (arbitrarily defined as the field at which the current density reaches 100 mA/cm^2) are 1.3 MV/cm and 1.8 MV/cm for Dow metal and Al respectively. Devices with a Dow metal cathode also show a maximum quantum efficiency of 0.4 cd/A , a factor of 4 increase compared to identical devices with an Al cathode ($\sim 0.09 \text{ cd/A}$). The maximum power efficiency is 0.09 lm/W for Dow metal, a factor of 3 higher than for Al. An over two orders of magnitude improvement in the maximum luminance and efficiency and one order of magnitude improvement in the current density are achieved for the blend PFO:PFM LEDs compared to identical PFO LEDs.

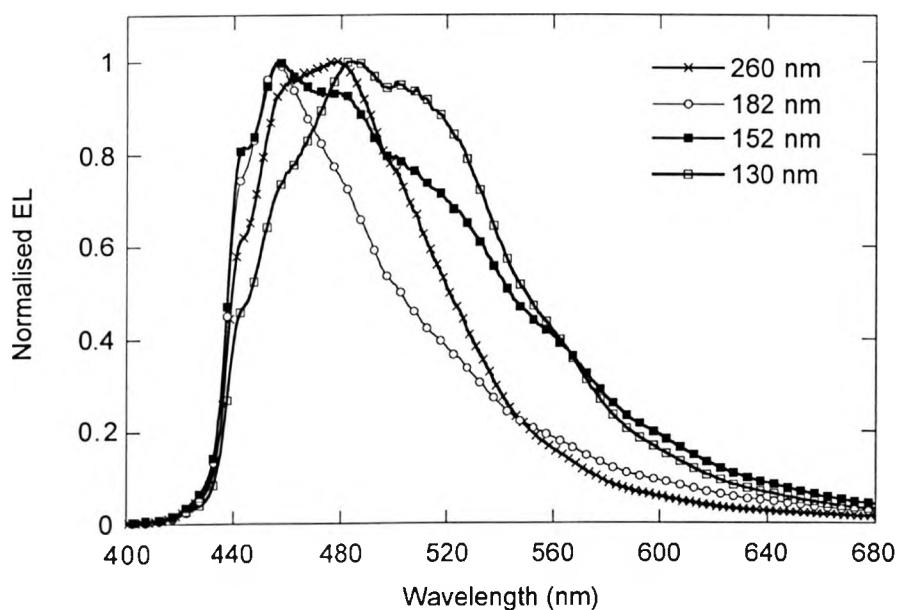


Figure 4.9: Electroluminescence spectra of LEDs (ITO / PFO:PFM / Dow metal) with different emissive layer thicknesses at a 20 wt % guest PFM concentration in the blend.

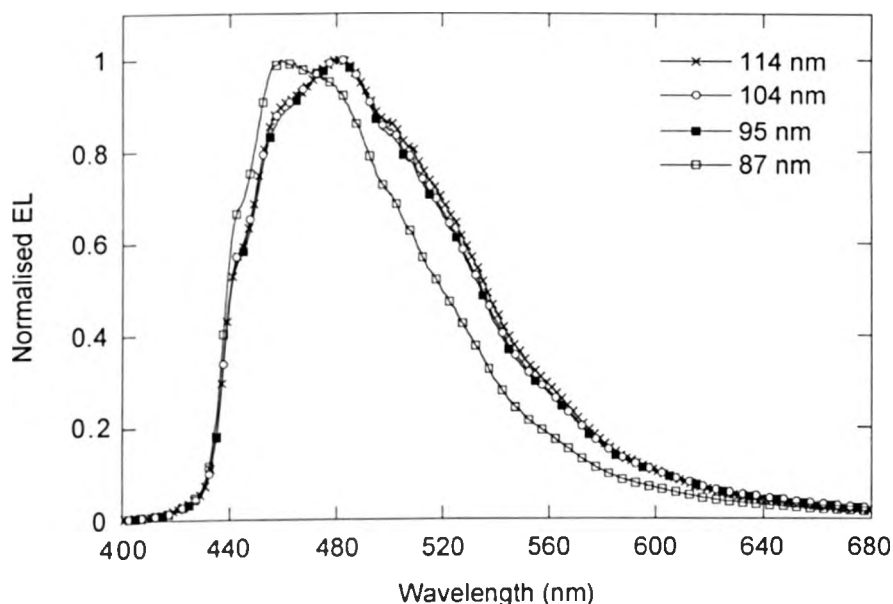


Figure 4.10: Additional electroluminescence spectra of LEDs (ITO / PFO:PFM / Dow metal) with different emissive layer thicknesses at a 20 wt % guest PFM concentration in the blend.

Figures 4.9 and 4.10 above show the electroluminescence spectra for a series of single layer blend LEDs with varying emissive layer thickness and a Dow metal cathode. They all had a 20-wt % PFM concentration. The shape of the EL spectrum was found to vary substantially with the thickness of the emissive layer. A possible explanation for these results is that significant interference effects between the directly emitted waves and the waves reflected from the cathode alter the radiative decay rate of the emissive species due to reflection from the metal cathode. This will depend on both the position of the recombination zone relative to the cathode and the relative orientation of the light emitting dipole moments.⁵⁰ Emission then can either be enhanced or reduced depending on whether there is a constructive or a destructive interference. The similar EL characteristics that were observed for both Al and Dow metal cathodes indicate that it is the reflection properties of the metal

Chapter 4: Blue light emitting diodes from blends of polyfluorene (PFO) and hole transporting materials

cathode and the orientation of the emitting dipoles relative to the cathode, rather than the position of the recombination zone in the bulk, that determine the interference effects which affect the shape of the emission spectrum. At shorter distances between the emissive dipoles and the metal electrode, we can also expect that an effective nonradiative energy transfer will take place to the metal which will further increase nonradiative decay pathways and quench the luminescence.⁵¹ The EL spectra of the LEDs resemble the PL spectrum of PFM suggesting that PFM molecules may act as dominant recombination sites in the blend with PFO. However, they generally show significant additional green and red components giving a broadened spectral width. A possible explanation also for this behavior is that there are strong interference effects at play, both at the cathode and the ITO/glass interface.⁵²⁻⁵³ This is supported by the observation that the spectral changes are not a monotonic function of thickness. As a result of the longer wavelength components that coexist in the EL spectra at different thicknesses, the light emitted from these devices in some cases appears whitish blue in color, rather than pure blue. The fact that the optical transitions show some broadening in their spectral characteristics can also be an indication of significant molecular dispersion of the fluorene and the amine units in the blend film. Another possibility concerning this bathochromic shift could be preferential recombination at charge (electron or hole) shallow trapping sites in the bulk.

Figures 4.11 and 4.12 below show the dependence of the current density and the luminance on the applied voltage for single layer ITO/PFO:PFM/Dow metal LEDs with different PFM concentrations. The emissive layer thickness was 100 nm for all the devices. Figure 4.13 shows the dependence of the quantum efficiency in cd/A on the voltage for the same set of devices.

Chapter 4: Blue light emitting diodes from blends of polyfluorene (PFO) and hole transporting materials

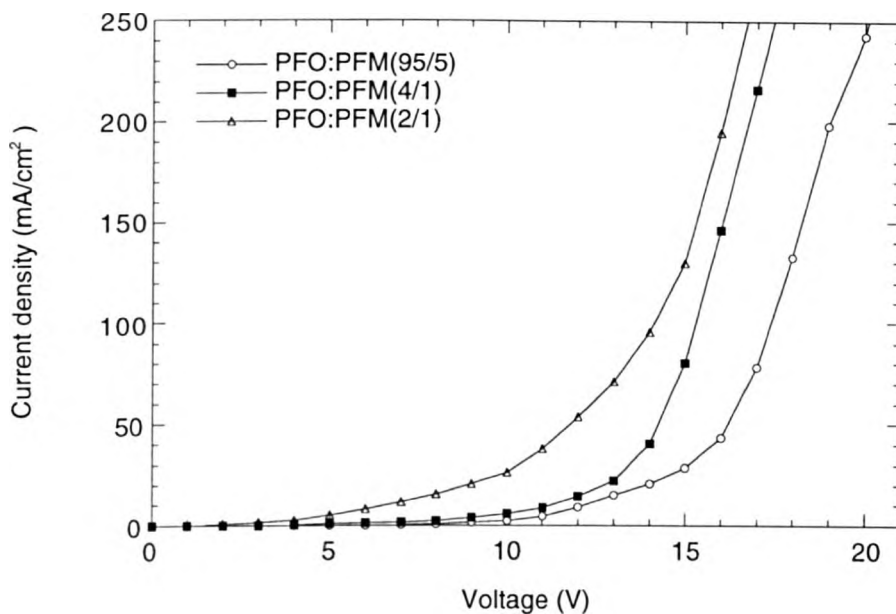


Figure 4.11: Current density vs. voltage characteristics for ITO/PFO:PFM(100nm)/Dow metal LEDs with varying PFM concentration [5wt.% (open circles), 20wt.% (filled squares) and 33wt.% (open triangles)].

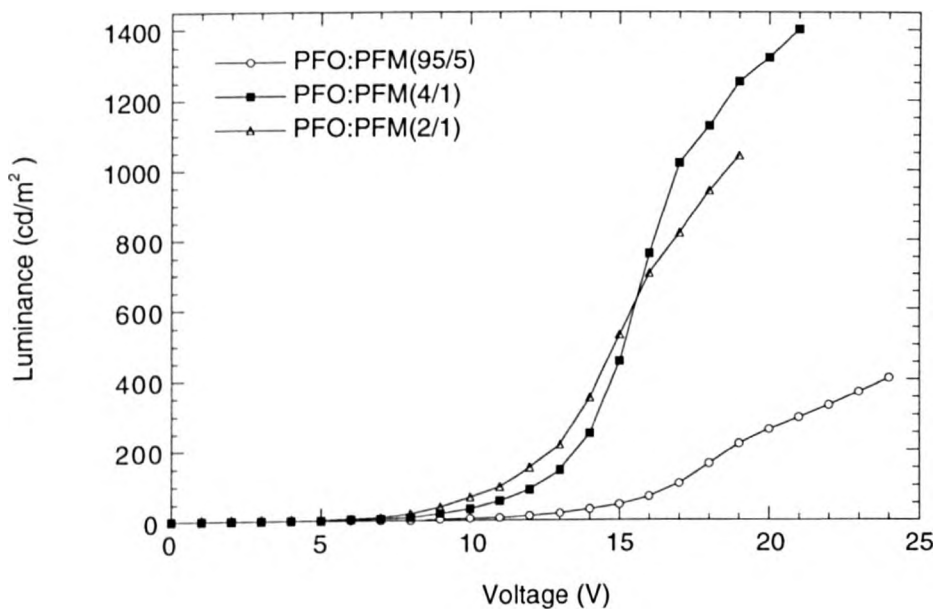


Figure 4.12: Luminance vs. voltage characteristics for ITO/PFO:PFM(100nm)/Dow metal LEDs with varying PFM concentration [5wt.% (open circles), 20wt.% (filled squares) and 33wt.% (open triangles)].

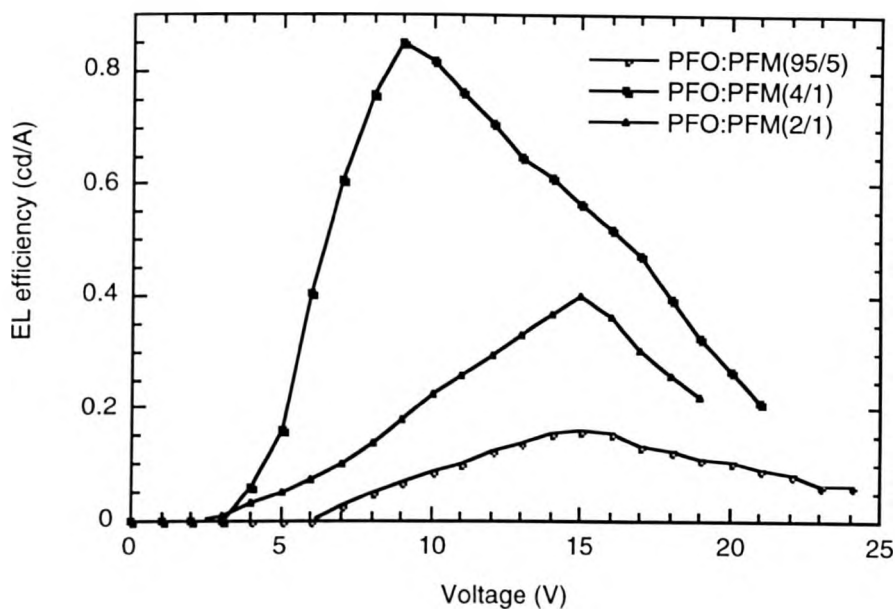


Figure 4.13: EL efficiency (cd/A) vs. voltage characteristics for ITO/PFO:PFM(100nm)/Dow metal LEDs with varying PFM concentration [5wt.% (open circles), 20wt.% (filled squares) and 33wt.% (open triangles)].

The doped devices showed an enhanced injection current density depending on the PFM concentration compared to the undoped PFO devices that showed a maximum current density of less than 100 mA/cm^2 at a high driving voltage of over 20 V. A significantly lower onset and operating voltage is thus achieved in the blend due to the reduced barrier for the injection of holes from the ITO to the PFM. In the absence of the hole transport material in the blend, hole injection is difficult due to the high ionization potential of PFO, namely 5.8 eV and is thus the limiting process for the overall device performance. Electrons appear to be the majority carriers in PFO LEDs with a Dow metal cathode and an ITO anode and the incorporation of an appropriate hole-transporting layer is expected to markedly improve the device performance. With the increase of the dopant concentration, the injection current was significantly increased. In particular, a current density of 50 mA/cm^2 was reached for PFM doping levels of 5, 20 and 33 wt% at 16V, 14V and 12V, respectively. Thus, the devices'

operating voltage was substantially lowered by increasing the PFM concentration. Figure 4.14 shows a schematic energy level diagram of the different components.

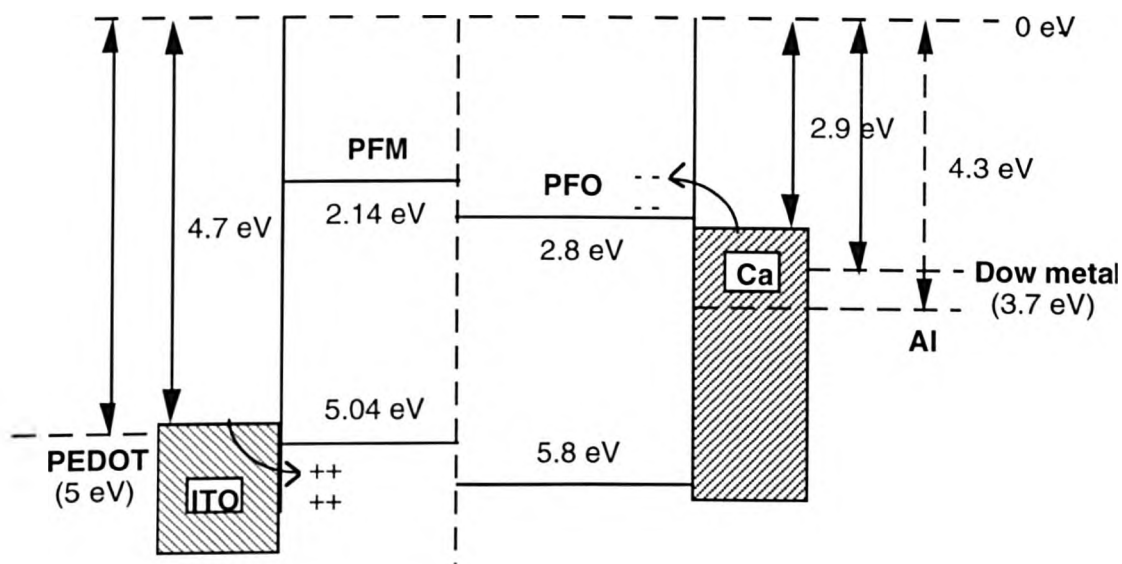


Figure 4.14: Energy level diagram of the different materials. Highest occupied molecular orbital (HOMO) levels were determined from cyclic voltammetry (CV) measurements. The PEDOT:PSS workfunction was estimated by applying electroabsorption spectroscopy to probe the electrode workfunction (more details for this estimation will be given on the next chapter). The LUMO level positions have not been measured directly but they were estimated by subtracting the optical gap from the HOMO value for each component.

The current voltage characteristics of the blend LEDs are mainly determined by the injection of the majority carriers in the bulk. By incorporating hole transporting molecules in the blend, a higher proportion of hole transporting HOMO energy levels will be available with increasing PFM concentration and this is expected to facilitate the hole injection from the ITO anode resulting in a lower operating voltage. On the other hand, the higher LUMO level position of PFM compared to PFO is not expected to affect electron transport in the blend to a large extent. By blending a hole transport material PFM into PFO, a significant increase of the bulk conductivity is also expected to occur that further accounts for the reduction in the

operating voltage with increasing PFM concentration. Another possibility is that PFM units provide intermediate energy levels, populated by rapid charge transfer between the HOMO levels of PFO and the ITO Fermi level that facilitate hole injection in the bulk of the device. The emission intensity is also limited by hole injection and the addition of hole transporting molecules increases significantly the device luminance. A maximum brightness of 1400 cd/m^2 is reached for the device with 20 wt.% PFM compared to a maximum brightness of 400 cd/m^2 for 5 wt.% PFM. The maximum luminance decreases to 1050 cd/m^2 for a device with 33 wt.% PFM concentration. Again the onset voltage for emission decreases with increasing PFM concentration as well as in comparison with pure PFO. Another trade off using a higher concentration of PFM is the reduction of the LEDs' efficiency because of an imbalance of electrons and holes in the device due to an excessive amount of holes that are transported through the device without recombination with electrons. The maximum quantum efficiency reaches 0.85 cd/A for a 20 wt.% PFM concentration compared to a maximum of 0.15 cd/A for 5 wt.% PFM but it is reduced to a maximum of 0.4 cd/A for 33 wt.% PFM.

Figures 4.15 and 4.16 compare the current density and luminance versus voltage characteristics for a series of single layer blend LEDs with 20 wt.% PFM, varying blend thickness and a Dow metal cathode. This concentration was used because it was found to give the best performance in terms of highest EL efficiency and brightness as we already showed before. Atomic force microscopy was also used to investigate the morphology of the blends and a $1 \mu\text{m} \times 1 \mu\text{m}$ AFM image of a PFO:PFM blend with 20 wt.% PFM is shown in Figure 4.17 below. This image shows that phase separation on a 20-30 nm scale occurs in the blend due to the low entropy of mixing, resulting in the presence of two distinct phases. Therefore a great deal of interfaces between the two polymers occurs in the blend that will significantly affect the transport and recombination processes, particularly under the influence of an external electric field during device operation.

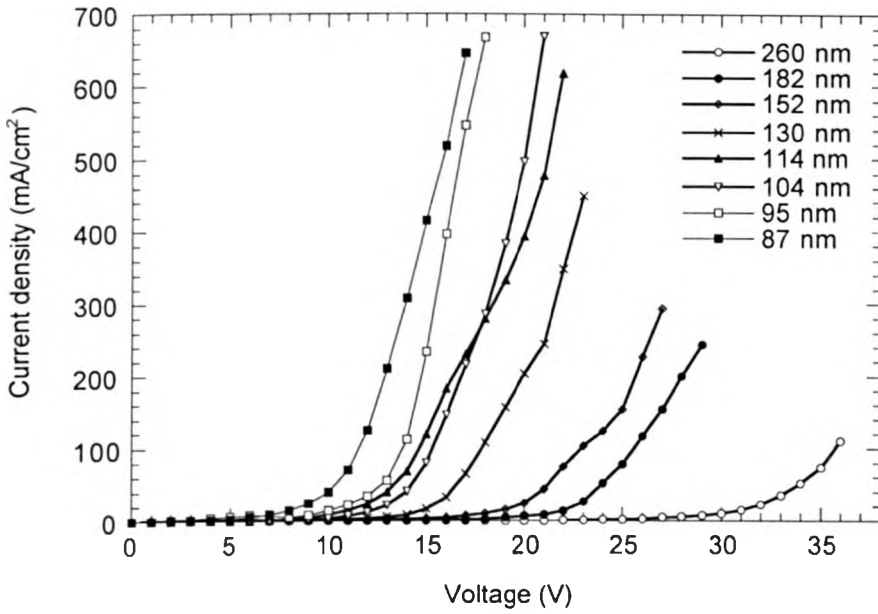


Figure 4.15: Current density - voltage characteristics for ITO/PFO:PFM(4/1)/Dow metal LEDs.

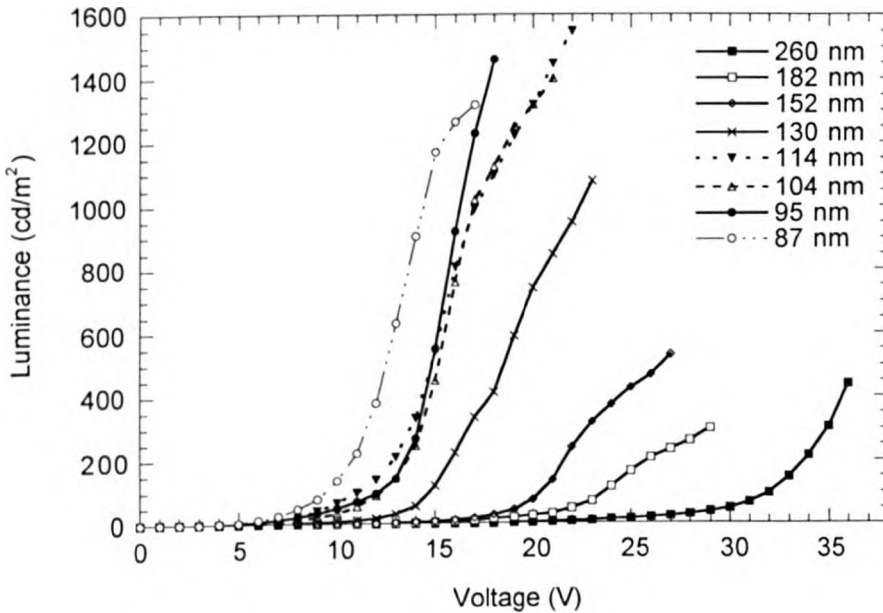


Figure 4.16: Luminance - voltage characteristics for ITO/PFO:PFM(4/1)/Dow metal LEDs.

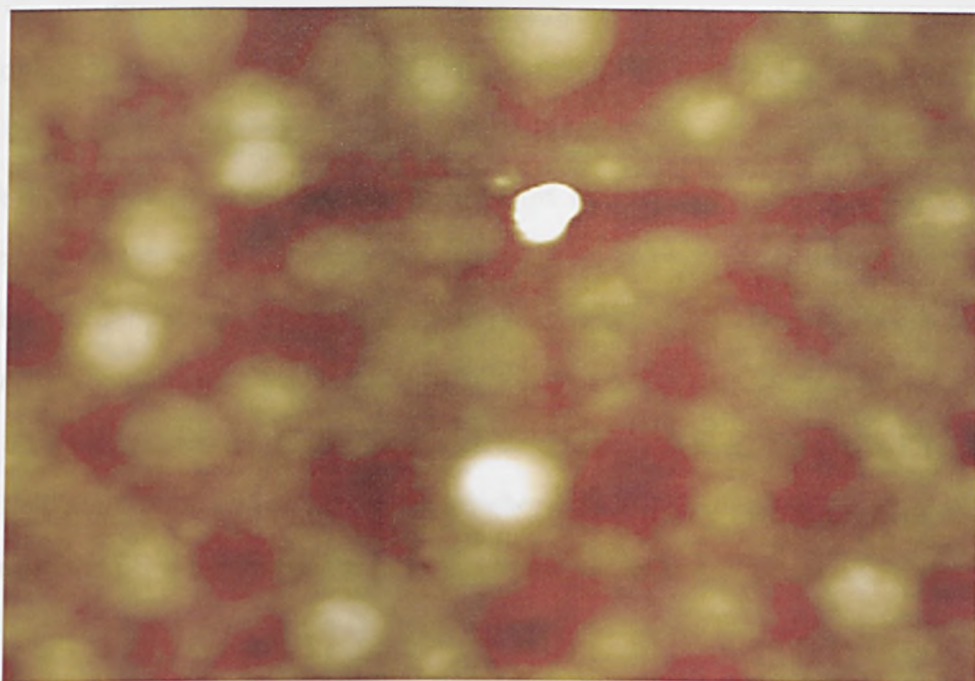


Figure 4.17: Topographical atomic force microscopy image of a PFO:PFM (20wt.%PFM) blend.

The best performance in terms of EL quantum efficiency at high brightness is achieved for a thickness of 104 nm. A maximum EL efficiency of 0.87 cd/A or 0.4% and a maximum power efficiency of 0.3 lm/W is achieved for a brightness of 40 cd/m^2 . This device turns on at 6.5 V (the bias required to give a luminance of 5 cd/m^2) which corresponds to an electric field of 0.6 MV/cm. At 100 cd/m^2 , the quantum efficiency is 0.65 cd/A or 0.33% and the power efficiency is 0.18 lm/W. The same device reaches a maximum brightness of 1550 cd/m^2 at 22 V and for a current density of 620 mA/cm^2 . At this maximum brightness, the external quantum efficiency is 0.25 cd/A or 0.13% and the power efficiency is 0.04 lm/W. The fact that the quantum efficiency is voltage dependent points towards an unbalanced electron and hole injection and transport in the blend. The maximum EL efficiency is achieved when the balance between the injected carriers is optimal in the film and the highest fraction of them radiatively recombines. Quenching of excitons from positively charged polarons can

reduce the EL efficiency at higher fields. A change of the local morphology (through the formation of aggregates) of the blend film under intense electrical excitation may also play a role in the quenching process. The significant reduction of the efficiency at high current densities can further be attributed to the transport of a significant number of holes that increases with electric field through the film without recombination with electrons. The barrier for electron injection from the Dow metal cathode to the LUMO of PFO is relatively high thus the contribution of the electrons to the total device current is expected to be injection limited. Due to the increase of the density of accumulated positive charges with increased electric field in the bulk, we can expect that a higher fraction of excitons that would otherwise contribute to the EL will be quenched from free or trapped holes at high electric fields.

Comparing devices with different emissive layer thickness we observe a significant increase in the current density for a fixed voltage as the thickness decreases. Both the onset and the operating voltage decrease continuously with decreasing thickness. The EL efficiency and the luminance increase with decreasing thickness until a thickness of ~ 100 nm and then decrease as the device become thinner. The lower current at a fixed voltage with increasing thickness is attributed to the lower electric field that results in a decreased carrier injection. The fact that the maximum efficiency starts to drop for films below a certain thickness, taken with the spectral changes, also points to the influence of interference effects. Exciton quenching at the cathode and nonradiative energy transfer to the metal electrode also reduce the luminance in thinner devices. The lower luminance at a fixed voltage with increasing thickness is attributed to the reduced number of excitons formed by carrier recombination. For thicker films, the charge trapping and the reduced hole mobility may reduce the charge recombination probability resulting in lower efficiencies compared to thinner films.

Chapter 4: Blue light emitting diodes from blends of polyfluorene (PFO) and hole transporting materials

An over two orders of magnitude improvement in the maximum luminance and efficiency is achieved for the doped LEDs compared to identical PFO devices. This occurs despite the reduction in PL efficiency for the blend. Consequently, a better charge balance that leads to more efficient recombination is implicated. The trapping of holes on the PFM sites can reduce their discharge at the cathode and may well increase the probability for encountering an electron and thus forming an exciton. It can also cause the formation of a hole space charge which adds to the external field. This will result in a redistribution of the electric field (enhancement at the cathode and reduction at the anode) which will enhance the electron injection rate from the cathode and block the hole leakage current that does not contribute to the emission finally resulting in a higher carrier recombination probability.

Charge trapping is thought to play a significant role in the emission process under electrical operation. PFM molecules are thought to act as dominant recombination centers. Förster transfer of excitons formed on PFO to PFM can still occur but charge (electron) transfer from PFO to PFM via a hopping mechanism can be an important pathway leading to substantial emission preferentially originating from PFM. By comparing the spectra of the films excited optically versus electrically it is concluded that the EL spectra have an increased contribution from PFM emission at a given PFM concentration which indicates the importance of charge transfer in the operation of LEDs based on a host-guest system.⁵⁴⁻⁵⁵ Both Förster transfer and charge transfer from PFO to PFM occur under electrical operation. Only Förster transfer is expected for optical excitation. Recombination on the PFM molecules may become more favorable due to their dual action as hole traps in PFO and as electron hopping sites. Electron transport can take place by hopping between PFO and PFM molecules. As the PFM concentration is increased, the distance between the PFM molecules becomes shorter and electrons may be shared more equally between PFO and PFM molecules resulting in an increased probability of electron hopping between adjacent host-guest sites.⁵⁶

4.5 Time of flight and electroabsorption spectroscopy

The interpretation that the introduction of the hole transporting molecules modifies the charge trapping is supported by transient electroabsorption measurements, time of flight (TOF) spectroscopy and electrical measurements of hole and electron only LEDs. Below, an analytical description of the results obtained using the above techniques will be presented with emphasis given on the interpretation of the results and how they account for the improved performance of the blend LEDs. Figure 4.18 presents current mode TOF transients for holes and electrons in PFO:PFM blends with 20-wt % PFM concentration. The device configuration was ITO/PFO:PFM(4/1)/Au(35nm) with a semitransparent gold cathode. The thickness of the blend was 1 μm and the applied field was 0.5 MV/cm.

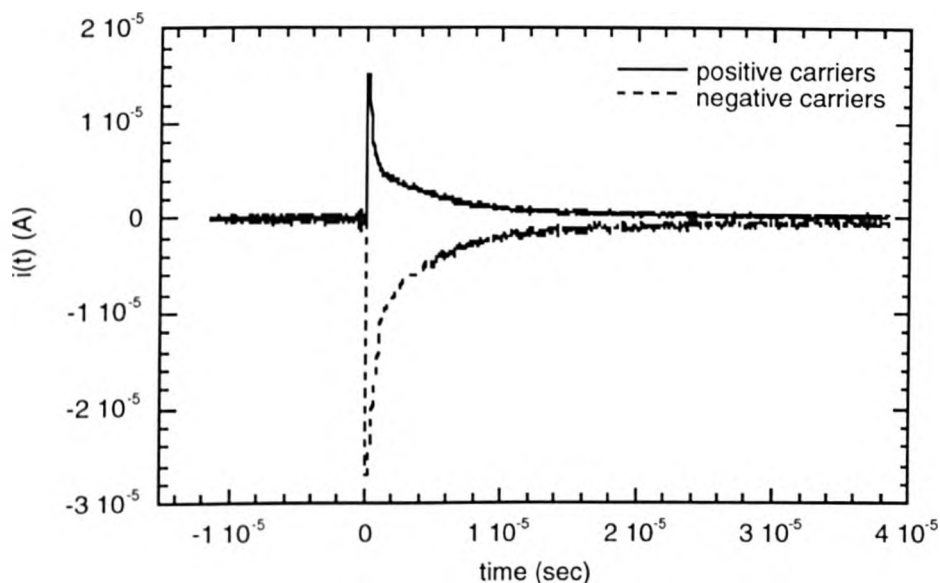


Figure 4.18: Typical current mode time of flight (TOF) transients for both holes (continuous line) and electrons (dashed line) in PFO:PFM blend films with 20-wt.% PFM concentration. The device configuration was ITO/PFO:PFM(4/1)/Au(35nm).

Evidence for hole trapping on PFM is obtained from these measurements. The shape of the positive transient photocurrent signal changes from the nondispersive transient, characteristic of both PFO⁴³ and PFM⁴⁴ polymers, to a dispersive transient for the blend. No clear carrier transit times could be obtained even from the corresponding current vs. time log-log plot for holes. Hole transport has become dispersive in the blend with a hole mobility apparently orders of magnitude below than that in PFO and PFM due to the trapping of holes in the bulk. The formation of traps is also consistent with the large difference in the ionization potential between the host PFO and the guest PFM. These localized hole trapping sites in the bulk of the film can act as efficient quenching centers for singlet excitons formed at the PFM sites further reducing the radiative decay rate and thus the quantum efficiency with increased voltage. The negative carrier transient also shows no discernible carrier transit time for electrons on the log-log plot. Electron transport in the blend is highly dispersive in agreement with the dispersive electron transport that has been observed in each of the individual components.⁴³⁻⁴⁴ Any photogenerated or injected electrons will thus be heavily trapped.

However, we observed that when the applied voltage is switched from positive to negative to record electron transients the signal decreases in magnitude with repeated photoexcitation. When the voltage is switched from negative to positive to record hole transients the signal decreases more substantially. The steady state signal magnitude was about a factor of 2 smaller for holes than that for electrons which provides a good indication that holes are trapped to a similar extent to the electrons. It is clear that the trapping will lead to a reduction in the hole mobility for the blend compared to the hole mobilities of the two individual compounds but it is not clear to what extent it will affect the electron mobility of the blend with regard to the individual electron mobilities. However, hole and electron mobilities are expected to be more similar in the blend configuration which implies than a significantly better charge balance between the majority hole current and the minority electron

current will occur in the blend compared to the individual compounds where the hole mobility is at least 3 orders of magnitude higher than the electron mobility.⁴³⁻⁴⁴ The recombination zone, which would otherwise be expected to lie closer to the cathode due to the fact that the electron mobilities are much lower than the hole mobilities, may be located further into the bulk in the case of the blend. This is expected to reduce the probability of nonradiative recombination for the blend LEDs and thus contribute to the increase of the device efficiency.

Electroabsorption (EA) spectroscopy in LEDs was also employed in order to study charge trapping as well as a probe technique for the cathode workfunction.⁵⁷ Single layer LEDs were prepared with an ITO anode, PFO, PFM or a PFO:PFM blend with varying PFM concentration and a semitransparent Al or Dow metal cathode. The EA spectrum was measured with a $V_{AC} = 1.5$ V. The spectrum of a PFO LED shows a broad peak at 402 nm. The EA spectrum of a PFM LED for different d.c. voltages is shown in Figure 4.19.

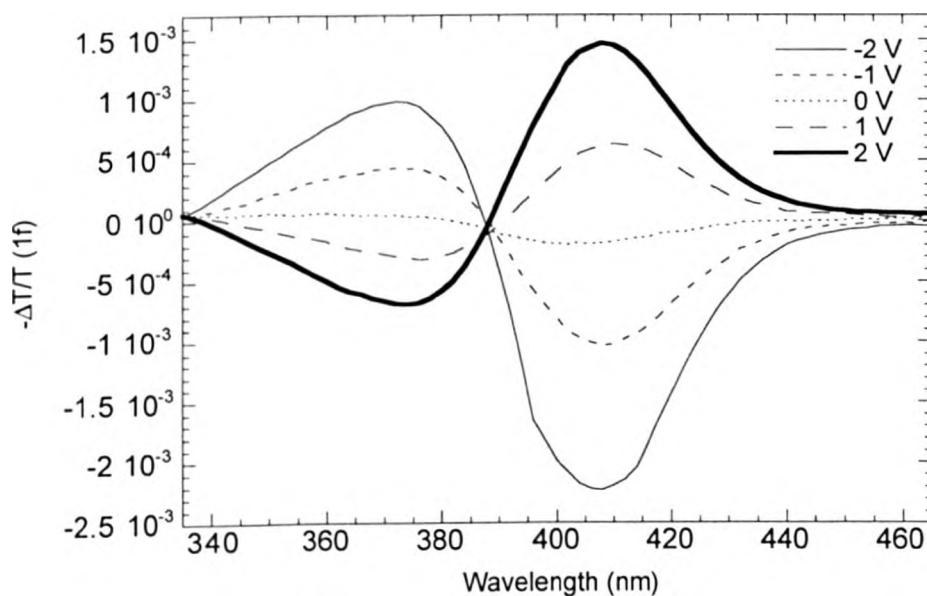


Figure 4.19: The EA spectrum of a PFM LED for different d.c. voltages at the frequency 1f.

The EA spectrum of a PFM LED (typical thickness of 100 nm) shows two peaks; a main peak at 406 nm and a secondary peak at 372 nm. The main peak coincides approximately with the peak of the first derivative of the absorption spectrum as expected from the equation that gives the Stark shift (see chapter 2) although deviations that have a very small effect on the EA peak have been found at wavelengths where the absorption is strong due to the use of reflection geometry that probes reflections at all the associated electrode/polymer interfaces. The EA spectrum has the same lineshape for all voltages with its magnitude depending linearly on the applied d.c. bias. Figure 4.20 presents typical EA spectra of PFO:PFM blends (20-wt.% PFM concentration) (100 nm thickness) for different applied d.c. voltages at the fundamental frequency $1f$.

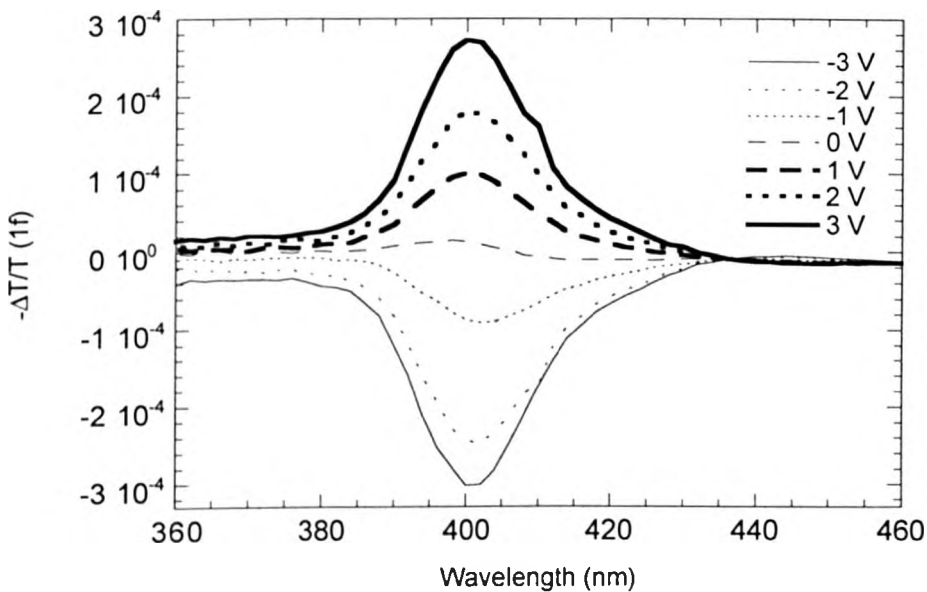


Figure 4.20: EA spectra of PFO:PFM blends (20-wt.% PFM) for different applied d.c. voltages at $1f$.

The EA spectra of the PFO:PFM (4/1) blend LEDs are almost identical to the EA spectra of the PFO LEDs with a main peak at 402 nm. They have the same lineshape for all

applied d.c. biases and their magnitude is controlled by the d.c. bias. The EA signal for both PFO and PFM LEDs varied linearly with the applied d.c. bias and it becomes null at the bias which corresponds to the workfunction difference (built in potential) of the two electrodes assuming that no band bending occurs at the anode and cathode interfaces.⁵⁸ For an Al cathode, the signal is zero at $V_{DC} = 0.4$ V while for a Dow metal cathode it is nulled at a d.c. bias of 0.9 V. If we assume that the work function of ITO is 4.6 eV, then an estimation of the workfunction of Al and Dow metal can be given by subtracting the above numbers from this value. Al's workfunction is found to be 4.2 eV and that of Dow metal is approximately 3.7 eV. An excellent agreement is found between the value of Al's workfunction from the literature and that from the experiment. Dow metal's workfunction is almost equal to the work function of Mg, again in excellent agreement with the theoretical value. Figure 4.21 shows the peak EA response versus d.c. bias for ITO/PFO:PFM (4/1)/Dow metal LEDs.

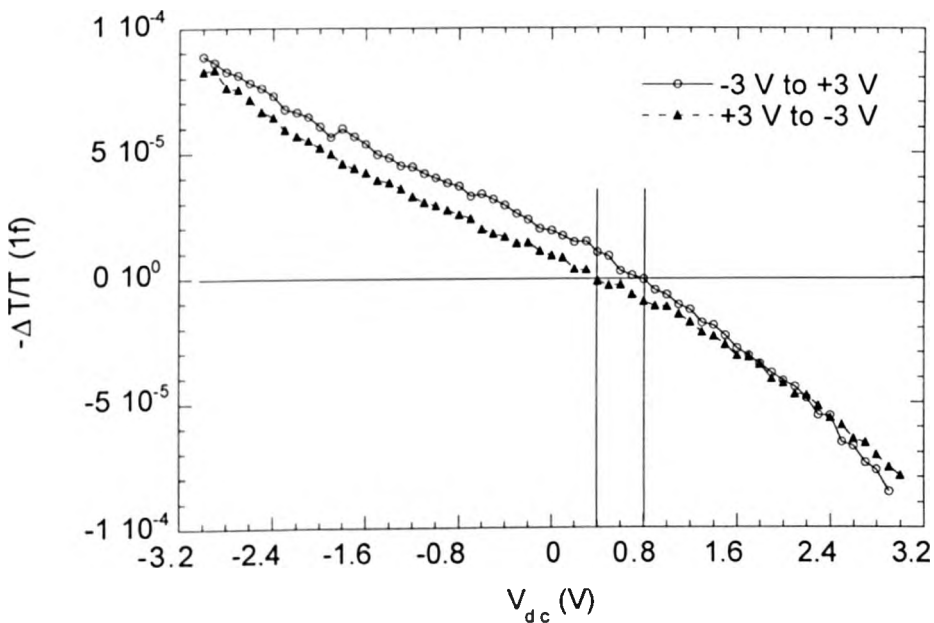


Figure 4.21: Peak EA response versus d.c. bias for ITO/PFO:PFM(4/1)/Dow metal LEDs.

The probe wavelength was the wavelength where the EA signal exhibits a maximum (402 nm). The AC bias was 1 V and the d.c. bias was scanned first from -3 to +3 V in the forward bias direction and then from +3 to -3 V in the reverse bias direction. For PFO and PFM, the plot is simply a linear function of the applied bias. However, the plot for the blend is not a linear function of the applied voltage but it shows a deviation above 1 V. Also the response of the LED is different depending on whether the sweep is performed in the forward bias or the reverse bias direction. We found that the zero point when the device is swept from -3 to +3 V (forward bias direction) occurs at 0.8 V which is 0.4 V higher than when the device is swept from +3 to -3 V (reverse bias direction). This is explained as a hysteresis effect due to the modification of the electric field distribution within the blend.⁵⁹

In order to test the influence of this dynamic effect on the internal electric field of the devices, we applied a d.c. voltage of 4 V to each device (which was always below the onset voltage for light emission in order to avoid any possible distortion from the emitted light on the measured EA signal) and we then recorded the EA signal as the DC bias was first switched to the built-in potential and then turned off (0 V) and on (4 V) again, for a few subsequent cycles. The voltage was “on” and “off” for 30 and 100 sec, respectively in each cycle. Each device was probed with monochromated light of wavelength equal to that where the EA response shows its maximum value. Figure 4.22 presents the EA(1f) signal dynamics of ITO/PFO/Dow metal LEDs as a function of time. The inset shows the EA(1f) signal dynamics of ITO/PFM/Dow metal LEDs. A fit of the EA(1f) signal for the PFM based LEDs to a single exponential function (regarded as the first order approximation of a two order polynomial function) is also shown. Figure 4.23 shows the EA(1f) signal dynamics of ITO/PFO:PFM/Dow metal LEDs at a 10-wt.% concentration of PFM. A fit of the signal to a polynomial function with a table presenting the fit parameters is also shown.

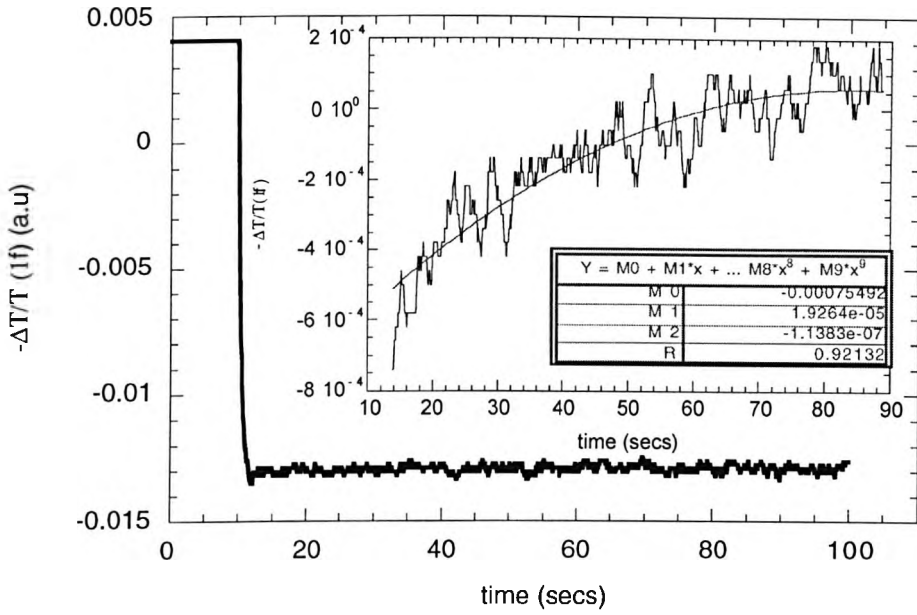


Figure 4.22: The EA(1f) signal dynamics of ITO/PFO/Dow metal LEDs. The inset shows the EA(1f) signal dynamics of ITO/PFM/Dow metal LEDs. A fit of the signal to a polynomial function is also shown.

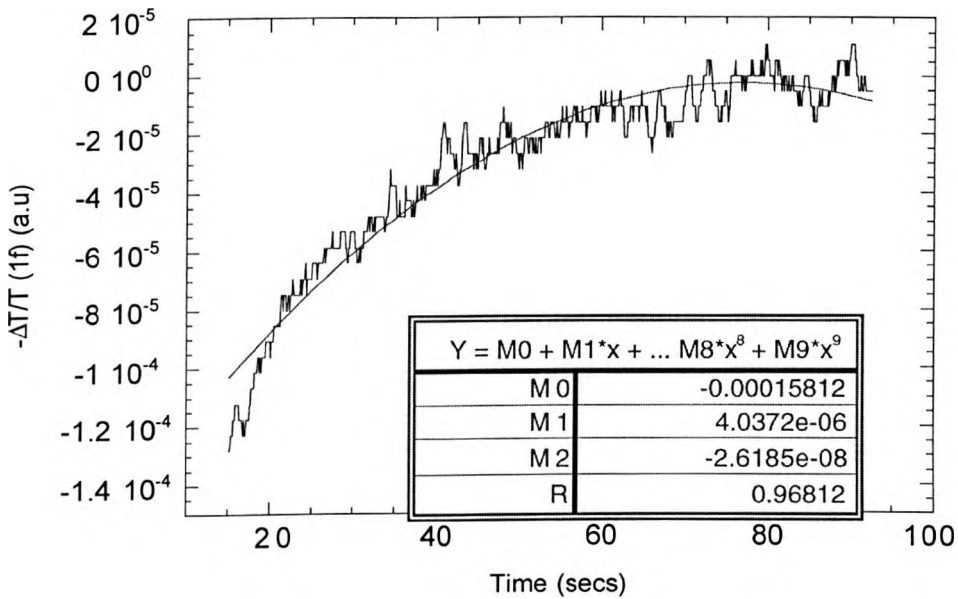


Figure 4.23: The EA(1f) signal dynamics of ITO/PFO:PFM/Dow metal LEDs at a 10-wt.% concentration of PFM. A fit of the signal to a polynomial function with a table presenting the fit parameters is also shown.

Chapter 4: Blue light emitting diodes from blends of polyfluorene (PFO) and hole transporting materials

For pure PFO LEDs, when the DC bias is turned off we observed that the EA signal also falls to zero. In contrast, for PFM LEDs the situation is somewhat different. When the DC bias was turned off, the EA signal does not fall to zero. It rather reverses sign and then it slowly decays to zero. The dynamics of the EA response could be fit to an exponential decay function. The time constant of this decay was in the range of 35 to 40 seconds depending on the applied d.c. bias. The induction of an internal counter electric field that opposes the external applied field has been proposed by Giebeler *et. al.* to account for the dynamics of the EA response in MEH-PPV diodes.⁵⁹ This counter electric field will result in a redistribution of the electric field within the device and it has further been attributed to trapped charge within the bulk of the device. Its existence also explains the hysteresis effect observed before. While it develops quickly enough so that during the forward voltage sweep only the steady electric field within the device will be measured, it decays more slowly so that during the reverse voltage sweep a steady electric field will not be restored in the bulk resulting in some hysteresis of the EA peak signal. For PFM doped PFO LEDs with a 5 wt-% PFM concentration, the EA signal is dominated by the PFO EA signal and falls to zero with turning off the device with no discernible EA decay. However, when the PFM concentration is increased to 10%, the EA signal shows a dynamic effect with a decay of the signal to zero with turning off the applied bias. Its dynamics could also be fit to an exponential decay function with a time constant in the range between 30 and 35 seconds. It should be pointed out that in reality we have been able to fit the EA dynamics with a second order polynomial function which results in a single exponential decay function if only the first order term of the polynomial is used on a Taylor polynomial series. The very similar dynamics of the EA response and the counter electric field in PFM and doped PFO LEDs with 10 wt.% PFM is a strong indication that the trapped charge is related to holes that are deeply trapped in PFM HOMO sites which are molecularly dispersed in the PFO layer. The fact that the traps were observed only at a PFM concentration higher than 5% in PFO may indicate that the

population threshold of the intermediate PFM low HOMO levels for holes to be trapped is between 5% and 10%. For 20% PFM concentration in PFO, trap decay times in the order of 30 seconds were also obtained. The trap decay time τ depends on the trap activation energy or in other words the trap energy level according to the following relation:⁵⁹

$$E_{\text{trap}} = kT \ln(-\tau/\sigma N \langle v \rangle) \quad (\text{assuming trap degeneracy of 1})$$

where E_{trap} is the trap activation energy, σ the capture cross section that is defined by the physical size of the traps, N the density of transport states, $\langle v \rangle$ the mean carrier velocity [$\langle v \rangle = (3kT/m)^{1/2}$], k the Boltzmann constant and T the temperature (kT is the thermal energy). We can estimate that N is in the order of 10^{20} cm^{-3} from conjugation length size, that σ is in the order of 10^{-14} cm^2 and that $\langle v \rangle$ is in the order of 10^2 cm/sec from estimates of the effective polaron mass m^* .⁵⁹ At room temperature $T = 300 \text{ K}$ we can then estimate a trap energy, $E_{\text{trap}} = 0.4 \text{ eV}$ ($\tau = 30 \text{ sec}$). These traps are associated with the low HOMO PFM levels and may compete with them in the trapping/detrapping process in the blend.

Unipolar carrier devices were also fabricated in order to study the effect of the dopant on the trap distribution in the emission layer. Electron only LEDs were fabricated with a Dow metal semitransparent metal anode (40 nm), a single layer of PFO, PFM or the blend and a Ca cathode. Hole only devices were fabricated with a 40 nm thick Au layer as the anode, a single layer of PFO, PFM or the blend and a 200 nm thick Au cathode. The J-V characteristics of these LEDs obeyed the power law expressed as $J \propto V^{m+1}$ fairly well, where m varies depending on the dominant charge transport process and the trap distribution in the bulk. If the transport is dominated by the ohmic law, the m value is 0. If it is dominated by the square law (space charge limited current), the m value is 1 when either no traps or a discrete trap level are present. For $m > 1$, the current obeys space charge limited law with traps and the m value gives information for the characteristics of the trap distribution.

For hole only PFO devices with a Au hole-injecting contact, we observed an m value of 0.5 up to an electric field of 1.5 MV/cm which indicates that the current conduction follows a combination of ohmic and trap-free space charge limited law. For hole only PFM devices with a Au contact, an m value of 2 was observed up to the same electric field indicating space charge limited hole conduction with traps. When ITO coated with PEDOT/PSS was used as the anode, we observed m values of 1 and 0 for PFO and PFM for all electric fields indicating trap-free space charge limited conduction (SCLC) and ohmic conduction, respectively. This indicates that for PFM, PEDOT/PSS is an ohmic contact for holes in contrast to Au which is a hole-blocking contact. For PFO, neither Au nor PEDOT/PSS can provide an ohmic contact. The low ionization potential of PFM, 5.04 eV (in contrast to the high HOMO of 5.8 eV for PFO) and the non-dispersive hole transport in PFM⁴⁴ can account for the above observations. Similar results have been obtained for a PFM fluorene-triarylamine copolymer (with a low ionization potential of 4.98 eV) with the same contacts in hole only LEDs by Campbell *et. al.*⁶⁰ For the case of PFO:PFM (4/1) blends, the I-V profile for either contact had two parts with different voltage dependence. It varied from a square-law profile ($m = 1$) up to 0.8 MV/cm to an m value of 2.5 for higher electric fields with a Au contact indicating that hole transport occurs through the PFM HOMO levels that act as hole traps in the blend. With a PEDOT/PSS contact the profile varied from $m = 0$ below 3 V (ohmic law) to $m = 1.5$ (SCLC with traps) above 3 V indicating that hole injection takes place to the PFM HOMO levels at low voltages which act as shallow traps limiting the mobility. Hole transport then proceeds by hopping between the HOMO levels of PFM chains with detrapping eventually taking place followed by holes moving towards the cathode. Blom *et. al.*⁶¹ have also found that lowering the hole mobility to an optimum value can result in significantly higher device efficiencies for single layer PLEDs based on poly (p-phenylene vinylene) derivatives compared to similar compounds that have much higher hole mobilities.

For electron only PFO devices, we obtained an m value of 0 in the range 0 to 2.5 V indicating that ohmic conduction may take place between Ca and the LUMO of PFO although doping of PFO with Ca that would result in an ohmic contact can not be excluded. The m value increased to 5 and 7 at low (< 1 MV/cm) and moderate (1-1.7 MV/cm) electric fields indicating that the electron current follows a space charge limited current law and is affected by the presence and filling of traps. Reaching the trapped charge filled limit above a field of 1.8 MV/cm, we observed an abrupt change of the I-V profile with the m value approaching 20 which is a result of the double charge carrier injection taking place at high fields reaching the EL threshold field. For PFO:PFM(4/1) electron only LEDs, m values of 1 were obtained below 2.5 V indicating that electron transport follows space charge limited conduction and is affected by the presence of PFM. Transport takes place by a hopping process not only between the PFO LUMO levels but probably also between adjacent PFM and PFO LUMO levels. The I-V profile had two parts with different voltage dependence. It first followed square law profile with traps ($m = 2.5$) below 1.3 MV/cm. The m value then increased to 6 until a field of 2.1 MV/cm and above this field an abrupt current increase occurred accompanied by a large increase in the m value to 24 as the onset field for emission was reached. These differences in the m value between PFM and PFM doped PFO LEDs indicate that the electron transport and the distribution of trap states in PFO is significantly affected by PFM electron traps although the relative position of the LUMO levels of PFO and PFM would imply that electron transport in the blend should not be significantly affected by PFM.

So far we have only employed Al and Dow metal cathodes. Electron injection is thus the limiting factor in the device performance as a high barrier for electron injection occurs between the LUMO level of PFO and the Fermi level of those electrodes. Therefore, we employed a Ca cathode in order to improve the electron injection. Figures 4.24 and 4.25 show the EL spectra of ITO/PFO:PFM(4/1)/Ca LEDs as a function of thickness and current.

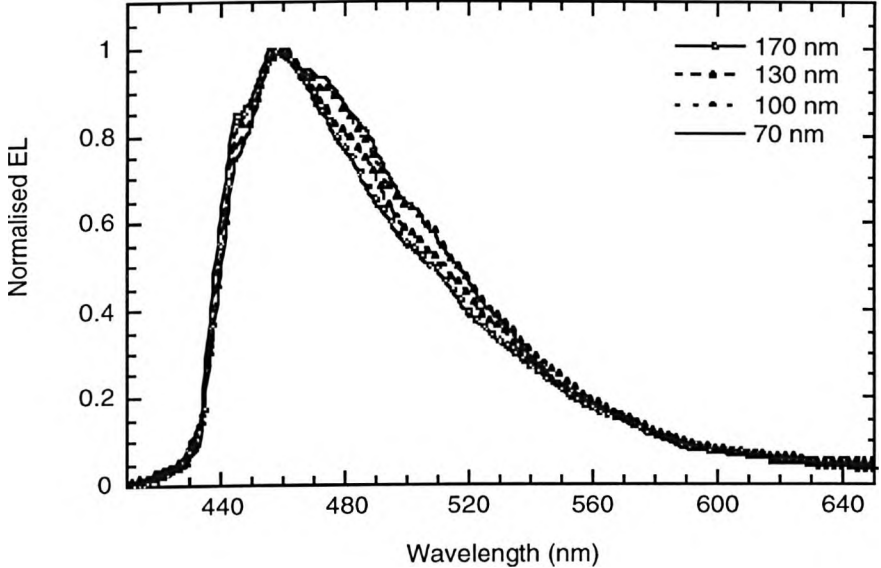


Figure 4.24: The EL spectra of a series of ITO/PFO:PFM(4/1) Ca LEDs with varying blend thickness.

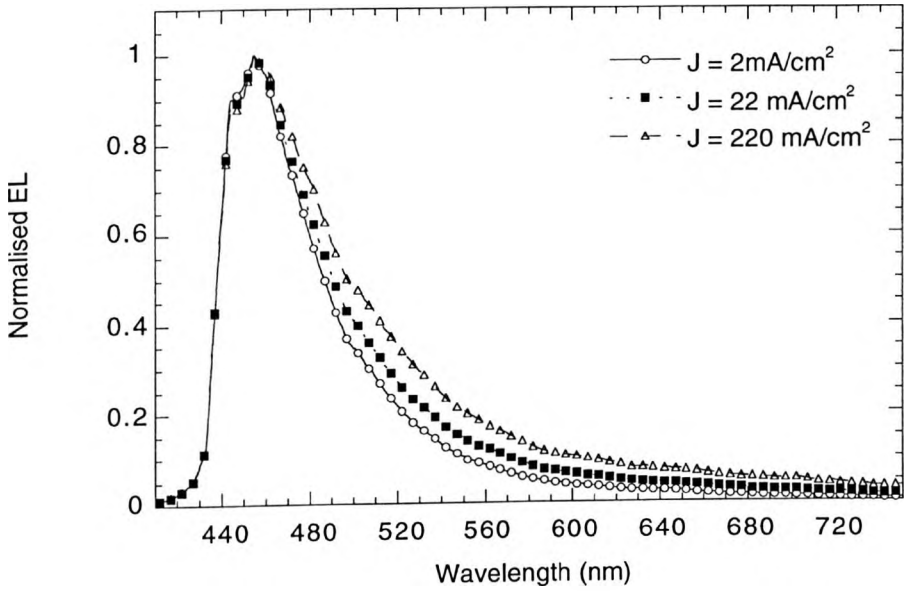


Figure 4.25: The EL spectra of ITO/PFO:PFM(4/1)/Ca LEDs as a function of the current density.

The EL spectra of the LEDs with a Ca cathode vary with the thickness of the emissive layer, however the variation is far less pronounced compared to the LEDs with a Dow metal cathode. This is probably due to two different reasons a) the significantly lower reflectivity of Ca which is expected to reduce the influence of interference effects on the EL spectrum and b) the higher electron injection ability of Ca that is expected to move the recombination and the emission zone further away from the cathode in the bulk and thus it will reduce undesirable charge transfer processes that are taking place between the emitting dipoles and the metal cathode and can influence the spectrum as well as reduce the emission efficiency. Also the peak wavelength at 455 nm is slightly shifted to the blue (about 15 nm for a thickness of 100 nm) and more closely resembles the PL spectrum of PFM for Ca cathodes, probably due to the effective combinatorial effect of the lower reflectivity and higher electron injection efficiency Ca which moves the recombination and emission zone away from the cathode. We also observed that a broadening of the EL spectrum with an increasing long wavelength tail takes place as the current density increases. However, no shift of the peak wavelength and no substantial difference on the relative oscillator strengths of the main peak and shoulder were observed with increasing current. This broadening of the spectrum is most probably associated with electrochemical degradation and reduced thermal stability of the blend due to the passage of electrical current and the exposure to heat due to the concomitant increase of the device temperature during operation. The low glass transition temperature of the two components (~ 70 °C) increases the tendency for spectral broadening at high currents. This has already been observed to be a common feature for most blue polyfluorenes although in some cases excimer emission or aggregate formation was considered to cause spectral broadening.³¹⁻³² This leads to reduced color purity (whitish-blue rather than pure blue) at high luminance levels in these LEDs. In Figures 4.26 and 4.27 the current and luminance vs. voltage characteristics of a series of ITO/PFO:PFM(4/1)/Ca LEDs with varying thickness are presented. Figure 4.28 shows the EL efficiency as a function of voltage for these LEDs.

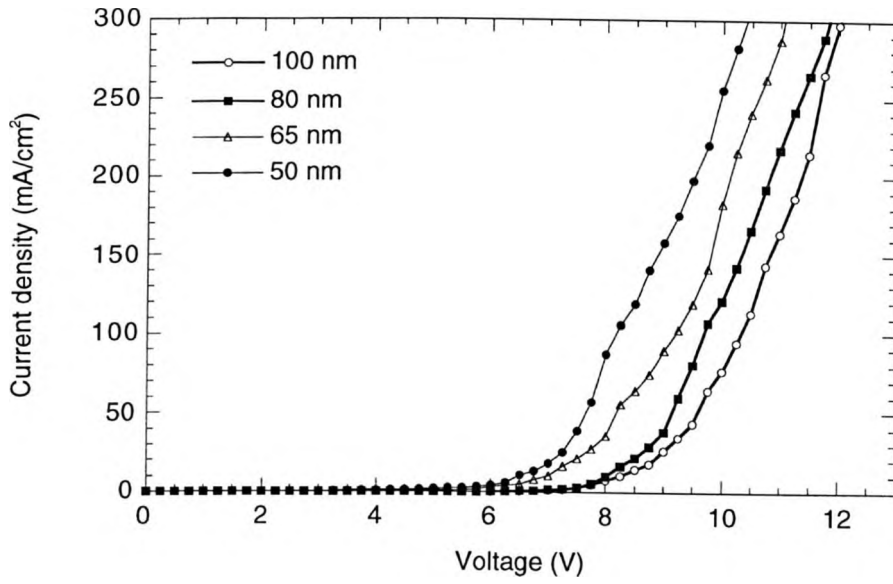


Figure 4.26: Current density vs. voltage characteristics of ITO/PFO:PFM(4/1)/Ca LEDs with varying thickness.

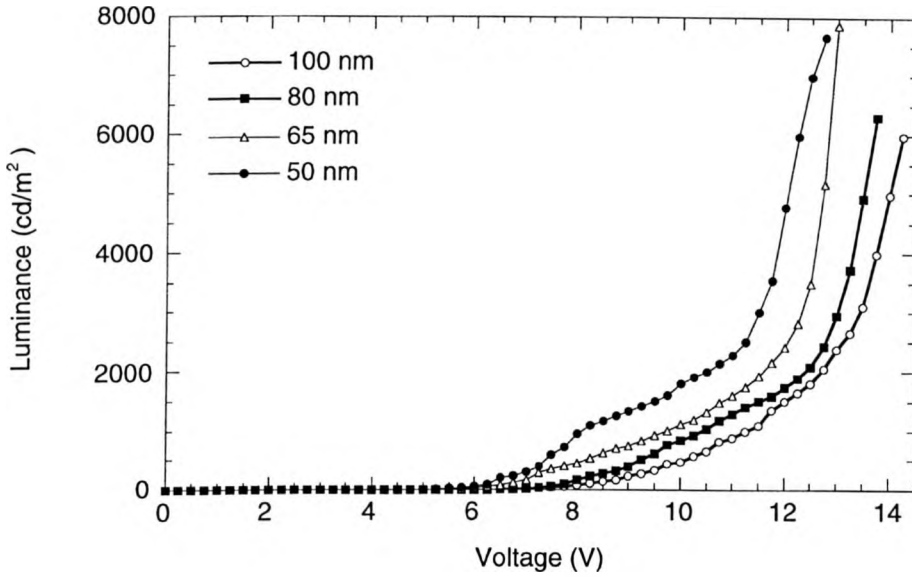


Figure 4.27: Luminance vs. voltage characteristics of ITO/PFO:PFM(4/1)/Ca LEDs with varying thickness.

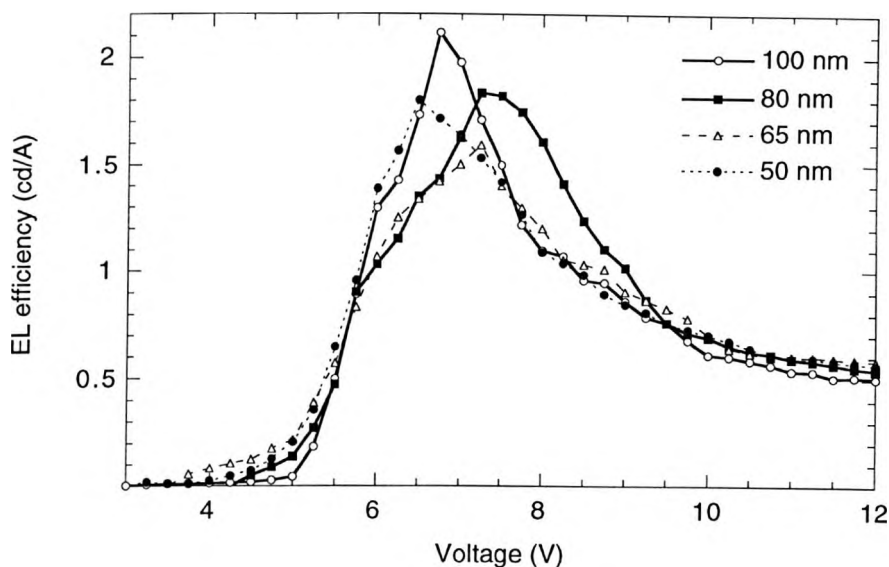


Figure 4.28: The external quantum efficiency as a function of voltage for this series of LEDs.

The best device performance in terms of maximum efficiency is achieved for a 100 nm thick blend layer. This device shows a maximum efficiency of 2.1 cd/A and a power efficiency of 1 lm/W at 15 cd/m² and also reaches a luminance of 6000 cd/m² at 14 V. The efficiency and brightness of the Ca devices are a factor of 2.5 and 4 higher compared to an identical device with a Dow metal cathode. This increase is attributed to the improved electron injection with Ca due to the lower injection barrier that electrons face at the interface which also moves the recombination zone further away from the cathode where emission quenching processes occur. However the imbalance of electrons and holes in the device with increasing charge carrier densities (with an excess hole current sweeping across the device) again results in a voltage dependent efficiency after a very fast and efficient electron-hole recombination at low voltages due to the facilitation of the hole injection by the PFM molecules. A thinner device (65 nm) reached a higher luminance of 8000 cd/m² at 13 V but the maximum EL efficiency was lowered to 1.6 cd/A. This optimized device also exhibits a peak brightness of

35,000 cd/m² at 50 V under a pulsed driving scheme (pulse width = 1 μs, pulse duration = 500 μs). We also fabricated blend LEDs with an emissive layer thickness of 100 nm and a 15 nm PEDOT/PSS layer on top of ITO. Figure 4.29 compares the current density and luminance vs. field characteristics of PFO:PFM blend LEDs with and without PEDOT:PSS.

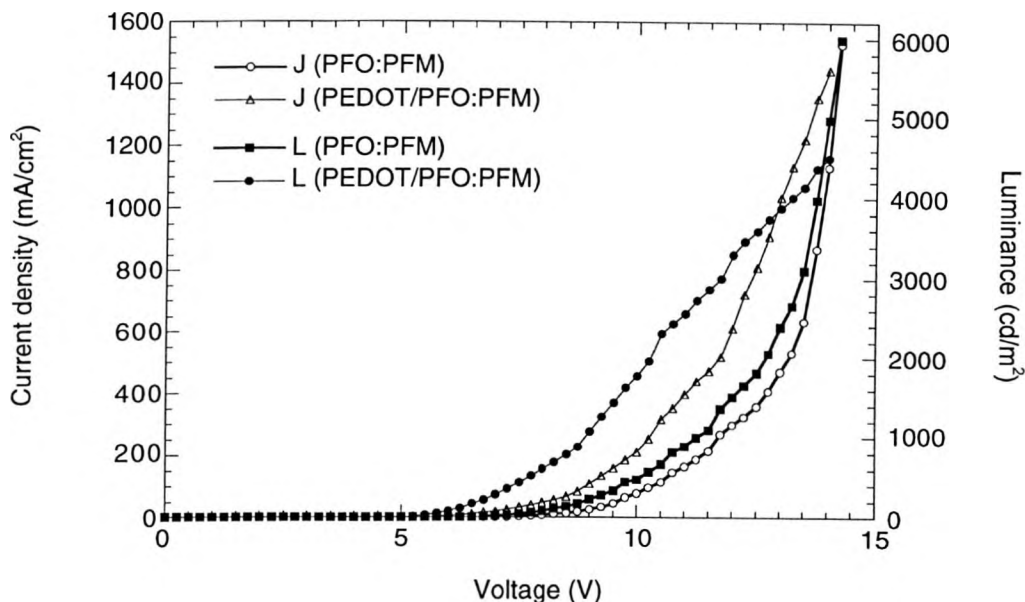


Figure 4.29: The current density and luminance versus electric field characteristics of a) ITO/PFO:PFM(4/1)(100 nm)/Ca and b) ITO/PEDOT:PSS(45 nm)/PFO:PFM(4/1)(100 nm)/Ca LEDs

Devices with PEDOT exhibit lower turn on as well as operating voltage and a higher luminance and current density at a certain voltage compared to devices without PEDOT. They reach a luminance of 100 cd/m² and a current density of 10 mA/cm² (arbitrarily defined as turn-on conditions) at 6 V compared to 8 V for devices without PEDOT due to the higher conductivity of PEDOT compared to PFM that allows more efficient hole injection especially at lower voltages. They also show a maximum power efficiency of 1.25 lm/W compared to 1 lm/W for devices without PEDOT:PSS. However they exhibit a lower maximum

brightness of 4500 cd/m^2 (compared to a luminance of 6000 cd/m^2 without PEDOT) while they show similar maximum quantum efficiencies of up to 2.1 to 2.2 cd/A ($\sim 1\%$) at 15 to 20 cd/m^2 . PEDOT has a workfunction of approximately 5.1 eV which aligns very well with the HOMO level of PFM (5.04 eV) and thus readily allows for holes to be conducted into PFM sites and then either transferred in the bulk and towards the cathode with or without recombination or get trapped to PFM sites that act as shallow traps before they are detrapped and recombine with electrons. Similar devices without PFM exhibit a much lower luminance of 800 cd/m^2 and an EL efficiency of 0.5 cd/A which confirms the significant role of hole trapping on the enhancement of the device performance. In general, we should note that the efficiencies quoted in this chapter are measured on fresh devices during the first voltage ramps and a small decrease of the efficiency was observed after a few successive runs due to electrical current assisted degradation, a characteristic observed in most blue PLEDs.

4.6 Conclusions

This chapter addresses the concept of blending an emissive conjugated polymer with a hole transport material as a means of improving the performance of single layer PLEDs. Applying this concept, bright and efficient blue LEDs based on a host-guest system with a poly(9,9-dioctylfluorene) (PFO) as a host and a hole-transport copolymer, poly(9,9-dioctylfluorene-co-bis-N,N'-(4-methylphenyl)-bis-N,N'-phenyl-1,4 phenylenediamine) (PFM) as a guest are realized. An optimum guest concentration of 20% by weight was found for maximum device efficiency and brightness. Despite the fact that the PL efficiency of the blend is lower compared to that of the host and guest polymers on their own, an enhancement in the efficiency is seen for the blend. A higher brightness and a lower turn on voltage are also achieved for the blend. This observation indicates that the hole transport material leads

to a significant improvement in hole injection and transport which consequently results in an improved charge balance factor and an increased exciton formation efficiency. Optimized LEDs showed blue emission with a peak wavelength at 455 nm, a maximum efficiency of 2.2 cd/A or 1%, a power efficiency of 1.25 lm/W and a luminance of 8,500 cd/m² at 13 V. A comparison of the PL and EL spectra also revealed that more emission originates from PFM for EL than for PL. This can be rationalized by the expectation that both weak Förster transfer and charge transfer from PFO to PFM occur under electrical operation. Resemblance of the EL spectra of the doped devices with the PL spectrum of PFM indicates that charge transport via hopping between adjacent sites followed by carrier recombination preferentially occurs on the PFM molecules. Only Förster transfer is expected for optical excitation. This is supported by time resolved PL measurements which show a reduction of the PFO lifetime in the blend with increasing PFM concentration. Hole trapping was also evidenced by time resolved EA measurements as well as from the dispersive shape of the TOF signal in the blend.

References

1. Burroughes, J.H., Bradley, D.D.C., Brown, A.B., Marks, R.N., Mackay, K., Friend, R.H., Burn, P.L. & Holmes, A.B. *Nature (London)* **347**, 539 (1990).
2. e.g. see CDT website, <http://www.cdilttd.co.uk> for latest results and developments.
3. Bernius, M., Inbasekaran, M., Woo, E., Wu, W. & Wujkowski, L. *Journal of Materials Science: Materials in Electronics* **11**, 111 (2000).
22. Ho, P.K.H., Kim, J.S., Burroughes, J.H., Becker, H., Li, S.F.Y., Brown, T.M., Cacialli, F. & Friend, R.H. *Nature* **404**, 481 (2000).
5. Speitzer, H., Becker, H., Kluge, E., Kreuder, W., Schenk, H., Demandt, R., & Soo, H. *Advanced Materials* **10**, 1340 (1998).
6. Gao, Y., Yu, G. & Heeger, A.J. *Advanced Materials* **10**, 917 (1998).

**Chapter 4: Blue light emitting diodes
from blends of polyfluorene (PFO) and hole transporting materials**

7. He, Y., Gong, S., Hattori, R. & Kanicki, J. *Applied Physics Letters* **74**, 2265 (1999).
8. He, Y. & Kanicki, J. *Applied Physics Letters* **76**, 661 (2000).
9. Steuber, F., Staudigel, J., Stossel, M., Simmerer, J., Winnacker, A., Spreitzer, H., Weissortel, F. & Salbeck, J. *Advanced Materials* **12**, 130 (2000).
10. Blom, P.W.M., Berntsen, A.J.M., Liedenbaum, C.H.T.F., Schoo, H.F.M., Croonen, Y. & Van De Weijer, P. *Journal of Materials Science: Materials in Electronics* **11**, 105 (2000).
11. Gross, M., Muller, D.C., Nothofer, H.-G., Scherf, U., Neher, D., Brauchle, C. & Meerholz, K. *Nature* **405**, 661 (2000).
12. Grem, G., Leditzky, G., Ulrich, B. & Leising, G. *Advanced Materials* **4**, 36 (1992).
13. Tasch, S., Niko, A., Leising, G. & Scherf, U. *Applied Physics Letters* **68**, 1090 (1996).
14. Yang, Y., Pei, Q. & Heeger, A.J. *Journal of Applied Physics* **79**, 934 (1996).
15. Tang, H, Li, F. & Shinar, J. *Applied Physics Letters* **71**, 2560 (1997).
16. Tao, Y.T., Balasubramaniam, Danel, A. & Tomasik, P. *Applied Physics Letters* **77**, 933 (2000).
17. Basca, W.S., Schaer, M., Zuppiroli, L. & Siove, A. *Journal of Applied Physics* **84**, 5733 (1998).
18. Shaheen, S.E., Jabbour, G.E., Morrell, M.M., Kawabe, Y., Kippelen, B., Peyghambarian, N., Nabor, M.F., Schlaf, R., Mash, E.A. & Armstrong, N.R. *Journal of Applied Physics* **84**, 2324 (1999).
19. Haskal, E.I. *Synthetic Metals* **91**, 187 (1997).
20. Noda, T., Ogawa, H. & Shirota, Y. *Advanced Materials* **11**, 283 (1999).
21. Tao, X.T., Suzuki, H., Wada, T., Sasabe, H. & Miyata, S. *Applied Physics Letters* **75**, 1655 (1999).

22. Grice, A.W., Tajbakhsh, A., Burn, P.L. & Bradley, D.D.C. *Advanced Materials* **9**, 1174 (1997).
23. Jen, A.K.-Y., Liu, Y., Hu, Q.-S. & Pu, L. *Applied Physics Letters* **75**, 3745 (1999).
24. Bernius, M., Inbasekaran, M., Woo, E., Wu, W. & Wujkowski, L. *Thin Solid Films* **363**, 55 (2000).
25. Grice, A.W., Bradley, D.D.C., Bernius, M.T., Inbasekaran, M., Wu, W.W. & Woo, E.P. *Applied Physics Letters* **73**, 629 (1998).
26. Grice, A.W. *Device physics of conjugated polymer LEDs* (Sheffield University, 1998).
27. Bradley, D.D.C., Grell, M., Long, X., Mellor, H., Grice, A., Inbasekaran, M. & Woo, E.P. *SPIE Proceedings* **3145**, 254 (1997).
28. Yu, W.-L., Cao, Y., Pei, J., Huang, W., & Heeger, A.J. *Applied Physics Letters* **75**, 3270 (1999).
29. Chen, J.P., Klaerner, G., Lee, J.-I., Markiewicz, D., Lee, V.Y., Miller, R.D. & Scott, J.C. *Synthetic Metals* **107** 129, (1999).
30. Chen, J.P., Markiewicz, D., Lee, V.Y., Klaerner, G., Miller, R.D. & Scott, J.C. *Synthetic Metals* **107** 203, (1999).
31. Klaerner, G., Lee, J.-I., Davey, M. & Miller, R.D. *Advanced Materials* **11**, 115 (1999).
32. Klaerner, G., Davey, M.H., Chen, W.-D., Scott, J.C. & Miller, R.D. *Advanced Materials* **10**, 993 (1998).
33. Kreyenschmidt, M., Klaerner, G., Fuhrer, T., Ashenurst, J., Karg, S., Chen, W.D., Lee, V.Y., Scott, J.C. & Miller, R.D. *Macromolecules* **31**, 1099 (1998).
34. Yu, W.-L., Pei, J., Huang, W. & Heeger, A.J. *Advanced Materials* **12**, 828 (2000).

35. Jiang, X., Liu, S., Ma, H. & Jen, A.K.-Y. *Applied Physics Letters* **76**, 1813 (2000).
36. Stephan, O. & Vial, J.-C. *Synthetic Metals* **106**, 115 (1999).
37. Setayesh, S., Marsitzky, D. & Müllen, K. *Macromolecules* **33**, 2016 (2000).
38. Uckert, F., Tak, Y.-H., Mullen, K. & Bassler, H. *Advanced Materials* **12**, 905 (2000).
39. Antoniadis, H., Inbasekaran, M. & Woo, E.P. *Applied Physics Letters* **73**, 3055 (1998).
40. Sainova, D., Miteva, T., Nothofer, H.G., Scherf, U., Glowacki, I., Ulanski, J., Fujikawa, H. & Neher, D. *Applied Physics Letters* **76**, 1810 (2000).
41. Cimrova, V., Neher, D., Remmers, M. & Kminek, I. *Advanced Materials* **10**, (1998).
42. Wu, C.C., Sturm, J.C., Register, R.A., Tian, J., Dana, E.P. & Thompson, M.E. *IEEE Transactions On Electron Devices* **44**, (1997).
43. Redecker, M., Bradley, D.D.C., Inbasekaran, M. & Woo, E.P. *Applied Physics Letters* **73**, 1565 (1998).
44. Redecker, M., Bradley, D.D.C., Inbasekaran, M., Wu, W.W. & Woo, E.P. *Advanced Materials* **11**, 241 (1999).
45. Miraura, N. & Suzuki, A., *Chem. Rev.* **95** 2457, (1995).
46. Förster, T. *Annalen der Physik* **2**, 55 (1948).
47. List, E.J.W, Creely, C., Leising, G., Schulte, N., Schluter, A.D., Scherf, U., Mullen, K. & Graupner, W. *Chemical Physics Letters* **325**, 132 (2000).
48. Buckley, A.R., Rahn, M.D., Hill, J., Cabanillas-Gonzalez, J., Fox, A.M. & Bradley, D.D.C. submitted to *Chemical Physics Letters* (2000).
49. Janietz, S., Bradley, D.D.C., Grell, M., Giebeler, C., Inbasekaran, M. & Woo, E.P. *Applied Physics Letters* **73**, 2453 (1998).

50. So, S.K., Choi, W.K., Leung, L.M. & Neyts, K. *Applied Physics Letters* **74**, 1939 (1999).
51. Becker, H., Burns, S.E. & Friend, R.H. *Physical Review B* **56**, 1893 (1997).
52. Wan, W.M.V., Greenham, N.C. & Friend, R.H. *Journal of Applied Physics* **87**, 2542 (2000).
53. Bulovic, V., Khalfin, V.B., Gu, G., Burrows, P.E., Garbuzov, D.Z. & Forrest, S.R. *Physical Review B* **58**, 3730 (1998).
54. Shoustikov, A., You, Y. & Thompson, M.E. *IEEE Journal of Selected Topics in Quantum Electronics* **4**, 3 (1998).
55. Shaheen, S.E., Kippelen, B., Peyghambarian, N., Wang, J.-F., Anderson, J.D., Mash, E.A., Lee, P.A., Armstrong, N.R. & Kawabe, Y. *Journal of Applied Physics* **85**, 7939 (1999).
56. Murata, H., Merritt, C.D. & Kafafi, Z.H. *IEEE Journal of Selected Topics in Quantum Electronics* **4**, 119 (1998).
57. Heller, C.M., Campbell, I.H., Smith, D.L., Barashkov, N.N. & Ferraris, J.P. *Journal of Applied Physics* **81**, 3227 (1997).
58. Yoon, J., Kim, J.-J., Lee, T.-W. & Park, O.-O. *Applied Physics Letters* **76**, 2152 (2000).
59. Giebeler, C., Whitelegg, S.A., Campbell, A.J., Liess, M., Martin, S.J., Lane, P.A., Bradley, D.D.C., Webster, G. & Burn, P.L. *Applied Physics Letters* **74**, 3714 (1999).
60. Campbell, A.J., Bradley, D.D.C., Antoniadis, H., Inbasekaran, M., Wu, W.W. & Woo, E.P. *Applied Physics Letters* **76**, 1734 (2000).
61. Blom, P.W.M., Vissenberg, M.C.J., Huiberts, J.N., Martens, H.C.F. & Schoo, H.F.M. *Applied Physics Letters* **77**, 2057 (2000).

CHAPTER 5

GREEN LIGHT EMITTING DIODES FROM BLENDS OF A BENZOTHIADIAZOLE DOPED POLYFLUORENE (5BTF8) AND TRIARYLAMINE COPOLYMERS

5.1 Introduction

Light emitting diodes (LEDs) based on conjugated polymers¹ have been the subject of intense research effort in the last few years due to their potential use for full-color display applications. PLEDs are now approaching commercial requirements in terms of high efficiency, high brightness, low operating voltage and long operating lifetimes.²⁻⁸ The ease of fabrication based on solution processing techniques offers a significant advantage over their inorganic counterparts. Many different electroluminescent conjugated polymers have been reported in the literature which emit colors that cover the whole of the visible spectrum.⁹⁻¹¹ However, most of them have the characteristic that one charge carrier is preferentially injected and/or transported. This unipolar injection and transport ability generally results in low efficiencies and brightnesses when they are used to fabricate single layer PLEDs. Therefore, multilayer structures are often employed in order to improve the

Chapter 5: Green light emitting diodes from blends of a benzothiadiazole doped polyfluorene (5BTF8) and triarylamine copolymers

device performance by achieving better charge injection from both electrodes and charge confinement at the heterojunction interface.¹²⁻¹³ However, as was noted in the last chapter, the construction of multilayer structures with polymers is in general problematic due to the limited choice of organic solvents that can be employed for spin-casting of the different layers. It is important that a solvent employed for the casting of one layer will not dissolve the layers already deposited. Moreover, even if a system of mutually incompatible solvents for the different polymers is found, a slight interpenetration of the polymer layers is likely to occur and a thin transition layer will then be formed at the interface which will be in the form of a blend. This blend structure can subsequently influence the operation of the device.

The incorporation of the functions of different polymers into a single film in the form of a blend¹⁴⁻¹⁵ has been proposed as an approach to avoid the use of multilayer structures. By mixing an emissive and a transport material together in a single solvent and then spin coating the mixture in a single step allows simplification of the device fabrication and can prove potentially important for full color display applications where a single fabrication step would be preferable. Single layer structures can thus be more useful for ink-jet printing techniques that have been recently used to print full color pixels on a substrate by employing a single component.¹⁶ Both the emissive and transport properties of the different materials in the blend are thought to be preserved by an appropriate choice of the blend composition.

We have validated this approach in the last chapter to fabricate bright, efficient and low operating voltage blue PLEDs by employing blends of appropriate conjugated polymers and hole transporting materials. The general concept of blending an emissive polymer with a hole transport material can be described under the following principles: a) The ionization potential of the hole transport layer is lower than that of the emissive polymer and this leads to a lower barrier for hole injection from the ITO anode. The hole injection may then occur

through the localized energy levels caused by the dopant in the blend. b) The improved hole injection leads to an increased density of holes in the bulk that may improve the charge carrier balance and result in higher current densities and brighter devices as the brightness is generally proportional to the recombination current c) The power efficiency which is of particular interest to the device engineer because of its importance for technological applications can be increased significantly as the lower barrier to hole injection leads to a reduction in the turn on and operating voltages (the power efficiency is proportional to $1/\text{voltage}$ so the lower the operating voltage the higher the power efficiency). d) Energy offsets for hole and electron transport at the HTL/polymer interface can still occur even though a distinct heterojunction interface is not present as in the case of two layer LEDs.

Here, the use of a green-emitting benzothiadiazole doped poly(9,9-dioctylfluorene) (namely 5BTF8) doped with a hole transport material consisting of a triarylamine copolymer (namely BFB) to fabricate green single layer PLEDs is reported. This blend was found to exhibit considerably enhanced performance in comparison with the undoped device. The composition of the blend was systematically varied to optimize the device performance. The optical and electrical characteristics of the individual components and the associated blends in a thin-film and a device configuration will also be presented in detail.

5.2 Experimental details

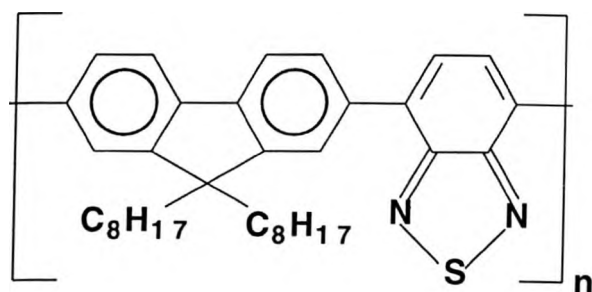
In order to compare directly the effect of blending the emissive polymer with a hole transport material, we fabricated two different kinds of devices: 'conventional' devices which have an active single layer of the emissive material (5BTF8) between the electrodes, and 'doped' devices which have a single layer of the emissive polymer doped with an amount of the hole transport material. Conventional and doped LEDs comprise an indium tin oxide

(ITO) anode, a single layer of the emissive polymer or the blend, spin cast from a solution in xylene (30 mg/ml) and a metal top cathode. Different cathodes were employed in this work. These include Al, Ca and bilayer cathodes consisting of LiF (1.5nm)/Al and CaO (2nm)/Al. All cathodes except Ca are air-stable. Deposition of Ca was done in a nitrogen-filled glove box. The typical deposition rate for Al and Ca was between 0.05 nm/sec (for the first 30 nm) and 0.4 nm/sec (after 30 nm) and 0.01-0.02 nm/sec for the inorganic LiF layer as LiF thermally deposited at a very low rate has been found to form excellent quality films. In order to form calcium oxide (CaO), a 2 nm layer of Ca was first deposited at a rate of 0.02 nm/sec. This layer was then oxidized by allowing oxygen to flow into the evaporator chamber for approximately 15 minutes. The partial pressure during the Ca oxidation process was around 8×10^{-6} mbar. The typical thickness for Al or Ca was around 250 nm. The blend was spin coated at various spin speeds (2000-8000 rpm) to give devices with emissive layer thickness ranging from 70 to 180 nm. In some cases a PEDOT:PSS hole injection layer was also used. PEDOT:PSS was spin-cast at 2000 rpm to form a 30 nm thick layer on top of ITO. It was then baked at 130 °C for 15 minutes in air to render it insoluble before spin-casting the polymer blend on top. All device measurements were carried out at room temperature either under a dynamic vacuum of 10^{-1} mbar or in a nitrogen filled glove box. Films of the 5BTF8/BFB blend were prepared by spin-coating the solutions onto quartz substrates. Films of 5BTF8 and BFB were also prepared as control samples. The 354 nm line of a HeCd laser or a xenon lamp was used as the excitation light source for PL measurements.

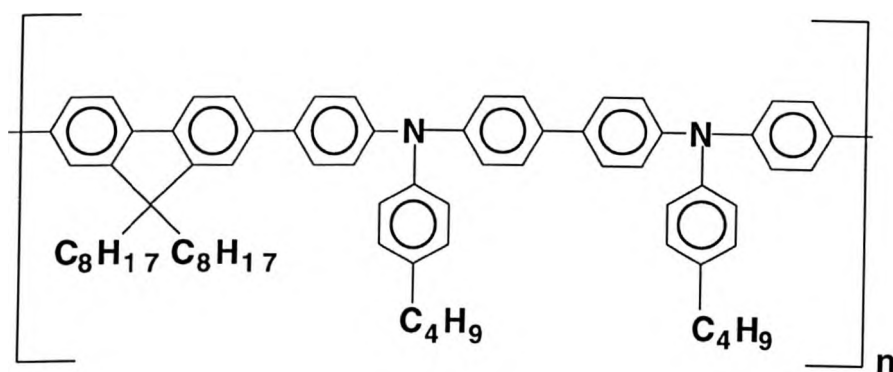
5.3 Optical spectroscopy of BFB, 5BTF8 and 5BTF8:BFB blends

The green-emitting polymer (namely 5BTF8) that was used as the host material is a blend which consists of 95% of the blue emitting poly(9,9-dioctylfluorene) (PFO) and 5% of a green emitting polymer, namely poly(9,9-dioctylfluorene-co-benzothiadiazole) (BT). The

hole transport material that was used as a guest is a triarylamine copolymer namely poly(9,9-dioctylfluorene-co-bis-N,N'-(4-butylphenyl)-bis-N,N'-phenylbenzidine) (BFB). Figure 5.1 shows the chemical structures of BT and BFB.



i) BT



ii) BFB

Figure 5.1: Chemical structures of BT and BFB.

Very high performance bilayer PLEDs that make use of a BT group in a similar polyfluorene copolymer to the one we use here have been demonstrated recently by He *et. al.*^{8,10} The devices were fabricated with an amine-fluorene polymer as a separate hole transport layer and showed green emission peaking at around 545 nm with a FWHM of about 80 nm. When an ITO coated glass substrate was used as the anode and Al as the cathode, brightnesses up to 10000 cd/m², external quantum efficiencies up to 3.8% (~ 14.5 cd/A) and

Chapter 5: Green light emitting diodes from blends of a benzothiadiazole doped polyfluorene (5BTF8) and triarylamine copolymers

power efficiencies up to 2.25 lm/W were demonstrated.⁸ When the ITO coated glass substrate was replaced by an ITO coated flexible plastic substrate, the device performance was significantly enhanced due to a better matching between the refractive indices of the substrate and the polymer. Although the brightness decreased to $\sim 2000 \text{ cd/m}^2$, the quantum efficiency increased to 15% ($\sim 56.2 \text{ cd/A}$) and the power efficiency increased to 9 lm/W.¹⁰

The LUMO level in BT is at 3.5 eV which is well below the common impurity trap states usually seen in polymers. Therefore, the introduction of the electron-withdrawing benzothiadiazole group shifts the LUMO further away from vacuum and results in a substantial improvement of the electron injection and transport. The emissive 5BTF8 blend can thus be used for both the electron transport and the emission of light. By doping BT into PFO the emission will originate from the guest dopant due to Förster energy transfer. This approach has been extensively used to change the emission wavelength from blue to green¹⁷ in PLEDs and from blue to red¹¹ in dye-doped PLEDs. PFO possesses a large hole mobility of order 10^{-4} to $10^{-3} \text{ cm}^2 \text{V}^{-1} \text{s}^{-1}$ with weak field dependence and supports non-dispersive hole transport. Electron transport is much weaker and highly dispersive.¹⁸ BT shows dispersive electron transport with a high electron mobility of order $10^{-3} \text{ cm}^2 \text{V}^{-1} \text{s}^{-1}$. The hole transport in BT is very poor and highly dispersive.¹⁹ The triarylamine electron donating functionality in BFB leads to a significant reduction in the ionization potential from the 5.8 eV value deduced from cyclic voltammetry measurements for the PFO homopolymer.²⁰ BFB has an ionization potential of 5.26 eV that facilitates hole injection from ITO (workfunction $\sim 4.7 \text{ eV}$). It also possesses a large hole mobility of $3 \times 10^{-4} \text{ cm}^2 \text{V}^{-1} \text{s}^{-1}$.²¹ The rather dispersive signal of the transient photocurrent in BFB is indicative of the existence of shallow traps for holes on this material. All polymers were synthesized via a Suzuki reaction²² and were purified to remove catalyst residues and ionic impurities. The absorption and photoluminescence spectra of PFO and BT are shown in Figure 5.2 below.

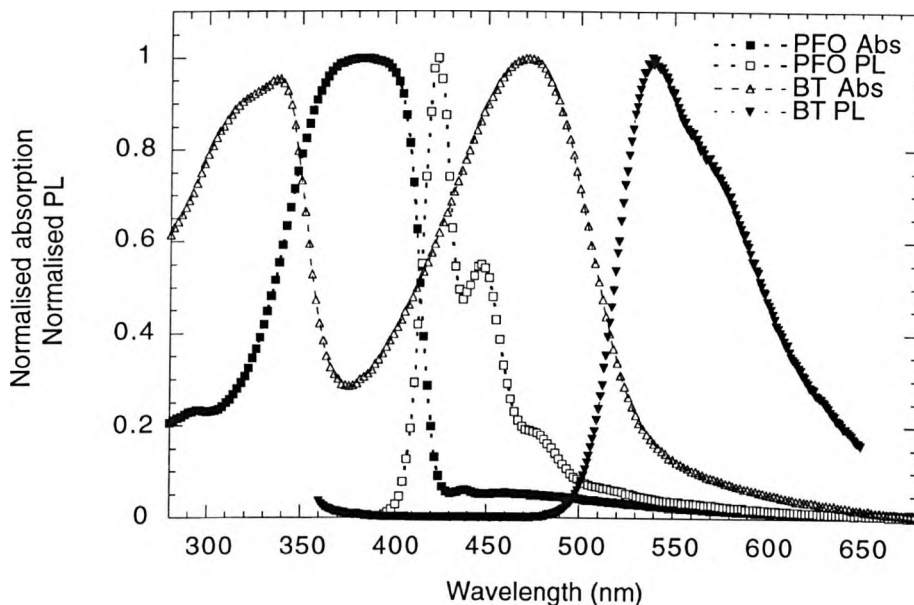


Figure 5.2: Absorption of PFO (filled squares), photoluminescence of PFO (open squares), absorption of BT (open triangles) and photoluminescence of BT (filled triangles).

The absorption spectrum of PFO consists of a featureless peak at 385 nm. The maximum intensity of the PL spectrum corresponds to the 0-0 transition at 422 nm with a clearly resolved vibronic feature appearing at 447 nm corresponding to the 0-1 transition. A rather broad shoulder is also apparent at 473 nm. The absorption spectrum of BT shows two broad peaks of similar intensity at 322 and 464 nm respectively. The PL spectrum of BT has a broad peak at around 540 nm and shows no resolved vibronic structure. Due to the significant spectral overlap between the PL spectrum of PFO and the absorption spectrum of BT, an efficient excitation transfer of singlet excitons from the host to the guest is energetically favorable and a direct dipole-dipole interaction (i.e. Förster energy transfer²³) is expected to occur. Time resolved measurements of PFO PL emission in 5BTF8 support the energy transfer mechanism. While the PL lifetime of PFO is about 350 ps, the lifetime of PFO emission in 5BTF8 is significantly reduced and consists of two components; a fast

component with a 12 ps lifetime and a slower component with a lifetime of 35 ps.²⁴ The fast and slow components have been associated with Förster energy transfer and excitation energy migration followed by Förster transfer, respectively. The nonradiative energy transfer from PFO to BT is the dominant excited state decay route of PFO. The radiative lifetime of BT is of the order of 1 ns. Absorption, PL and EL spectra of 5BTF8 are shown in Figure 5.3.

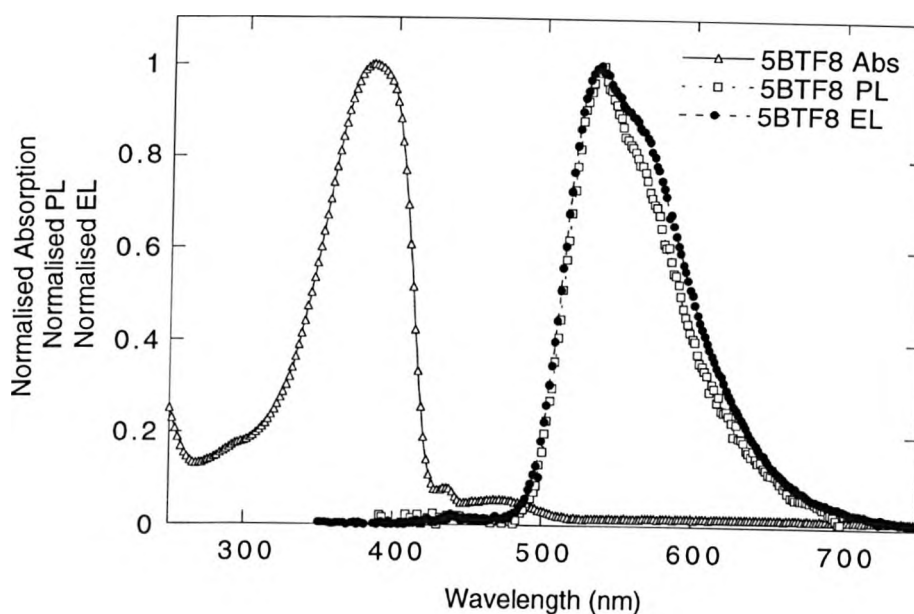


Figure 5.3: Absorption (open triangles), PL (open squares) and EL spectra (filled circles) of 5BTF8.

The absorption spectrum of 5BTF8 exhibits its main featureless peak due to the PFO absorption at 384 nm and has a relatively narrow line width with a full width at half maximum of 68 nm. It also shows a small shoulder at 465 nm due to the contribution of the BT absorption in the blend. The 5BTF8 blend is expected to have some polymer chains with BT HOMO and LUMO parameters and others with PFO parameters. However, there will be no chains with the HOMO energy level of PFO and the LUMO energy level of BT. The high electron affinity of BT (~3.5 eV) compared to that of PFO (~2.8 eV) suggests that the use of

use of a high workfunction air-stable cathode might be sufficient to achieve efficient electron injection. The PL spectrum of 5BTF8 shows a peak located at 537 nm and a small shoulder at 564 nm. It arises solely from BT due to efficient Förster transfer between PFO and BT. The EL spectrum also peaks at 535 nm with a half width at half maximum of about 80 nm that is about 10 nm wider than its PL counterpart. The small spectral broadening in EL probably arises from weak interference effects from the reflective Al cathode as a result of the proximity of the recombination/emission zone close to the cathode. Absorption and PL spectra of the BFB guest are shown in Figure 5.4.

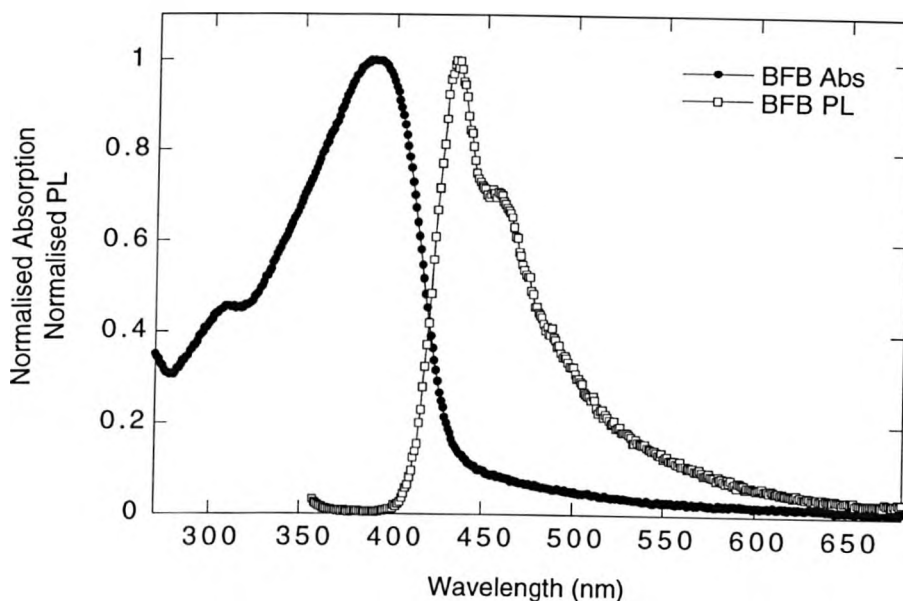


Figure 5.4: Absorption (filled circles) and photoluminescence spectra (open squares) of BFB.

The absorption spectrum shows a broad featureless peak at 386 nm. The PL spectrum peaks at 433 nm (0-0 transition) with a shoulder at 457 nm (0-1 transition). The radiative lifetime of the PL emission is 150 ps and can be fitted accurately with a single exponential decay. The PL quantum efficiency of BFB was $(15 \pm 2)\%$. The low efficiency is due to the low portion of

the photogenerated excitations that produce singlet excitons and the efficient nonradiative decay processes that are dominant in this material and lead to a high nonradiative recombination probability. The PL efficiency of the 5BTF8:BFB blend was $(48\pm 3)\%$ for a BFB concentration of 20% which is almost as high as the efficiency of 5BTF8 ($\sim 55\pm 5\%$) indicating that no significant exciton dissociation or transfer to BFB occurs in the blend. PL and EL spectra of the 5BTF8:BFB blend (20 wt.% BFB) are shown in Figure 5.5.

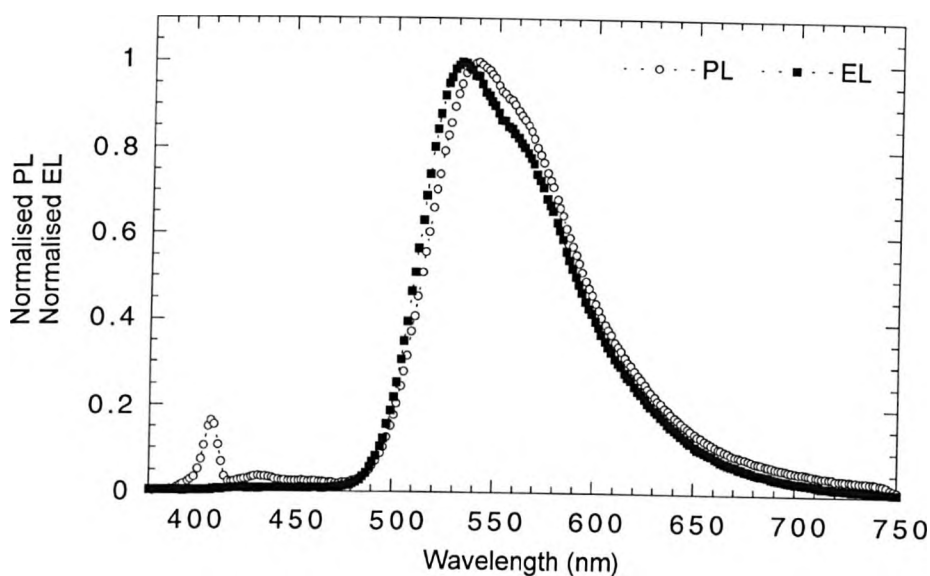


Figure 5.5: PL (open circles) and electroluminescence (EL) spectra (filled squares) of 5BTF8:BFB(4:1).

The EL spectrum peaks at 534 nm and very closely resembles the PL spectrum (the small peak at 400 nm in PL is due to the excitation source) indicating that both the EL and the PL arise from the same emissive species. The CIE 1931 chromaticity color coordinates are (0.39, 0.58). Moreover, both spectra are identical to the emission spectrum of 5BTF8 and this confirms that emission solely originates from the radiative carrier recombination and decay of singlet excitons within 5BTF8. A small emission band which is evident only in the PL spectrum is located at around 435 nm. This band may be attributed to emission from lower

energy PFO excited conjugation segments in 5BTF8 due to incomplete energy transfer from PFO to BT under photoexcitation. Association of this band with residual emission from individual BFB excited states can not be totally excluded, however in this occasion any singlet excitons that are formed in BFB are energetically favorable to migrate and relax to the lower energy (longer conjugation length) 5BTF8 sites and also contribute to the emission.

5.4 LEDs based on 5BTF8 and 5BTF8:BFB blends

LEDs were first fabricated with ITO as the anode and Al as the cathode. Figure 5.6 compares current density versus voltage characteristics of 5BTF8 and BFB doped 5BTF8 LEDs with varying BFB concentration and an emissive layer thickness of around 85 nm.

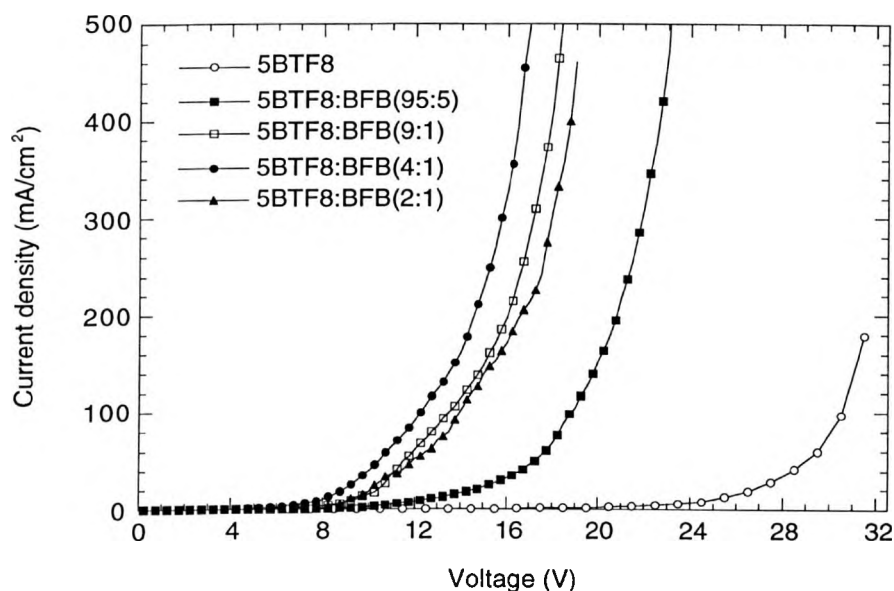


Figure 5.6: Current density vs. voltage characteristics of ITO/5BTF8/Al, ITO/5BTF8:BFB(95:5)/Al, ITO/5BTF8:BFB(9:1)/Al, ITO/5BTF8:BFB(4:1)/Al and ITO/5BTF8:BFB(2:1)/Al LEDs.

Chapter 5: Green light emitting diodes from blends of a benzothiadiazole doped polyfluorene (5BTF8) and triarylamine copolymers

Figures 5.7 and 5.8 compare luminance and EL efficiency vs. voltage of this series of LEDs.

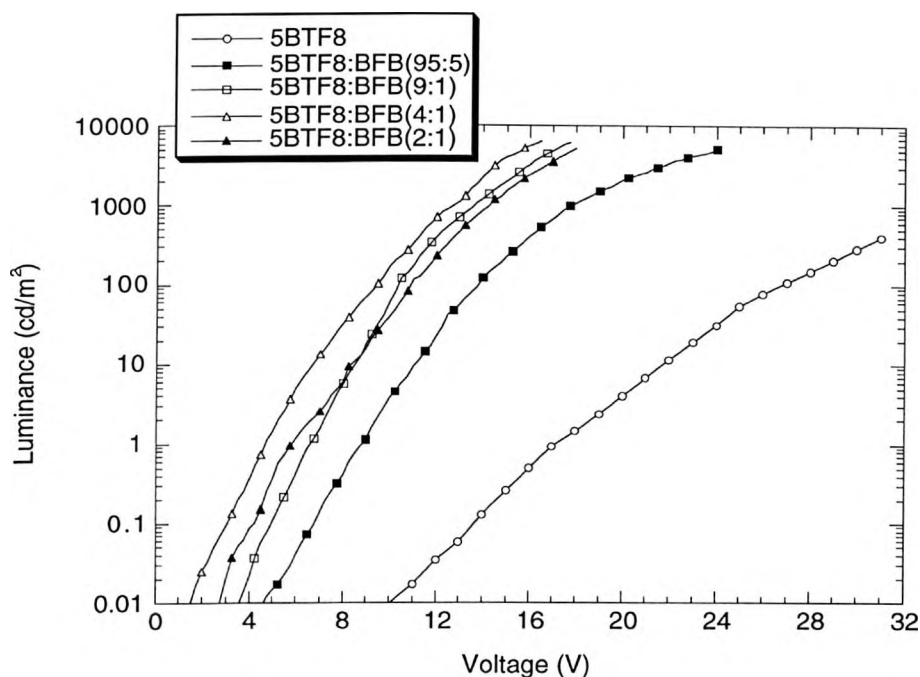


Figure 5.7: Luminance vs. voltage of 5BTF8 and 5BTF8:BFB LEDs with varying BFB concentration.

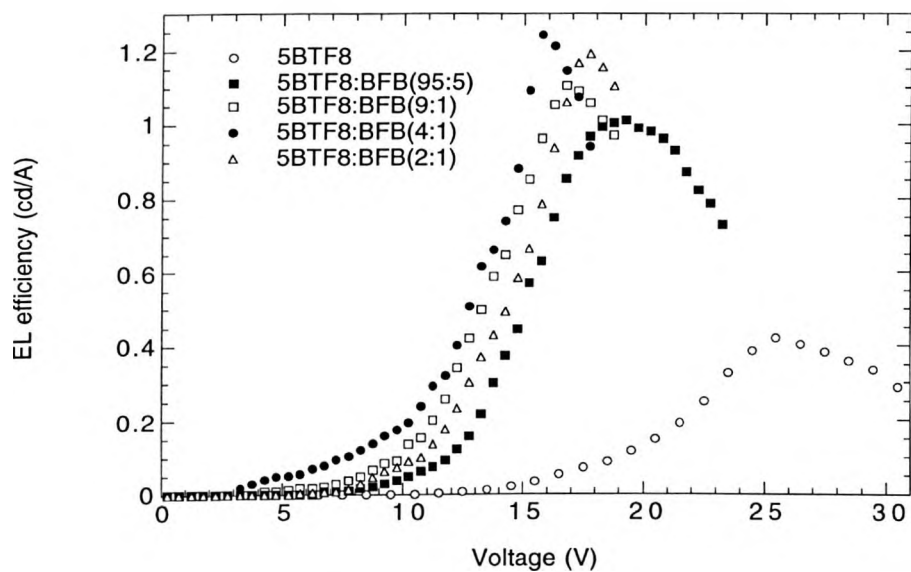


Figure 5.8: EL efficiency vs. voltage of 5BTF8 and 5BTF8:BFB LEDs with varying BFB concentration.

Chapter 5: Green light emitting diodes from blends of a benzothiadiazole doped polyfluorene (5BTF8) and triarylamine copolymers

Undoped 5BTF8 devices exhibit a poor performance. They reach a maximum brightness of 400 cd/m^2 and a current density of 185 mA/cm^2 at 32 V. The maximum EL efficiency is 0.42 cd/A and the maximum power efficiency is 0.05 lm/W, both obtained at 55 cd/m^2 . The doped devices however exhibit a significantly improved performance. More than one order of magnitude enhancement in the maximum brightness is found in the blend compared to the undoped device. The maximum brightness is achieved for a 20 wt.% BFB concentration. The brightness reaches 6450 cd/m^2 at 16.5 V. The corresponding current density is 750 mA/cm^2 , a factor of 4 larger than the maximum current density sustained by the undoped device. The quantum and power efficiency also increase by approximately a factor of 3 and 4, respectively. The quantum efficiency and the power efficiency increase to 1.25 cd/A and 0.2 lm/W, respectively. The greatly enhanced device performance is due to the improved hole injection and transport as a direct result of the presence of the hole transporter in the blend that leads to an increased current flow through the device and a corresponding increase in the brightness. Although the PL efficiency of the blend is slightly lower than that of 5BTF8, the EL efficiency is much higher in the blend due to an improvement of the charge carrier balance factor that determines the exciton generation rate. An increase in the charge balance factor will result in an increased exciton formation rate. We therefore propose that the increase of this factor is the major reason for the increased efficiencies and the higher luminances observed in the doped devices.

This is further evidenced by the comparison of the turn on and operating voltages in the two devices. The undoped device turns on (arbitrarily defined as the bias required to give a measurable luminance of 5 cd/m^2) at 20.5 V and the operating voltage is 27 V for a luminance of 100 cd/m^2 . A substantial decrease of the turn on and the operating voltage is achieved for the 20 wt.% device. The turn on and operating voltage is reduced to 6 and 9.5 V, respectively. This is due to the reduced barrier for hole injection from the ITO to the

HOMO level of BFB in the blend. In the absence of BFB in the blend, hole injection is particularly difficult due to the high ionization potentials of PFO and BT (~5.8 and 5.9 eV, respectively) but the incorporation of BFB will lead to a reduction of the injection barrier to half of its original value. Another possibility in terms of energy levels is that the BFB units provide intermediate energy levels, populated by rapid charge transfer between the HOMO levels of PFO and BT and the ITO Fermi level that facilitate hole injection in the bulk while the high mobility of the holes that will predominantly be transported by the BFB molecules can further contribute to lowering the operating voltage of the blend device. The position of the HOMO level of BFB that is more shifted towards the vacuum level compared to that of PFO or BT will result in hole transport taking, initially, place mainly through the lowest energy BFB chains. A hopping process will then transfer holes to the PFO or BT chains. Holes will preferentially hop to the lower energy (longer conjugation length) PFO chains but some holes may also hop to the BT chains as they are only at slightly higher energy. On the other hand, electron transport will mainly take place through the LUMO levels of BT as BT has a considerably larger electron affinity compared to PFO or BFB. The higher hole mobility in BFB and the higher electron mobility in BT may also favor hole transport initially in BFB and electron transport in BT although in the 5BTF8:BFB blend there will be a composite hole and electron mobility for the blend and not individual values for each constituent. The application of an electric field will then lead to the formation of positively and negatively charged polarons through charge carrier-phonon lattice coupling that will mainly recombine on BT sites to form singlet excitons. Also any singlet excitons formed initially in the higher energy PFO chains will finally migrate to the lower energy BT sites. If these excitons decay radiatively then light emission will occur.

Phase separation, as expected due to the poor miscibility of polymeric materials, was also found to occur in the blend. BFB dispersed in 5BTF8 represents the minority phase and

yields a great deal of interfaces between the two polymer phases that can clearly affect the transport and recombination under an applied field. The increased interface area between BFB, PFO and BT is expected to have a beneficial effect on the charge transport and the radiative exciton recombination. Some redistribution of the internal electric field due to the build up of a hole space charge at the host/guest interfaces, that may occur due to the 0.5 eV barrier for hole transport from BFB to PFO or BT, will also facilitate electron injection from the cathode by increasing the effective electric field close to the cathode while it can also block the excessive hole current that does not contribute to radiative recombination. This would also result in more efficient carrier recombination and a higher exciton formation rate.

By comparing the maximum brightness and efficiency for different BFB concentrations we found that the optimum composition was 20 wt.% BFB. A further increase in the BFB concentration had no beneficial effect on the LED characteristics. The maximum brightness reaches 5200, 6200 and 5300 cd/m^2 and the corresponding maximum EL efficiencies are 1, 1.1 and 1.2 cd/A at high luminances of the order of 1000 cd/m^2 for 5, 10 and 33 wt.% BFB concentration, respectively. The improved hole injection and transport induces higher current flow and this is also revealed in the plot of current density as a function of voltage where a steep increase in the current is observed at higher BFB concentrations. The operating voltage decreases monotonically until 20 wt.% and then slightly increases as the BFB concentration is further increased to 33 wt.%. Although by increasing the BFB concentration the average hopping distance for holes becomes smaller resulting in a higher “effective” hole mobility, this voltage increase may indicate that a very high density of BFB HOMO levels can result in hole trapping with BFB HOMOs acting as shallow hole traps that hinder hole transport. Exciton quenching from free or trapped holes can also account for the reduction of efficiency at higher fields and BFB concentrations. An electrically induced modification of the local film morphology through the formation of

aggregated species can also attribute to the quenching of singlet excitons in the bulk or at the blend surface and thus reduce the luminance and efficiency. An increased fraction of holes is also expected to cross the device at higher fields and BFB concentrations without recombining with oppositely charged carriers to form excitons thus further reducing the quantum efficiency.

However, the large barrier for electron injection from Al to the LUMO of BT (~1eV) limits the device performance and the enhancement of the electron injection rate is expected to increase the efficiency. Among other methods, the insertion of a dielectric layer such as LiF between Al and the active polymer layer has been reported to enhance the device performance.²⁵⁻²⁶ We thus deposited a 1.5 nm thick LiF layer before the deposition of Al and examined its effect on the LED performance. Figure 5.9 compares current density vs. voltage characteristics of ITO/5BTF8:BFB/LiF-Al LEDs with a 20-wt.% BFB concentration.

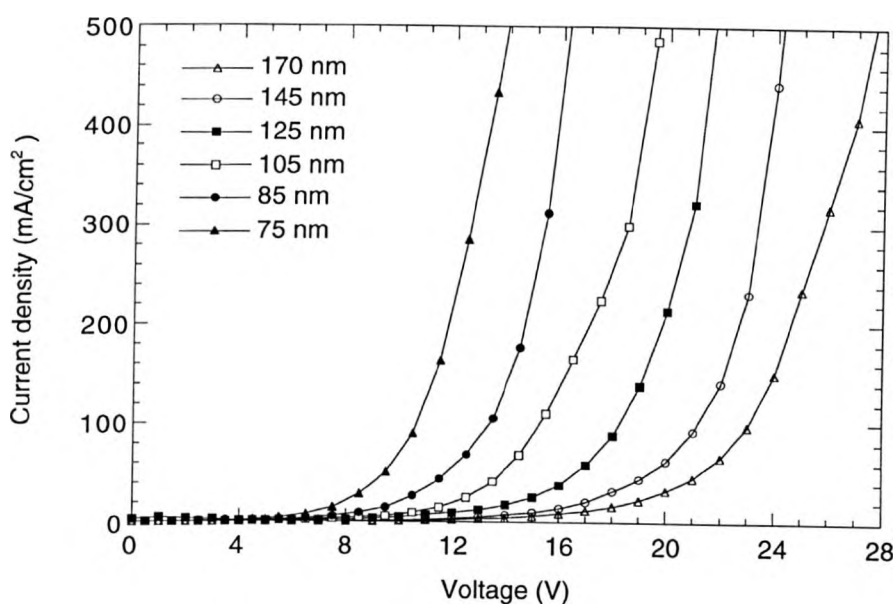


Figure 5.9: Current vs. voltage of ITO/5BTF8:BFB(4:1)/LiF(1.5nm)-Al LEDs with varying thickness.

Chapter 5: Green light emitting diodes from blends of a benzothiadiazole doped polyfluorene (SBTF8) and triarylamine copolymers

Figures 5.10 and 5.11 compare luminance and EL efficiency vs. voltage for these devices.

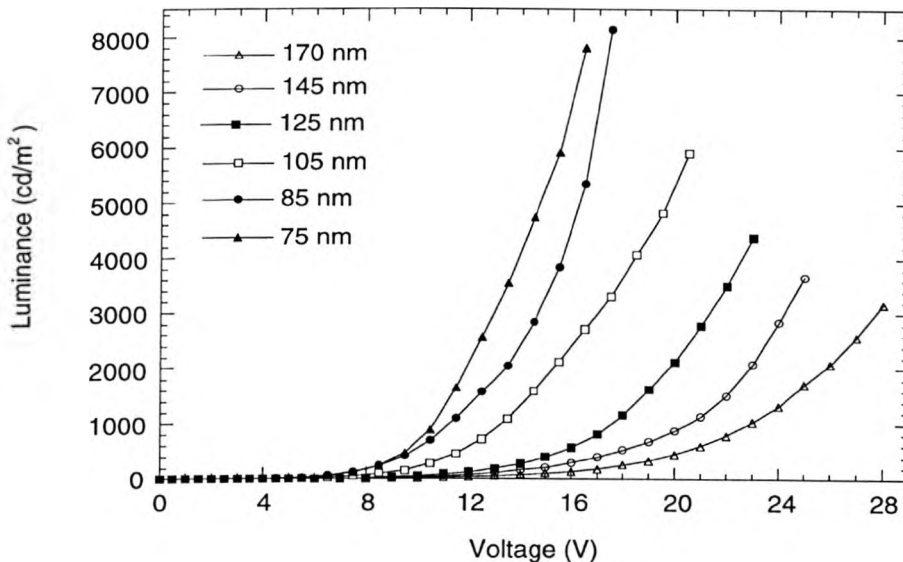


Figure 5.10: Luminance vs. voltage characteristics of ITO/5BTf8:BFB(4:1)/LiF(1.5nm)-Al LEDs.

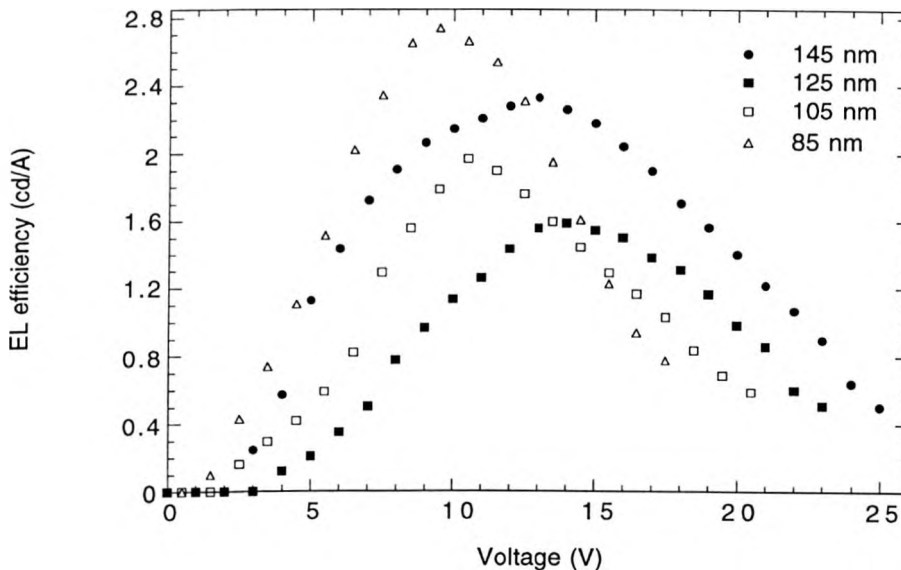


Figure 5.11: EL efficiency vs. voltage characteristics of ITO/5BTf8:BFB(4:1)/LiF(1.5nm)-Al LEDs.

Chapter 5: Green light emitting diodes from blends of a benzothiadiazole doped polyfluorene (SBTF8) and triarylamine copolymers

For maximum EL quantum and power efficiency at a high light output, a thickness of 85 nm yields an optimal rate of charge carrier injection and exciton recombination. At an applied voltage of 17.5 V a maximum luminance of 8150 cd/m^2 at a corresponding current density of 1050 mA/cm^2 was obtained. The turn on voltage is 3 V (for a luminance of 5 cd/m^2) and the operating voltage is 7 V (for a luminance of 100 cd/m^2). We also calculate the maximum external quantum efficiency to be 0.9% or 2.75 cd/A and the corresponding power efficiency to be approximately 1 lm/W at a brightness of 420 cd/m^2 . At an operating brightness of 100 cd/m^2 which is typical of a computer or a TV monitor, the EL efficiency is 2.2 cd/A or 0.72 % and the power efficiency is 0.95 lm/W. LED performance is therefore enhanced significantly upon deposition of a very thin layer of LiF under the Al electrode due to improved electron injection. This is evidenced by the lower turn-on and operating voltage, the higher luminance at a fixed voltage and the higher efficiencies compared to the Al devices. The fact that the quantum efficiency is voltage dependent points to unbalanced electron and hole injection and transport in the blend. The maximum efficiency is achieved when the charge balance reaches its optimum in the bulk and the fraction of charge carriers radiatively recombining to emit light reaches its highest value.

If we also compare devices with different thickness we observe a significant increase in the current density for a fixed voltage as the thickness decreases. The turn on and operating voltages for both luminance and current decrease continuously with decreasing thickness as a result of the more efficient exciton recombination and the improved transport, respectively. However below a certain device thickness of about 65 nm we found that the turn on voltage for luminance increases. This is attributed to the increased nonradiative recombination losses at the cathode interface as a result of exciton quenching. The maximum EL efficiency does not show a continuous trend with decreasing thickness but it rather “oscillates” with thickness, probably due to the influence of constructive or destructive

interference effects on the exciton recombination rate as the relative distance between the light emitting dipoles and the cathode changes with device thickness which may affect the position of the recombination zone. The interplay between the probability for a carrier to encounter an oppositely charged carrier and form an exciton or to discharge at the counter electrode will also influence the efficiency. The maximum luminance increases monotonically with decreasing thickness until a certain thickness of about 85 nm and then decreases again as the device becomes thinner. The lower current density at a fixed voltage with increasing thickness is attributed to the lower electric field that results in a decreased carrier injection. The fact that the maximum efficiency starts to drop below a certain thickness points to the influence of the exciton quenching and the increased nonradiative energy transfer to the cathode on the nonradiative and thus the total exciton decay rate. The lower luminance at a fixed voltage with increasing thickness is also attributed to the decreased carrier injection and therefore to the reduced number of excitons formed by radiative recombination. Field induced exciton dissociation at high electric fields is considered to be a possible factor in luminescence quenching so the decreased operating voltage due to enhanced electron injection will result in a decreased field strength and therefore in reduced exciton quenching. Antoniadis *et. al.*²⁷ and Giebeler *et. al.*²⁸ have emphasized the influence of the anode/HTL interface on the operating voltage and the importance of the HTL/ETL interface in determining the efficiency and our results are in agreement with their conclusions.

An increased electron injection from the bilayer cathode can be expected as a result of the presence of the LiF layer. However the exact mechanism of electron injection by inserting an insulating LiF layer between the emitting layer and the cathode remains elusive. Different mechanisms have been proposed that include the decrease of the effective barrier height for electron injection,²⁹⁻³¹ the large voltage drop across LiF that facilitates electron tunneling,²⁵⁻²⁶ removal of the exciton-quenching states from the cathode interface,^{29,32-33}

Chapter 5: Green light emitting diodes from blends of a benzothiadiazole doped polyfluorene (5BTF8) and triarylamine copolymers

band bending by Fermi level alignment,³⁴ dissociation of LiF to form a low workfunction Li contact²⁹ and formation of interfacial dipoles or surface states that facilitate the injection by charge transfer.³⁵ A recent combined UPS and XPS study on polyfluorene/Al and LiF/Al interfaces has shed some light at this interface which is subjected to strong chemical interactions between Al and C atoms of the polymer backbone. In that case, Al was found to form Al-C complexes with C atoms at the interface disrupting the conjugation along the backbone.³⁶ The inclusion of a LiF layer between the polymer and Al was proposed to decrease these chemical interactions, stabilize the interface and reduce the number of exciton quenching sites. So such a thin interfacial layer would rather improve the device performance by a similar mechanism as no LiF dissociation or band bending was found to occur.

In order to gain some insight into the mechanism behind the enhancement of the device performance in our LEDs, we employed the electroabsorption (EA) technique to directly measure the barrier height for electron injection at the polymer/(LiF/Al) interface. The results we obtained showed a significant reduction of the cathodic barrier height brought about by the LiF layer; this effect was more pronounced with increasing thickness of LiF. We first measured the EA spectra of the individual components BT, 5BTF8, BFB and the EA spectrum of the blend 5BTF8:BFB (20 wt.% BFB) in order to obtain both the spectral dependence of the EA signal which is related to the nature of the excited states in each material and the peak wavelengths which we will then use to probe the blend devices and measure their EA response at this wavelength. All the EA spectra were measured on devices with ITO and Al electrodes. The applied DC and AC bias was -3 and 1.5 V, respectively. Figure 5.12 compares the electroabsorption spectra of PFO, BT and 5BTF8 at the fundamental frequency 1f. The EA spectrum of PFO is given for comparison. Similarly, Figure 5.13 directly compares the 1f EA spectra of 5BTF8, BFB and 5BTF8:BFB (20 wt.% BFB).

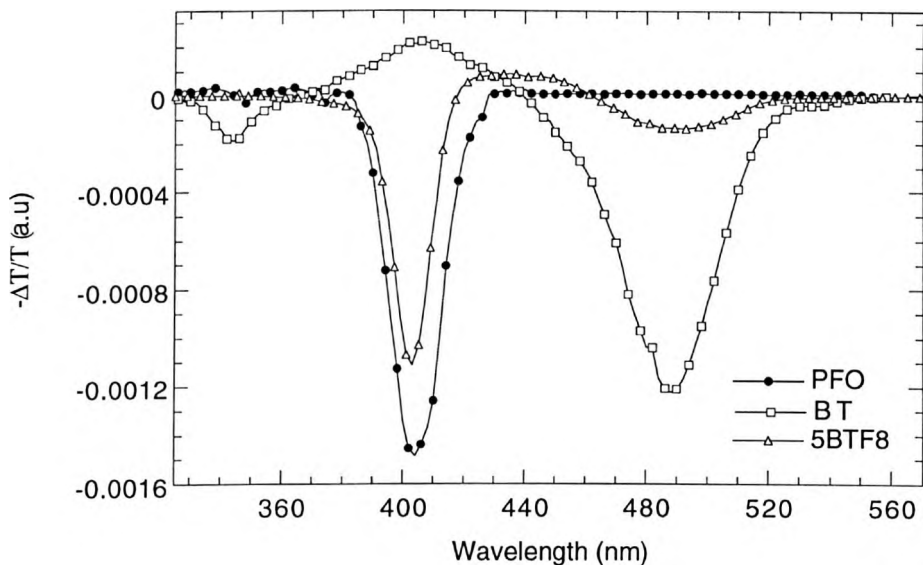


Figure 5.12: 1f EA spectra of PFO (filled circles), BT (open squares) and 5BTF8 (open triangles).

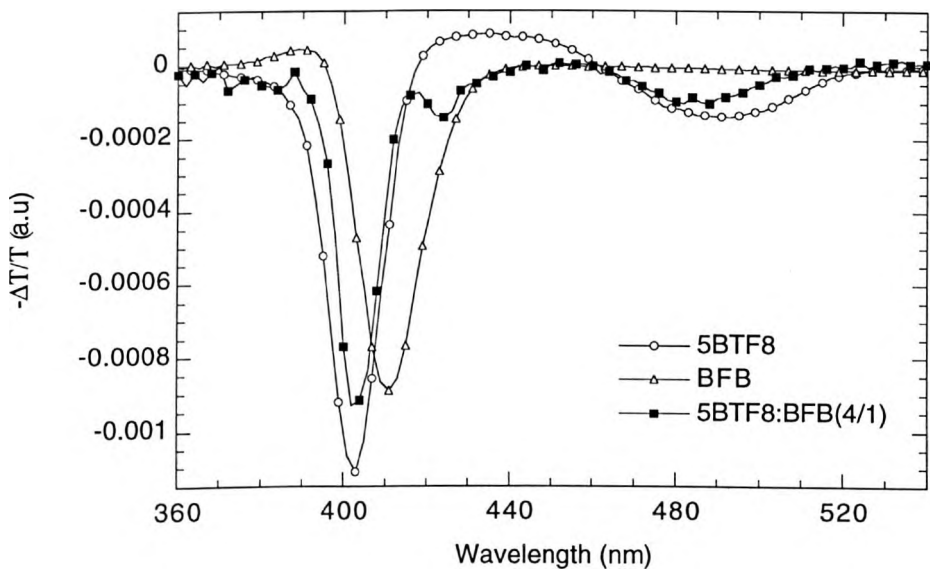


Figure 5.13: EA of 5BTF8 (open circles), BFB (open triangles) and 5BTF8:BFB(4/1) (filled squares).

**Chapter 5: Green light emitting diodes
from blends of a benzothiadiazole doped polyfluorene (5BTF8) and
triarylamine copolymers**

The EA spectrum of PFO peaks at 402 nm. The peak of the BT EA signal occurs at 488 nm with a secondary peak occurring at 406 nm. The EA spectrum of 5BTF8 is a linear superposition of the EA spectra of PFO and BT with the main peak associated to PFO and the smaller peak associated to BT. The EA of BFB peaks at 412 nm. The EA of the 5BTF8:BFB blend merely resembles the EA of 5BTF8 with almost no apparent contribution from BFB. We also found that the signal increases with either the DC or the AC voltage in a linear way and that even when no DC bias was applied the signal was not zero due to the presence of a built in field across the device. We then scanned the blend BFB/5BTF8 device structures in forward DC bias from -3 to +3 V while probing the device at 402 nm and recorded the EA signal as a function of DC voltage at the fundamental frequency and at the peak wavelength. The EA signal was measured with an AC bias of 1 V. Figure 5.14 shows the 1f EA spectrum peak response as a function of DC voltage for 5BTF8:BFB blend LEDs with Al, LiF(1nm)/Al, LiF(2nm)/Al and LiF(5nm)/Al cathodes.

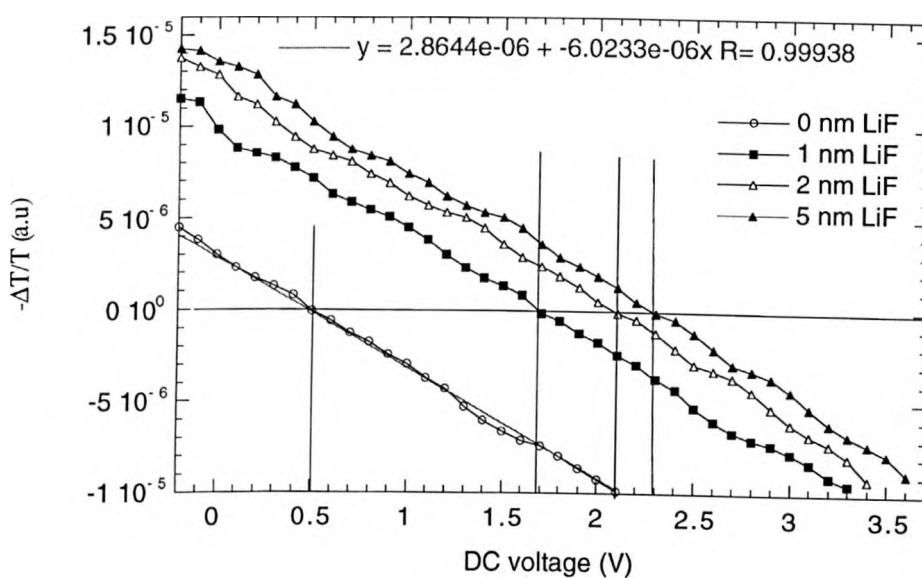


Figure 5.14: 1f electroabsorption spectrum peak response as a function of DC voltage with Al (open circles), LiF(1nm)/Al (filled squares), LiF(2nm)/Al (open triangles) and LiF(5nm)/Al (filled triangles) cathode.

The voltage at which the EA signal becomes zero corresponds to the voltage necessary to cancel the internal electrostatic potential produced by the different contacts. This energy difference between the workfunctions of the two electrodes is termed as the built-in potential and requires that no significant charge accumulation takes place inside the bulk due to either intrinsic or extrinsic defect states. Devices with different LiF thickness were fabricated in order to measure the effect of the LiF thickness on the workfunction of the bilayer cathode. The bias required to null the EA signal for a 1 nm thick LiF layer was 1.7 V compared to 0.5 V for Al. This value increased to 2.1 and 2.3 V for a 2 and 5 nm thick LiF layer, respectively. This is entirely consistent with internal photoemission results reported by Shaheen *et. al.* where a sharp decrease of the Al workfunction was observed upon deposition of LiF monolayers.²⁹ These results are also in good agreement with recently published work by Cacialli *et. al.* on polyarylene LEDs with a LiF/Al cathode where a similar reduction of the LiF/Al workfunction was observed with a saturation value reached for a 7 nm thick LiF layer.³⁸ The thicker the LiF layer, the larger the reduction of the barrier height for electron injection. In other words the further towards the vacuum level the Fermi level of the cathode shifts with increasing LiF thickness which results in a concomitant decrease of the LiF/Al “effective” workfunction. These results provide clear evidence that no band bending occurs at the polymer/LiF/Al interface in contrast to other reports on MEHPPV LEDs which suggested band bending as the mechanism behind the improvement of electron injection.³⁴ They also suggest that the main reason for the enhancement of the device performance (lower turn-on voltage, higher efficiency, higher luminance and current density) upon insertion of LiF is the decrease of the barrier height at the interface for electron injection from the cathode to the LUMO of the polymer. The significant reduction of the barrier height compared to Al which is up to 1.8 V for a 5 nm thick LiF layer results in a significant enhancement of the electron injection rate which will result in a better balance of the hole and electron currents. If we take into account that Al has a workfunction of 4.3 eV we estimate that the workfunction of ITO is

Chapter 5: Green light emitting diodes from blends of a benzothiadiazole doped polyfluorene (5BTF8) and triarylamine copolymers

~ 4.8 eV and the “effective” workfunction of a bilayer LiF(5nm)-Al cathode is ~ 2.5 eV. However, we note that LEDs with a 3 nm thick LiF layer did not show any further improvement in the performance compared to LEDs with 1.5 nm LiF. This suggests that thicker LiF layers may not further improve the performance as the detrimental effect of the insulating character of LiF on the electron conduction may overcome the beneficial effect of the continuous reduction of the electron barrier height. We also note that interfacial dipoles can influence the built in potential by shifting the energy levels and therefore can affect the “effective” workfunction of the cathode resulting in an overestimation of the reduction in the barrier height. We also examined the possibility of charge trapping in BT, 5BTF8, BFB and 5BTF8:BFB by employing the time resolved EA technique as presented in Chapter 4. The LEDs were biased, relative to the built in potential, and the EA signal was measured following removal of the bias. Figure 5.15 shows the EA peak response of 5BTF8. The inset shows the response of BT. Figures 5.16 and 5.17 show the peak responses of BFB and 5BTF8:(20 wt.%)BFB, respectively.

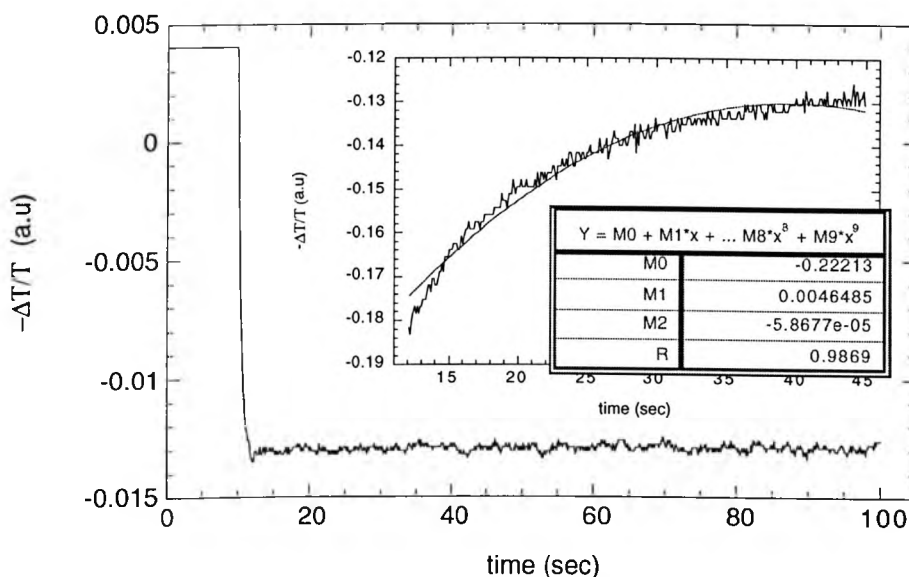


Figure 5.15: EA peak response of 5BTF8. The inset shows the response of BT.

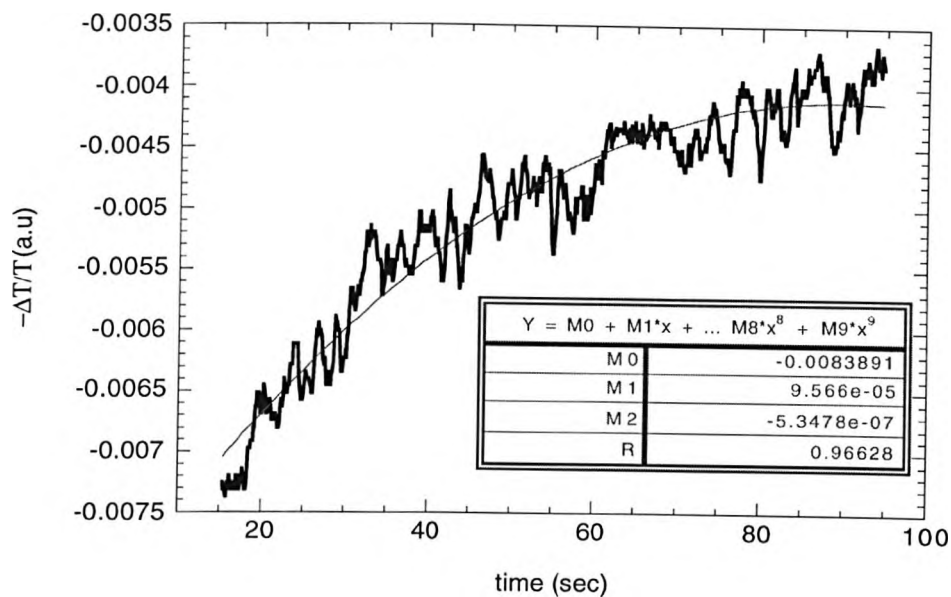


Figure 5.16: EA peak response of BFB with the parameters of a polynomial function used to fit the curve.

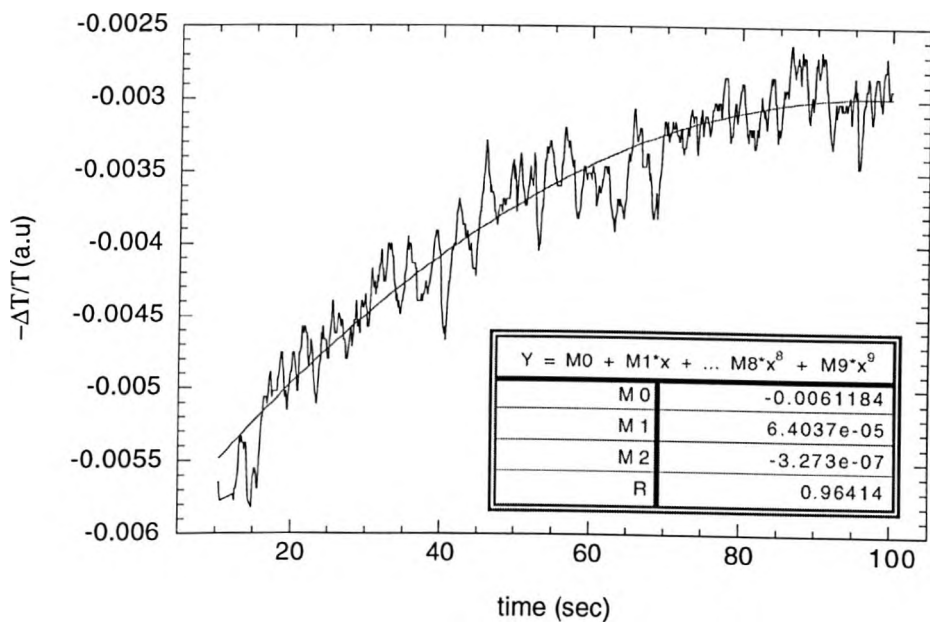


Figure 5.17: Time resolved EA spectrum peak response of 5BTF8:BFB(4/1) with the calculated parameters of a polynomial function used to fit the curve.

**Chapter 5: Green light emitting diodes
from blends of a benzothiadiazole doped polyfluorene (5BTF8) and
triarylamine copolymers**

Following removal of the applied bias, the EA signal reversed sign and exponentially decayed to zero in all cases except in 5BTF8. The decay can be accurately fit by a second order polynomial function which can be approximated to an exponential decay function (with an $\exp(-t/\tau)$ dependence where τ is the decay constant). The sign reversal of the EA signal has been associated by Giebeler *et. al.* with trapped charges in the bulk as a result of an induced field that opposes the external field.³⁷ In BT, we observed the reversal above the onset of the EL emission and therefore we can expect that electrons will be the trapped charges with an increased magnitude of the induced field with increasing applied bias until the onset of EL followed by a slight decrease due to recombination occurring at trap sites. We did not observe any counter electric field in 5BTF8 which suggests that trapping in the blend may be suppressed as a result of the decreased concentration of BT hopping sites and the increased separation distance of the BT chains by the PFO matrix. Electron only 5BTF8 LEDs (with a Dow metal anode and a Ca cathode) were found to sustain a space-charge limited electron current without traps at low and medium fields while BFB was not found to influence electron transport in the blend. In BFB and the 5BTF8:BFB blend the sign reversal and the decay to zero occurred before the EL onset which indicates that the trapped charges are holes that are associated with BFB sites and influence the hole transport in the blend. We calculate the decay constant for BT to be ~ 45 sec. For BFB the decay constant is calculated to be ~ 85 sec while for the 5BTF8:BFB blend it was ~ 95 sec. All the decay constants did not vary significantly with bias. The decay time t is related to the trap activation energy E_{trap} by the relation $\tau = \sigma N \langle u \rangle \exp(-E_{\text{trap}}/kT)$ ($\langle u \rangle$ is the carrier thermal velocity, T is room temperature, N is the density of states and σ is the trap capture cross section).³⁷ If we use similar parameter values for the polyfluorene derivatives we examine here to those we used for PFM ($N \sim 10^{20} \text{ cm}^{-3}$, $\langle u \rangle \sim 10^2 \text{ cm/sec}$ and $\sigma \sim 10^{-14} \text{ cm}^2$) we estimate that the activation energies are ~ 0.50 , 0.65 and 0.7 eV for BT, BFB and 5BTF8:BFB, respectively. In order then to examine the effect of Ca, which has been shown to exhibit superior electron

injection compared to other metals, on the LED performance we fabricated ITO/5BTF8:BFB(4:1)/Ca LEDs with the optimized blend thickness of the LiF LEDs (~ 90 nm). Figure 5.18 shows the luminance and the EL efficiency vs. voltage of these devices.

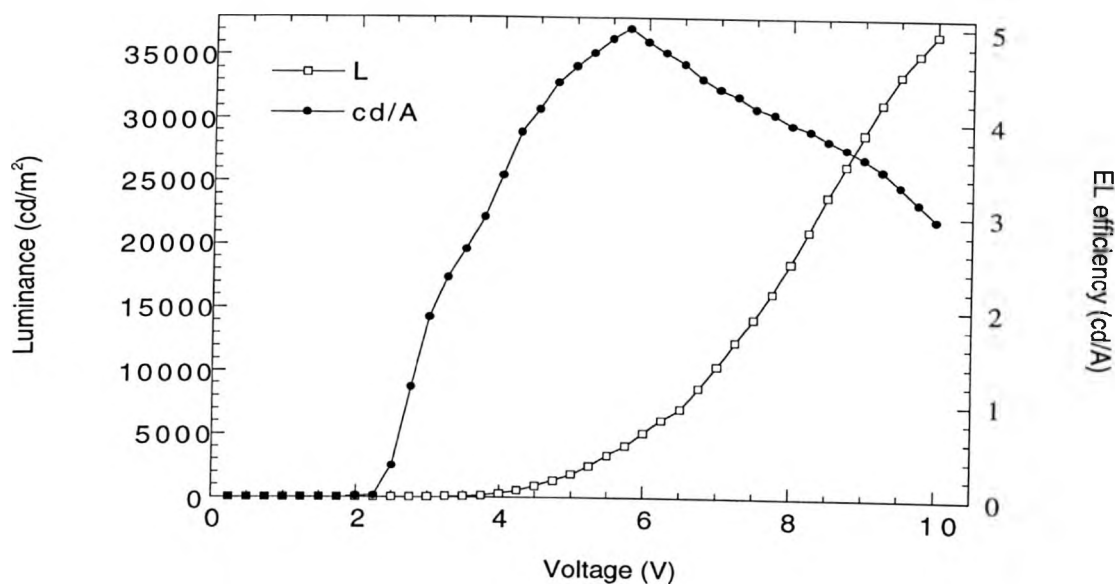


Figure 5.18: Luminance and EL efficiency vs. voltage of an ITO/5BTF8:BFB(4:1)/Ca LED.

This device reaches 100 cd/m^2 at 3.65 V and has a maximum luminance of 36500 cd/m^2 at 10 V and at a corresponding current density of 1250 mA/cm^2 . This is a factor of 4.5 higher than the luminance with a LiF/Al cathode. We calculate the maximum external EL efficiency to be 1.5% or 5 cd/A (a factor of 1.8 higher than with LiF/Al) at a brightness of 4000 cd/m^2 . The maximum power efficiency is 3 lm/W. At a brightness of 100 cd/m^2 , this device shows an efficiency of 2.8 cd/A or 0.85% and a power efficiency of 2.4 lm/W. Under pulsed operation (1 μ s pulses, 0.3% duty cycle) the device exhibits a maximum luminance of $250,000 \text{ cd/m}^2$ with an efficiency of 2 cd/A at 70 V. These results suggest that Ca is the optimum cathode for the BFB/5BTF8 blend as it yields the highest luminance, the lowest

Chapter 5: Green light emitting diodes from blends of a benzothiadiazole doped polyfluorene (5BTF8) and triarylamine copolymers

operating voltage and the highest efficiency. Apparently this is due to the superior electron injection ability of Ca compared to LiF/Al that results in highly efficient exciton recombination even though its workfunction (2.9 eV) is similar to that of the LiF(1.5nm)/Al cathode as extracted from the EA measurements. It may also indicate that the facilitation of electron injection could also be due to other factors such as the formation of midgap bipolaron energy states induced by doping the first few nm of the polymer with Ca atoms or the pinning of the surface states' energy levels through band bending. Similar observations were made by Bharathan *et. al.* on MEH-PPV LEDs where a 0.2 nm layer of Ca was sufficient to n-dope the polymer surface.³⁹ Stoessel *et. al.*⁴⁰ also demonstrated using the TOF-SIMS technique that Ca atoms diffuse into an F8BT polyfluorene at this interface and the thickness of Ca was found to affect the luminescence efficiency as the degree of diffusion depended on the Ca layer thickness. More recently, Liao *et. al.*⁴¹ showed by employing UPS and XPS techniques that bipolaron states are formed in the energy gap of PFO upon deposition of a Ca layer and that this reduces the recombination efficiency. The situation might be different here though due to the significantly higher electron mobility of 5BTF8 compared to PFO. There is also more balanced electron and hole transport⁴² and thus the recombination zone may move away from the doped interfacial region. The same authors also reported that the Ca-induced bipolaron states in the forbidden gap of polyfluorene could be removed upon oxygen exposure of Ca.⁴³ This stimulated our interest to examine the effect of oxygen exposure on the performance of 5BTF8 LEDs with Ca cathodes. A 2 nm Ca layer was deposited on top of 5BTF8 and then exposed to oxygen to form a CaO layer, which was then capped with an Al overlayer. For comparison, identical LEDs with Ca and Al cathodes were tested and the effect of depositing a 30 nm PEDOT layer on top of ITO on the device performance was also examined. Figure 5.19, 5.20 and 5.21 compare current, luminance and EL efficiency vs. field characteristics of LEDs with an ITO anode, 90 nm 5BTF8 and different cathodes; a) Al, b) Ca, c) CaO(2nm)-Al and d) Ca (with an ITO/PEDOT anode).

Chapter 5: Green light emitting diodes from blends of a benzothiadiazole doped polyfluorene (5BTF8) and triarylamine copolymers

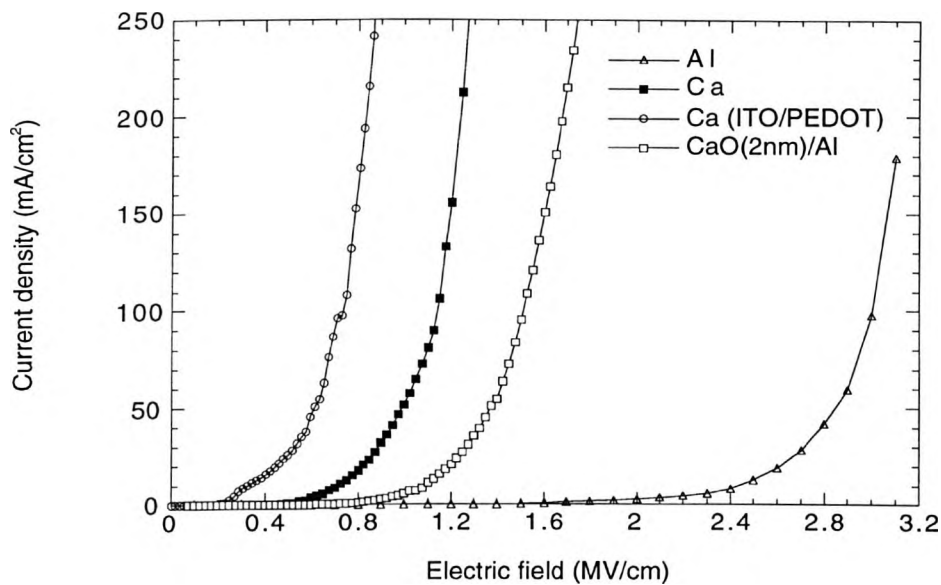


Figure 5.19: Current density vs. electric field characteristics of a) ITO/5BTF8/Al, b) ITO/5BTF8/Ca, c) ITO/PEDOT/5BTF8/Ca and d) ITO/5BTF8/CaO(2nm)-Al LEDs.

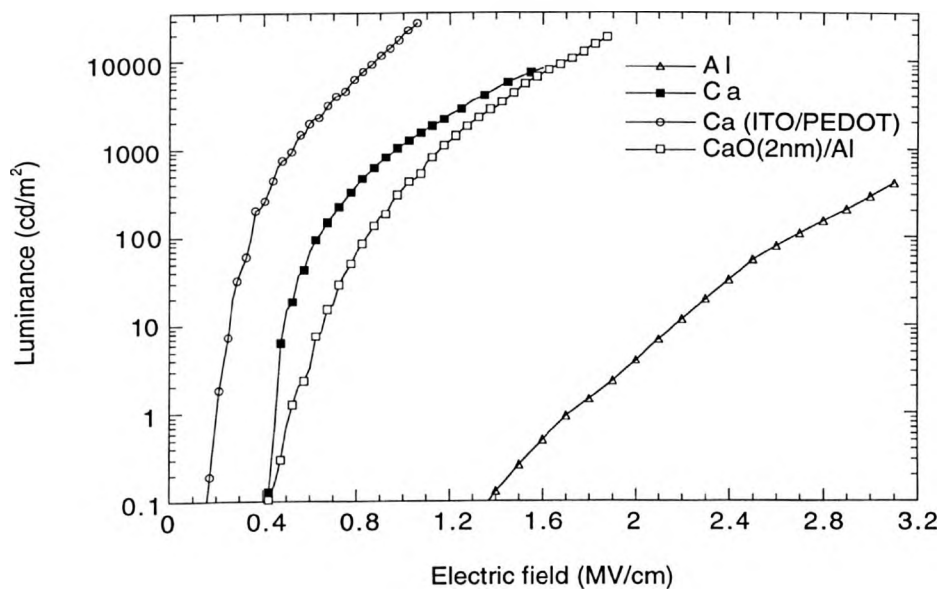


Figure 5.20: Luminance vs. electric field characteristics of 5BTF8 LEDs with different cathodes.

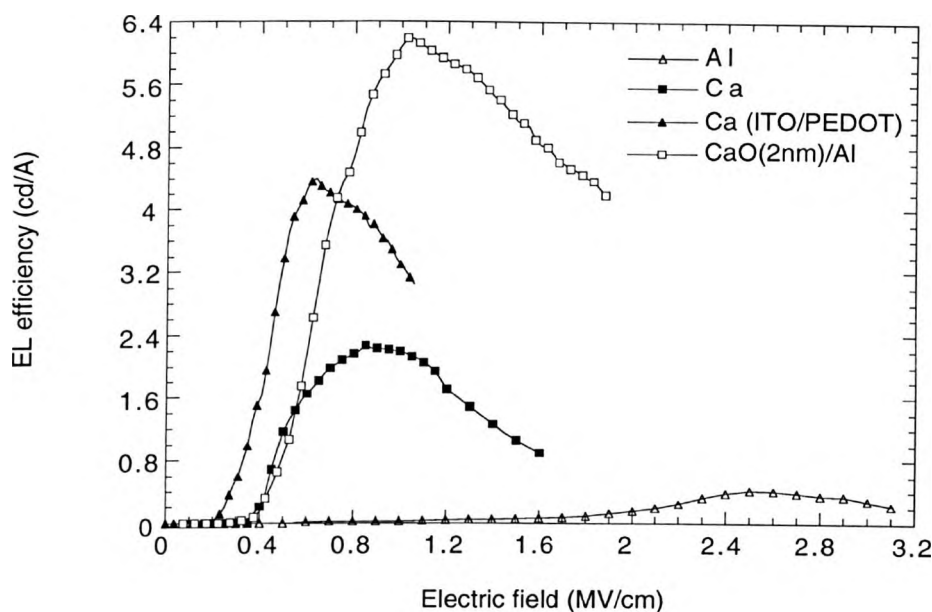


Figure 5.21: EL efficiency vs. electric field characteristics of the same series of LEDs.

With an Al cathode the device shows a maximum luminance of 400 cd/m^2 at an electric field of 3.1 MV/cm . With Ca the maximum light output increases to $\sim 8000 \text{ cd/m}^2$ at 1.6 MV/cm . A further increase to a luminance of $\sim 18500 \text{ cd/m}^2$ is obtained for CaO/Al at 1.85 MV/cm . The turn on luminance field (arbitrarily defined as the field at which the brightness is 100 cd/m^2) is 2.7 , 0.65 and 0.85 MV/cm for Al, Ca and CaO/Al, respectively. An identical trend is obtained for the turn on current field with Al yielding the highest and Ca the lowest. The maximum EL photometric efficiency is 0.4 , 2.2 and 6.2 cd/A for Al, Ca and CaO/Al, respectively. These results suggest that a thin CaO layer before Al reduces significantly the operating voltage and enhances tremendously the luminance and efficiency (by more than a order of magnitude) compared to bare Al and also performs better than Ca (with the only drawback being the slightly higher operating voltage). This improvement could be due to the n doping effect of Ca that dopes the first polymer monolayers and increases the electron injection or the removal of the gap states by exposure to oxygen. The latter process

Chapter 5: Green light emitting diodes from blends of a benzothiadiazole doped polyfluorene (5BTF8) and triarylamine copolymers

would depend on the exposure time as if the oxygen was enough to convert all the Ca atoms to CaO then the removal of the gap states would be complete. Reduction of the chemical interactions at the polymer/Al interface would also contribute to the improved performance.

Further investigations on the effect of CaO on the device performance are in progress and recent results suggest that CaO is an excellent hole blocking material.⁴⁴ This suggests that such a buffer layer will also act as to block holes from discharging at the cathode and thus to improve the electron-hole balance factor and result in more efficient recombination in the bulk by also forming a hole space charge that would enhance electron injection by redistributing the electric field near the cathode. We thus propose that a combination of the hole blocking effect of CaO and the removal of the gap states is most probably the reason for the improved performance. Also the lower operating voltage and the steeper increase of the current and luminance with Ca compared with CaO/Al indicate that the electron injection is better with Ca but that a more balanced charge transport and efficient exciton recombination is favored with CaO/Al.

The incorporation of PEDOT:PSS as a hole injection layer yields the lowest operating voltage (~ 0.45 MV/cm for 100 cd/m^2) and the highest maximum luminance ($\sim 27500 \text{ cd/m}^2$). Although it shows considerably improved performance compared to the device without the PEDOT layer, its efficiency (~ 4.4 cd/A) is lower than that of CaO/Al (~ 6 cd/A). We also measured the barrier height for hole injection at the ITO/PEDOT:PSS/polymer interface by employing the EA technique following the same experimental procedure as for LiF to see if there is a similar effect. Figure 5.22 shows the EA spectrum peak response as a function of DC voltage for 5BTF8:BFB (20wt.% BFB)/LiF(1nm)-Al LEDs with ITO and ITO/PEDOT anodes, respectively.

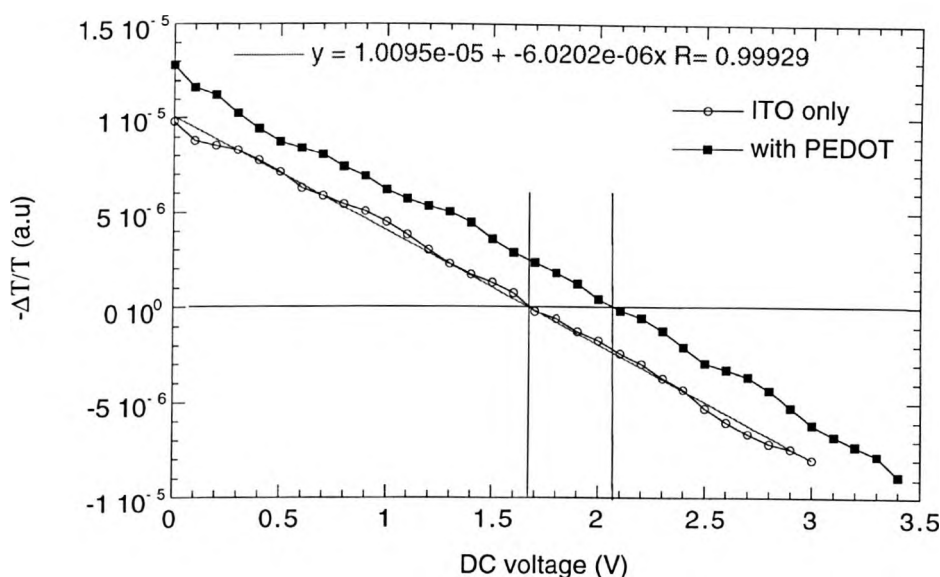


Figure 5.22: EA spectrum peak response as a function of DC voltage for 5BTF8 based LEDs with an ITO anode (open circles) and an ITO/PEDOT anode (filled squares). The straight lines are a guide to the eye.

A reduction of the anodic barrier height brought about by the deposition of PEDOT:PSS on ITO is found. More specifically, we found that in the case where ITO is used as anode the voltage necessary to null the built in electric field is 1.7 eV, whereas when ITO/PEDOT:PSS is used as anode then the built in potential is 2.1 eV. We estimated the workfunction of LiF(1nm)-Al to be 3.1 eV, thus by subtracting this value from the above experimental values, an estimate of the workfunction of ITO/PEDOT:PSS can be made. ITO/PEDOT:PSS has a workfunction of approximately 5.2 eV considering that the ITO workfunction is 4.8 eV. These results also indicate that no significant band bending occurs at the anode/polymer interface and are in excellent agreement with results reported by Brown *et. al.* on poly(phenylene-vinylene) derivative LEDs with a PEDOT:PSS coated ITO anode.⁴⁵ The reduction of the anodic barrier height brought about by PEDOT:PSS can explain the improved hole injection, the increase of the luminance and efficiency and the reduced operating voltage. The negligible voltage drop at the ITO/PEDOT interface will also result in reduced heating and therefore in more stable devices. Also the improved efficiency with

PEDOT is attributed to a combined effect of the improved hole injection at the PEDOT/5BTF8 interface compared to the ITO/5BTF8 interface, the high conductivity of PEDOT that facilitates hole transport and its electron-blocking effect which confines charges to the emitting layer. The latter is evident by the very low current flow in reverse bias.

5.5 Conclusions

In this chapter we have applied the concept of blending emissive and hole transporting polymers in order to produce high brightness, efficiency and low operating voltage green single layer PLEDs. A significant improvement of the device performance is achieved in terms of higher efficiency and brightness and lower operating voltage compared with undoped devices. The improvement of the device performance in the blend is mainly due to improved hole injection and transport in the presence of the guest hole transporting material. The host polymer termed 5BTF8 is itself a blend of a green electron transporter namely poly(9,9-dioctylfluorene-co-benzothiadiazole), (BT) and a blue poly(9,9-dioctylfluorene), (PFO) in a 5:95 ratio. The guest is a fluorene-triarylamine hole transport copolymer namely poly(9,9-dioctylfluorene-co-bis-N,N'-(4-butylphenyl)-bis-N,N'-phenylbenzidine), (BFB). Förster transfer occurs from PFO to BT in the 5BTF8 host and the improvement of the charge carrier balance factor by blending 5BTF8 with BFB increases the device brightness by more than two orders of magnitude (from $\sim 400 \text{ cd/m}^2$ to $\sim 36500 \text{ cd/m}^2$) and the efficiency by a factor of 12 (from $\sim 0.4 \text{ cd/A}$ to $\sim 5 \text{ cd/A}$) compared with the undoped device. Single layer devices with a peak emission wavelength at 535 nm that exhibit brightnesses up to $36,500 \text{ cd/m}^2$ at 10 V have been realized. The effect of a bilayer LiF/Al cathode on the device performance was also examined. The improvement of the device performance with LiF was attributed to enhanced electron injection due to a lowering of the “effective” electron injection barrier as evidenced by EA measurements. A similar decrease of

the hole injection barrier was also found on devices where a PEDOT:PSS layer was spin coated between ITO and the polymer resulting in a significant reduction of the operating voltage. Finally, exposure of Ca to oxygen to form a CaO layer was found to improve the performance of a single layer SBTF8 LED due to the combined action of CaO to improve the charge balance by acting as a hole blocking layer and to remove the exciton quenching gap states formed at the Ca,Al/polymer interface. The findings described above demonstrate that by using an appropriate blend composition both charge carrier injection and transport can be enhanced in a single-layer LED to the same level as in a bilayer device. They also illustrate the importance of the cathode/polymer interface in achieving high performance and the advantages of single-layer PLEDs with bipolar charge-carrying properties in comparison to more complicated to fabricate multilayer PLEDs.

References

1. Burroughes, J.H., Bradley, D.D.C., Brown, A.B., Marks, R.N., Mackay, K., Friend, R.H., Burn, P.L. & Holmes, A.B. *Nature* **347**, 539 (1990).
2. Speitzer, H., Becker, H., Kluge, E., Kreuder, W., Schenk, H., Demandt, R. & Soo, H. *Advanced Materials* **10**, 1340 (1998).
3. Gao, Y., Yu, G. & Heeger, A.J. *Advanced Materials* **10**, 917 (1998).
4. Becker, H., Spreitzer, H., Kreuder, W., Kluge, E., Schenk, H., Parker, I. & Cao, Y. *Advanced Materials* **12**, 42 (2000).
5. Bernius, M., Inbasekaran, M., Woo, E., Wu, W. & Wujkowski, L. *Journal of Materials Science: Materials in Electronics* **11**, 111 (2000).
6. Cao, Y., Yu, G., Parker, I.D. & Heeger, A.J. *Journal of Applied Physics* **88**, 3618 (2000).

**Chapter 5: Green light emitting diodes
from blends of a benzothiadiazole doped polyfluorene (SBTF8) and
triarylamine copolymers**

7. Ho, P.K.H., Kim, J.S., Burroughes, J.H., Becker, H., Li, S.F.Y., Brown, T.M., Cacialli, F. & Friend, R.H. *Nature* **404**, 481 (2000).
8. He, Y., Gong, S., Hattori, R. & Kanicki, J. *Applied Physics Letters* **74**, 2265 (1999).
9. Yang, Y., Pei, Q. & Heeger, A.J. *Journal of Applied Physics* **79**, 934 (1996).
10. He, Y., & Kanicki, J. *Applied Physics Letters* **76**, 661 (2000).
11. Virgili, T., Lidzey, D.G. & Bradley, D.D.C. *Advanced Materials* **12**, 58 (2000).
12. Brown, A.R., Bradley, D.D.C., Burn, P.L., Burroughes, J.H., Friend, R.H., Greenham, N.C., Holmes, A.B. & Kraft, A. *Applied Physics Letters* **61**, 2793 (1992).
13. Greenham, N.C., Moratti, S.C., Bradley, D.D.C., Friend, R.H. & Holmes, A.B. *Nature* **365**, 628 (1993).
14. Cimrova, V., Neher, D., Remmers, M. & Kminek, I., *Advanced Materials* **10**, 676 (1998).
15. Wu, C.C., Sturm, J.C., Register, R.A., Tian, J., Dana, E.P. & Thompson, M.E. *IEEE Transactions On Electron Devices* **44**, 1269 (1997).
16. Yang, Y., Chang, S.C., Bharathan, J. & Liu, J. *Journal of Materials Science-Materials in Electronics* **11**, 89 (2000).
17. Roitman, D.B., Antoniadis, H., Hueschen, M., Moon, R. & Sheats, J.R., *IEEE Journal of Selected Topics in Quantum Electronics* **4**, 58 (1998).
18. Redecker, M., Bradley, D.D.C., Inbasekaran, M. & Woo, E.P. *Applied Physics Letters* **73**, 1565 (1998).
19. Campbell, A.J. (unpublished results).
20. Grice, A.W., Bradley, D.D.C., Bernius, M.T., Inbasekaran, M., Wu, W.W. & Woo, E.P. *Applied Physics Letters* **73**, 629 (1998).
21. Redecker, M., Bradley, D.D.C., Inbasekaran, M., Wu, W.W., Woo, E.P. *Advanced Materials* **11**, 241 (1999).

**Chapter 5: Green light emitting diodes
from blends of a benzothiadiazole doped polyfluorene (5BTF8) and
triarylamine copolymers**

22. Miraura, N. & Suzuki, A. *Chem. Rev.* **95**, 2457 (1995).
23. Pope M. & Swenberg S.E. *Electronic processes in organic crystals*, Oxford University Press, New York (1982).
24. Buckley, A.R., Rahn, M.D., Hill, J., Cabanillas-Gonzalez, J., Fox, A.M. & Bradley, D.D.C. *Chemical Physics Letters* (in press).
25. Hung, L.S., Tang, C.W. & Mason, M.G. *Applied Physics Letters* **70**, 152 (1997).
26. Jabbour, G.E., Kawabe, Y., Shaheen, S.E., Wang, J.F., Morrell, M.M., Kippelen, B. & Peyghambarian, N. *Applied Physics Letters* **71**, 1762 (1997).
27. Antoniadis, H., Miller, J.N. & Roitman, D.B. *IEEE Electron Devices* **44**, 1289 (1997).
28. Giebeler, C., Antoniadis, H., Bradley, D.D.C. & Shirota, Y. *Journal of Applied Physics* **85**, 608 (1999).
29. Shaheen, S.E., Jabbour, G.E., Morrell, M.M., Kawabe, Y., Kippelen, B., Peyghambarian, N., Nabor, M.F., Schlaf, R., Mash, E.A. & Armstrong, N.R. *Journal of Applied Physics* **84**, 2324 (1998).
30. Schlaf, R., Parkinson, B.A., Lee, P.A., Nebesny, K.W., Jabbour, G., Kippelen, B., Peyghambarian, N. & Armstrong, N.R. *Journal of Applied Physics* **84**, 6729 (1998).
31. Mori, T., Fujikawa, H., Tokito, S. & Taga, Y. *Applied Physics Letters* **73**, 2763 (1998).
32. Tang, H., Li, F. & Shinar, J. *Applied Physics Letters* **71**, 2560 (1997).
33. Park, Y., Choong, V.-E., Hsieh, B.R., Tang, C.W. & Gao, Y. *Physical Review Letters* **78**, 3955 (1997).
34. Yoon, J., Kim, J.-J., Lee, T.-W. & Park, O.-O. *Applied Physics Letters* **76**, 2152 (2000).
35. Lee, H.-M., Choi, H.-J., Hwang, D.-H., Do, L.-M., Zyung, T., Lee, J.-W. & Park, J.-K. *Applied Physics Letters* **72**, 2382 (1998).

**Chapter 5: Green light emitting diodes
from blends of a benzothiadiazole doped polyfluorene (SBTF8) and
triarylamine copolymers**

36. Greczynski, G., Fahlman, M. & Salaneck, W.R. *Journal of Chemical Physics* **113**, 2407 (2000).
37. Giebeler, C., Whitelegg, S.A., Campbell, A.J., Liess, M., Martin, S.J., Lane, P.A., Bradley, D.D.C., Webster, G. & Burn, P.L. *Applied Physics Letters* **74**, 3714 (1999).
38. Brown, T.M., Friend, R.H., Millard, I.S., Lacey, D.J., Burroughes, J.H. & Cacialli, F. *Applied Physics Letters* **77**, 3096 (2000).
39. Bharathan, J.M. & Yang, Y. *Journal of Applied Physics* **84**, 3207 (1998).
40. Stoessel, M., Wittmann, G., Staudigel, J., Steuber, F., Blassing, J., Roth, W., Klausmann, H., Rogler, W., Simmerer, J., Winnacker, A., Inbasekaran, M. & Woo, E.P. *Journal of Applied Physics* **87**, 4467 (2000).
41. Liao, L.S., Cheng, L.F., Fung, M.K., Lee, C.S., Lee, S.T., Inbasekaran, M., Woo, E.P. & Wu, W.W. *Chemical Physics Letters* **325**, 405 (2000).
42. Fletcher, R.B. *PH.D Thesis* (Sheffield University, 2000).
43. Liao, L.S., Cheng, L.F., Fung, M.K., Lee, C.S., Lee, S.T., Inbasekaran, M., Woo, E.P. & Wu, W.W. *Physical Review B* **62**, 10004 (2000).
44. Wilkinson, C.I. (unpublished results).
45. Brown, T.M., Kim, J.S., Friend, R.H., Cacialli, F., Daik, R. & Feast, W.J. *Applied Physics Letters* **75**, 1679 (1999).

CHAPTER 6

ELECTROPHOSPHORESCENCE FROM PTOEP- DOPED POLYFLUORENE RED LIGHT-EMITTING DIODES

6.1 Introduction

A continuous research effort in numerous academic and industrial labs worldwide to improve the performance of polymer light-emitting diodes (PLEDs) over the last decade has now led to devices that are rapidly approaching the performance levels needed for commercial applications and the first products are expected to appear in the market soon.¹ Much of the work undertaken has focused on increasing the efficiency of LEDs by either balancing the charge carrier injection and transport² or doping the host with a highly emissive fluorescent dye.³⁻⁴ However, these efficiencies are still limited by the use of fluorescent materials where only the singlet excitons emit. Theoretically, a 1:3 ratio of singlet to triplet excitons will be formed upon charge carrier recombination under electrical excitation, assuming similar cross sections for formation of singlets and triplets and no correlation of electrons with holes prior to exciton formation.⁵

While this ratio has been experimentally confirmed by the Princeton group on OLEDs based on aluminum tris(8-hydroxyquinoline) (Alq3) doped with phosphorescent materials,⁶ other recent reports on PLEDs have brought this number into question.⁷⁻¹⁰ First, the group at Uniax reported a value of ~50% for the ratio of internal EL to PL efficiency in PLEDs with MEH-PPV blended with a PBD electron transport material.⁷ They suggested that either the exciton binding energy is small or that singlets are formed with a higher probability than triplets. The Cambridge group also reported results from LEDs based on PPV derivatives for which the internal EL efficiency was ~ 50% of the PL quantum yield of the emitter.⁸ They then calculated that the lower limit for the probability of forming a singlet exciton from electrical injection is 35%-45% in these polymers by taking into account interference effects on the radiative rate. They attributed this result to the more extended nature of the singlet state that leads to a higher probability formation during electron-hole capture and possibly to the extended conjugation that can modify the recombination process. Wohlgenannt et. al. also reported that the ratio of the formation cross-section of singlets to triplets depends systematically on the optical gap of the material and reaches a value of 5 for red-emitting polymers.⁹ The Mons group also performed theoretical calculations by applying a molecular orbital perturbation approach to a model poly(paraphenylenevinylene) system and found that the ratio between EL and PL quantum yields exceeded the 25% limit.¹⁰ This was also attributed to the higher singlet formation cross-section imposed by bond-charge interactions.

However even if the formation cross-section of singlets is significantly higher than that of triplets or the spin-degeneracy limit is not valid in some fluorescent materials, the efficiency is still limited by the fact that emission occurs only from singlet states. Hence, radiative recombination of both singlet and triplet states would substantially increase the EL quantum efficiency. While highly luminescent fluorescent dyes can improve the efficiency and tune the color of OLEDs,¹¹⁻¹⁴ the utilization of both singlet and triplet excitons in the recombination process requires the use of phosphorescent materials. In a phosphorescent

material, the incorporation of a heavy metal atom results in strong spin-orbit coupling which makes the transition from the triplet excited to the ground singlet state weakly allowed. Thus emission from both singlet and triplet states can be harvested and the internal EL efficiency can theoretically reach 100% of the PL efficiency of the emitting material.

The first report of electrophosphorescent OLEDs came from the Princeton group. They reported high efficiency energy transfer from both singlet and triplet states, in a Alq₃ host material doped with the phosphorescent dye 2,3,7,8,12,13,17,18-octaethyl-21H,23H-porphyrin platinum (II) (PtOEP).¹⁵ They demonstrated doped OLEDs with saturated red emission and peak external quantum efficiencies of 4% at low brightness due to emission from both singlet and triplet states. A significant decrease of the quantum efficiency at high current densities and dopant concentrations, associated with bimolecular interactions such as triplet-triplet annihilation and concentration quenching, was also observed in these devices. Since then, PtOEP and several other phosphorescent dyes have been employed in a variety of LEDs, doped either into a small molecule¹⁶⁻²¹ or a conjugated polymer²²⁻²⁵ host in an effort to utilise both singlets and triplets in the recombination process. Very high maximum external quantum efficiencies of 5.5% from platinum (II) porphyrins (PTOX) based OLEDs²⁶⁻²⁷ and 15% from iridium (III) tris (2-phenylpyridine) [Ir (ppy)₃] based OLEDs²⁸⁻³⁰ have been achieved, demonstrating the potential arising from the use of phosphorescent dopants in organic LEDs. Furthermore, red phosphorescent OLEDs with extremely long operating lifetimes that approach 10⁷ hours under pulsed operation (projected to 50% initial brightness) have been demonstrated,³¹ thus addressing another advantage the phosphorescent devices may possess when compared with the fluorescent ones.

Efficient, pure red PLEDs are necessary in order to develop full-color displays. However they are particularly difficult to make because red-emitting materials remain elusive and the human eye is more sensitive to the orange than to the red emission; thus if the

spectrum falls slightly in the orange, the color perceived will be "orangish red". Europium (Eu) complexes have been widely investigated due to their sharp emission bands and their potential to utilize triplets, either by using them as single emissive compounds or by doping them into blue emitting host materials.³²⁻³⁵ Porphyrin compounds have also been found to produce efficient saturated red LEDs when doped in appropriate small molecule hosts.³⁶⁻³⁷

Here, we will show that highly efficient pure red emission can be achieved in polymer LEDs by using a host-guest system configuration where the energy is efficiently transferred from the blue to the red. A blue emissive poly (9,9-dioctylfluorene) (PFO) is used as a host. The red emissive phosphorescent dye, 2,3,7,8,12,13,17,18-octaethyl-21H,23H-porphyrin platinum (II) (PtOEP), is doped into PFO at different concentrations up to 8% by weight resulting in sharp, bright and efficient red electroluminescence emission peaked at 646 nm with a full width at half maximum (FWHM) of 17 nm. It is demonstrated that the maximum external EL efficiency of the doped PFO devices increases by an order of magnitude compared to that of the undoped devices. This is a direct consequence of the successful utilization of both singlet and triplet excitons in the radiative recombination and electroluminescence emission process in these doped LEDs. We will also describe the fabrication and the performance of phosphorescent red PLEDs with emphasis given to the factors that affect the device performance and result in different spectral dependence for the PL and EL emission as a function of the dopant concentration.

6.2 Experimental details

PtOEP was purchased from Porphyrin Products Inc.³⁸ and used without any further purification. PtOEP was dissolved in toluene at a concentration of 0.2% by weight. The solution was first heated at 80°C for a few minutes and then it was left in an ultrasonic bath for 10 minutes in order to obtain a clear homogeneous solution. PFO emits blue light with a

high photoluminescence quantum efficiency of 55% and efficient multilayer PLEDs with a PFO emissive layer were first demonstrated by Grice *et al.*³⁹ These devices emitted blue light with a peak wavelength of 436 nm and with maximum external quantum efficiency of 0.2%. In addition to the neat films of PFO, doped PFO:PtOEP films were also prepared with concentrations ranging from 0.1% up to 8% by weight for optical and electrical measurements. LEDs are fabricated using indium tin oxide (ITO) as an anode and Ca as a cathode. For single layer devices, the blend was spin coated from a toluene solution. For double layer LEDs, N,N-di (3-hydroxycarbonyl-phenyl)-N,N-diphenylbenzidine (BFA) and PEDOT/PSS were used as a separate hole transport layer (HTL) and hole injection layer, respectively. BFA is insoluble in toluene so a distinct heterojunction interface is expected to be formed between this and the second layer upon spin casting without significant interpenetration taking place between the 2 layers. BFA was dissolved in tetrahydrofuran (THF) at a concentration of 15 mg/mL and spun at 6000 rpm to form a 40 nm thick layer. BFA was baked at 60 °C for 2 hours under vacuum to remove any residual solvent. PEDOT/PSS was spun from a methanol solution at 2500 rpm to form a 40 nm thick layer on top of ITO and it was then baked at 150 °C for 15 minutes in air to render it insoluble. Thickness measurements of the double layer devices show that the total thickness is approximately equal to the sum of the thicknesses of the two layers as measured separately on a glass substrate. This indicates that the desired total thickness of the double layer LEDs has been preserved during the spincoating process. The devices were then transferred to a nitrogen filled glove box where a 250 nm thick Ca cathode was thermally evaporated at a basic pressure of 10^{-6} Torr. All the device characterization was done inside the glove box.

Double layer devices with a HTL have been extensively reported in the literature since the first reports of a two layer organic LED by Tang *et al.*⁴⁰ and a two layer polymer LED by Brown *et al.*⁴¹ They have been shown to improve the external EL quantum efficiency and to reduce the turn on electric field of polymer LEDs by improving the injection and transport of

Chapter 6: Electrophosphorescence from PtOEP-doped polyfluorene red light-emitting diodes

the charge carriers (electrons and holes). They allow for a separate optimization of the injection and the transport of both charge carrier types. They can also introduce energy level offsets at the heterojunction that act as a feedback mechanism to the injection process and due to the accumulation of charge carriers at this interface a redistribution of the internal electric field and an enhancement on the injection of the minority charge carriers is expected to occur. This structure can also help in keeping the recombination zone away from the cathode where exciton quenching effects are present due to defects that are generated during the metal deposition and usually act as luminescence quenching sites.

Figure 6.1 shows the chemical structures of the materials used as a host and as a dopant.

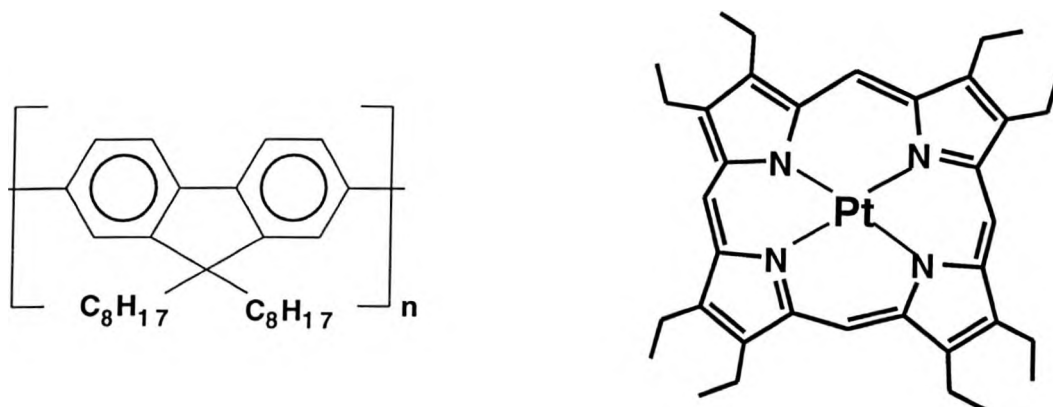


Figure 6.1: The chemical structures of the host PFO and the dopant PtOEP.

6.3 Optical spectroscopy studies of blends of PtOEP and PFO

Figure 6.2 shows the optical absorption spectra of PFO and 0.1 wt% PtOEP:PMMA, the photoluminescence spectrum of PFO and the phosphorescence spectrum of 0.1 wt% PtOEP:PMMA.

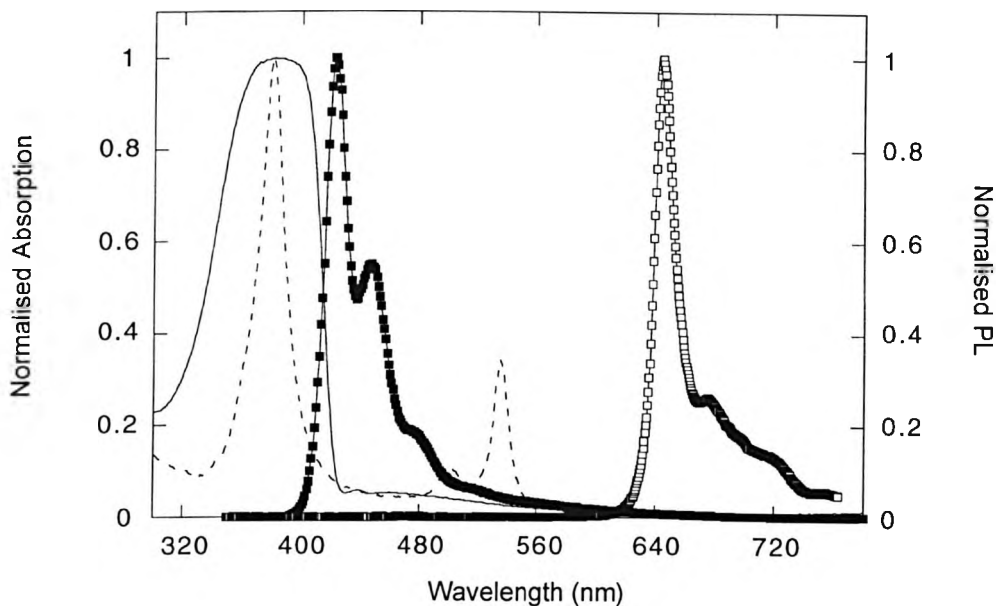


Figure 6.2: Absorption spectra of PFO (solid line) and 0.1 wt% PtOEP in PMMA (dashed line), PL spectrum of PFO (filled squares) and phosphorescence spectrum of 0.1 wt% PtOEP in PMMA (open squares).

As shown in Figure 6.2 above, there is a weak overlap between the photoluminescence spectrum of PFO and the Soret absorption band of PtOEP at 380 nm such that Förster energy transfer is possible. The Q band of the PtOEP absorption is at 536 nm and a small spectral overlap also occurs between this band and the emission of PFO. PtOEP was dissolved in an inert polymer matrix, polymethylmethacrylate (PMMA) in order to isolate the PtOEP molecules and reduce intermolecular interactions between them that would result in aggregation-induced concentration quenching of its emission. Figure 6.3 shows the absorption spectra of PFO/PtOEP blends with different PtOEP concentrations. The spectra are normalised to the PFO absorption peak at 380 nm and are offset for comparison. The PL spectra of PFO/PtOEP blends (normalised to the phosphorescence peak at 646 nm) as a function of the PtOEP concentration are also shown in Figure 6.4.

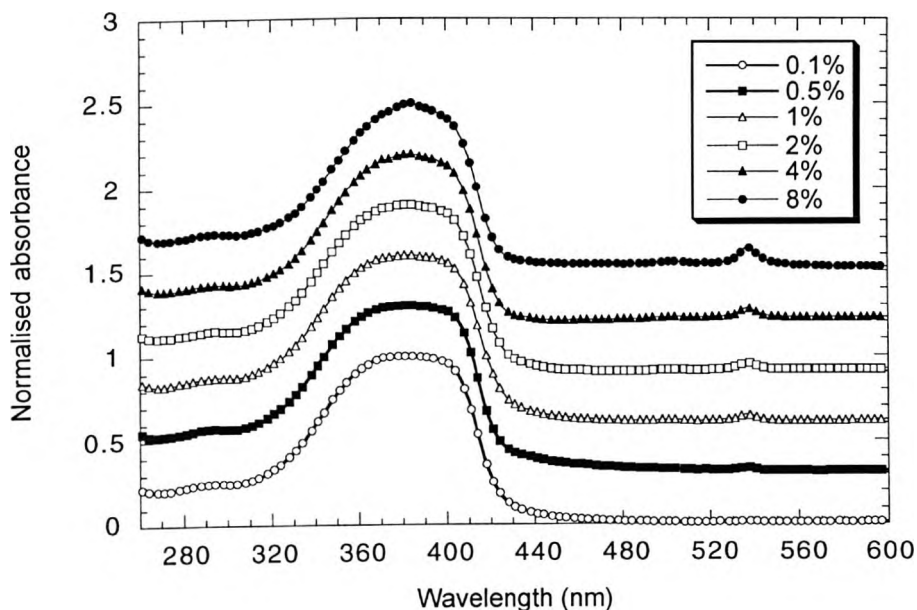


Figure 6.3: The absorption spectra of PtOEP doped PFO films with different PtOEP concentrations. The spectra are normalised to the PFO absorption peak at 380 nm and offset for comparison.

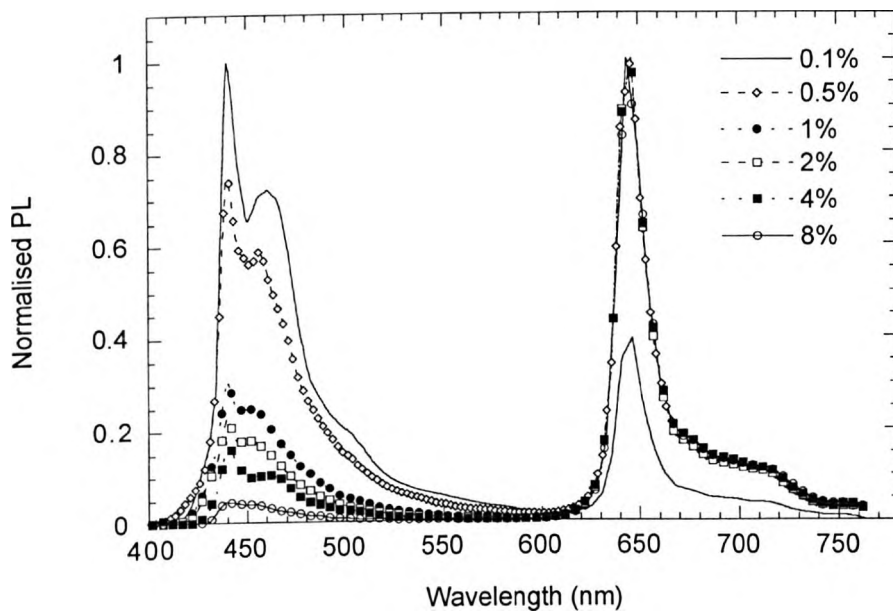


Figure 6.4: The photoluminescence emission spectra of a series of PFO:PtOEP films with varying concentrations of PtOEP ranging from 0.2% to 8%.

The absorption spectra of the PtOEP/PFO blends are superpositions of the individual spectra of PFO and PtOEP. The PL spectra of the PFO/PtOEP blends testify to the occurrence of only weak energy transfer in this system. As the concentration of the PtOEP increases in the blend, the contribution of the PFO blue emission to the PL decreases and that of the red emission of PtOEP increases. At 0.2% PtOEP concentration, PFO emission dominates the PL while above 1% PtOEP concentration, PtOEP emission is dominant. However even at 8% doping, some emission from PFO still remains which strongly implies that the energy transfer is not complete and that the efficiency of the transfer is moderate. Singlet exciton transfer from the host to the guest will occur by a long-range dipole-dipole coupling process (Förster transfer). Triplet excitons cannot be transferred from the host to the guest with a Förster transfer process due to lack of spin conservation, rather transfer can only occur by direct electron exchange between the host and the guest. Energy transfer of singlet excitons can be characterised by the Förster radius, which is defined as the distance between the host and the guest for which intermolecular energy transfer to the guest and radiative recombination and decay on the host are equally probable.

The Förster transfer radius can be calculated by using the following relation:

$$R_0 = \left(0.527K^2T / N_A n^4\right)^{1/6}$$

where K^2 is an orientation factor ($2/3$ for random dipole orientation), N_A is Avogadro's number, n is the refractive index of the host and T is the overlap integral between the absorption spectrum of the acceptor and the fluorescence spectrum of the donor molecules.⁴²

By comparing the fluorescence spectrum of PFO and the absorption spectrum of PtOEP, we have calculated the Förster radius of the PFO/PtOEP system and found it to be 1.7 nm. This is a rather small value, as expected by the weak overlap of the donor emission and the acceptor absorption spectra, compared to typical Förster radii of 5 nm found for other host-guest systems.^{3,37} It indicates that high dopant concentrations would be needed in order for a complete transfer of singlet excitons from PFO to PtOEP to occur.

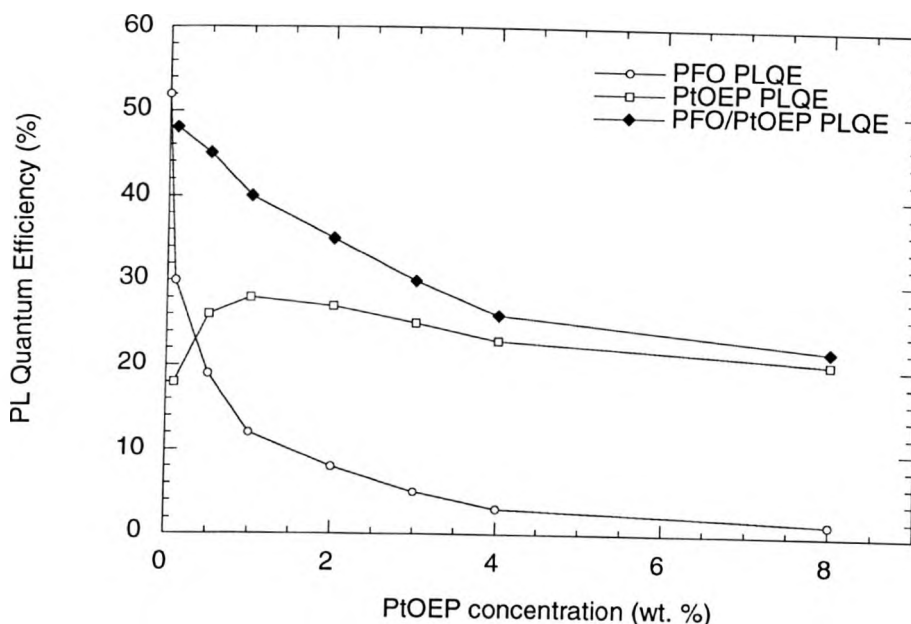


Figure 6.5: PFO PL (open circles), PtOEP phosphorescence (open squares), and total PL efficiencies (filled diamonds) as a function of the PtOEP concentration (The standard error of the PLQE measurement is ~ 2%).

In Figure 6.5 above, the PFO photoluminescence, the PtOEP phosphorescence, and the total photoluminescence quantum efficiencies as a function of the PtOEP concentration are shown. The contribution of the PFO yield to the total yield decreases significantly as the PtOEP dopant concentration increases. As the samples are excited at 354 nm where PtOEP absorption is quite weak, virtually all of the absorption will be on the PFO. The ratio of the photoluminescence quantum efficiencies of the blend components can then be used to independently calculate the Förster radius.⁴³ As the PL quantum yield of PFO is approximately 52% and that of PtOEP in PMMA is approximately 26%, the distance between the dopant molecules at which the PL efficiency of PFO is approximately 2 times that of PtOEP will be equal to the Förster transfer radius. Energy transfer is found to be equally probable at a typical separation between the PtOEP molecules of 1.9 nm (we have assumed that the PtOEP molecules are dispersed uniformly in the host PFO). This value is in good

Chapter 6: Electrophosphorescence from PtOEP-doped polyfluorene red light-emitting diodes

agreement with the overlap integral calculation. The decrease of the PtOEP phosphorescence quantum efficiency from 28% at 1 wt% PtOEP concentration to 20% at 8 wt% PtOEP is attributed to significant intermolecular interactions between PtOEP molecules that reduce the PtOEP quantum yield below that of dilute PtOEP in PMMA. Evidence for aggregation is seen in the absorption spectrum of a high concentration of PtOEP in a polystyrene host where significant scattering in the absorption tail and some splitting of the spectrum was observed.

Further evidence that Förster energy transfer occurs was obtained by time resolved PL measurements. Figure 6.6 presents typical data from time resolved photoluminescence experiments on PtOEP:PFO blends. Time resolved fluorescence decay curves of PFO emission from different concentration PtOEP:PFO blends are shown.

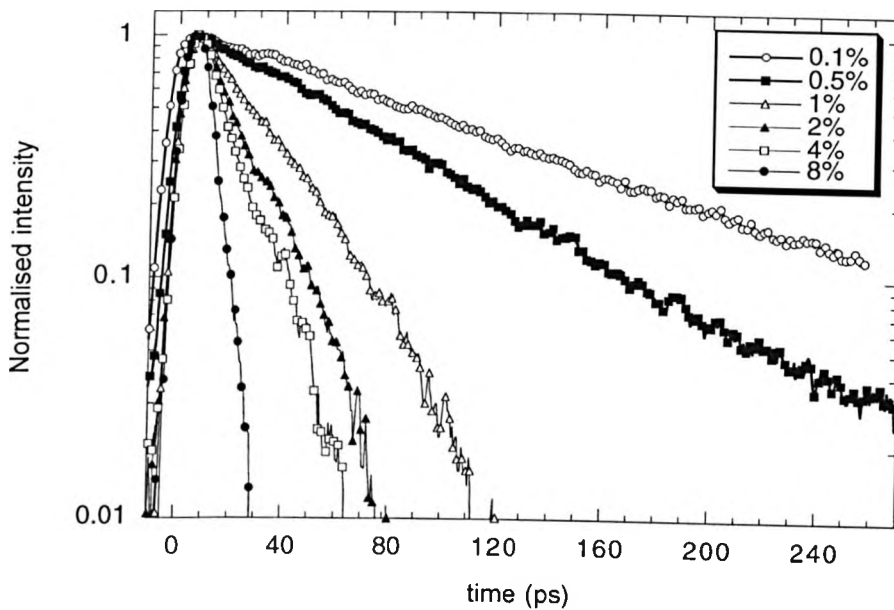


Figure 6.6: Time resolved fluorescence decay of PFO emission from different concentration PtOEP:PFO blends. Each of the curves is fitted well with a single exponential function indicating a single decay component. The resolution of the measured decay times is about 5 ps.

Chapter 6: Electrophosphorescence from PtOEP-doped polyfluorene red light-emitting diodes

All the fluorescent decays were fit with a single exponential function, according to the equation $I=I_0\exp(-t/\tau)$ where τ is the PL lifetime indicating a single decay component. The resolution of the measured decay times is about 5 ps. A significant reduction of the emission lifetime of the PFO host is observed with increasing PtOEP concentration in the blend. By recording the luminescence decay with a streak camera, the fluorescence lifetime of the PFO emission was estimated to be approximately 20 ps in a 4% (by weight) PtOEP:PFO blend compared to a radiative emission lifetime of approximately 350 ps obtained for a spin-coated PFO film. Figure 6.7 below, shows fitted PFO fluorescence lifetimes for different concentration PtOEP:PFO films. It is noted that at low PtOEP concentrations the values for the PFO component lifetime extrapolate to the pure PFO PL lifetime of 350 ps.

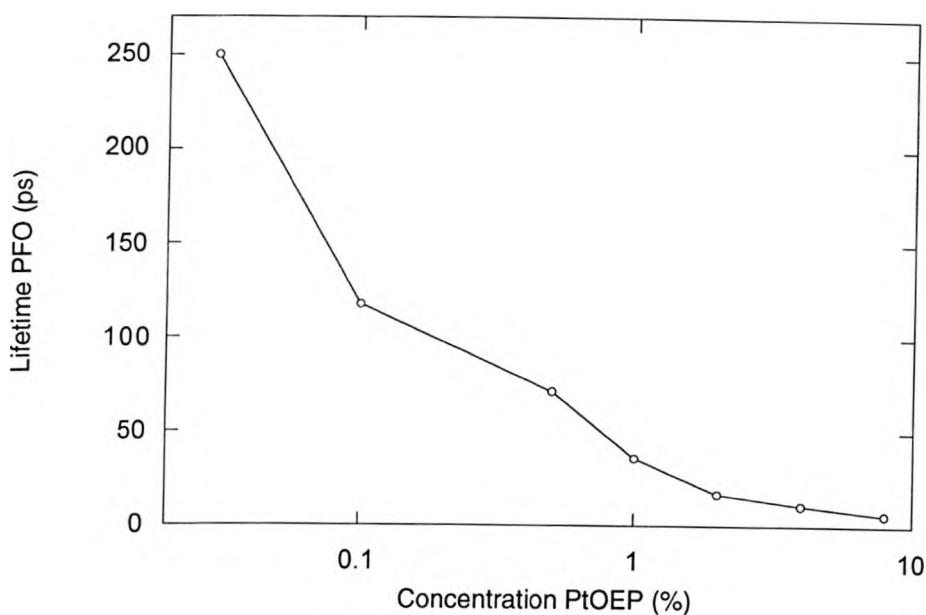


Figure 6.7: Fitted PFO component PL lifetimes for different concentration PtOEP:PFO films.

In Figure 6.8 that follows, a plot of the energy transfer rate as a function of the square of PtOEP concentration in PtOEP:PFO blends is presented.

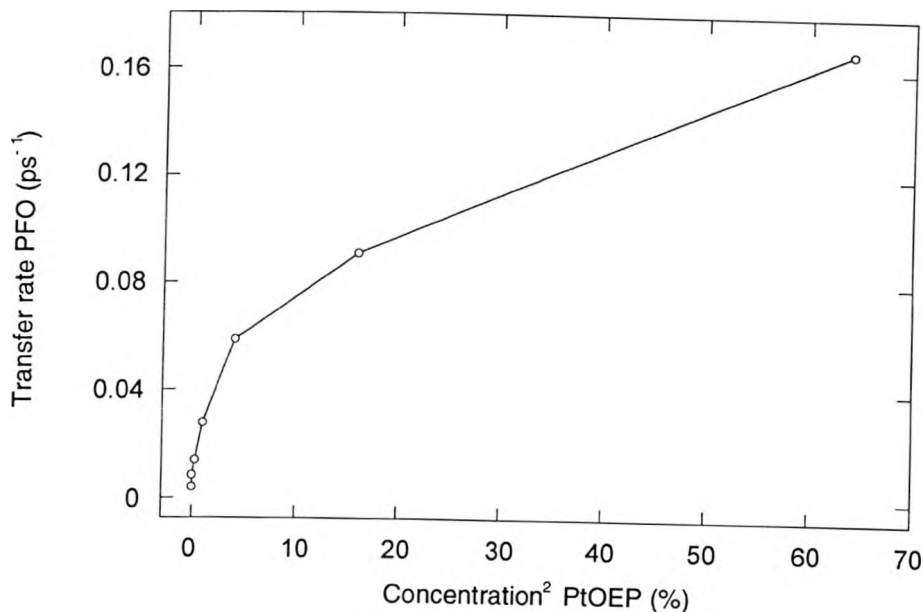


Figure 6.8: Energy transfer rate as a function of the square of PtOEP concentration in PtOEP:PFO blends.

The rate for non-radiative dipole-dipole energy transfer is given by:

$K_{ET} = 1/\tau_D(R_0/R)^6$, where τ_D is the fluorescence lifetime of the donor, R_0 is the Förster radius and R is the separation between donor and acceptor and where it has been assumed that the energy transfer is much slower than vibrational relaxation in both the donor and the acceptor. The total rate of the decay of the donor emission in the blend is given by:

$$K = K_R + K_{NR} + K_{ET} ,$$

where K_R and K_{NR} are the radiative and the nonradiative decay rates. Thus,

$$K_{ET} = K - K_R - K_{NR} \text{ or } K_{ET} = (1/\tau) - (1/\tau_D),$$

where τ is the lifetime of the donor emission in the blend. As K_{ET} has an inverse sixth power dependence on the donor-acceptor separation and the concentration of the molecules has an inverse third power dependence on their separation distance, the transfer rate should be proportional to the square of the concentration and thus a plot of the energy transfer rate versus the square of the concentration should be linear and fit to a straight line. No such dependence however was observed for the whole concentration range which implies that the

hard spheres model (according to which the guest molecules are considered as hard spheres in the host) might not be appropriate to describe this host-guest system and thus that the Förster rate equation cannot adequately describe the dependence of the transfer rate on the guest concentration. For low concentrations (<1%), a reasonable fit characteristic of the Förster kinetics could be obtained; however a significant deviation was observed at higher concentrations. Similar conclusions have been drawn by Buckley *et. al.*⁴⁴ and List *et. al.*⁴⁵ when studying polymer-polymer blends where energy migration in the host was found to occur and accounted for the inadequacy of that model to explain the experimental results.

6.4 Electrical characterization of phosphorescent PLEDs

Figure 6.9 shows the electroluminescence emission spectra of a series of ITO/PFO_(1-x):PtOEP_(x) (x=0.2%-8%)/Ca LEDs at a current density J = 10 mA/cm².

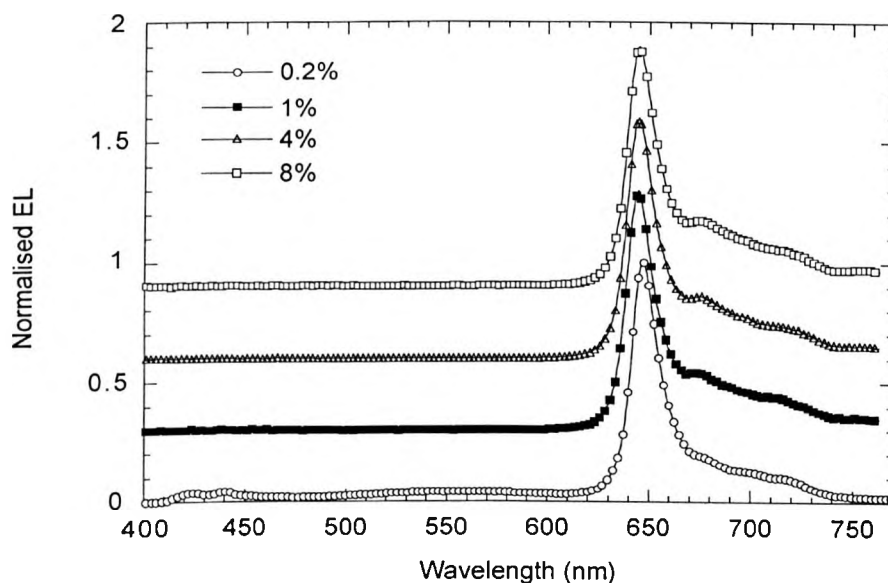


Figure 6.9: EL spectra of a series of ITO/PFO_(1-x):PtOEP_(x) (x=0.2%-8%)/Ca LEDs at a current density J = 10 mA/cm². The spectra are normalised to the phosphorescence peak at 646 nm and offset for comparison.

Unlike the PL spectra of the doped PFO:PtOEP films, the red emission characteristic of the PtOEP dominates the EL spectra at doping concentrations as low as 1%. All the EL spectra show a sharp emission peak at 646 nm with a FWHM of 17 nm and weak vibronic progression with sidebands appearing at 685 nm and 718 nm. Only the 0.2% doped device shows weak emission from the PFO singlet state at 440 nm and from the excimer PFO band at 550 nm. Almost no emission from PFO was observed at dopant concentrations above 1%. Figure 6.10 shows the EL spectra of PtOEP:PFO LEDs with a 0.1 wt% PtOEP concentration recorded at different current densities (normalised to the phosphorescence peak at 646 nm).

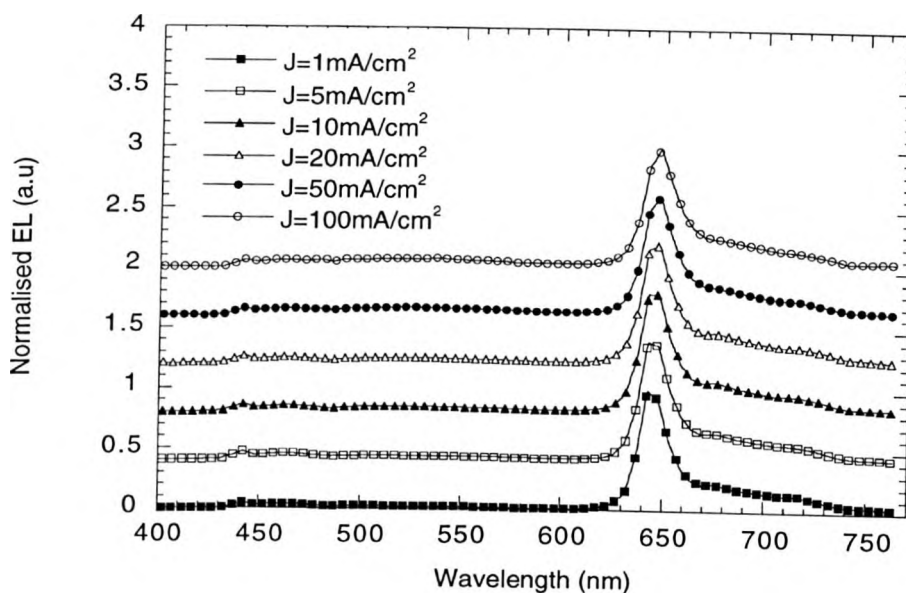


Figure 6.10: The EL spectra of PtOEP:PFO LEDs with 0.1 wt% PtOEP concentration recorded at different current densities. The spectra are normalised to the peak at 646 nm and are offset for comparison.

The EL spectra of 0.1 wt% PtOEP doped PFO LEDs are almost identical regardless of the current density. Figures 6.11 and 6.12 show in detail the wavelength region between 410 and 610 nm of the EL spectra of PtOEP:PFO LEDs with 0.1 and 4 wt.% PtOEP concentration, respectively where the growth of a new peak at 540 nm is shown with increasing current.

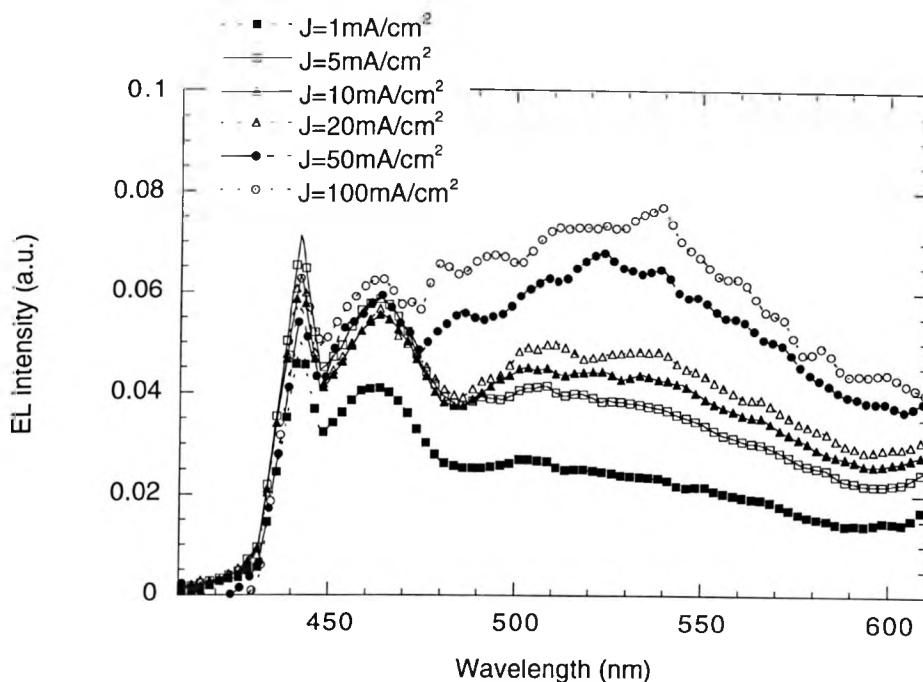


Figure 6.11: EL spectra of PtOEP(0.1wt%):PFO LEDs recorded at different current densities. The growth of a new peak at 540 nm is shown as the current density increases.

This feature, which appears as a broad shoulder at low currents, grows with increasing current and is finally resolved to a sharp feature peaked at 540 nm in both cases. It can not be ascribed to emission from either the PtOEP or the PFO singlet state as they are located around 570 and 430 nm, respectively. A possible explanation could be that this feature is due to emission from a charge transfer state formed between a PFO molecule in its ground state and a PtOEP molecule in its excited singlet state. The fact that this feature has a significantly reduced intensity (relative to the PtOEP triplet peak) in the 4% device compared to the 0.1% device further supports this argument as it indicates that the formation of this state is less likely in the presence of a higher density of PtOEP molecules that would decrease the donor-acceptor separation distance and reduce the probability of forming a PFO-PtOEP charge transfer complex with regard to the formation of a PtOEP excited state.

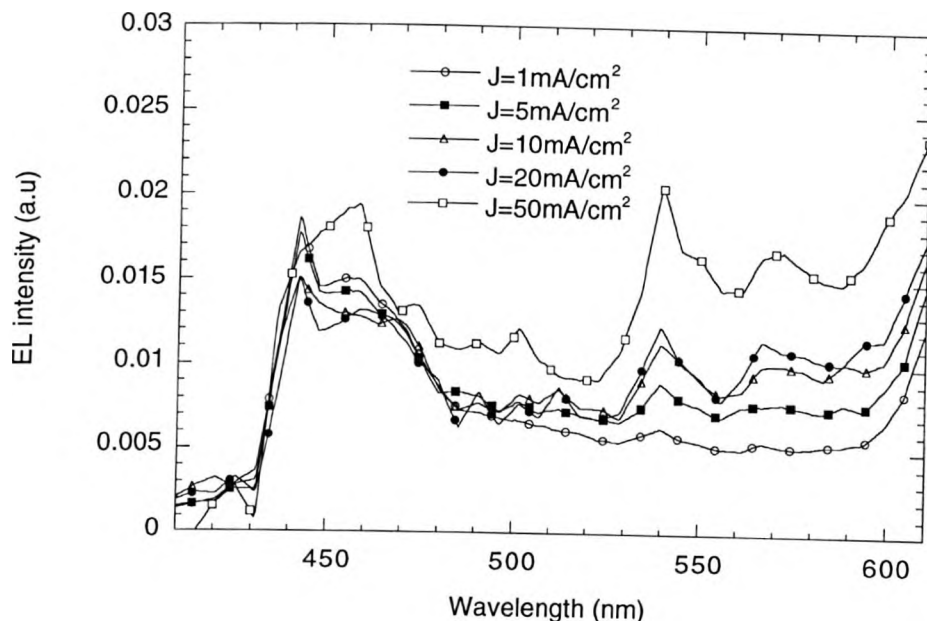


Figure 6.12: EL spectra of 4 wt% PtOEP doped PFO LEDs for different current densities. The growth of two new peaks, at 540 and 570 nm, respectively is shown as the current density increases.

The 4% doped LED also shows another distinct feature at 570 nm evolving with current which can probably be attributed to weak fluorescence from the PtOEP singlet state. The increased concentration of PtOEP molecules in the 4% device might increase the probability of radiative singlet recombination compared to the 0.1% device where this feature is not resolved even at very high current densities. Also a feature that is ascribed to PFO singlet emission is seen at around 440 nm in both devices.

The different dopant concentration dependence of the PL and EL spectra suggest that although energy transfer due to weak coupling of the guest absorption and the host emission occurs under optical excitation of the blend films, it cannot account for the dominant PtOEP emission at low dopant concentrations in the EL spectra. Rather, the additional mechanism of charge carrier trapping must be operating upon electrical operation of the devices. Ultraviolet photoelectron spectroscopy (UPS) measurements in PtOEP/Alq₃ blends have shown that the

Chapter 6: Electrophosphorescence from PtOEP-doped polyfluorene red light-emitting diodes

highest occupied molecular orbital (HOMO) of PtOEP in an Alq₃ host lies 0.5 eV below the HOMO of Alq₃ (5.9 eV).⁴⁶ This result provides strong evidence that PtOEP molecules could act both as hole traps and as recombination centres in PtOEP doped PFO LEDs. PFO has an ionisation potential of 5.8 eV and a similar energy level scheme for PtOEP should occur in a PFO host. To support this picture, the position of the PtOEP lowest unoccupied molecular orbital (LUMO) relative to that of PFO was estimated via the known optical gap of 2.2 eV for PtOEP. This calculation leads to a LUMO level of approximately 3.2 eV which lies at least 0.4 eV above the corresponding LUMO level of PFO. PtOEP could then also act as an electron trap. In that case, electrons would recombine with holes directly on the PtOEP molecules and form singlet and triplet excitons with singlets being converted to triplets via efficient intersystem crossing and resulting in phosphorescence. Triplet excitons could also be expected to transfer their energy from PFO to PtOEP by means of a Dexter transfer mechanism.⁴⁷ However, no evidence of Dexter transfer was found to occur in the PFO:PtOEP system; this is supported by the fact that the long PFO triplet lifetime (0.3-3.2 ms) did not depend on the PtOEP concentration and did not decrease in the doped system compared to the undoped PFO.⁴⁸ This allows to conclude that all the excitons except the PFO triplets are available to the recombination and emission process in the doped LEDs. The next step was the fabrication and characterization of PtOEP:PFO blend LEDs. Figure 6.13 shows the chemical structure of BFA that was used as a HTL in LEDs with a blend emissive layer.

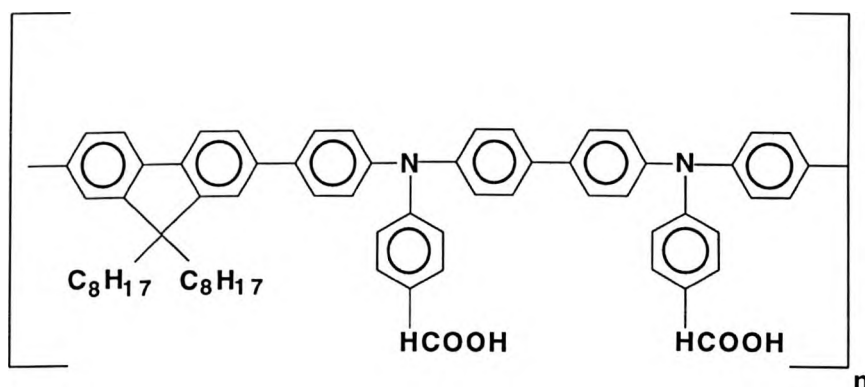


Figure 6.13: The chemical structure of the hole transporting polymer BFA.

Chapter 6: Electrophosphorescence from PtOEP-doped polyfluorene red light-emitting diodes

Figures 6.14 and 6.15 show luminance vs. voltage and EL efficiency vs. luminance characteristics of 2 wt.% PtOEP doped PFO LEDs with varying emissive layer thickness.

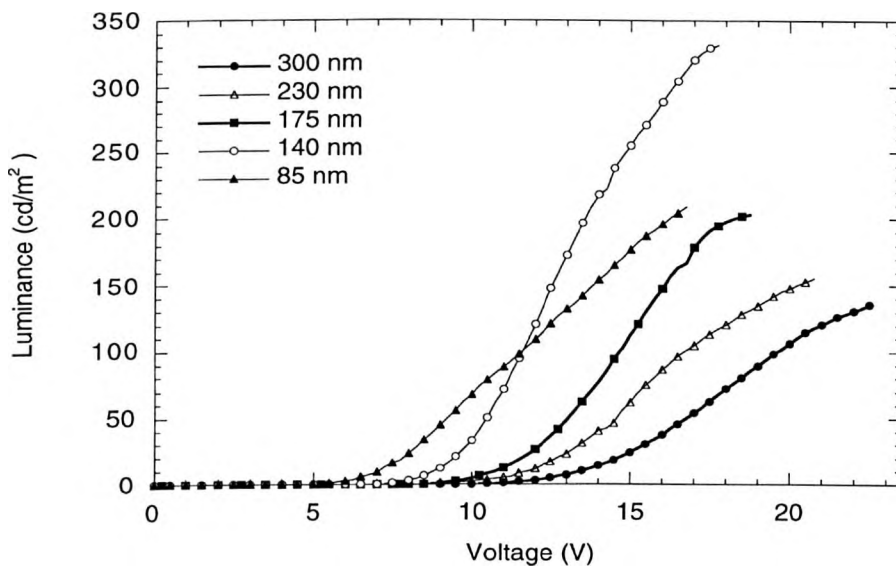


Figure 6.14: Luminance vs. voltage characteristics of 2 wt.% PtOEP doped PFO LEDs.

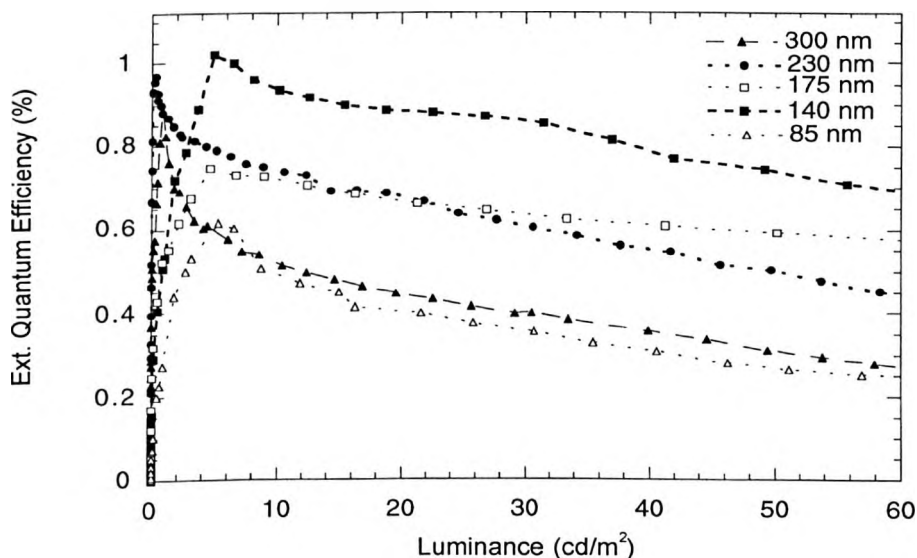


Figure 6.15: EL efficiency as a function of luminance for 2 wt.% PtOEP doped PFO LEDs.

Chapter 6: Electrophosphorescence from PtOEP-doped polyfluorene red light-emitting diodes

The optimum thickness of the blend in terms of maximum light output was approximately 140 nm. The maximum brightness of this device reached 340 cd/m^2 at 18V. The 140 nm thick layer shows the maximum EL quantum efficiency that reaches almost 1% at 5 cd/m^2 . The efficiency decreases with increasing current (it reaches 0.7% at 60 cd/m^2). It is suggested that the decrease of the efficiency at high current densities and luminance levels which has been observed as a general phenomenon among most OLEDs with phosphorescent dyes is partly due to the effects of triplet-triplet annihilation and saturation of the emissive dopant sites at a high triplet exciton population,^{15,27} and partly due to the lower recombination efficiency caused by charge imbalance at high injection levels. Current density and luminance vs. voltage (J/V & L/V) characteristics of 2 wt% PtOEP doped single and two layer (with BFA or PEDOT as a hole transport layer) PFO LEDs are shown in Figure 6.16.

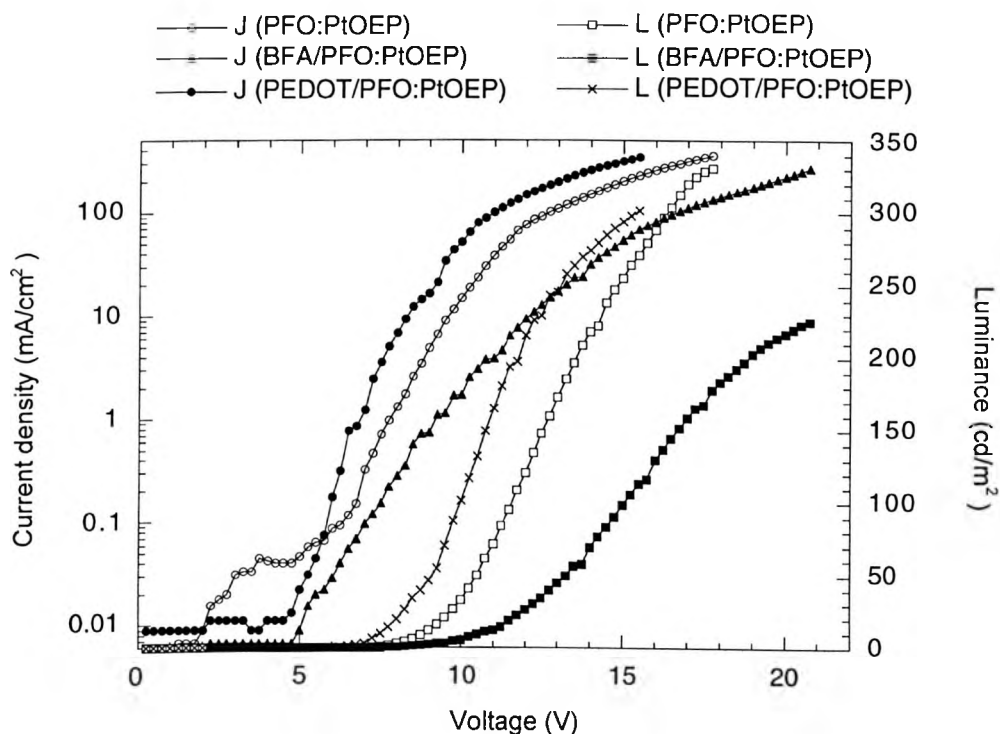


Figure 6.16: Current density and luminance vs. voltage characteristics for a) ITO/PFO:PtOEP(2%)/Ca b) ITO/BFA/PFO:PtOEP(2%)/Ca and c) ITO/PEDOT:PSS/PFO:PtOEP(2%)/Ca LEDs.

Chapter 6: Electrophosphorescence from PtOEP-doped polyfluorene red light-emitting diodes

The optimum concentration of PtOEP in PFO was found to be 2% by weight in terms of maximum EL quantum efficiency and brightness (not shown here). Both the BFA and the PEDOT:PSS layers were 40 nm thick while the PFO/PtOEP layer was 140 nm thick. It has to be noted that the 4 wt% single layer LED required a thicker layer for optimum performance probably due to the increased density of dopant molecules which in turn will increase the width of the recombination zone and thus would lead to more significant efficiency losses for thinner layers due to the long triplet exciton diffusion length. The two-layer device with PEDOT showed the lower turn on as well as operating voltage that is attributed to the much higher conductivity of PEDOT compared to that of ITO. The turn on voltage for light emission (arbitrarily defined as the voltage at which the device luminance reaches 10 cd/m^2) is 8.5, 10 and 7 V for the one layer, two layer with BFA and two layer with PEDOT LEDs, respectively. The corresponding voltage required for a current density of 1 mA/cm^2 is 6.5 V for the PEDOT device, 7.5 V for the single layer device and 9 V for the BFA device. A maximum brightness of 340 cd m^{-2} was observed at a corresponding current density of 400 mA cm^{-2} and a maximum external EL efficiency of 1% was obtained at low brightness. The quantum efficiency is almost a factor of 5 higher than that obtained for optimized PFO devices in a similar two-layer device configuration with a BFA hole transport layer.³⁹ We attribute the higher efficiency observed here to the efficient use of both singlet and triplet excitons in the radiative recombination and emission process in the doped LEDs.

Under pulsed driving operation (500 ns pulses with 300 μs period from a pulse generator were used for this purpose), a peak emission brightness of $15,000 \text{ cd/m}^2$ was obtained at 70 V. Transient EL decay measurements of a 4% doped PFO LED reveal an EL transient decay time of $55 \mu\text{s}$ ⁴⁹ which is consistent with previously reported PtOEP emission lifetime data ($\tau=70 \mu\text{s}$).¹⁷ The slight decrease of the PtOEP lifetime in our LEDs might be due to the exciton confinement in a very narrow recombination zone region on the dopant sites that could lead to increased triplet exciton annihilation.

Chapter 6: Electrophosphorescence from PtOEP-doped polyfluorene red light-emitting diodes

In order to improve further the quantum efficiency of these LEDs, we employed ITO from a different supplier as an anode. This ITO has a lower workfunction (4.3 eV) compared to our standard ITO (4.7 eV) and thus a higher barrier for hole injection to the HOMO level of BFA (5.3 eV) is expected to be formed. Shaheen *et al.*⁵⁰ have shown that the device efficiency increases by shifting the ionization potential of the hole transport material further away from the HOMO level of the emitting material in a two layer configuration. In other words, the higher the barrier that holes had to cross at the HTL/EML interface was, the higher was the device efficiency. This enhancement was attributed to the improved carrier balance achieved that increases the recombination efficiency. A similar improvement should be expected by increasing the barrier for hole injection from the anode to the HTL, aiming to improve the electron-hole balance in the device.

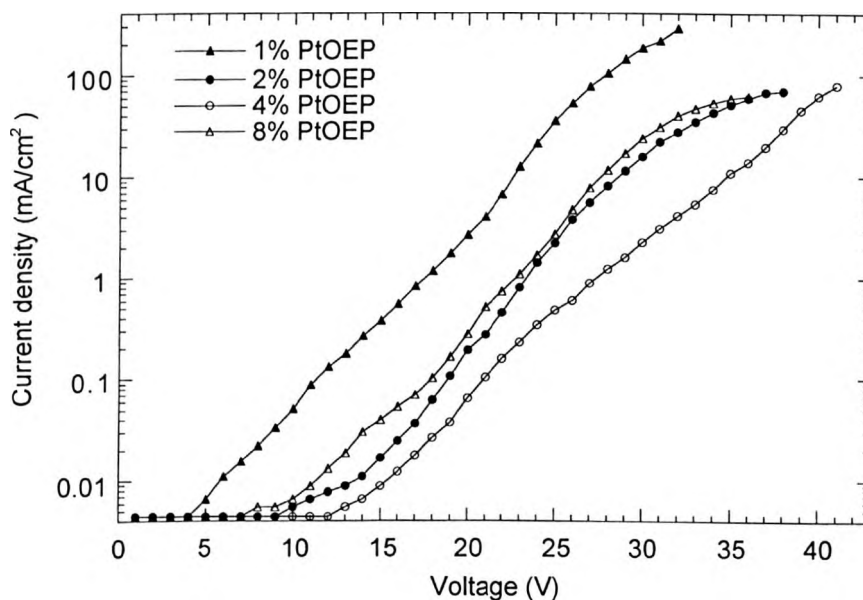


Figure 6.17: The current density as a function of applied voltage for doped PFO:PtOEP LEDs with PtOEP concentrations of 1%(filled triangles), 2% (filled symbols), 4% (open symbols) and 8% (open triangles) by weight.

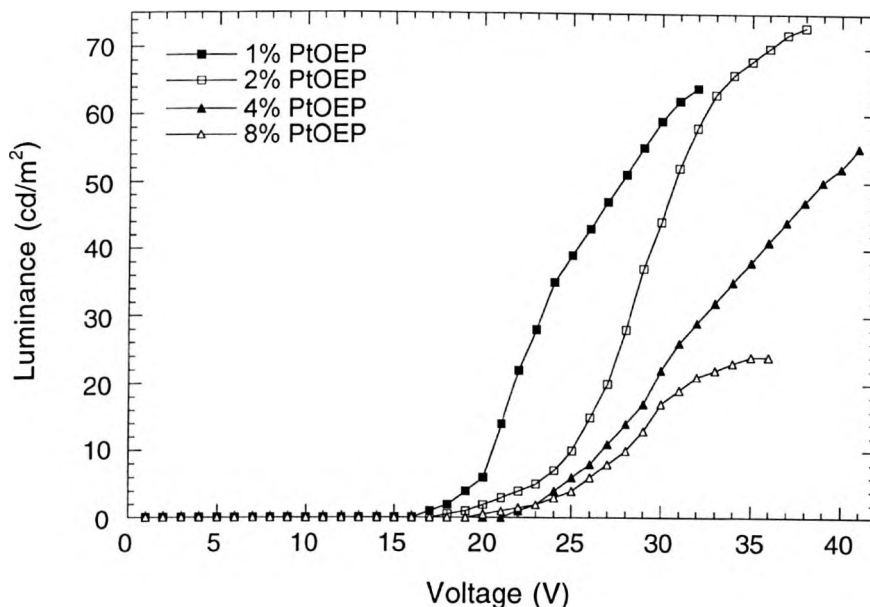


Figure 6.18: The luminance as a function of applied voltage for doped PtOEP:PFO LEDs with PtOEP concentrations of 1%(filled squares), 2%(open squares), 4% (filled triangles) and 8% (open triangles).

Figures 6.17 and 6.18 show the dependence of the current density and luminance, respectively, on the applied bias for doping concentrations of 1%, 2%, 4% and 8% by weight. All the devices had a 140 nm thick emissive layer. The operating as well as the turn on voltage (arbitrarily defined as the voltage required for $J = 5 \text{ mA/cm}^2$) required for charge injection and onset of the emission increase with doping concentration up to 4 wt% PtOEP concentration and then decreases for the 8 wt% blend. The increase of the operating voltage of the doped LEDs with PtOEP concentration is clear evidence for charge carrier trapping in the doped system where PtOEP molecules become dominant recombination centres. Table I below shows the voltage required for a current density of 5 mA/cm^2 and for a luminance of 5 cd/m^2 together with the maximum external EL quantum and power efficiencies obtained.

**Chapter 6: Electrophosphorescence
from PtOEP-doped polyfluorene red light-emitting diodes**

PtOEP concentration (wt%)	Voltage at 5 mA/cm ² (V)	Voltage at 5 cd/m ² (V)	Maximum EL quantum efficiency (%)	Power efficiency (lm/W)
0 ³⁸	11.5	10.5	0.2	0.07
1	21	19.5	1.5	0.10
2	27	23	3	0.18
4	33	24.5	3.5	0.16
8	26	25.5	0.6	0.03

Table 1: Operating conditions of PtOEP:PFO LEDs with a low workfunction ITO anode.

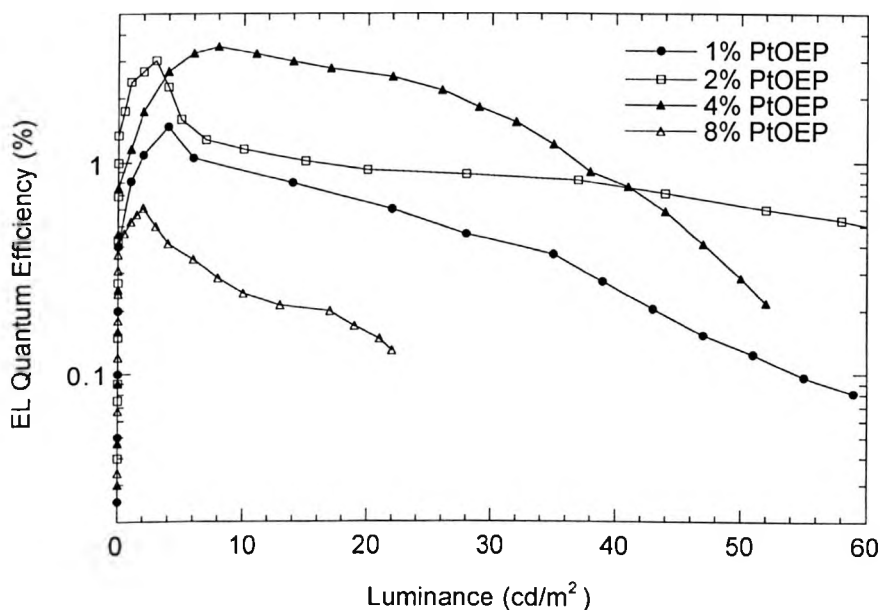


Figure 6.19: The external EL quantum efficiency versus luminance of PtOEP:PFO LEDs with PtOEP concentrations of 1%, 2%, 4% and 8% by weight.

Figure 6.19 shows the variation of the EL quantum efficiency for the different PtOEP doping concentrations as a function of the LED luminance. In each case, the efficiency peaks at a luminance below 10 cd/m^2 . The EL efficiency of the 2% device reaches 3% at a brightness of 3 cd/m^2 . A 4% doped PFO/PtOEP device showed a maximum EL efficiency of 3.5% at a brightness of 8 cd/m^2 . The efficiency increases by a factor of 3 compared to the higher workfunction ITO LEDs and is now more than an order of magnitude higher than the ELQE of optimized undoped PFO LEDs.³⁹ The external EL quantum efficiency vs. luminance results for two layer doped 2 wt% PFO LEDs with a BFA layer employing the two different workfunction ITOs are shown in Figure 6.20.

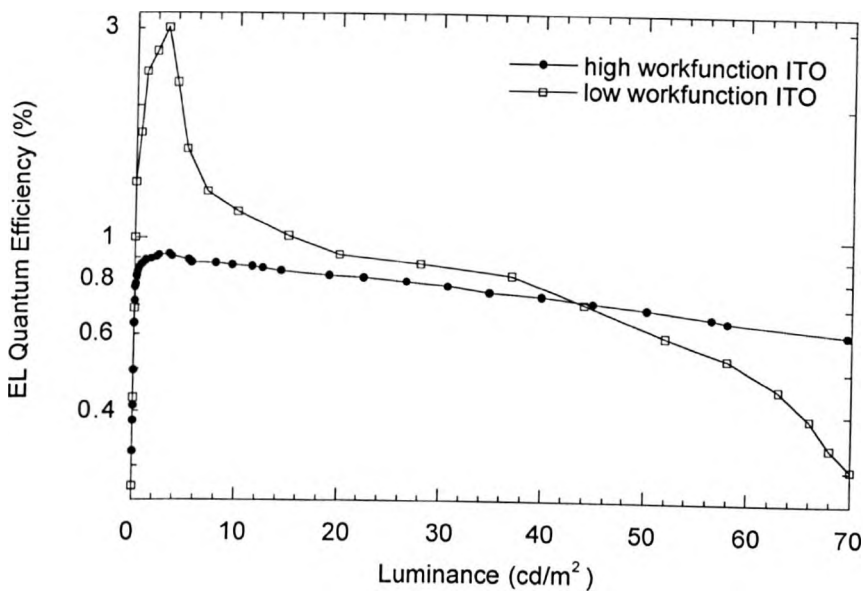


Figure 6.20: EL efficiency vs. luminance for BFA/PFO:PtOEP(2%) LEDs that employ different workfunction ITOs as the anode [high workfunction (filled symbols), low workfunction (open symbols)].

These efficiencies are also higher than efficiencies reported in the literature for other polymer hosts and a PtOEP dopant. For example, Cleave *et. al.*¹⁷ reported a maximum efficiency of 0.5% for a PNP polymer host and Guo *et. al.*²³ reported a maximum efficiency

of 2.3% for another polyfluorene derivative host at low luminance levels. We attribute this further increase in the efficiency to the improved balance of the injected carriers in the bulk. As the barrier for hole injection increases, we expect a smaller number of holes to be injected and then transported to the BFA/PFO:PtOEP interface where they will recombine with electrons mainly on the dopant molecules. Again the efficiency significantly drops at higher brightness levels and reaches 0.7% at 50 cd/m^2 for the 2% device. At PtOEP concentrations above 4%, a significant decrease of the quantum efficiency was observed due to concentration quenching of the dopant molecules. The decrease of the efficiency is more rapid in this set of devices; this may be due to the fact that a more balanced injection of electrons and holes is achieved at lower injection and luminance levels due to very fast and efficient electron-hole recombination which quickly then becomes less efficient due to a combination of the effects of the excess electron injection relative to hole injection and the high barrier that holes face at the ITO/BFA interface. The formation of a hole space charge at this interface will also inhibit the injection of more holes and redistribute the electric field in the device in favour of an increased electron injection that will reduce further the recombination efficiency at higher voltages. However, the increase of the EL efficiency is at the expense of a higher operating voltage and a lower maximum light output as well as current. This is due to the increased barrier for hole injection that mainly determines the J/V characteristics of the doped devices. A reduced number of holes are injected at a given voltage and hence a lower exciton recombination rate occurs.

Further information on the carrier trapping in these devices can be determined from the high field regime of the J/V characteristics of the bilayer devices. The low field regime is characterised by a combination of Ohmic and space charge limited conduction, with an $I \propto V^{1.5}$ dependence. In the high field regime (above the turn-on voltage) the current follows a trapped-charge limited power law dependence, $I \propto V^{m+1}$, where m is a function of the trap distribution within the PFO:PtOEP layer. For the undoped PFO devices, $m=6$ while for the

Chapter 6: Electrophosphorescence from PtOEP-doped polyfluorene red light-emitting diodes

doped devices $m=10-12$ which suggests that upon doping the trap distribution is modified in the bulk; this is also consistent with the increase observed in the operating voltage of the doped LEDs compared with the undoped ones.

More analytical information was obtained from analysis of the J/V characteristics of hole and electron only LEDs. Hole-only LEDs were fabricated with a PEDOT/PSS anode and an Au cathode. Upon doping of PFO with PtOEP, it was observed that the exponent m of the current density power law changes. It changes from 1 for PFO indicative of trap free space charge limited conduction, to 1.5 and 2.5 respectively, for low and high fields in PtOEP doped PFO. This indicates that in the blend space charge limited conduction with an exponential distribution of traps in energy (trapped-charge limited conduction) dominates for all electric fields with the traps to be presumably induced by the PtOEP molecules. The increase of m with field indicates that the energetics of the trap distribution is modified with the electric field. At higher fields, m increases to 4 indicating that the hole trap distribution is further modified with filling of trap states. Electron only LEDs were fabricated with a Ca cathode and a Dow metal anode. A strong variation of m with field was observed in these devices. For PFO, $m=5-6$ at low and moderate fields while for doped PtOEP PFO, m varies significantly with field from 1.5 for low fields to between 8 and 12 for moderate fields suggesting a significant variation of the distribution of the electron trap energies with doping and electric field. This also implies that while the hole mobility of PtOEP doped PFO is rather weakly dependent on the electron field, the electron mobility is strongly field dependent. The electron trapping may also contribute to the carrier imbalance at high voltages that results in a decrease of the quantum efficiency.

Transient electroabsorption spectroscopy was also employed to provide information about possible charge trapping in the doped LEDs.⁵¹ Figure 6.21 shows typical EA spectra of single layer PFO/PtOEP (4-wt%) and PtOEP (5-wt%)/PMMA devices. The inset shows

Chapter 6: Electrophosphorescence from PtOEP-doped polyfluorene red light-emitting diodes

the EA spectrum of the PtOEP (5-wt%)/PMMA device in more detail. The EA spectra were recorded at $V_{AC} = 2V$ and $V_{DC} = -4V$. ITO and Al electrodes were used in this set of devices.

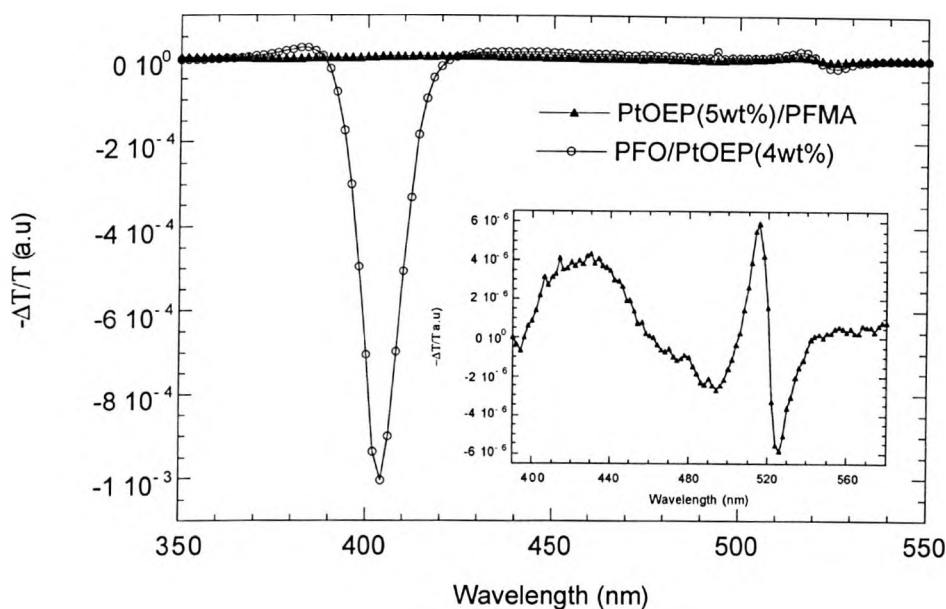


Figure 6.21: Typical 1f electroabsorption (EA) spectra of single layer PFO/PtOEP (4-wt%) and PtOEP (5-wt%)/PMMA devices. The inset shows the spectrum of a PtOEP (5-wt%)/PMMA device in detail.

The 1f spectrum of the blend is a superposition of the 1f spectra of the individual components. The EA spectrum of PtOEP exhibits two sharp features at 514 and 526 nm associated with the Q absorption band and a broad shoulder at around 425 nm probably associated with the Soret absorption band. Figure 6.22 shows the dynamics of the EA signal response of a PtOEP (4wt%)/PFO LED after turning the 5V DC voltage off at 10 sec and back on at 85 sec. As explained in chapter 4, the EA signal is monitored after initially biasing the device at 5 V and then varying the DC voltage following a cycle where the device is first off and then on.

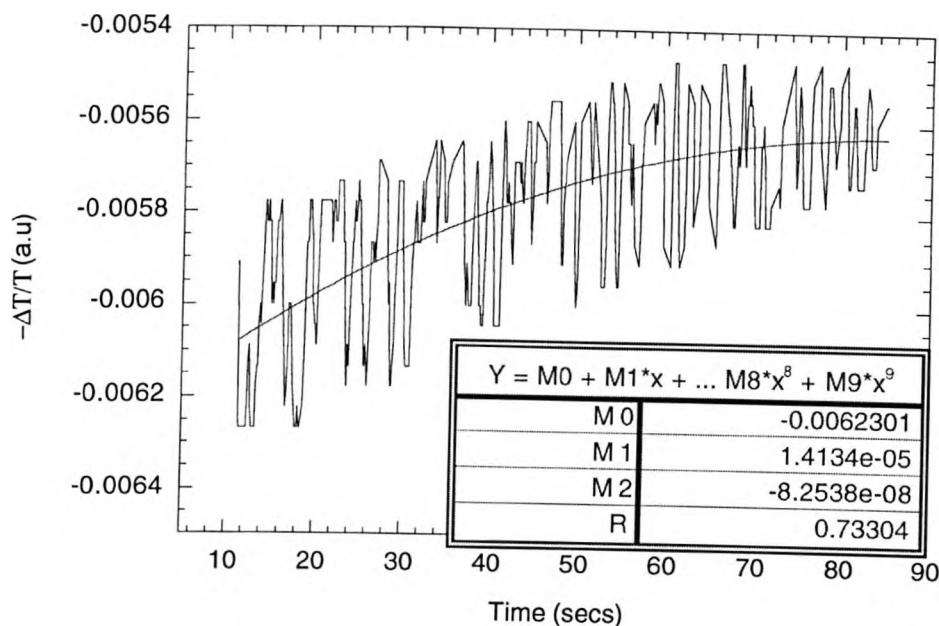


Figure 6.22: Dynamics of the electroabsorption response of a PtOEP (4wt%)/PFO LED after turning the 5V dc voltage off at 10 sec and back on at 85 sec.

Although the dynamics of the EA signal is very noisy, the signal can be fit with a polynomial decay function (which is in first order an approximation of an exponential function decay). The time constant of the decay is approximately 400 sec. As proposed by Giebeler *et al.*⁵¹ an electric field opposing the applied voltage will be induced in the device by trapped charge and will change the internal electric field distribution. As the decay time is proportional to the exponential of the trap activation energy E_{trap} , the very slow decay time of the traps implies that they are deep traps that require a large activation energy. These data provide further strong evidence that the PtOEP molecules act as deep traps in PFO though they do not allow the sign of the trapped charge to be determined with accuracy.

6.5 Utilizing a polymer blend host - Improved efficiency phosphorescent LEDs.

So far we have demonstrated that upon doping PtOEP in a PFO host, dopant molecules can selectively trap charges upon electrical excitation and act as the dominant recombination and emission centres. This permits external EL quantum efficiencies as high as 1% to be achieved even though Förster energy transfer is not particularly efficient for this host-guest system.

In this second part of the chapter we will show that the use of a blend of PFO and a hole transport material, namely PFM, as the host and PtOEP as the guest allows improved efficiency electrophosphorescent PLEDs to be obtained. The maximum external EL quantum efficiency of the doped PtOEP:PFO:PFM devices can be increased by a factor of 2 to 3 compared to that of identical PtOEP:PFO devices. The important role that charge carrier trapping and subsequent exciton recombination on the dopant molecules plays in the light emission mechanism of LEDs based on a host-guest system will be further discussed.

6.6 Spectroscopic studies of blends of PtOEP and PFO:PFM

PFO:PFM blends with a ratio of 4 to 1 by weight were prepared in toluene. This ratio was chosen because it was found to give the best performance in terms of high brightness and efficiency in blue LEDs based on that blend (analytical details are given in chapter 4). In addition to films of PFO:PFM (4:1), doped PFO:PFM (4:1):PtOEP films were also prepared with PtOEP concentrations ranging from 0.1% up to 8% by weight. The films were studied by absorption, PL and PLQE spectroscopy. The samples were excited by a HeCd laser at 354 nm. Both single and two layer devices were fabricated for comparison. BFA or PEDOT /

PSS was used as a separate HTL in the two-layer devices. BFA and PEDOT / PSS were thermally treated as before and the devices had an ITO anode and a Ca cathode.

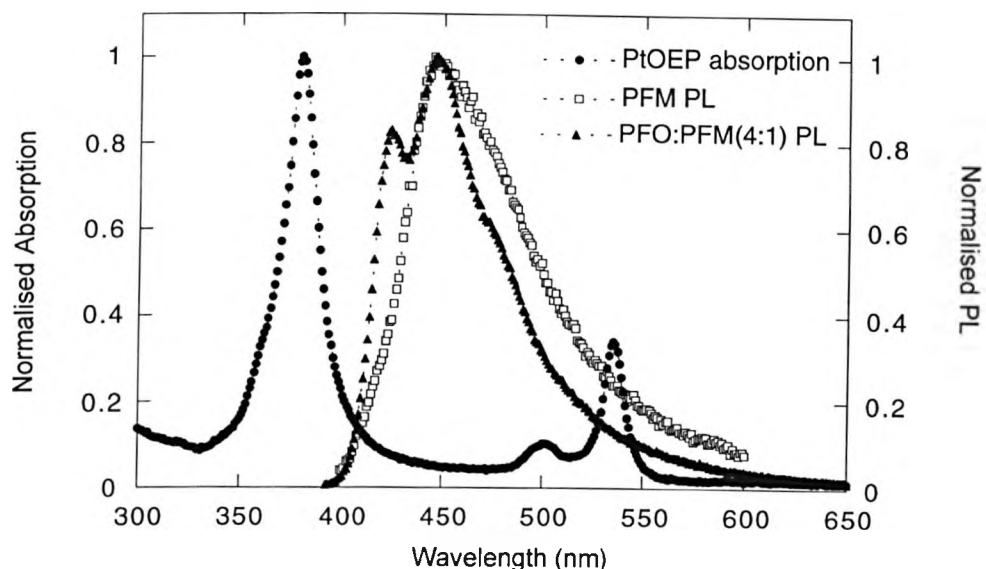


Figure 6.23: Absorption spectrum of 0.1 wt% PtOEP:PMMA (filled circles), photoluminescence spectrum of PFM (open squares) and photoluminescence spectrum of PFO:PFM (20 wt%) (filled triangles).

Figure 6.23 shows the absorption spectrum of PtOEP in PMMA at a concentration of 0.1% by weight, the PL spectrum of PFM and the PL spectrum of a PFO/PFM blend containing 20 wt.% PFM. There is a significant spectral overlap between the PL of the blend and the Q absorption band of PtOEP at 530 nm and also some weak overlap with the Soret absorption band of PtOEP at 380 nm. The spectral overlap of the PFO:PFM blend emission with the PtOEP absorption is larger than that for PFO and thus energy transfer of singlet excitons is expected to be more efficient in this system. Using the Förster radius relation, we find $R_0 = 2.6$ nm which is almost a factor of 1.5 larger than that for PFO:PtOEP (1.7 nm). Thus we expect that singlet energy transfer will be more efficient in the PFO:PFM:PtOEP system than the PFO:PtOEP system. We speculate that this will result in an improved

electrophosphorescence efficiency. The quantum efficiencies of the PFO:PFM (4:1) PL, the PtOEP phosphorescence and the total PL emission as a function of the PtOEP concentration are shown in Figure 6.24.

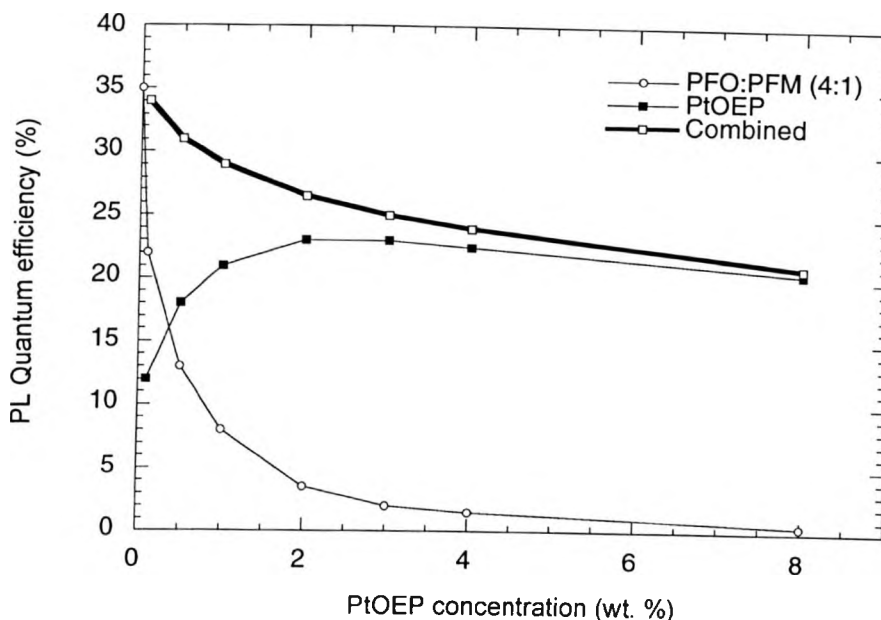


Figure 6.24: PFO:PFM PLQE (open circles), PtOEP phosphorescence QE (filled squares), and total photoluminescence quantum efficiency (open squares) as a function of the PtOEP concentration.

The PL spectra of the PFO:PFM/PtOEP blends (not shown here) are non-linear superpositions of the individual PL spectra with a decreased contribution of the PFO:PFM blue emission to the overall PL spectrum as the concentration of PtOEP increases. A notable difference observed here is that at 8 wt% PtOEP concentration, emission from PFO:PFM is almost completely quenched while a relatively larger component of PFO emission is present at this concentration when PFM is not used in the host. Also these high dopant concentrations give rise to enhanced concentration quenching as evidenced by a 30% decrease of the PLQE of the PtOEP emission in a 8 wt% (by weight) PtOEP:(PFO:PFM) blend compared to a 0.1

wt% PtOEP:PMMA film. The stronger energetic overlap of the excitonic states in PtOEP and PFO:PFM leads to a higher probability for reverse energy transfer from PtOEP to PFO:PFM and this will result in an increased nonradiative quenching of the PtOEP emission and thus to a lower PL efficiency when doped in a PFO:PFM host compared to that of PtOEP in PMMA. The Marburg group has recently measured phosphorescence from a polyfluorene to be within 0.1 eV of the PtOEP emission⁵², thus it is expected that there will be an increased probability that reverse Dexter transfer and migration of triplet excitons could occur from the guest to the host when polyfluorene-based materials are used as hosts.

6.7 Phosphorescent PLEDs from blends of PFO:PFM and PtOEP

The electroluminescence spectra of the PtOEP doped PFO:PFM (4:1) LEDs are identical in shape to the PtOEP phosphorescence spectra (with a peak wavelength of $\lambda_{\text{max}}=646$ nm). There is a negligible contribution from the PFO:PFM (4:1) host emission to the EL even at 0.2-wt% PtOEP concentration in the blend host. The CIE chromaticity coordinates of (0.67, 0.28) are almost identical to those obtained from the PL spectrum of PtOEP in a PMMA matrix. No significant emission from the PFO:PFM host was observed at high current densities (until up to 100 mA/cm^2) which suggests that the degree of saturation of the long-lived triplet PtOEP sites in this host-guest system at low dopant concentrations is reduced enough, probably due to a shorter triplet exciton diffusion length in this host, that no residual emission occurs from the host. Similar observations were made by Guo *et. al.*²³ in doped LEDs with a polyfluorene-based host and a porphyrin based guest. These results are in contrast to the cases where either Alq₃ or Ir(ppy)₃ was used as a host.^{15-16,29} Figure 6.25 shows the external EL quantum efficiency versus luminance results for a series of three different sets of devices, a) single layer, PFO:PFM(4:1):PtOEP b) double layer with a BFA hole transport layer, BFA/PFO:PFM(4:1):PtOEP and c) double layer with a PEDOT hole conducting layer, PEDOT/PFO:PFM(4:1):PtOEP.

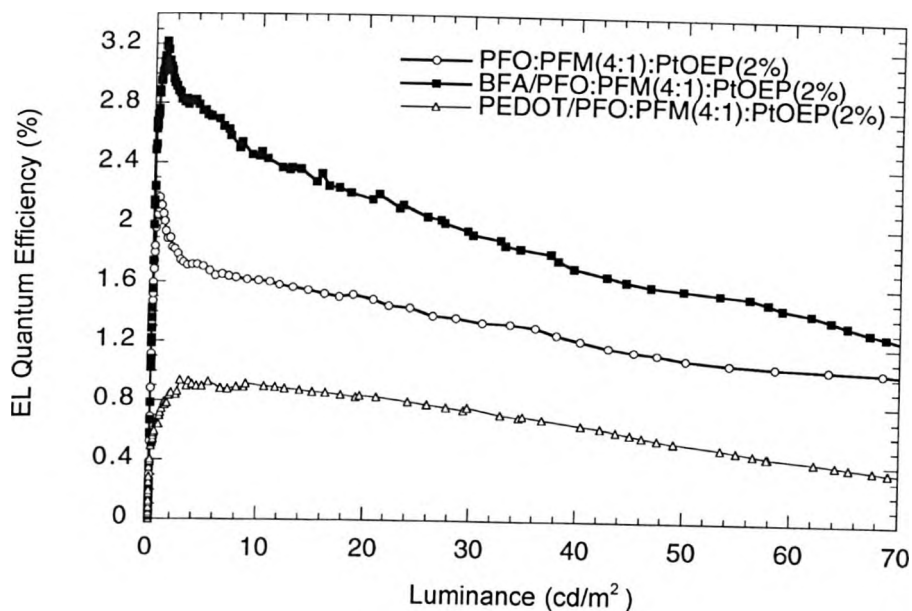


Figure 6.25: EL quantum efficiency vs. luminance for a series of doped LEDs with an ITO anode and a Ca cathode a) PFO:PFM (4:1):PtOEP(2%) single layer (open circles) (b) BFA/PFO:PFM(4:1):PtOEP(2%) double layer (filled squares) and c) PEDOT:PSS/PFO:PFM(4:1):PtOEP(2%) double layer LEDs (open triangles).

PtOEP was doped in the host at a concentration of 2% (by weight). Both BFA and PEDOT had a thickness of 40 nm. The thickness of the emissive layer was 190 nm and was found to give the higher efficiencies in single layer devices. The device with a BFA layer shows the maximum EL quantum efficiency of all three LEDs; The efficiency reaches 3.2 % at a low brightness of 2 cd/m² and decreases to 0.9% at 100 cd/m². The single layer device shows a maximum efficiency of 2.2% at low brightness and 0.9% at 100 cd/m² while the device with PEDOT exhibits a max efficiency of 0.8% at 5 cd/m² (the efficiency at 100 cd/m² is 0.2%). The position of the energy levels of the materials used allows PFM sites to act as hole traps when BFA is used as a HTL thus allowing better charge balance in these 2 layer LEDs as evidenced by the higher efficiency they exhibit compared to the single layer LEDs where holes are directly injected through a small barrier preferentially to the PFM molecules.

When PEDOT is used as a HTL, the efficiency decreases significantly and we attribute this to the fact that the HOMO energy levels of PEDOT and PFM are well aligned and that readily allows holes to be easily conducted through the PtOEP layer to the cathode, leading to carrier imbalance and thus to low carrier recombination efficiency.

There are two mechanisms for electroluminescence from PFO:PFM films doped by PtOEP: (I) Förster transfer of singlet excitons formed on either PFO or PFM to PtOEP singlet states followed by intersystem crossing to triplet states and emission. This is the dominant mechanism for photoluminescence from a PtOEP-doped PFO:PFM film. (II) Direct trapping of holes on the PtOEP molecules followed by recombination. The highest occupied molecular orbital (HOMO) of PFM is 5.04 eV below vacuum, whereas the HOMO of PtOEP is 5.4 eV below vacuum.⁴⁶ Holes will therefore be preferentially injected from the hole transport layer (BFA or PEDOT) into the HOMO of PFM and then be transferred on PtOEP by a hopping process. PFM should act as a shallow hole trap when BFA is used as a hole transport layer, because the HOMO level of PFM lies about 0.3 eV above that of BFA. This will reduce hole conduction to the PtOEP sites and result in improved carrier balance and a higher carrier recombination probability than for a PFO host. Further hole injection will be blocked by the formation of a positive space charge in the bulk and the redistribution of the electric field is expected to increase electron injection from the cathode. Trapped holes on PtOEP molecules will then recombine with electrons injected from the Ca cathode to the LUMO level of PtOEP resulting in direct exciton formation on PtOEP. PtOEP singlets will be converted to triplets via intersystem crossing and thus also result in phosphorescence. Excitons will be confined in PtOEP since the energy of the PtOEP triplet exciton is significantly lower than the energy gaps of PFM and PFO. This will further increase the recombination efficiency and reduce exciton quenching. The different dependence of the EL and PL spectra on the PtOEP concentration is again a strong indication that carrier trapping is the dominant process leading to exciton formation under charge carrier injection.

A comparison of the current density and luminance vs. electric field (J/E & L/E) characteristics of doped double layer (BFA is used as HTL) PFO and PFO:PFM (4:1) LEDs (with a 2 wt% PtOEP concentration in the host) is shown in Figure 6.26.

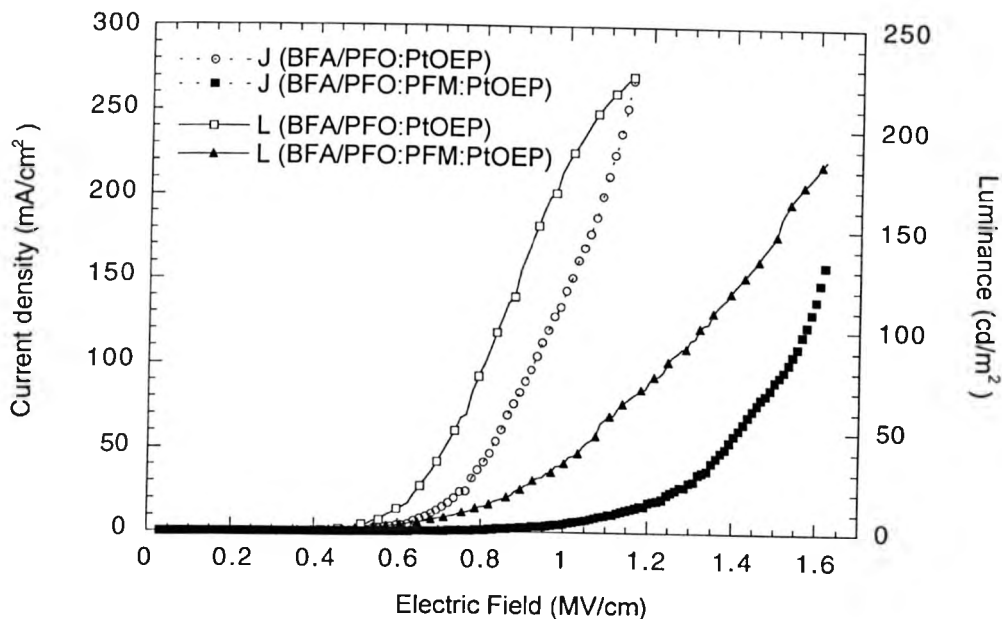


Figure 6.26: Current density and luminance as a function of the applied electric field of a) BFA/PFO:PtOEP(2%) and b) BFA/PFO:PFM(4:1):PtOEP(2%) LEDs.

This graph clearly demonstrates the role of PFM molecules as hole traps in the 2-layer device configuration with a BFA hole transport layer. The current-field characteristics shifts to higher fields when PFM is introduced in the PFO host and a similar effect is also observed on the luminance-field characteristics. The threshold electric field required for a current density of 20 mA/cm^2 increases from 0.75 MV/cm for the PFO host to 1.25 MV/cm for the PFO:PFM (4:1) host. For a luminance of 20 cd/m^2 , the field also increases from 0.6 MV/cm to 0.85 MV/cm . A maximum luminance of 190 cd/m^2 is obtained at a corresponding current density of 160 mA/cm^2 for the PFO:PFM host. These values are lower than the

corresponding values for the PFO host and this is due to a reduced component of hole current that contributes to the device current when PFM is incorporated in PFO which also leads to a reduced light output at a certain electric field. Figure 6.27 compares directly the EL efficiency vs. luminance of double layer doped 2-wt% PFO LEDs with and without PFM.

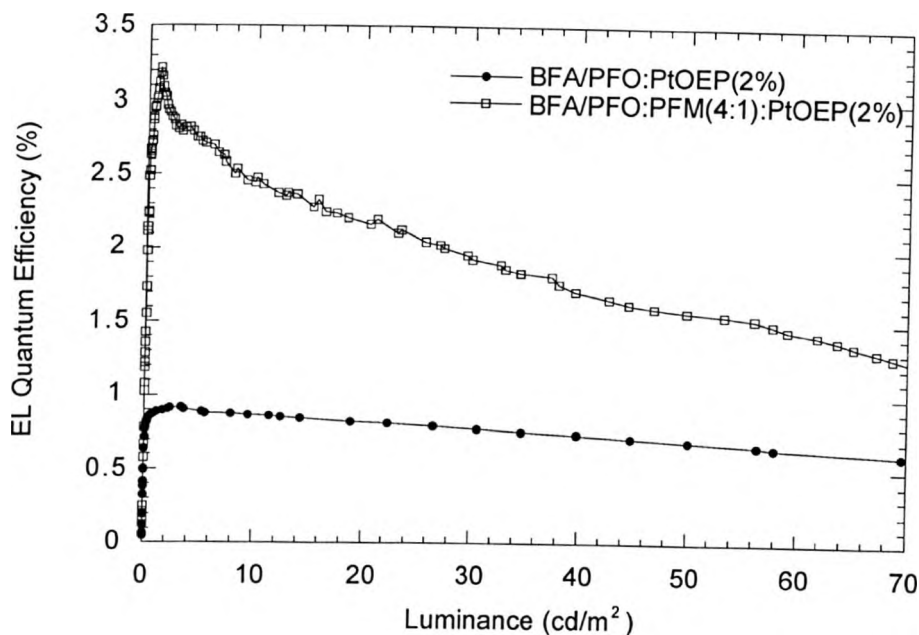


Figure 6.27: External quantum efficiency versus luminance of a) ITO/BFA/PFO:PtOEP(2%)/Ca (filled symbols) and b) ITO/BFA/PFO:PFM(4:1):PtOEP(2%)/Ca (open symbols) LEDs.

The results shown here are for the high workfunction ITO; a similar trend is observed when the lower workfunction ITO is used instead. The maximum efficiency of the device with PFM is a factor of 3 higher than the device without PFM at low brightness levels and a factor of 1.5 higher at high brightness levels (100 cd/m^2). We propose this increase is due to the dual action of PFM molecules both as hole traps as well as singlet exciton recombination centres in the PFO host that leads to a host-guest system with increased energy transfer probability. Similar to our previous work with PFO as a host, a maximum external EL

efficiency of 5.8% was obtained at a low brightness of 5 cd/m^2 when a lower workfunction ITO was employed with the PFO/PFM/PtOEP blend. We attribute this to the improved charge balance of the injected carriers that is achieved in the bulk of the device with PFM at low charge injection levels.

Finally, it is important to note that all the fabricated devices based on a PtOEP-doped host showed significantly higher quantum efficiencies (about 2 orders of magnitude) compared to that of a neat PtOEP LED (where the luminescent region was a homogeneous film of PtOEP prepared by spin casting from a toluene solution) in which triplet exciton interactions effectively quench the luminescence by increasing the nonradiative recombination/decay probability (the aggregate-induced self-quenching effect).

6.8 Conclusions

This chapter is concerned with electrophosphorescence, the process that utilizes both singlet and triplet excitons, aiming to produce highly efficient PLEDs. A red phosphorescent emitter namely 2,3,7,8,12,13,17,18-octaethyl-21H,23H-porphyrin platinum (II), (PtOEP) was employed as the dopant in a host-guest system configuration with a blue PFO host. By varying the concentration of PtOEP a spectral range of bluish-red to pure red emission can be obtained. Blue emission from PFO could be observed even at 8% dopant concentration under optical excitation of a PFO:PtOEP film, while at 1% dopant concentration only red emission from PtOEP could be observed upon electrical excitation of the corresponding LEDs.

Analysis of the absorption spectra of films of PtOEP in PMMA shows that the intermolecular interactions are sufficient to change the absorption spectrum. At concentrations of 8% PtOEP in PFO, concentration quenching induced by strong intermolecular interactions significantly reduces the efficiency of the phosphorescence emission in the blend. From

analysis of the absorption, PL and EL spectra together with time resolved PL and electroabsorption measurements, we conclude that direct carrier trapping and subsequent exciton recombination occurring on the PtOEP molecules is the dominant EL emission mechanism whereas Förster transfer observed to occur from the host to the dopant dominates the PL emission. Singlets formed on the PtOEP molecules will be converted to triplets via efficient intersystem crossing and thus also result in phosphorescence. Any singlets formed directly on PFO by recombination of untrapped charges can subsequently transfer their energy by Förster transfer to the PtOEP singlets and also contribute to the phosphorescence emission. Saturated red emission centred at 646 nm was obtained and optimised doped LEDs with external EL efficiencies up to 1% at low brightness were realised. By decreasing the workfunction of the hole injecting contact, efficiencies up to 3% were reached due to the improved balance of the injected carriers. The direct trapping of holes and electrons and the subsequent formation of excitons on PtOEP as well as the use of both singlet and triplet states to generate light results in high recombination efficiencies. The increase of the operating voltage of the doped devices with increasing PtOEP concentration is a direct consequence of the charge trapping on PtOEP. The decrease of the operating voltage at sufficiently high PtOEP concentrations (8 wt.%) is attributed to the fact that charge transport at these concentrations occurs directly by hopping between the PtOEP molecules; thus a reduction of the space charge formed and the EL quantum efficiency is expected to occur.

PFO was also doped with a fluorene-triarylamine hole transporting copolymer, namely PFM and this blend was used as a host with a PtOEP guest. The incorporation of a hole transporting material in PFO in the form of a blend results in a host system that has improved energy transfer coupling with a PtOEP guest compared to that of when PFO is used as a host. Another fluorene-triarylamine copolymer, namely BFA was used as a separate HTL in a two-layer device configuration. The efficiency of these devices increased by a factor of 3 and reached 3.2% at low brightness and 0.9% at 100 cd/m^2 for a high workfunction ITO

anode. For a low workfunction ITO, an external EL quantum efficiency of 5.8% was obtained at a low brightness of 5 cd/m². The improved performance of the blend LEDs is attributed to more efficient energy transfer from the host to the guest as well as to improved charge carrier balance due to hole trapping on the PFM molecules.

Charge carrier trapping is found to play a very important role in achieving high quantum efficiency electrophosphorescent polymer LEDs from host-guest systems with relatively weak energy transfer coupling. Other approaches that could result in very highly efficient phosphorescent polymer LEDs could be either doping other phosphorescent materials that possess shorter exciton lifetimes into an appropriate combination of an emissive and a hole transporting material used as a host or selecting guest-host combinations with a stronger energy transfer coupling and thus a higher probability for energy transfer.

References

1. e.g. see CDT website, <http://www.cdttld.co.uk> for latest results and developments.
2. Strukelj, M., Papadimitrakopoulos, F., Miller, T.M. & Rothberg, L.J. *Science* **267**, 1969 (1995).
3. Virgili, T., Lidzey, D.G. & Bradley, D.D.C. *Advanced Materials*, **12**, 58 (2000).
4. Tasch, S., List, E.J.W., Hochfilzer, C., Leising, G., Schlichting, P., Rohr, U., Geerts, Y., Scherf, U. & Mullen, K. *Physical Review B* **56**, 4479 (1997).
5. Pope, M. & Swenberg, C.E. *Electronic Processes in Organic Crystals and Polymers*, 2nd Edition, Oxford University Press, Oxford (1999).
6. Baldo, M.A., O'Brien, D.F., Thompson, M.E. & Forrest, S.R. *Physical Review B* **60**, 14422 (1999).
7. Cao, Y., Parker, I.D., Yu, G., Zhang, C. & Heeger, A.J. *Nature* **397**, 414 (1999).
8. Kim, J.-S, Ho, P.K.H., Greenham, N.C. & Friend, R.H. *Journal of Applied*

**Chapter 6: Electrophosphorescence
from PtOEP-doped polyfluorene red light-emitting diodes**

- Physics* **88**, 1073 (2000).
9. Wohlegenannt, M., Tandon, K., Mazumdar, S., Ramasesha, S. & Vardeny, Z.V. *Nature* **409**, 494 (2001).
 10. Shuai, Z., Beljonne, D., Silbey, R.J. & Bredas, J.L. *Physical Review Letters* **84**, 131 (2000).
 11. Murata, H., Merritt, C.D. & Kafafi, Z.H. *IEEE Journal of Selected Topics in Quantum Electronics* **4**, 119 (1998).
 12. Shoustikov, A., You, Y. & Thompson, M.E. *IEEE Journal of Selected Topics in Quantum Electronics* **4**, 3 (1998).
 13. Bulovic, V., Shoustikov, A., Baldo, M.A., Bose, E., Koslov, V.G., Thompson, M.E. & Forrest, S.R. *Chemical Physics Letters* **287**, 455 (1998).
 14. List, E.J.W., Holzer, L., Tasch, S., Leising, G., Scherf, U., Müllen, K., Catellani, M. & Luzzati, S. *Solid State Communications* **109**, 455 (1999).
 15. Baldo, M.A., O'Brien, D.F., You, Y., Shoustikov, A., Sibley, S., Thompson, M.E. & Forrest, S.R. *Nature (London)* **395**, 151 (1998).
 16. Kwong, R.C., Lamansky, S. & Thompson, M.E., *Advanced Materials* **12**, 1134 (2000).
 17. Cleave, V., Yahioglu, G., Le Barny, P., Friend, R.H. & Tessler, N. *Advanced Materials*, **11**, 285 (1999).
 18. Baldo, M.A., Thompson, M.E. & Forrest, S.R. *Nature (London)*, **403**, 750 (2000).
 19. Adachi, C., Baldo, M.A. & Forrest, S.R. *Journal of Applied Physics* **87**, 8049 (2000).
 20. Ma, Y.G., Lai, T.S. & Wu, Y. *Advanced Materials* **12**, 433 (2000).
 21. Ma, Y., Che, C.-M., Chao, H.-Y., Zhou, X., Chan, W.-H. & Shen, J. *Advanced Materials* **11**, 852 (1999).
 22. Tessler, N., Ho, P.K.H., Cleave, V., Pinner, D.J., Friend, R.H., Yahioglu, G., Le Barny, P., Gray, J., de Souza, M. & Rumbles, G. *Thin Solid Films* **363**, 64 (2000).

23. Guo, T.-F., Chang, S.-C., Yang, Y., Kwong, R.C. & Thompson, M.E., *Organic Electronics* **1**, 15 (2000).
24. Lee, C. -L., Lee, K.B. & Kim, J.-J. *Applied Physics Letters* **77**, 2280 (2000).
25. Cleave, V., Tessler, N., Yahioglu, G., Le Barny, P., Facchetti, H., Boucton, N. & Friend, R.H. *Synthetic Metals* **102**, 939 (1999).
26. O'Brien, D.F., Baldo, M.A., Thompson, M.E. & Forrest, S.R., *Applied Physics Letters* **74**, 442 (1999).
27. Kwong, R.C., Sibley, S., Dubovoy, T., Baldo, M., Forrest, S.R. & Thompson, M.E. *Chemistry of Materials* **11**, 3709 (1999).
28. Adachi, C., Baldo, M.A., Thompson, M.E. & Forrest, S.R. *Applied Physics Letters* **77**, 904 (2000).
29. Baldo, M.A., Lamansky, S., Burrows, P.E., Thompson, M.E. & Forrest, S.R. *Applied Physics Letters* **75**, 4 (1999).
30. Tsutsui, T., Yang, M.J., Yahiro, M., Nakamura, K., Watanabe, T., Tsuji, T., Fukuda, Y., Wakimoto, T. & Miyaguchi, S. *Japanese Journal of Applied Physics* **38**, L1502 (1999).
31. Burrows, P.E., Forrest, S.R., Zhou, T.X. & Michalski, L. *Applied Physics Letters* **76**, 2493 (2000).
32. McGehee, M.D., Bergstedt, T., Zhang, C., Saab, A.P., O'Regan, M.B., Bazan, G.C., Srdanov, V. & Heeger, A.J. *Advanced Materials* **11**, 1349 (1999).
33. Jabbour, G.E., Wang, J.-F., Kippelen, B. & Peyghambarian, N. *Japanese Journal of Applied Physics* **38**, L1553 (1999).
34. Liang, C.J., Zhao, D., Hong, Z.R., Zhao, D.X., Liu, X.Y., Li, W.L., Peng, J.B., Yu, J.Q., Lee, C.S. & Lee, S.T. *Applied Physics Letters* **76**, 67 (2000).
35. Hu, W., Matsumura, M., Wang, M. & Jin, L. *Applied Physics Letters* **77**, 4271 (2000).

**Chapter 6: Electrophosphorescence
from PtOEP-doped polyfluorene red light-emitting diodes**

36. Sakakibara, Y., Okutsu, S., Enokida, T. & Tani, T. *Applied Physics Letters* **74**, 2587 (1999).
37. Shoustikov, A., You, Y., Burrows, P., Thompson, M.E. & Forrest, S.R. *Synthetic Metals* **91**, 217 (1997).
38. PtOEP was purchased from Porphyrin Products Inc., P.O.Box 31, Logan, UT, USA.
39. Grice, A.W., Bradley, D.D.C., Bernius, M.T., Inbasekaran, M., Wu, W.W. & Woo, E.P. *Applied Physics Letters* **73**, 629 (1998).
40. Tang, C.W. & VanSlyke, S.A. *Applied Physics Letters* **51**, 913 (1987).
41. Brown, A.R., Bradley, D.D.C., Burn, P.L., Burroughes, J.H., Friend, R.H., Greenham, N.C., Holmes, A.B. & Kraft, A. *Applied Physics Letters* **61**, 2793 (1992).
42. Förster, T. *Annalen der Physik* **2**, 55 (1948).
43. Virgili, T. *PhD thesis*, Sheffield University (1999).
44. Buckley, A.R., Rahn, M.D., Hill, J., Cabanillas-Gonzalez, J., Fox, A.M. & Bradley, D.D.C. *Chemical Physics Letters* (in press).
45. List, E.J.W, Creely, C., Leising, G., Schulte, N., Schluter, A.D., Scherf, U., Mullen, K. & Graupner, W. *Chemical Physics Letters* **325**, 132 (2000).
46. Hill, I.G., Makinen, A.J. & Kafafi, Z.H. *Applied Physics Letters* **77**, 2003 (2000).
47. Dexter, D.L. *Journal of Chemical Physics* **21**, 836 (1953).
48. P.A.Lane, *personal communication*.
49. Cadby, A.J. *personal communication*.
50. Shaheen, S.E., Jabbour, G.E., Kippelen, B., Peyghambarian, N., Anderson, J.D., Marder, S.R., Armstrong, N.R., Bellman, E. & Grubbs, R.H. *Applied Physics Letters* **74**, 3212 (1999).
51. Giebeler, C., Whitelegg, S.A., Campbell, A.J., Liess, M., Martin, S.J., Lane, P.A., Bradley, D.D.C., Webster, G. & Burn, P.L. *Applied Physics Letters* **74**, 3714 (1999).
52. Bässler, H. University of Marburg, (*unpublished results*).

CHAPTER 7

INCORPORATION OF A SMALL AREA STRUCTURE IN POLYMER LIGHT-EMITTING DIODES AND MICROCAVITIES

7.1 Introduction

The performance of polymer light emitting diodes has approached a commercially viable level for applications such as low-cost flat-panel displays and the first products are expected to appear in the market soon.¹ Advanced applications are likely to be both active matrix² and passive matrix³ LED displays. For high-resolution passive matrix displays, it will be of practical importance to develop LEDs of a few hundred μm -size that will be capable of exhibiting high peak brightness (in excess of 200 kcd m^{-2}), high emission efficiency (in excess of 5 cd/A) and fast ($< 5 \text{ ms}$) switching times (the LED switching speed will determine how many rows can be addressed in a display). High-resolution patterning of LEDs will thus be necessary towards the fabrication of full-color flat panel displays. In order to fabricate high-resolution fine pixels, different techniques can be employed such as photolithography, vacuum deposition with a fine shadow mask or laser photoablation.⁴⁻⁵ Tian *et. al.*⁴ have succeeded in fabricating a few hundred by a few hundred μm pixels using

a simple shadow mask method. However, cathodes that are patterned via shadow-masking techniques make it difficult to fabricate individual devices with feature sizes smaller than 100 μm . Noach *et. al.*⁵ have succeeded in employing an excimer-laser-ablation technique to fabricate 20x20 μm LEDs. More recently, Suganuma *et. al.*⁶ reported the fabrication of a 200 nm x 2 mm array of OLEDs on a glass substrate by employing a photolithographic technique which used an optical phase shift mask. In this case, anisotropic emission spectra were observed between the directions perpendicular and parallel to the patterning of the arrays with large differences in their relative intensities; these characteristics were attributed to the confinement effect of the photons in a very narrow emitting area as defined by the submicrometer-sized OLED.

Although the fabrication of high-resolution fine pixels using different techniques has proved successful, the optimization of the LED structure and/or the use of new materials in order to achieve high peak brightness and high sustainable current densities still remains an open challenge. Lidzey *et. al.*⁷ first reported tip current densities as high as 10,000,000 A/m^2 in scanning tunneling microscopy (STM) injection experiments of PPV structures. Kozlov, *et. al.*⁸ have studied OLED structures under intense optical and electrical excitation and found that multilayer DCM doped Alq_3 devices with a Mg:Ag cathode can exhibit peak current densities up to 3,000,000 A/m^2 under pulsed excitation which would give excitation densities in excess of those required for lasing in optically pumped structures provided there is efficient conversion of injected carriers into excitons. However, current-induced absorption primarily due to polarons (or trapped charge carriers) does not allow lasing to occur under electrical operation. Tessler *et. al.*⁹⁻¹⁰ have reported “small area” (dimensions were kept below 1 mm^2) optimized PPV based LED structures with Ca cathodes that allow exceptionally high current densities and luminances to be achieved by using short pulsed driving schemes. In these devices and to avoid problems associated with series resistance

within the ITO, a 100 nm Al layer was deposited underneath 100 nm thick SiO₂ insulating strips that were deposited on top of ITO. The distance between the Al and the active pixel was also kept to less than 0.5 μm. Current densities between 1 and 10 kA cm⁻² and peak brightnesses between 5,000,000 and 20,000,000 cd m⁻² were demonstrated from these LEDs with a quantum efficiency of up to 1 cd/A at high current densities. The exceptionally high charge carrier mobilities found at high current densities, close to 0.1 cm²/(Vs) a factor of 5 higher than at low fields, are believed to partly account for such high device performance. Jabbour *et. al.*¹¹ have also reported two layer small-molecule based LEDs with a hole transport polymeric material, a quinacridone doped Alq₃ emissive layer and a LiF/Al cathode that when tested under pulsed voltage mode showed a peak brightness of 4,400,000 cd/m² at 1,000,000 A/m² and an efficiency of 4.4 cd/A. Such a high efficiency at such peak brightness is very encouraging for the development of electrically pumped organic/polymer lasers. Frolov *et. al.*¹² have also fabricated micro-LEDs from disubstituted polyacetylene using a micro-disk configuration with diameters in the order of 100 μm that reached maximum current densities of 20000 A/m² in d.c. current mode. As it has also been shown by Fletcher *et. al.*¹³, PLEDs can emit EL pulses of duration < 150 ns which allows the devices to be driven to very high voltages (up to 100 V) without significant degradation. Although these results prove that high current densities, previously thought to be unattainable in electrically driven organic LEDs due to the low carrier mobilities and various exciton quenching mechanisms, can be achieved, significant interest still remains in understanding what ultimately limits the maximum emission brightness, the maximum sustainable current-density and therefore the quantum efficiency in a PLED.

In this chapter the performance of PLEDs has been investigated as their active areas are reduced to dimensions typical for pixellated displays. As will be shown below, the emission properties of PLEDs are modified by the physical size of the device. It is

demonstrated that the maximum current density and luminance that can be sustained by an LED prior to catastrophic failure under intense electrical excitation increases significantly as the active emissive area is reduced. This is a direct consequence of improved thermal management within the LED structure. Pulsed operation with a low duty cycle can also assist in thermal management and results for driving with 1 μ s voltage pulses at low duty cycles will be reported. Small area LEDs were also incorporated in a microcavity configuration in order to fabricate novel small area microcavity LEDs towards the goal of obtaining lasing emission from a PLED. Results for both 5BTF8 and PFO cavity LEDs will be reported and discussed in detail with emphasis given to some interesting changes that are observed in the spectral properties of the PFO cavity LEDs under intense electrical excitation.

7.2 Experimental details

The small area LEDs employed in this chapter utilize the 5BTF8 blend. As has been presented in detail in Chapter 5, this blend consists of 95% PFO with 5% BT, it operates as a guest-host energy transfer system with efficient Förster transfer from the PFO to the BT and is 55% PL efficient with emission at 535 nm. TOF work carried out by Campbell has indicated that 5BTF8 has reasonably balanced electron and hole carrier mobilities.¹⁴ The combination of high PL efficiency and good transport will be vital if large current densities and high brightnesses and quantum efficiencies are to be achieved.

LEDs were fabricated using indium tin oxide (ITO) coated glass substrates as the anode. To investigate the role of the device emissive area on LED performance, a layer of an insulating dielectric silicon nitride, (Si_xN_y), was patterned on top of the ITO anode. This effectively defines the area through which current can flow and thus controls the device emissive area. In a standard LED, this area is defined by the overlap of the cathode and the

ITO anode. The use of a resistive interlayer patterned by photolithography allows the area of the LED to be controlled with high precision. The small area LEDs were fabricated as follows: A 300 nm thick layer of Si_xN_y was deposited on ITO by plasma enhanced chemical vapor deposition (CVD). A photoresist layer was spin-coated onto the silicon nitride, which was then patterned using photolithography. The structure was then exposed to a halocarbon / oxygen plasma, which selectively removed the Si_xN_y unprotected by the photoresist. The remaining photoresist was finally removed using an acetone wash. Using this technique, 'holes' in the Si_xN_y having diameters of 500, 100 and 50 μm were created. This plasma etch process had very little effect on the ITO. A 30 nm layer of the hole injecting PEDOT / PSS was then spin coated onto the Si_xN_y and baked at 150 °C for 10 minutes in air to render it insoluble. 5BTF8 from a 20 mg/ml toluene solution was then spin coated onto the PEDOT to form a 130 nm thick layer. Finally, a 300 nm thick Ca cathode was thermally evaporated onto 5BTF8. Figure 7.1 shows a schematic diagram of the structure of a small area LED.

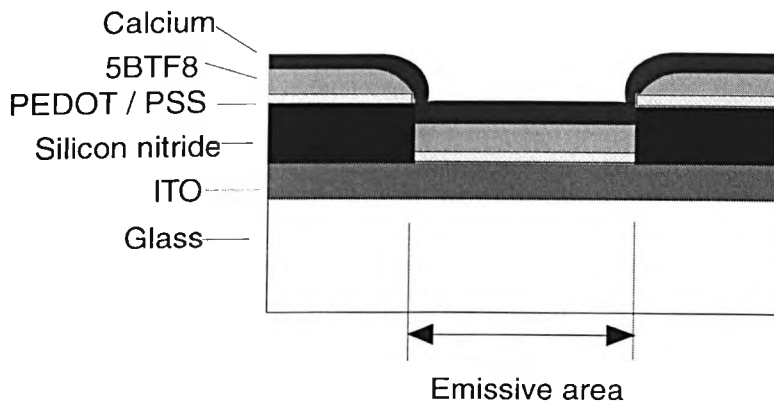


Figure 7.1: Schematic structure of a small area LED with a 5BTF8 emissive layer.

For comparison, standard area LEDs whose active area (1.5 x 3 mm) was defined by the overlap between ITO anode and Ca cathode were also fabricated. The devices have been electrically characterized by measuring the maximum brightness and the maximum current density that can be sustained prior to catastrophic failure. The LEDs were investigated using

both DC and pulsed driving schemes. For pulsed driving, the devices were driven by a HP 8114A pulse generator which can supply up to 100 V and 2 A. The rise time of the pulses is in the order of a few ns. Typically, a short pulse width in the order of a few hundred ns to a few μs was applied, to avoid heating problems, with a pulse period in the order of a few hundred μs to a few ms. The devices were tested under a high pump vacuum of $\sim 5 \times 10^{-6}$ mbar that simulates an encapsulation environment. This environment is expected to reduce the degradation effects of oxygen and moisture on the device stability and also preserve the calcium cathode used.

The current flowing during a voltage pulse was measured using a Tektronix oscilloscope by observing the voltage drop across a 10Ω series resistor which is connected in parallel to the LED. The data (voltage, current and light pulses) on the oscilloscope was typically averaged 32 to 64 times although this depended on the strength of the signal detected. For d.c. drive, the average brightness of the devices was measured using a Si photodiode calibrated with a Topcon luminance meter. The calibration was made for the standard devices and according to it 1 V from the photodiode corresponds to an absolute luminance of 90 cd/m^2 for 5BTF8. To determine the “true” brightness of the small area LEDs, the average d.c. brightness as recorded by the photodiode was multiplied by a factor that corresponds to the ratio between the standard LED device area and the small LED device area. This factor had values of 23, 573 and 2293 for $500 \mu\text{m}$, $100 \mu\text{m}$ and $50 \mu\text{m}$ diameter LEDs, respectively. Further, to determine the brightness during pulsed operation, the average d.c. brightness was scaled by a factor that corresponds to the operational duty cycle (typically $< 1\%$). The EL intensity was then detected using a calibrated fast photodiode (with a response time of approximately 50 ns) connected to the oscilloscope. Device storage and, where possible, device processing were performed in a dry nitrogen-filled glove box.

7.3 Device performance under d.c. and pulsed driving schemes

AFM images of a 50 μm device prior to the cathode deposition have shown that the side-walls of the hole are not coated by polymer and that the average depth of the hole is approximately 300 nm, corresponding to the thickness of the silicon nitride.¹⁵ The spin-coating process appears to coat the bottom of the holes with the same thickness of polymer as it does on the surrounding silicon nitride medium. Figure 7.2 compares the luminance versus voltage characteristics of standard and small area LEDs with varying diameter of the active device area in d.c. mode. The luminance versus current density characteristics measured under d.c. drive is shown in Figure 7.3. The performance of the standard area devices is compared with devices with diameters of 500 μm and 100 μm .

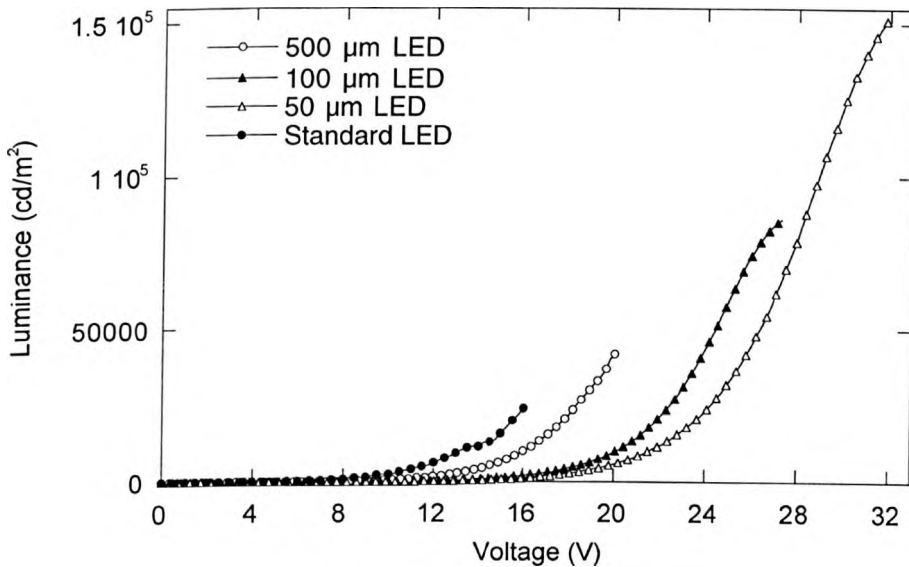


Figure 7.2: Luminance vs. voltage characteristics for different sized LEDs: “Standard” device (filled circles), 500 μm diameter (open circles), 100 μm diameter (filled triangles) and 50 μm diameter (open triangles).

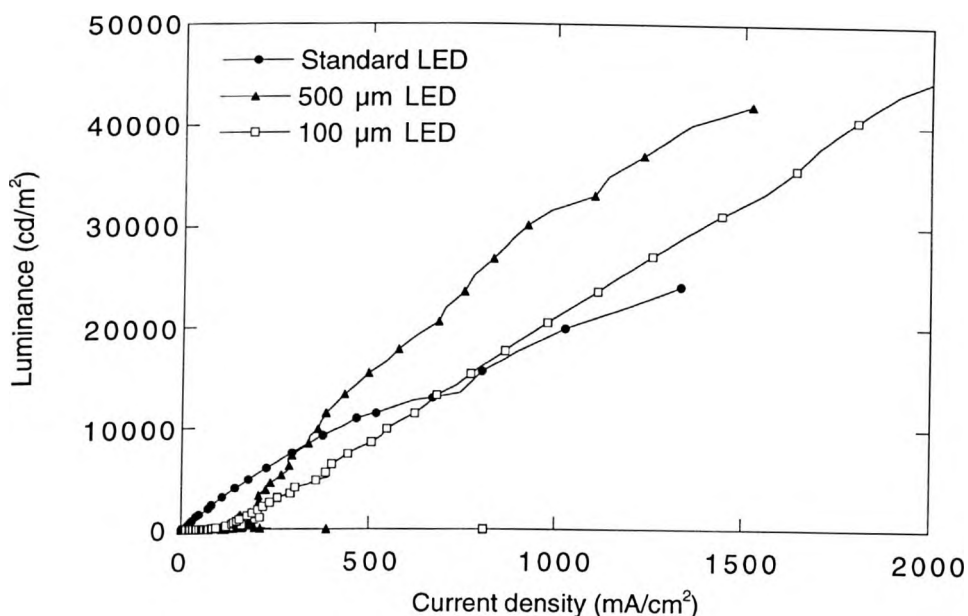


Figure 7.3: Luminance vs. current density characteristics (d.c. drive) for the different sized LEDs.

For the standard devices, the luminance and current density reach peak values of 24 kcd m^{-2} and 13 kA m^{-2} , respectively at 15 V. A monotonic increase in both the maximum current density and luminance sustained by the device is observed as the device emissive area is reduced: The peak luminance obtained for the $500 \text{ }\mu\text{m}$ device was 42 kcd m^{-2} at a current density of 15 kA m^{-2} and a voltage of 20 V. The $100 \text{ }\mu\text{m}$ device reached a peak brightness of 86 kcd m^{-2} at 27 V and at a current density of 43 kA m^{-2} . For the $50 \text{ }\mu\text{m}$ diameter devices, the peak luminance was 153 kcd m^{-2} at a current density of 125 kA m^{-2} at 32 V. The $100 \text{ }\mu\text{m}$ device therefore sustained a brightness (current density) more than 3.5 (3) times as large as that found for the standard device. The $50 \text{ }\mu\text{m}$ device also exhibited an increase of the maximum luminance and current density in d.c. mode by a factor of 6(9) compared to the standard device. We speculate that the increase of the driving voltage in the small area LEDs is probably due to the increased thickness gradient of the 5BTF8 layer towards the edge of the coated “hole” as it was observed on the AFM images. This would result in a thicker layer

and therefore in a lower local electric field at the contact (at a given voltage) which would reduce the charge injection in the bulk. From Figure 7.3, it can be seen that all the LEDs almost follow the same luminance versus current curve regardless of the size of the emissive area, indicating that the EL efficiency ($\sim 3 \text{ cd/A}$) is largely independent of the size of the device. The peak efficiency was 3.2 cd/A for a $500 \mu\text{m}$ device at 30 kcd m^{-2} and 9 kA m^{-2} . The standard device had a turn-on voltage of 5 V (defined as the voltage at a brightness of 100 cd m^{-2}). At this brightness, the device had an efficiency of 1.1 cd/A which increases to 2.8 cd/A at 1000 cd m^{-2} . The best performance figures for standard optimized LEDs are 8.5 cd/A (ELQE $\sim 2.5 \%$) at 4.4 V . These LEDs reached a brightness of 100 cd m^{-2} at 3.2 V .¹⁶ Figure 7.4 shows luminance vs. voltage characteristics of the different sized LEDs under a pulsed driving scheme while Figure 7.5 shows luminance vs. current density characteristics for these LEDs. Pulses with $1 \mu\text{s}$ width, $100 \mu\text{s}$ period and 1% duty cycle (except the $50 \mu\text{m}$ LEDs where the period was $300 \mu\text{s}$ and the duty cycle was 0.3%) were used.

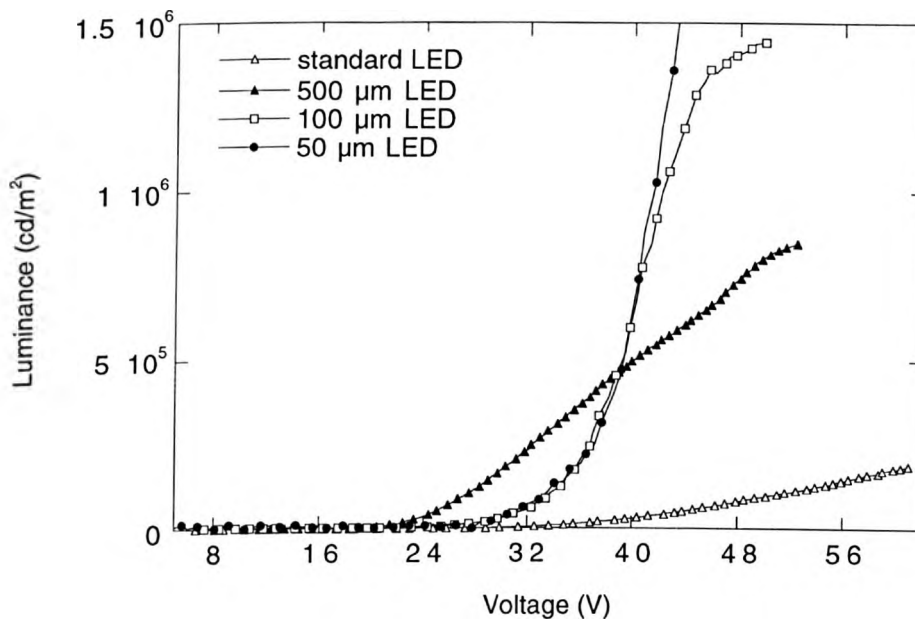


Figure 7.4: Luminance vs. voltage characteristics [$1 \mu\text{s}$ pulse width, $100 \mu\text{s}$ period ($300 \mu\text{s}$ for $50 \mu\text{m}$)].

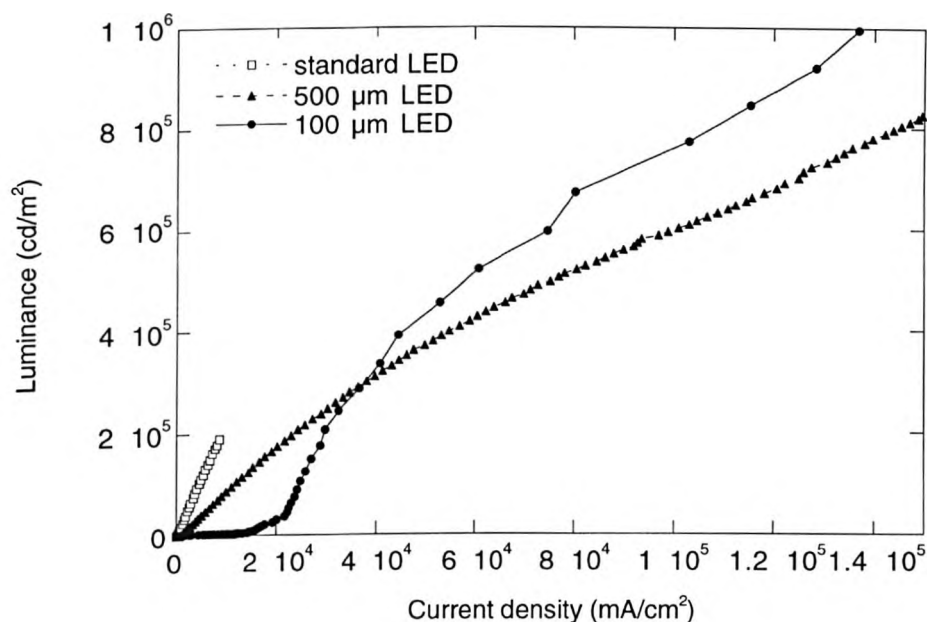


Figure 7.5: Luminance vs. current density characteristics (pulsed drive, 1 μ s pulses, 1 % duty cycle).

For the standard LED, the maximum luminance measured was 189 kcd m^{-2} , an increase of 8 times the d.c. brightness. The maximum current density sustained before device failure increased by approximately the same amount to 86 kA m^{-2} . As was observed in d.c. drive excitation, a reduction in the device active area also results in an increase in the maximum brightness. However in contrast to what happens in d.c. mode, here the operating voltage of the small area LEDs is significantly lower than that of the standard LEDs. This can be attributed to either the beneficial effect of the pulsed excitation on the capacitance loss and thus the average power dissipated in the bulk of the device or the trapped-charge-limited (TCL) conductivity of 5BTF8. The different slopes of the I-V characteristics measured under d.c. and pulsed conditions may provide some evidence for the latter explanation. The 500 and 100 μm devices had peak luminance values of 845 kcd m^{-2} and 1.4 Mcd m^{-2} respectively (an increase of 20 and 16 times, respectively, the d.c. luminance). The maximum current density sustained by the 500 and the 100 μm devices was 1.56 MA m^{-2} and 2.6 MA m^{-2} ,

respectively (an increase of 100 and 60 times, respectively, the d.c. peak current density). The 500 μm device showed an increase of the maximum current density and peak brightness by a factor 18 (4.5) compared to the standard device under the same pulsed scheme. The 100 μm device also showed an increase of the maximum current density and luminance by a factor of 8 (30) compared to the standard LED. The EL efficiency of the standard LED is higher than the efficiency of the small area LEDs under pulsed driving in contrast to d.c. mode. Current leakage conduction paths at low voltages were observed to occur both in the 50 and 100 μm LEDs and can account for the reduced efficiency of the small area LEDs in pulsed mode. The maximum efficiency of the standard device is ~ 2 cd/A while that of the small area LEDs is lower than 1 cd/A although it almost remains constant at high currents in contrast to d.c. mode where it falls off at high currents. This is a result of the reduced power dissipated in the device under pulsed drive (device is “off” for most of the pulse duration) that allows for efficient recombination at high current densities.

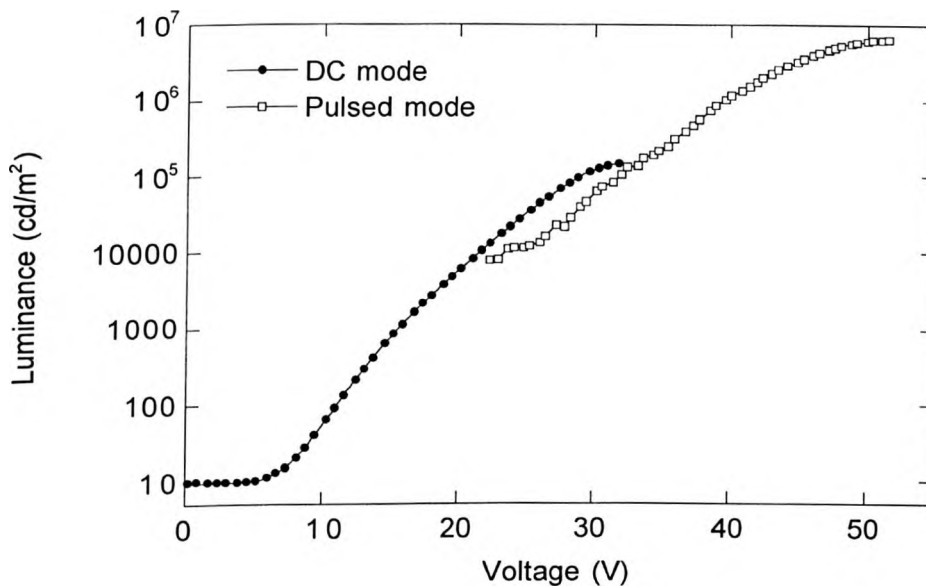


Figure 7.6: Luminance vs. voltage characteristics of a 50 μm device under both d.c. and pulsed driving.

Chapter 7: Incorporation of a small area structure in polymer light-emitting diodes and microcavities

Figure 7.6 shows the luminance versus voltage measured for a 50 μm device under both d.c. and pulsed drive. A peak luminance of 6.5 Mcd m^{-2} at 5.1 MA m^{-2} was sustained for the 50 μm LED using $1 \mu\text{s}$ pulses at a 0.3 % duty cycle (300 μs pulse period). Both the peak luminance and current density of the 50 μm LEDs increase by almost a factor of 40 compared to the corresponding d.c. drive peak values. The maximum luminance (current density) sustained in pulsed mode also increases by a factor of 35 (60) compared to the standard device. The corresponding factor for comparing the same magnitudes in d.c. mode is 6 for the luminance and 9 for the current density, therefore the pulsed driving scheme “adds” another factor of 6 increase in the peak values for both luminance and current density on top of the factors already calculated for reducing the device size from a standard 4.5 mm^2 device to a 50 μm diameter LED in d.c. driving. The slight difference of the duty cycles used for the standard (1%) and the 50 μm device (0.3%) was not found to influence the comparison of the results. Table 1 summarizes all the results obtained for the different sized LEDs under both d.c. and pulsed driving schemes.

Device	Current density (A/m^2)	Luminance (cd/m^2)
Standard (4.5 mm^2) (d.c)	13000	24000
500 μm (d.c)	15000	42000
100 μm (d.c)	43000	86000
50 μm (d.c)	125000	153000
Standard (pulsed)	86000	189000
500 μm (pulsed)	1560000	845000
100 μm (pulsed)	2600000	1400000
50 μm (pulsed)	5100000	6500000

Table 1: Summary of results for the different sized LEDs under both d.c. and pulsed driving schemes.

As it is well known, in an LED some of the energy that is not emitted as light will be converted to heat. The existence of unavoidably large current densities, in general, will make devices more susceptible to Joule heating problems. The effect of current-induced heating on the LED operation has been measured and modeled and is considered to play a major role in limiting the maximum efficiency and brightness and in initiating the degradation mechanism.¹⁷⁻¹⁸ Zhou *et. al.*¹⁷ have found that the temperature rise due to the Joule heating effect inside an LED is significant and can be higher than 60 °C under high driving conditions. They also proposed that the electric-field-induced decomposition of the ITO and the electromigration of the indium atoms (or ions) are responsible for the catastrophic failure of LEDs. In another study, Tessler *et. al.*¹⁸ found that the temperature in the recombination zone may be elevated by at least 60 K above ambient if the LED is run at a d.c. current density equivalent to 25 kA m⁻² and this temperature rise will eventually limit the maximum efficiency attainable in the device. This current density is twice as large as the maximum current density that can be sustained by the standard LEDs under d.c. drive. Therefore it can be concluded that when the standard LED is run at its maximum sustainable current density, the temperature of the recombination zone might rise by some tens of degrees. Pinner *et. al.*¹⁹ have proposed that the mechanism for the current/heat-induced failure of LEDs can be considered as follows: at current densities higher than 1 kA m⁻², the increase in the device temperature results in an increase in the charge carrier mobility. At a constant operating voltage, this increases the current flow, which in turn increases localized Joule heating. Thus a positive feedback loop is expected to be established which can lead to thermally activated degradation pathways and localized melting followed by delamination of the cathode. This process eventually results in catastrophic failure or thermal breakdown of the LED.

Hence the enhanced performance of the small-area device structures can be explained by their significantly improved thermal properties. Two different thermal based processes are

proposed to influence the thermal properties of the small area LEDs. The first process involves the Si_xN_y medium. As the LED active area becomes smaller, the average distance between any emissive volume within the active area and the cooler surrounding silicon nitride medium decreases. This results in a more efficient heat exchange with the surrounding medium and thus to an efficient heat dissipation from the polymer, allowing the LED to sustain higher current densities and higher peak brightnesses. A similar effect should be expected to occur between the emissive medium and the Ca cathode; this is the second process involved. As the device area becomes smaller, a larger part of the Ca cathode will not directly participate in the injection and emission process thus allowing to act as an efficient heat sink for the heat produced inside the device. The significantly higher conductivity of the Ca metal compared to the Si_xN_y dielectric may also determine the relative contribution of each of the two processes (by increasing the contribution of the Ca “heat sink”) on the improved thermal stability of the small area LEDs. The effect of heating on device failure is also confirmed by the ability of LEDs to sustain much larger current densities when run under pulsed schemes, as a low operational duty cycle significantly reduces the average power dissipated in the LED (the device is in the “off” state for most of the duration of the pulse). Thus an overall improved thermal management of the small area LEDs can account for their significantly improved performance compared to standard LEDs.

We finally note that in some cases a layer of gold was photolithographically patterned onto the ITO with small holes for the active area of the device and then on top of this a Si_xN_y layer was deposited and also patterned to finally leave the small active area through which current flow occurs. This allows for intrinsic device characteristics to be measured and for problems associated with the series resistance due to the ITO to be removed. Robert Fletcher has used this structure to fabricate 5BTF8 based PLEDs with a BFA hole transporting polymer that exhibited maximum brightnesses of 2 Mcd^{-2} and sustained current densities

over 1 MA/m^2 when driven with a 200 ns pulse (and a 400 μs period) at 99 V.²⁰ Identical 50 μm PEDOT/PSS/5BTf8 devices with gold on top of Si_xN_y showed a maximum brightness of 2.5 Mcd m^{-2} at 40 V and sustained current densities over 2.5 MA/m^2 resulting in efficiencies of 1 cd/A under identical pulse excitation conditions. However, no improvement was realized on the device performance compared to identical small area LEDs that only had a Si_xN_y layer on top of ITO. Although the operating voltage was slightly lower due to the fact that gold provides a low resistance path for holes to be injected into the polymer, significantly higher hole leakage currents were also observed at low voltages in the case of gold devices that also made the devices more susceptible to electrical shorts. It should be finally noted that the EL spectrum of the small area LEDs is identical to the EL spectrum of the standard LEDs (emission peak at 535 nm) and no angular dependence of the emission color or modification of the spectrum under intense pulsed excitation was observed.

7.4 Small area microcavity LEDs

7.4.1 Introduction

Although PLEDs show high brightness and efficiency, their emission characteristics are usually characterized by a wide viewing angle and a broad spectral width due to inhomogeneous broadening and coupling to vibronic modes. Full color displays will require materials with narrow emission spectra that can provide saturated colors. A modification of the emission characteristics is possible by using planar microcavity structures which alter the optical mode density. Several research groups have reported different microcavity structures²¹⁻²⁶ that narrow the emission linewidth significantly, enhance the emission intensity in the cavity mode wavelength and provide a feedback mechanism for lasing emission; thus they have been extensively used to overcome the problem of the broad

emission spectra of PLEDs. In the second part of this chapter, incorporation of the small area structure into a microcavity configuration and results from electrically pumped microcavity 5BTF8 and PFO LEDs will be presented. The novel application of small area microcavity LEDs was investigated in the context of efforts towards electrically pumped lasing after the group at Bell Labs demonstrated, for the first time, lasing from a tetracene organic crystal.²⁷

7.4.2 Theory and experimental details

A microcavity is analogous to a Fabry Perot resonator where a standing wave is set up between the two mirrors that define the two ends of the cavity. Light emitted from the emissive medium will be coupled to the standing wave and enhanced only at the cavity mode wavelength while suppressed elsewhere. The principal effect of the microcavity on the spontaneous emission is to redistribute the photon density of states such that only certain wavelengths, which correspond to allowed cavity modes, are emitted in a given direction. The intensity of the spontaneous emission will be enhanced in the direction normal to the cavity axis relative to a non cavity device. Another effect of the microcavity is that the emission wavelength, its intensity and linewidth exhibit an angular dependence. The cavity length is defined as the distance between the two mirrors (typically one dielectric mirror and a metallic mirror are used). The emission wavelength λ depends on the cavity length according to the following relation:

$$2nd\cos\{\sin^{-1}[(\sin\theta)/n]\} = m\lambda \quad (1)$$

where d is the distance between the two mirrors, n the refractive index of the emissive medium, m the mode integer and θ is the emission angle. At normal incidence, $\theta=0$ and for $m=1$, the emission wavelength will be given by the relation: $\lambda=2dn$. If more than one layer is placed between the two mirrors then the thickness and the refractive index of each individual layer has to be taken into account in order to calculate the cavity mode wavelength. Figure

7.7 shows a schematic diagram of a microcavity with a DBR (distributed Bragg reflector) mirror consisting of alternate Si_xN_y and SiO_2 layers, an active layer and a metal mirror.

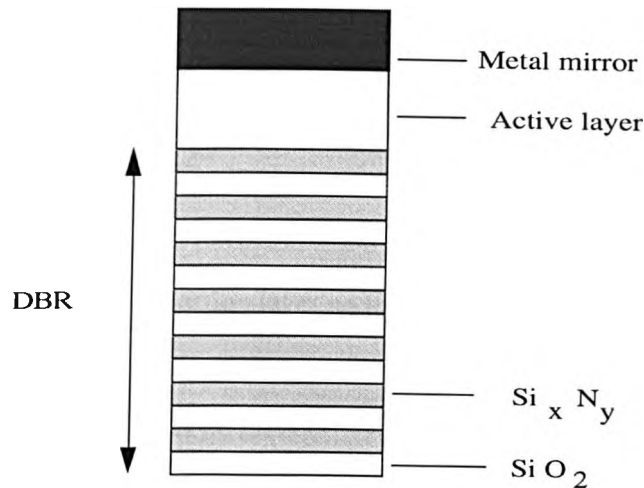


Figure 7.7: Schematic diagram of the microcavity.

The bottom DBR mirror was a dielectric mirror which consists of 4 or 6 pairs of alternate silicon nitride Si_xN_y (high refractive index material, $n=1.95$) and silicon dioxide SiO_2 (low refractive index material, $n=1.45$) layers. Each individual layer is $\lambda/4$ thick where λ is the cavity mode wavelength. Each layer was deposited by plasma enhanced chemical vapor deposition at 300°C at the Department of Electronic Engineering at the University of Sheffield. The mirrors were designed so that they have a high reflectivity over the wavelength range where the active layer is emissive and with the center of the DBR stop band designed to be close to the emission peak wavelength of the active material. The exact thickness and number of repeat units of the DBR mirror to be used were calculated using a transfer matrix (TM) model that is able to predict the emission from a set of oscillators that can be designed to replicate the emission from a specific material.²⁸ A 300 nm thick ITO layer ($n=2.0$) was next deposited on top of the DBR by DC magnetron sputtering. The ITO deposition was done at the Dow Chemical Company in USA. The $50\ \mu\text{m}$ small area LED

structure was then incorporated on top of the ITO with the only difference being that a 1 μm thick photoresist layer was used instead of Si_xN_y to define the active area. A composite Ca(15nm)/Al(300nm) cathode was used as the top mirror. Ca has a poor reflectivity so a Ca/Al composite cathode will combine the low workfunction and the high electron injection ability of Ca with the high Al reflectivity. This composite cathode has a reflectivity of $\sim 80\%$, similar to the reflectivity of Al^{20} , and thus is a relatively “good” mirror that will reduce optical losses and allow narrow emission linewidths to be achieved. A 15 nm PEDOT/PSS layer was also used as a hole injection layer on top of the ITO anode.

7.4.3 5BTF8 microcavity LEDs

5BTF8 has been shown to exhibit spectral narrowing under optical excitation only when the excitation is at the lower wavelength range where BT absorbs ($\sim 340 \text{ nm}$)²⁰, therefore an investigation of 5BTF8 in a cavity configuration under electrical excitation would be of significant interest with the possibility of achieving stimulated emission remaining elusive. For small area 5BTF8 cavity LEDs, a 110 nm thick 5BTF8 ($n=2.2$)²⁹ layer was used as emissive layer. This results in a total thickness of 125 nm (by adding the PEDOT thickness) which can then be added to the ITO thickness in order to define the cavity length. The cavity length defined by the separation between the top of the last SiO_2 layer of the DBR and the top mirror is 425 nm. The EL enhancement factor at the cavity mode wavelength ($\sim 525 \text{ nm}$) was found to increase up to 4 repeat pairs of mirrors. Therefore a DBR mirror consisting of 4 alternate pairs of Si_xN_y and SiO_2 layers was the choice for the 5BTF8 cavity LEDs. Its reflectivity spectrum is shown in Figure 7.8 (with ITO already deposited on the DBR). In order to measure the reflectivity, white light was focused at normal incidence on the DBR and the light reflected was passed through a fibre and recorded by a photomultiplier. The EL spectrum of a cavity 5BTF8 LED is also shown in the Figure 7.9 below.

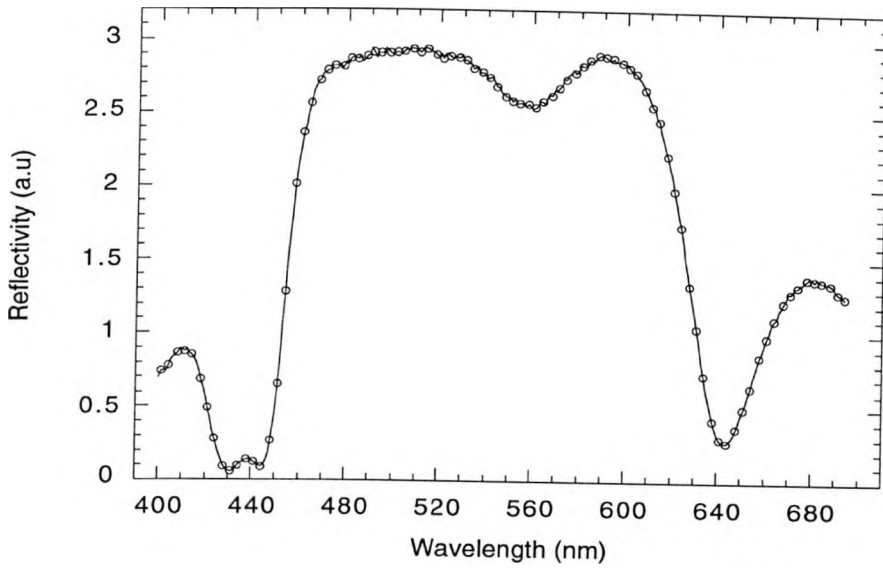


Figure 7.8: Reflectivity of a DBR mirror consisting of 4 alternate pairs of silicon nitride and silicon oxide.

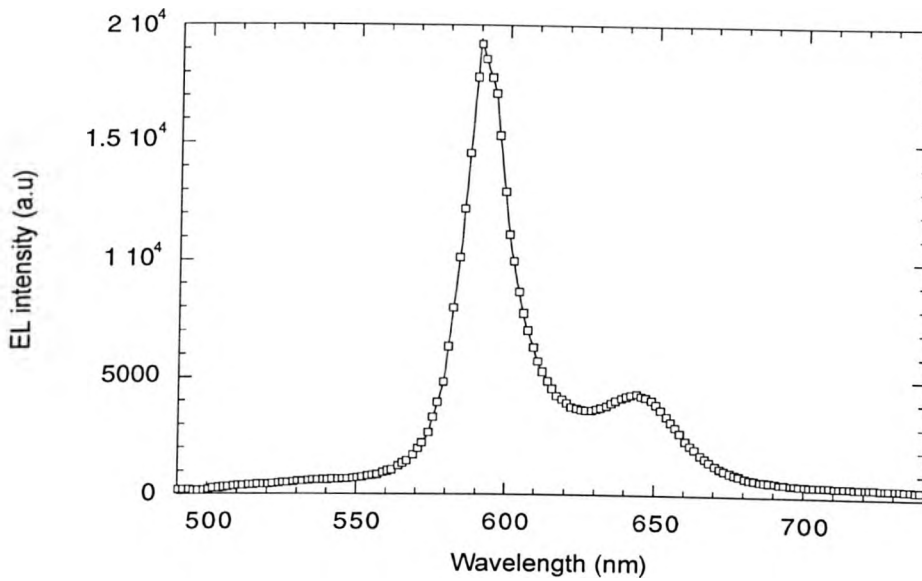


Figure 7.9: Electroluminescence spectrum of a small area microcavity 5BTF8 LED at normal incidence.

The DBR mirror has a high reflectivity between 500 and 600 nm where 5BTF8 emits. The small mode observed at 560 nm is due to weak reflection at the air/ITO interface that also acts

as a mirror due to the refractive index difference between ITO and air. The reflectivity spectrum of the cavity (not shown here) exhibits a sharp dip at 590 nm corresponding to the cavity mode. The EL spectrum of a non cavity LED shows emission characteristic of BT peaking at 535 nm (FWHM = 90 nm). The main cavity mode is at 590 nm (FWHM = 18 nm) while a second mode occurs at 640 nm. Although the main cavity mode does not coincide with the 5BTF8 peak as should be expected by taking into account the refractive indices and thicknesses of the different layers that are deposited between the mirrors, this could be achieved if the total thickness (excluding ITO) was reduced to 100 nm. The occurrence of a second mode is mainly related to the drop off in DBR reflectivity. Light then escapes from the cavity rather than couples to the standing wave. The optical field inside the cavity (along the cavity axis) also exhibits a mode at ~ 635 nm as demonstrated by Fletcher *et. al.*²⁹ The large electromagnetic field is expected to further enhance the mode observed at ~ 640 nm. Current and luminance vs. voltage characteristics of cavity 5BTF8 LEDs are shown in Figure 7.10.

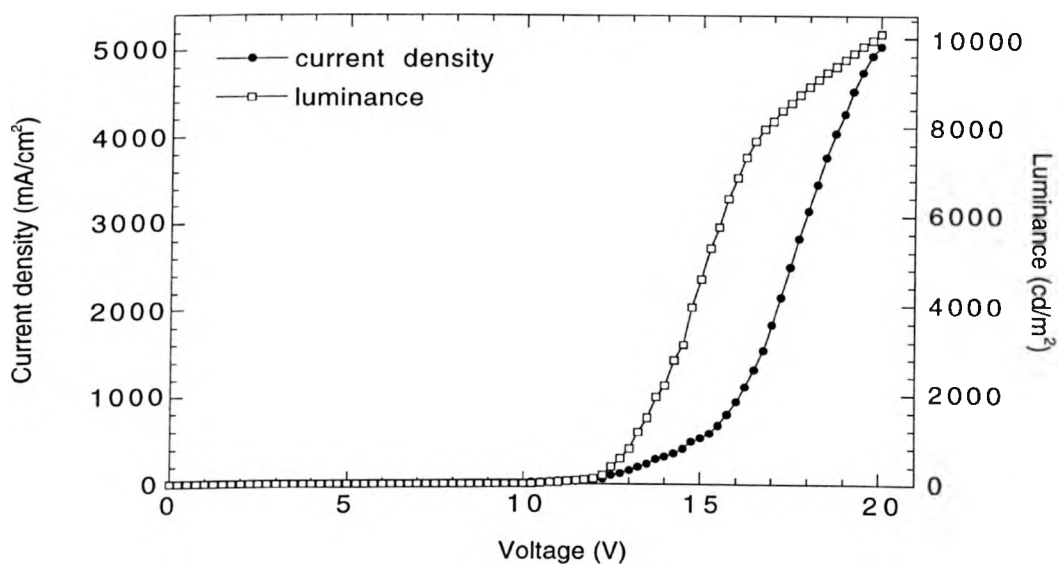


Figure 7.10: Current density and luminance vs. voltage characteristics of small area cavity 5BTF8 LEDs.

Under d.c. drive, a maximum brightness of 10000 cd/m^2 at a maximum current density of 5000 mA/cm^2 was obtained at 20 V; the maximum quantum efficiency was 1 cd/A obtained at a luminance of 5000 cd/m^2 and the turn on voltage was 11.5 V for a luminance of 100 cd/m^2 . A significant improvement of the device performance over identical standard microcavity 5BTF8 LEDs is achieved by integrating the small area device structure in the cavity configuration. Fletcher et. al. reported maximum luminances of 300 cd/m^2 and maximum sustainable current densities of 35 mA/cm^2 at 35 V with a corresponding efficiency of 0.95 cd/A for identical standard cavity LEDs.²⁹ Therefore the maximum luminance (current density) obtained from the small area cavity LEDs is almost a factor of 30 (150) higher than the standard cavity LEDs; an improvement attributed to the improved thermal properties of the small area structures as analytically explained earlier in the chapter. We also note that the phase change on reflection and the cavity mode wavelength have been shown to be a function of the mirror composition²⁹ and thickness³⁰, therefore the mirror properties could also partly account for the red-shifted position of the peak wavelength of cavity LEDs. No spectral changes were observed to occur under pulsed excitation resulting in an identical emission spectrum to the one obtained in d.c. mode.

7.4.4 PFO microcavity LEDs

PFO has been shown to exhibit optically pumped spectral narrowing, stimulated emission and gain narrowing of the cavity mode linewidth in a cavity configuration where optical feedback is provided,³¹⁻³² with evidence that lasing emission also occurs. The next step would be to examine the electrical operation of small area PFO cavity LEDs which can provide information on the possibility of spectral narrowing or spectral redistribution of the cavity modes under charge injection and particularly under intense pulsed electrical excitation. For PFO cavity LEDs, dielectric mirror substrates consisting of alternate quarter

wavelength ($\lambda/4$) layers of silicon oxide and silicon nitride on glass were used. The DBR mirrors consisted of 6 pairs of $\lambda/4$ layers; this number of pairs was found to exhibit the highest reflectivity in the blue spectral region where PFO emits and thus it is suitable for the preparation of PFO cavity LEDs. A 105 nm thick layer of PFO ($n=1.6$) was then spin coated onto the DBR/ITO substrate from a toluene solution. Figure 7.11 shows the reflectivity spectrum of the 6 pair DBR mirror (with ITO already deposited on top of the DBR).

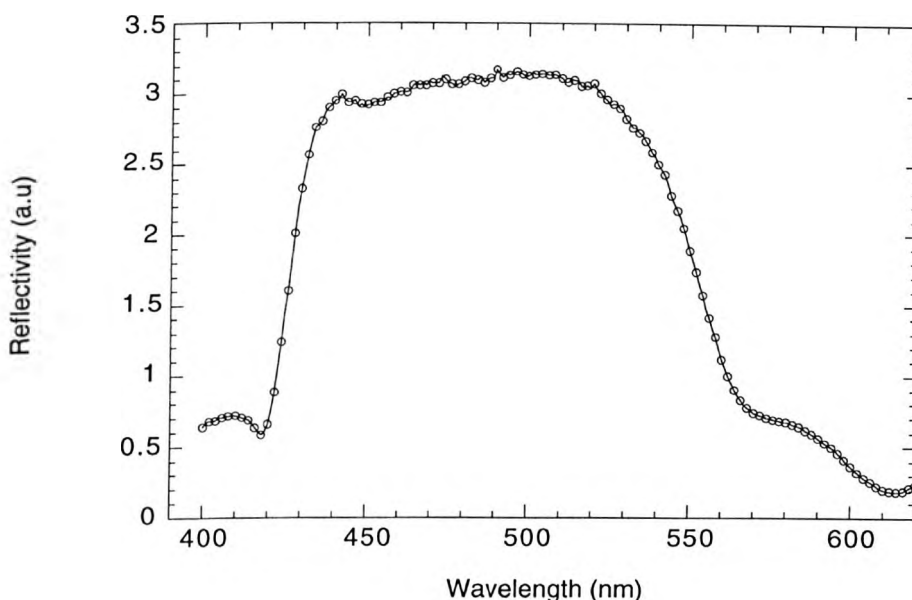


Figure 7.11: Reflectivity spectrum of a 6 pair DBR mirror.

The reflectivity spectrum shows a high reflectivity between 430 and 530 nm. This wavelength region coincides with the PFO emission spectral region. The reflectivity spectrum of the PFO cavity (not shown here) shows a sharp dip at 450 nm which will be identified later as the cavity emission mode. Current and luminance vs. voltage characteristics of cavity PFO LEDs are shown in Figure 7.12 while Figure 7.13 shows the EL spectrum of a PFO cavity LED under d.c. and pulsed driving. 1 μ s pulses with a 500 μ s period were used.

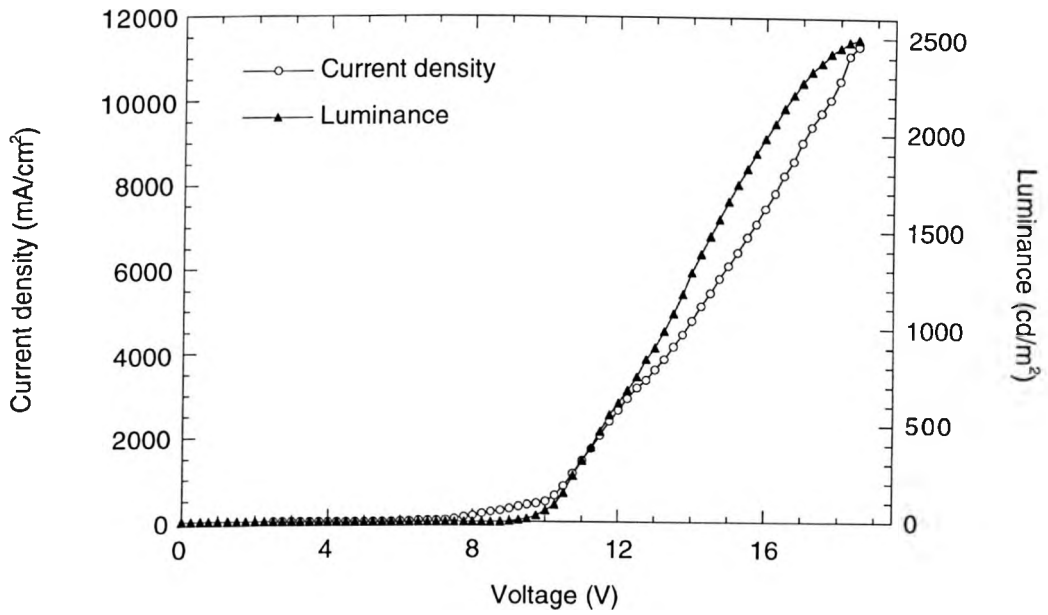


Figure 7.12: Current density and luminance vs. voltage characteristics of small area PFO microcavity LEDs.

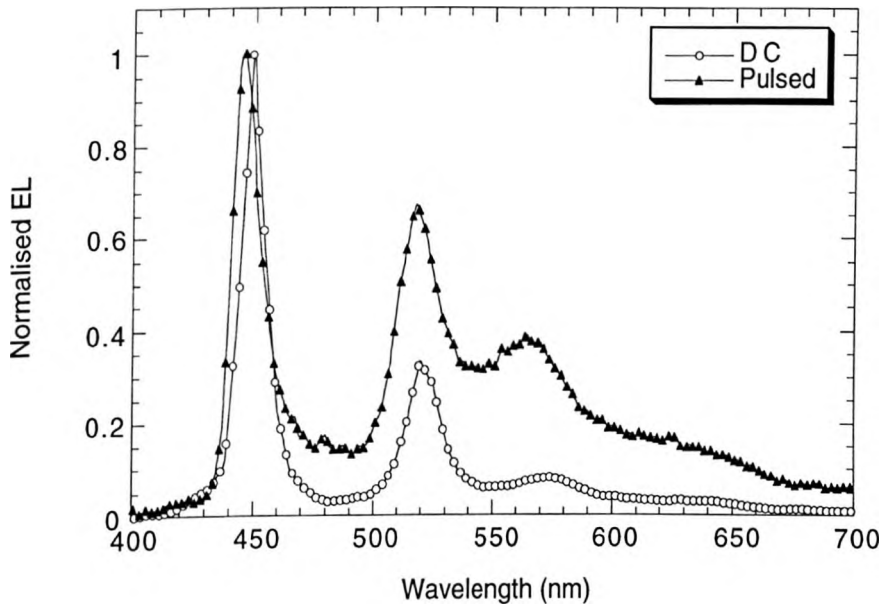


Figure 7.13: EL spectra of small area PFO cavity LEDs under d.c. and pulsed driving at normal incidence.

Electrically pumped PFO cavity LEDs exhibit a very high performance; they reach a maximum luminance of 2500 cd/m^2 at a current density of 11500 mA/cm^2 with a maximum EL efficiency of 0.03 cd/A in d.c. mode. The turn on voltage (arbitrarily defined as the voltage required to reach a luminance of 100 cd/m^2) is 10.5 V . A peak emission cavity wavelength of 449 nm with a narrow linewidth of 11 nm was obtained in d.c. mode for the cavity PFO LEDs. The applied current density was 10000 A/m^2 . A second mode is also present at 520 nm while a small shoulder band occurs at around 570 nm which may be associated with some small contribution from excimer emission. A small blue shift of the cavity mode at 449 nm of $\sim 4 \text{ nm}$ occurs under pulsed excitation thus resulting in a main cavity peak at 445 nm . This can not be attributed to thermal expansion as this process would result in a red shift of the cavity mode wavelength. It can rather be attributed to a small decrease of the refractive index of PFO at very high current densities i.e. by state filling. The spacing between the different modes is also mainly determined by the wavelength-dependent effective cavity length. For comparison, noncavity PFO LEDs also show blue emission with clear vibronic structure and well resolved peaks at 430 and 450 nm and with a full width at half maximum of approximately 45 nm . A broad unstructured band also appears at around 530 nm which is associated with excimer emission in noncavity LEDs. However under pulsed excitation ($1 \mu\text{s}$ pulses, 0.2% duty cycle) with an applied current density of $\sim 100000 \text{ A/m}^2$, a change of the cavity emission spectrum as a result of spectral redistribution occurs. While in d.c. mode emission is mostly distributed in the cavity mode at 449 nm with some emission in the mode at 520 nm , under pulsed excitation the relative weight of the mode at 520 nm increases with regard to the mode at 449 nm . In Figure 7.14 the EL spectrum of a PFO cavity LED as a function of the applied current under pulsed driving is presented while Figure 7.15 shows the ratio of the relative intensities of the two modes at 449 and 520 nm also as a function of the applied current.

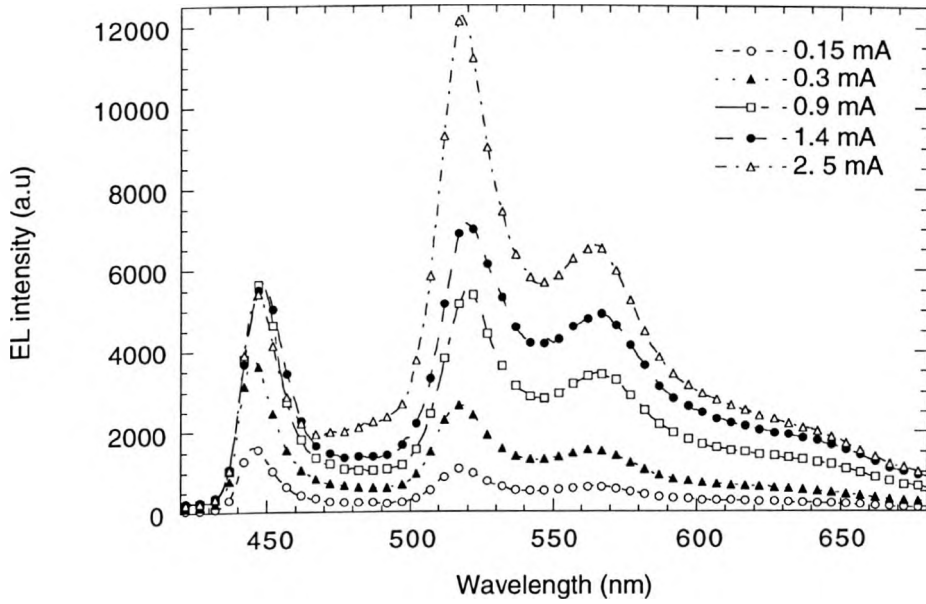


Figure 7.14: EL spectrum of a small area PFO cavity LED as a function of the applied current.

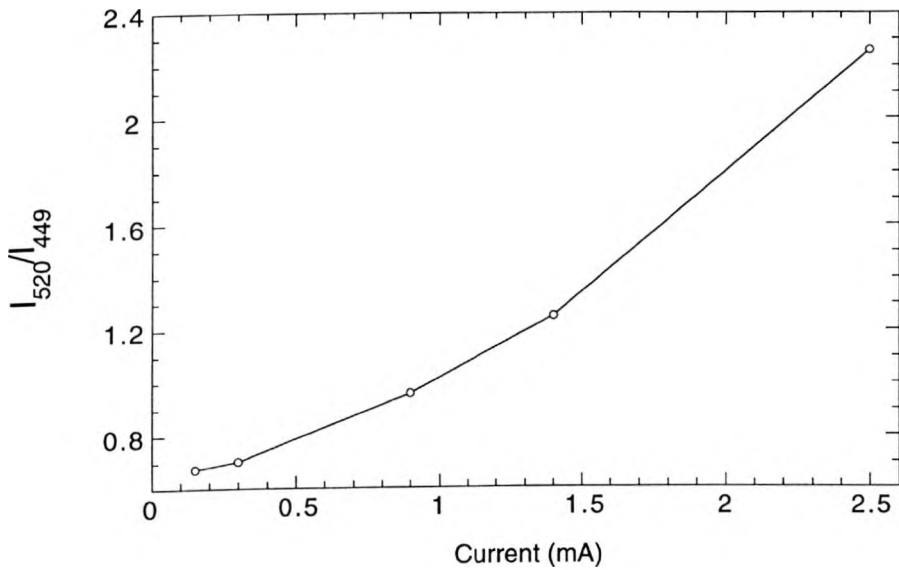


Figure 7.15: Ratio of relative intensities of the two modes at 449 and 520 nm as a function of current.

Below 0.3 mA (essentially when the device is still driven in d.c. mode) both modes increase in intensity at the same rate. Above this “threshold” the second peak increases quicker than the main peak indicating a preferential wavelength for emission. The change in the ratio of the intensity of the two cavity modes is almost a factor of 3 for a increase of the pulsed current density by a factor of 30. The spectral redistribution of the two cavity modes occurs above a “threshold” current of 0.3 mA which corresponds to a current density of 155000 A/m^2 . The maximum sustainable current before catastrophic failure of the device was 2.5 mA which corresponds to a current density of $1,250,000 \text{ A/m}^2$. We should expect that if no gain (stimulated emission) occurs, the spectrum would just scale with injected current and no spectral mode redistribution would take place. However, the fact that the spectral intensity enhancement occurs not on the main cavity mode (as should be expected from the fact that the main peak of the non cavity device is close to the position of the main cavity mode) but on the “secondary” lower oscillator strength mode indicates that it can not probably be attributed to gain. Either changes in the refractive index of PFO or possible electrical-induced degradation of PFO under intense excitation (as typically observed in PFO LEDs with an increase of the excimer emission component under high excitation conditions resulting in whitish-blue rather than pure blue color) are thought to be the likely causes for the spectral redistribution. Also the linewidth of either of the cavity modes is almost independent of the applied current which implies that no electrically induced spectral narrowing occurs and further indicates that probably no gain has been achieved during electrical operation. A transition from multi-mode to single-mode operation and a narrowing of the linewidth would be expected to occur under spatial coherence (or stimulated emission/lasing conditions) and we believe that the results presented here do not show strong evidence for stimulated emission. Although very high current densities were demonstrated, losses in the cavity/diode structure because of metal electrode absorption and charge-induced absorption are the main reasons for not observing lasing. Further investigations in addressing these issues are currently in progress.

7.5 Conclusions

The work described in this chapter shows how small area device structures can result in very high brightness and efficient LEDs that are able to sustain significantly higher current densities than normal structures. Small area device structures (with an active area down to 50 μm diameter) were fabricated and characterized. In this structure, a photolithographically patterned silicon nitride layer is deposited on top of the ITO in order to define active areas with diameters of 500, 100 and 50 μm , respectively. A significant improvement of the maximum brightness and the current density is achieved in these small area devices. We find that by reducing the active diameter of the device from the standard size (1.5 x 3 mm) to 50 μm , the current density that can be sustained increases by a factor of 9 in d.c. mode and by a factor of 60 in pulsed mode. This increase in current density is mirrored by similar increases in maximum brightness. The brightness of the 50 μm LED increases by a factor of 6 in d.c. mode and by a factor of 35 in pulsed mode compared to the standard LEDs. An improvement by approximately a factor of 6 is obtained for both the maximum current density and luminance sustained by the 50 μm small area LEDs in pulsed mode compared to d.c. mode which confirms that low duty cycle pulsing schemes can significantly reduce the average power dissipation in a device and thus improve the device stability and increase the operating lifetime. 50 μm diameter 5BTF8 LEDs emitted light with a brightness of $\sim 155,000 \text{ cd/m}^2$ in d.c. mode. Using pulsed driving schemes, the same devices reached a maximum brightness of $6,500,000 \text{ cd/m}^2$ and sustained current densities up to $5,000,000 \text{ A/m}^2$. These improvements are attributed to an overall improved thermal management of the small area devices due to reduced Joule heating effects. Both the Si_xN_y medium and the Ca cathode are proposed to act as efficient heat sinks that enable significant heat dissipation from the device as a result of the efficient heat exchange between the emissive medium and the surrounding

media. These results confirm that efficient thermal management will be particularly important in determining the operational stability and lifetime of PLED displays.

The incorporation of the small area structure in a microcavity configuration has also resulted in high brightness cavity LEDs with interesting spectral properties. By using highly reflective DBR mirrors and a composite Ca/Al cathode with a low workfunction and a high reflectivity, novel small area cavity 5BTF8 and PFO LEDs have been realized. Electrically pumped 5BTF8 cavity LEDs exhibit a maximum light output of 10000 cd/m^2 , a sustainable current density of 5000 mA/cm^2 , an EL efficiency of 1 cd/A and a narrow linewidth of 18 nm with an emission peak at 590 nm . Similarly, PFO cavity LEDs reach a maximum luminance of 2500 cd/m^2 at a current density of 11500 mA/cm^2 . A peak cavity wavelength of 450 nm with a narrow linewidth of 11 nm was obtained in d.c. mode. Spectral redistribution was observed to occur under intense pulsed excitation and led to EL spectral changes in PFO cavity LEDs. An increased relative weight of the emission peak at 520 nm compared to that at 449 nm was observed with increasing current density above a “threshold” current of 0.3 mA which corresponds to a current density of $\sim 155,000 \text{ A/m}^2$. Both the fact that the enhancement occurs on the secondary cavity mode and that we do not observe spectral narrowing leads us to attribute the spectral redistribution to either changes in the refractive index or electrical-induced degradation of PFO under intense excitation conditions. Future work will concentrate on improving the spectral properties of the small area cavity LEDs so that there is only a single cavity mode within the EL spectra. Optimization of the device structure and the pulsing scheme applied will also be a matter for future work.

References

1. e.g. see CDT website, <http://www.cdttld.co.uk>

2. Sirringhaus, H., Tessler, N. & Friend, R.H. *Synthetic Metals* **102**, 857 (1999).
3. Fukuda, Y., Watanabe, T., Wakimoto, T., Miyaguchi, S. & Tsuchida, M. *Synthetic Metals* **111-112**, 1 (2000).
4. Tian, P.F., Burrows, P.E. & Forrest, S.R. *Applied Physics Letters* **71**, 3197 (1997).
5. Noach, S., Faraggi, E.Z., Cohen, G., Anvy, Y., Neumann, R., Davidov, D. & Lewis, A. *Applied Physics Letters* **69**, 3650 (1996).
6. Sugamura, N., Adachi, C., Koyama, T., Taniguchi, Y. & Shiraishi, H. *Applied Physics Letters* **74**, 1206 (1999).
7. Lidzey, D.G., Bradley, D.D.C., Alvarado, S.F. & Seidler, P.F. *Nature* **386**, 135 (1997).
8. Kozlov, V.G., Parthasarathy, G., Burrows, P.E., Khalfin, V.B., Wang, J., Chou, S.Y. & Forrest, S.R. *IEEE Journal of Quantum Electronics* **36**, 18 (2000).
9. Tessler, N., Harrison, N.T. & Friend, R.H. *Advanced Materials* **10**, 64 (1998).
10. Pinner, D.J., Tessler, N. & Friend, R.H. *Synthetic Metals* **102**, 1108 (1999).
11. Jabbour, G.E., Shaheen, S.E., Morrell, M.M., Anderson, J.D., Lee, P., Thayumanavan, S., Barlow, S., Bellmann, E., Grubbs, R.H., Kippelen, B., Marder, S., Armstrong, N.R. & Peyghambarian, N. *IEEE Journal of Quantum Electronics* **36**, 13 (2000).
12. Fletcher, R.B., Lidzey, D.G., Bradley, D.D.C., Walker, S., Inbasekaran, M. & Woo, E.P. *Synthetic Metals* **111**, 151 (2000).
13. Frolov, S.V., Fujii, A., Chinn, D., Hirohata, M., Hidayat, R., Taraguchi, M., Masuda, T. Yoshino, K. & Vardeny, Z.V. *Advanced Materials* **10**, 869 (1998).
14. Campbell, A.J. (personal communication).
15. Martin, S.J. (personal communication).
16. Wang, X. & Bradley, D.D.C. (unpublished results).

17. Tessler, N., Harrison, N.T., Thomas, D.S. & Friend, R.H. *Applied Physics Letters* **73**, 732 (1998).
18. Zhou, X., He, J., Liao, L.S., Lu, M., Ding, X.M., Hou, X.Y., Zhang, X.M., He, X.Q. & Lee, S.T. *Advanced Materials* **12**, 265 (2000).
19. Pinner, D.J., Friend, R.H. & Tessler, N. *Synthetic Metals* **111-112**, 257 (2000).
20. Fletcher, R.B. *Engineering of Optoelectronics Devices based on Conjugated Polymers* (Sheffield University, 1999).
21. Lidzey, D.G., Bradley, D.D.C., Martin, S.J. & Pate, M.A. *IEEE Journal of Selected Topics in Quantum Electronics* **4**, 113 (1998).
22. Tokito, S., Tsutsui, T. & Taga, Y. *Journal of Applied Physics* **86**, 2407 (1999).
23. Tessler, N., Denton, G.J. & Friend, R.H. *Nature* **382**, 695-697 (1996).
24. Dodabalapur, A., Rothberg, L.J., Jordan, R.H., Miller, T.M., Slusher, R.E. & Phillips, J.M. *Journal of Applied Physics* **80**, 6954 (1996).
25. Gruner, J., Cacialli, F. & Friend, R.H. *Journal of Applied Physics* **80**, 207 (1996).
26. Bulovic, V., Kozlov, V.G., Khalfin, V.B. & Forrest, S.R. *Science* **279**, 553 (1998).
27. Schön, J.H., Kloc, C., Dodabalapur, A. & Batlogg, B. *Science* **289**, 599 (2000).
28. Born, M. & Wolf, E. *Principles in Optics* (Pergamon, Oxford, 1986).
29. Fletcher, R.B., Lidzey, D.G., Bradley, D.D.C., Bernius, M. & Walker, S. *Applied Physics Letters* **77**, 1262 (2000).
30. Becker, H., Burns, S.E., Tessler, N. & Friend, R.H. *Journal of Applied Physics* **81**, 2825 (1997).
31. Virgili, T., Lidzey, D.G., Bradley, D.D.C., Cerullo, G., Stagira, S. & De Silvestri, S. *Applied Physics Letters* **74**, 2767 (1999).
32. Long, X., Grell, M., Malinowski, A., Bradley, D.D.C., Inbasekaran, M. & Woo, E.P. *Optical Materials* **9**, 70 (1998).

CHAPTER 8

ENERGY TRANSFER FROM BLUE TO GREEN IN BENZOTHIADIAZOLE-DOPED POLYFLUORENE BASED LIGHT-EMITTING DIODES

8.1 Introduction

Development of full-color flat-panel displays using electroluminescent organic and polymeric materials has been intensively pursued in recent years because of the potential advantages of low cost fabrication, better contrast/viewing angle and flexibility compared to their liquid crystal and inorganic counterparts. For the realization of multicolor displays, bright, efficient and low operating voltage red, green and blue (RGB) light-emitting pixels will be necessary. One of the most attractive methods, with respect to the ease of production, for fabricating green and red LEDs is the internal colour conversion technique¹ which aims to efficiently convert blue emission internally into green or red emission by blending blue-light-emitting polymers with green or red dyes and light-emitting polymers. This technique requires good spectral overlap between the emission spectrum of the host and the absorption spectrum of the guest and is mainly based on internal excitation (Förster type) energy transfer and charge transfer from the host to the guest, so that a down conversion of the emission

color towards lower energies is achieved although different processes such as charge trapping or Dexter transfer can also be involved in device operation. This technique based on blue LEDs allows the realisation of all visible emission colours by using appropriate materials with high PL efficiency and good charge transport properties.

Electroluminescence color tuning by dye doping² and efficient blue³, green⁴⁻⁵, yellow⁶, orange⁷⁻¹¹, and red¹²⁻²⁰ LEDs have been demonstrated and reported in the literature by applying this technique. Shaheen *et. al.*⁴ demonstrated efficient green emission peaking at 533 nm from quinacridone doped 8-hydroxyquinoline aluminum (Alq₃) LEDs and shown that in addition to Förster energy transfer that occurs both under photoexcitation and electrical excitation, charge transfer from the host to the dopant also occurs during electrical operation. List *et. al.*⁶ have demonstrated efficient yellow PLEDs based on a blend of a blue-emitting ladder type poly (p-phenylene) (m-LPPP) and an orange-emitting poly(decylthiophene) (PDT) that exhibit quantum efficiencies of up to 4.2%. Bulovic *et. al.*⁸ demonstrated orange OLEDs exhibiting brightness of 15200 cd/m² by doping Alq₃ with the laser dye DCM2, with the emission color dependent on the concentration of DCM2 in the blend. Jin *et. al.*¹¹ also demonstrated orange LEDs peaking at 550 nm with an external efficiency of 2% by doping rubrene into Alq₃ and attributed the high efficiency achieved to a combination of energy transfer from the host to the dopant and direct carrier trapping and recombination on the dopant followed by fluorescence emission from rubrene. Regarding red LEDs, McGehee *et. al.*¹² demonstrated pure red-emission OLEDs by blending Eu complexes into poly[2-(6'-cyano-6'-methyl-heptyloxy)-1,4-phenylene] (CN-PPP). The EL spectrum peaked at 630 nm with a very narrow spectral linewidth of 3.5 nm and a maximum efficiency of 1.1%. Virgili *et. al.*¹³ demonstrated efficient red LEDs by doping the red fluorescent dye tetraphenylporphyrin (TPP) into the blue-emitting poly (9,9-dioctylfluorene) (PFO). These devices showed a main emission peak at 653 nm and reached a luminance of 90 cd/m² and an external efficiency of 0.9%. Shoustikov *et. al.*¹⁶ also demonstrated saturated red LEDs by

doping TPP into Alq₃ with predominant red emission even observed at very low doping levels as expected from the large Förster radius of 3.3 nm on this system. Red LEDs peaking at 660 nm with FWHM of 20 nm were also demonstrated by Sakakibara *et. al.*²⁰ by doping a reduced porphyrin compound, namely tetraphenylchlorin, into Alq₃.

In this chapter we follow this approach to demonstrate EL devices based on a blend of a blue-emitting poly (9,9-dioctylfluorene) copolymer with 1,4-phenylene, namely F8P, and a green-emitting poly (9,9-dioctylfluorene) copolymer with benzothiadiazole, namely BT. Optical spectroscopy such as absorption, photoluminescence, PL quantum efficiency and time resolved PL measurements will be presented in detail. Single layer LEDs based on this blend with a PEDOT/PSS hole injection buffer layer were also fabricated and exhibited bright and efficient green emission from BT peaking at 535 nm for BT concentrations as low as 0.5% as a result of almost complete excitation energy transfer from F8P to BT. Optimised devices (in terms of BT guest concentration and emissive layer thickness) showed a maximum EL quantum efficiency of 7 cd/A and a maximum brightness of 15000 cd/m².

8.2 Experimental details

F8P was supplied by the Dow Chemical Company. It is a high molecular weight alternating copolymer of poly (9,9-dioctylfluorene) (PFO) with 1,4-phenylene (named F8P) and was prepared via a Suzuki coupling reaction with Pd-catalysed polymerization.²¹ It is soluble in conventional organic solvents such as aromatic hydrocarbons, tetrahydrofuran and chlorinated hydrocarbons. Its chemical structure is shown in Figure 8.1 below.

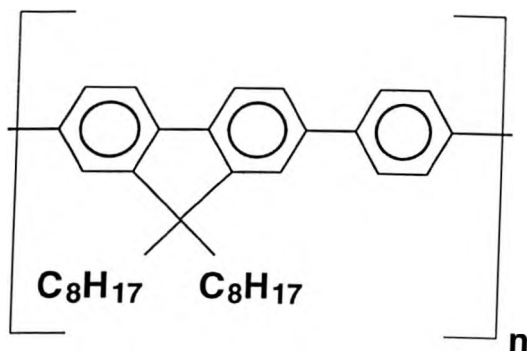


Figure 8:1 Chemical structure of F8P.

F8P was dissolved in toluene at a concentration of 20 mg/ml and used as a host in a host-guest system with BT as a guest. BT was added at concentrations (by weight) varying from 0.5% to 50%. Films of the F8P:BT blends were prepared by spin-coating the solutions onto quartz substrates suitable for absorption and photoluminescence measurements. Films of BT and F8P were also prepared as control samples for optical measurements. The 354 nm line of a HeCd laser was used to excite the samples. The samples were mounted inside an integrating sphere for PL quantum efficiency measurements. Single layer LEDs were prepared by first spin-coating a 45 nm layer of PEDOT/PSS onto ITO-coated glass substrates. On top of this layer, which was baked at 130 °C for 15 min in air, a solution of F8P having different BT concentrations was spin-coated, forming different thickness layers depending on the spin speed. A calcium cathode was then deposited onto the polymer films by thermal evaporation. All device testing was made in a nitrogen-filled glove box. All device processing steps were made in a clean room.

8.3 Optical spectroscopy of individual components and blends

Figure 8.2 compares the absorption spectra of F8P and BT and the photoluminescence spectra of F8P and BT while Figure 8.3 shows the absorption spectra of a series of F8P:BT blends with varying BT concentration.

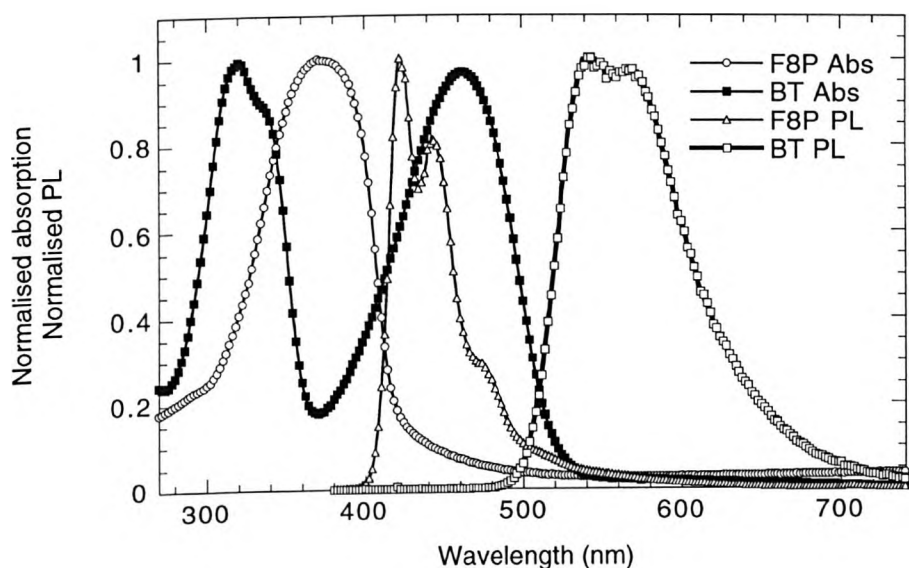


Figure 8.2: Absorption of F8P (open circles), photoluminescence of F8P (open triangles), absorption of BT (filled squares) and photoluminescence of BT (open squares).

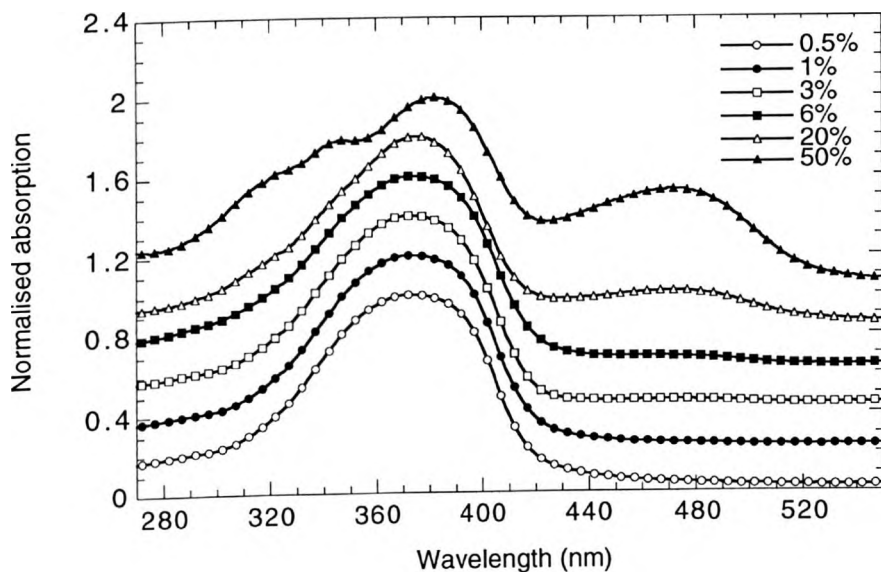


Figure 8.3: Absorption spectra of F8P:BT blends with varying BT concentration [0.5% (open circles), 1% (filled circles), 3% (open squares), 6% (filled squares), 20% (open triangles) and 50% (filled triangles)].

The absorption spectrum of F8P is broad and featureless while its photoluminescence spectrum shows well-defined vibronic features. The absorption maximum occurs at around 370 nm while the absorption onset occurs at approximately 420 nm. The FWHM is approximately 80 nm. The absorption maximum occurs at a shorter wavelength than that of PFO (which occurs at 385 nm). This can be explained by a difference in steric hindrance effects.²¹ The steric repulsion is more severe in F8P because of the proximity of the phenylene *peri*-hydrogen to the C-1 hydrogen of fluorene. This results in an increased torsional angle between fluorene and phenylene units and consequently in a blue-shifted absorption spectrum. The PL spectrum with a FWHM of 38 nm exhibits a main peak at 420 nm (corresponding to the 0-0 transition) and vibronic structure with a weaker peak at 440 nm (0-1 transition) and a shoulder at around 475 nm. The absorption spectrum of BT shows two broad featureless absorption bands of similar oscillator strength, one in the UV with a maximum at 320 nm and one in the visible part of the spectrum with a maximum at around 465 nm. The PL spectrum of BT with a FWHM of 80 nm shows emission in the green region with maxima at around 540 and 570 nm. F8P is thus a wide band gap blue material whose emission spectrum shows a very significant overlap with the absorption spectrum of BT and therefore excitation energy transfer (via a Förster mechanism) from the host (F8P) to the guest (BT) can be expected to take place. The absorption spectra of the F8P:BT blends are dominated by the absorption of F8P at low BT concentrations with an increasing contribution from the BT absorption band at around 465 nm as the concentration of BT increases in the blend. A linear superposition of the absorption spectra of the individual components results in the observed absorption spectra of the blends for all guest concentrations. At very high BT concentrations (~50%), both a small red shift of the absorption maximum by 10 nm and a broadening of the spectrum is observed which may indicate that some degree of phase segregation between F8P and BT occurs. Figure 8.4 and 8.5, respectively show the photoluminescence spectra and PL quantum efficiency measurements of a series of F8P/BT blends as a function of the BT concentration.

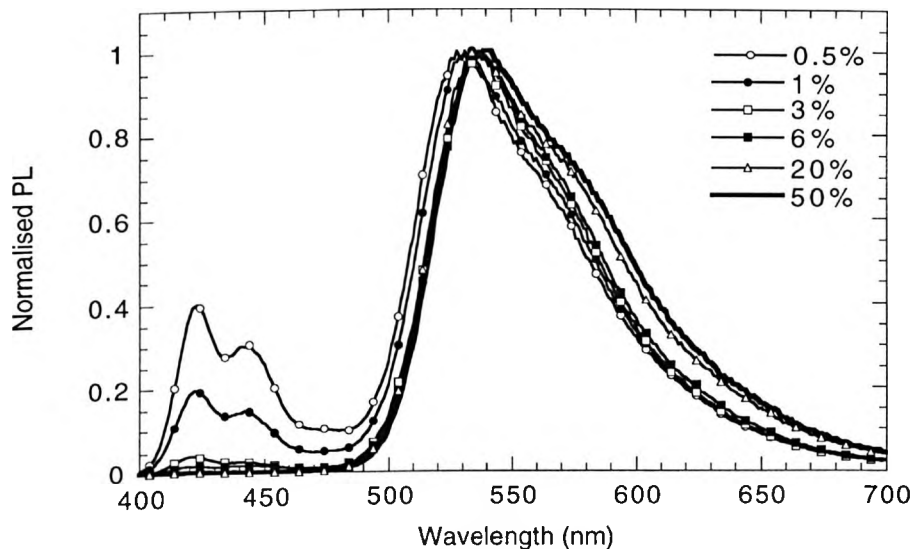


Figure 8.4: Photoluminescence spectra of F8P:BT blends with varying BT concentration.

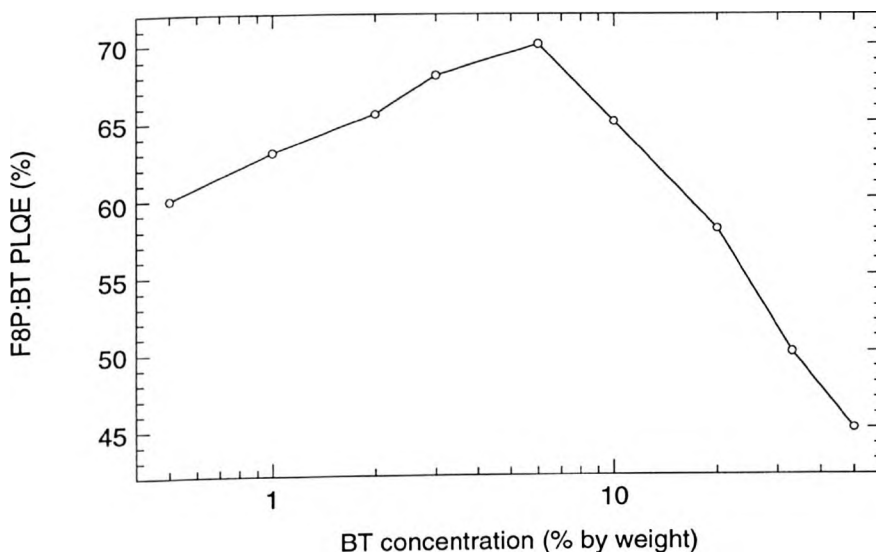


Figure 8.5: PL quantum efficiency measurements of F8P:BT blends as a function of BT concentration.

The F8P:BT films were excited at 354 nm where there is significant absorption from F8P to create a population of excited F8P states while direct absorption by BT is very small. The resulting PL spectra of the blends are a non-linear superposition of direct emission from

excited F8P states (420 nm peak) as well as luminescence from BT states (532 nm) that are excited via a Förster energy transfer mechanism. The measurement of the PL spectra of the blends provides a probe of the Förster transfer from F8P to BT under photoexcitation. By increasing the content of BT in the blend, the spectral contribution from F8P is decreased in the total spectrum. Although at 0.5-wt. % BT, emission from BT excited chains is already dominant in the blend emission, only for higher than 6-wt. % BT no F8P emission is observed. A small monotonic red shift of the emission spectrum of the blends is observed with increasing BT concentration; the peak at 532 nm for 0.5% BT is shifted by 8 nm to 540 nm for 50% BT. This redshift is probably associated with more BT sites becoming available for Förster transfer as the BT concentration increases. As we do not observe a strong contribution of BT to the absorption of the blends except for high BT concentrations, we suggest that at least for low BT concentrations, a process where photons emitted by F8P are reabsorbed from BT and therefore contribute to the emission stemming from BT plays a negligible role. However, over 20-wt.% BT, there is absorption stemming from segregated BT chains in the F8P host which indicates that the photon reabsorption process by BT may also account for the small redshift of the emission maxima in the blend. Exciton diffusion from F8P to BT chain segments is also energetically favourable and also accounts for the energy transfer. Exciton transfer is also evident by the PL efficiency measurements of the blends. F8P has a PLQE of around 55%. The efficiency of the blends initially increases as more BT chains become available for energy transfer and the efficiency of the transfer also quickly increases as a result of the reduced mean distance between host and guest molecules. The efficiency increases to 60, 65 and 70% for 0.2, 2 and 6-wt. % BT, respectively. It reaches a peak value of 70% at a doping level of 6-wt. %. At higher concentrations, it decreases significantly. It is reduced from 65% for 10-wt. % BT to 45% for 50-wt. % BT (BT has a PLQE of around 40%). This efficiency decrease is due to the combined effect of the aggregation-induced quenching of the BT chains and the reduced concentration of F8P chains that are available for excitation and transfer to BT with increasing BT concentration.

Figure 8.6 shows time resolved PL measurements of the F8P emission in F8P/BT blends while Figure 8.7 shows the extracted PL lifetimes of F8P as a function of BT concentration.

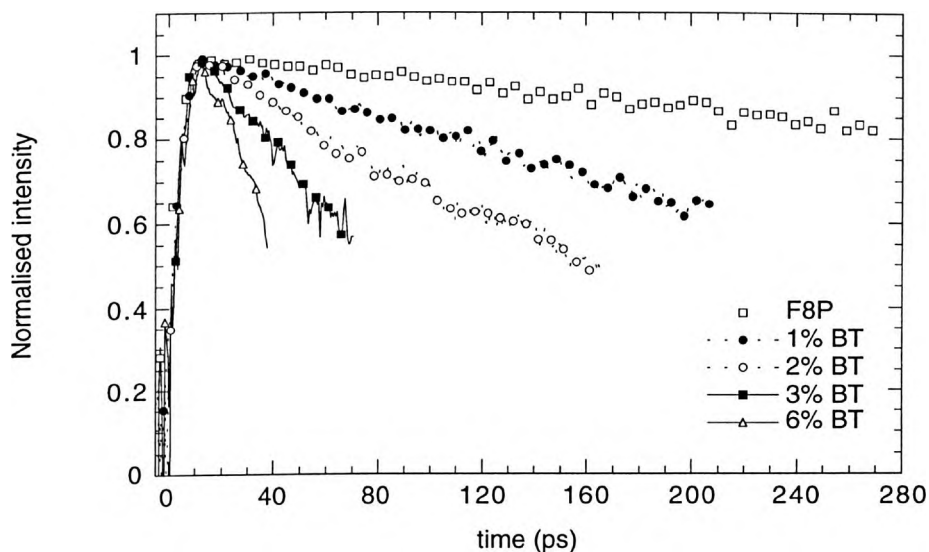


Figure 8.6: Fluorescence decay curves of F8P emission in F8P:BT blends for varying BT concentration.

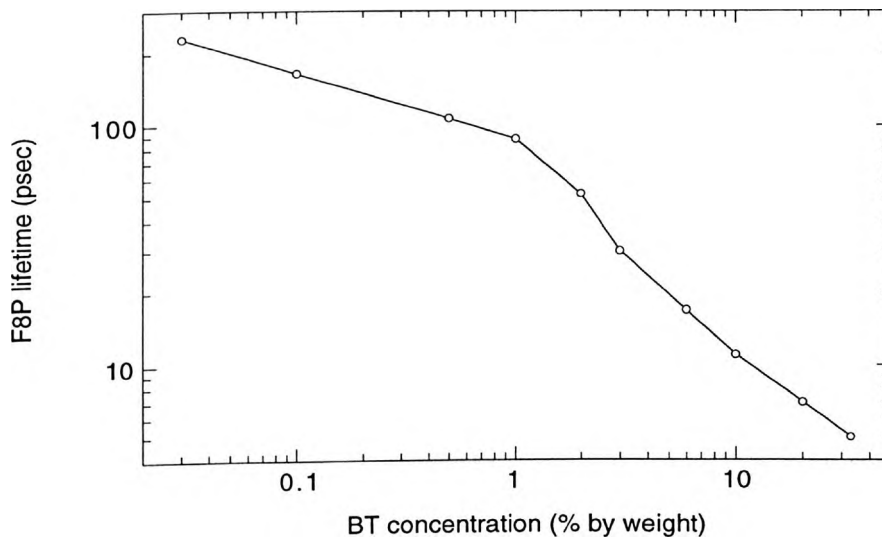


Figure 8.7: PL emission lifetime of F8P in F8P:BT blends as a function of BT concentration.

Time resolved PL measurements, performed at low excitation densities on F8P and F8P:BT blends, record the fluorescence decay of F8P emission. F8P has a photoluminescence lifetime of around 300 ps that can be accurately fitted with a single component exponential decay. The fluorescence decay curves from the high concentration samples (BT fraction $\geq 6\%$) could be accurately fitted with a single component exponential decay while the low concentration samples (BT fraction $< 6\%$) needed a double exponential component. By taking into account the relative weighting of each component in the double exponential fit, we deduced the average values of the F8P lifetime for each BT concentration. The F8P lifetime decreases from 230 ps for 0.03-wt. % BT to 107, 52 and 17 ps for 0.5-wt. %, 2-wt. % and 6-wt. % BT, respectively. For high BT concentrations (BT fraction $> 20\%$), the lifetime reached the resolution limit of the measurement which was approximately 5 ps. Hence for BT concentrations above 33% it was not possible to obtain lifetime measurements as the lifetime was then lower than the resolution of the experimental set-up. From the above graphs, it can be seen that with increasing concentrations of BT the lifetime of the F8P PL emission decreases. This provides clear evidence that the energy transfer becomes considerably more efficient as the concentration of BT increases. Also the monotonic increase of the relative contribution of the shorter lifetime component of F8P emission in the biexponential decay further suggests that the efficiency of energy transfer increases significantly with increasing BT concentration.

In pure F8P, the PL emission occurs from the lowest energy excited chain segments (longest conjugation length segments) subsequent to migration of the singlet excitons within the distribution of effective conjugation lengths. In the blend, excitation energy (exciton) transfer to a BT chain will stop the migration process within the F8P host. However as the BT concentration increases and the mean distance between donor and acceptor molecules decreases, the excitation will have to travel a smaller distance within F8P adjacent chains before it is transferred onto the nearest BT chain. The decrease of the relative contribution of

the longer lifetime component of F8P emission in the double exponential decay is a direct result of this process which results in an increase of the energy transfer rate with increasing BT concentration. The double exponential decay seen for low BT concentrations can then be associated with two different processes. The shorter lifetime is associated with direct energy transfer from F8P sites to BT chains via a Förster type mechanism. The longer lifetime can be associated with a two-step process. First, excitation energy migration (interchain or intrachain) on the F8P chain segments that are further away from the BT chain segments followed by a Förster type singlet exciton transfer onto the nearest BT chains and emission from the BT excited chains. The single lifetime seen for higher BT concentrations probably corresponds to a very fast and efficient direct energy transfer from F8P to BT with optical excitations of F8P chain segments created within a nearest neighbour distance of BT chains. Also the fact that the exciton transfer rate from F8P to BT is much faster than the combined radiative/non-radiative decay rate of F8P enables for efficient energy transfer as the exciton on the host will transfer to the guest before it decays.

List *et. al.*²³ have similarly proposed the excitation energy migration process in a polymer-macromolecule system to account for the experimentally attained temperature and concentration dependence of the steady state PL as a two-step process that involves initially a thermally activated migration within the host followed by transfer from the host to the guest. Förster energy transfer alone could not account for the observed behaviour. Buckley *et. al.*²² studied a polymer-polymer blend system with PFO as a host and BT as a guest that bears many similarities to the one we have studied here with the only difference that another host (F8P) is used. They found that at high BT concentrations (BT fraction > 0.5%), two distinct lifetimes describe the energy transfer process. A short 12 ps lifetime associated with Förster-type transfer between nearest neighbour sites from excited PFO chain segments to BT chains and a longer 35 ps lifetime associated with excitation energy migration in the host (occurring within ~ 20ps) followed by Förster-type energy transfer. The distinct differences found

between the PFO:BT and the F8P:BT systems for different BT concentrations are difficult to interpret as both F8P and PFO have similar PL spectra that show a large overlap with the BT absorption and also have similar PL emission lifetimes. Different molecular packing of the PFO and F8P chain segments relative to the BT chains in the blend films can influence the energy transfer processes and may play a significant role in determining which transfer mechanism will dominate the emission behaviour of the blends.

In Figure 8.8 the transfer rate from F8P to BT as a function of BT concentration is shown.

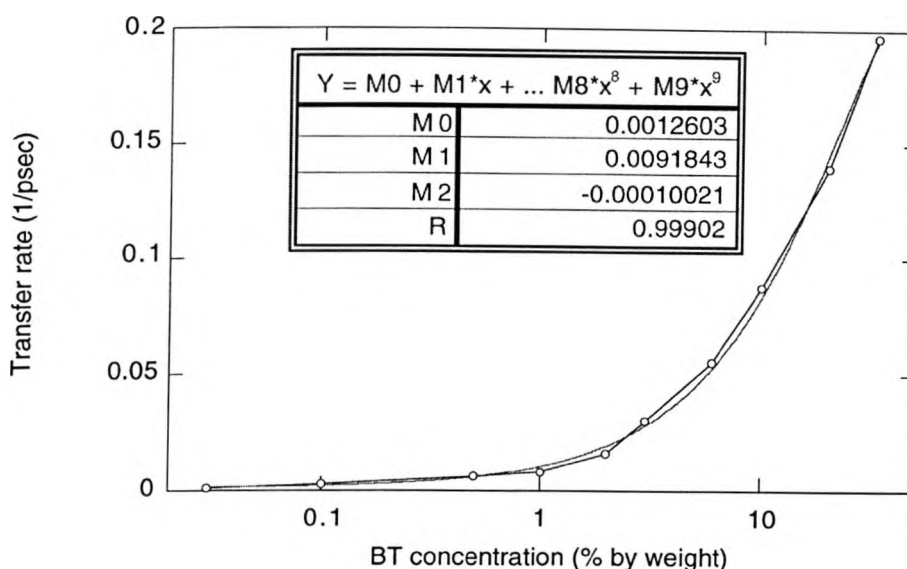


Figure 8.8: Transfer rate from F8P to BT in F8P:BT blends as a function of BT concentration.

The energy transfer rate K_{ET} , which is given by subtracting the decay rate of the pure host ($1/\tau_0$ where $\tau_0=300$ ps) from the total decay rate of the host in the blend, as a function of BT concentration c is accurately fitted with a second order polynomial function for all concentrations with $K_{ET} \propto xc+yc^2$ ($x \sim 90y$). If we consider that the energy transfer rate in its simplest form, for Förster-type transfer and a hard-sphere model ($c \propto R^{-3}$), is given by: K_{ET}

$= (1/\tau_0)(R_0/R)^6$, then we conclude that the Förster rate equation can not adequately describe the energy transfer rate dependence on concentration and thus an estimation of the Förster radius in this system cannot be made. Similar conclusions were drawn for the PFO:BT system presumably due to the inadequacy of the hard-sphere model to accurately describe a polymer-polymer blend as well as the lack of consideration of excitation energy migration.²²

Table 1 below summarizes the data from PLQE and time resolved PL measurements.

BT concentration (%)	PLQE of F8P:BT blends (%)	F8P lifetime (ps) (fast component)	F8P lifetime (ps) (slow component)	Relative weighting of fast (%)	Relative weighting of slow (%)
0.03	51	205	260	55	45
0.1	55	147	190	65	35
0.5	60	100	125	70	30
1	63	81	107	75	25
2	65	48	64	80	20
3	68	28	40	85	15
6	70	17	26	95	5
10	65	11	-	100	-
20	58	7	-	100	-
33	50	~5	-	100	-
50	45	<5	-	100	-

Table 1: Summary of data from PLQE and time resolved PL measurements on F8P:BT blends.

8.4 Electrical characteristics of LEDs made from F8P:BT blends

The EL spectra of F8P:BT blends with varying BT concentration are shown in Figure 8.9.

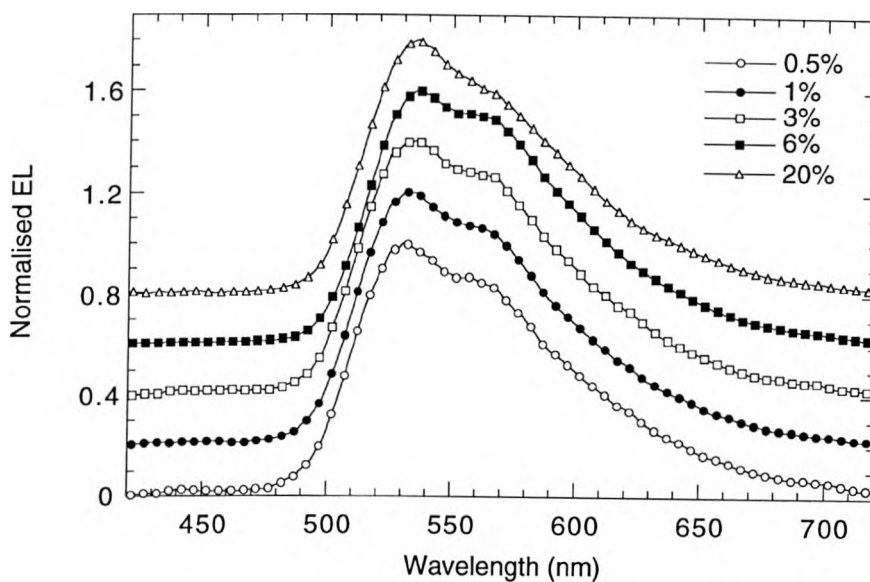


Figure 8.9: Electroluminescence spectra of F8P:BT blends with varying BT concentration.

Unlike the PL spectra of the F8P:BT blends where a 6-wt. % BT concentration is required to completely quench blue emission from F8P, the EL spectra show predominant green emission originating from excited states on BT chain segments for a BT concentration as low as 0.5-wt. %. The EL spectra thus show pure green emission at very low BT concentrations and the transition of spectral shapes occurs more rapidly as a function of concentration for the case of EL than for PL. The different concentration dependence observed in PL and EL suggests that additional mechanisms for emission occur under electrical operation. As in the PL, excited-state BT chain segments can be formed via Förster energy transfer from excited F8P sites. In addition, the charge-carrier trapping mechanism can be expected to occur. Excited BT states will then be formed by sequential charge trapping of a hole charge on BT (after transfer of the hole charge from F8P to BT) followed by trapping of an electron charge on BT. These processes are likely to occur only if they are energetically allowed. This is

defined by the relative positions of the HOMO and LUMO energy levels of the individual components and their energetic difference. The HOMO and LUMO levels of BT are at 5.9 and 3.5 eV, respectively while the respective levels of F8P are at 5.9 and 2.8 eV. Therefore the HOMO/LUMO levels of the guest are well within the respective levels of the host and are expected to retain their original energies in the blend. As the LUMO level of F8P is 0.7 eV higher than that of BT, electrons are expected to be injected from the cathode to the lowest energy BT sites and thus electron transport will predominantly occur on the BT chains. Also as the HOMOs of the two components are at similar energy levels, holes are expected to be injected from the anode to the lowest energy F8P sites (as they are available in a much higher population than the corresponding BT levels) and hole transport will then occur between F8P and BT HOMO levels through interchain hopping. The average hopping distance will be controlled by the concentration of BT. As the BT concentration increases, the average hopping distance for electrons will be shorter while that for holes will be longer if hole transport occurred predominantly on the F8P chains. However, also the distance between BT and F8P molecules will become shorter and the holes can then be shared between the F8P host and the BT guest. At higher BT concentrations, the hole transport will be dominated by hopping via the BT sites. Therefore, electron-hole recombination on BT molecules maximised by the role of BT acting as an electron trap as well as a hole hopping site is proposed to be the dominant emission mechanism and is mainly responsible for the enhancement of the EL emission. In conclusion, if the energy transfer from F8P to BT was the sole emission mechanism, a similar concentration dependence in both PL and EL should be expected. The significantly enhanced contribution from BT emission to the EL compared to the PL for a given concentration implies that BT chains selectively trap charge carriers leading to EL emission from these sites. Figures 8.10 and 8.11 compare current density and luminance vs. field characteristics of ITO/PEDOT(45nm)/F8P:BT(~150nm)/Ca LEDs with varying BT concentration and a blend layer thickness of around 150 nm while Figure 8.12 shows the EL quantum efficiency vs. field characteristics for the same series of LEDs.

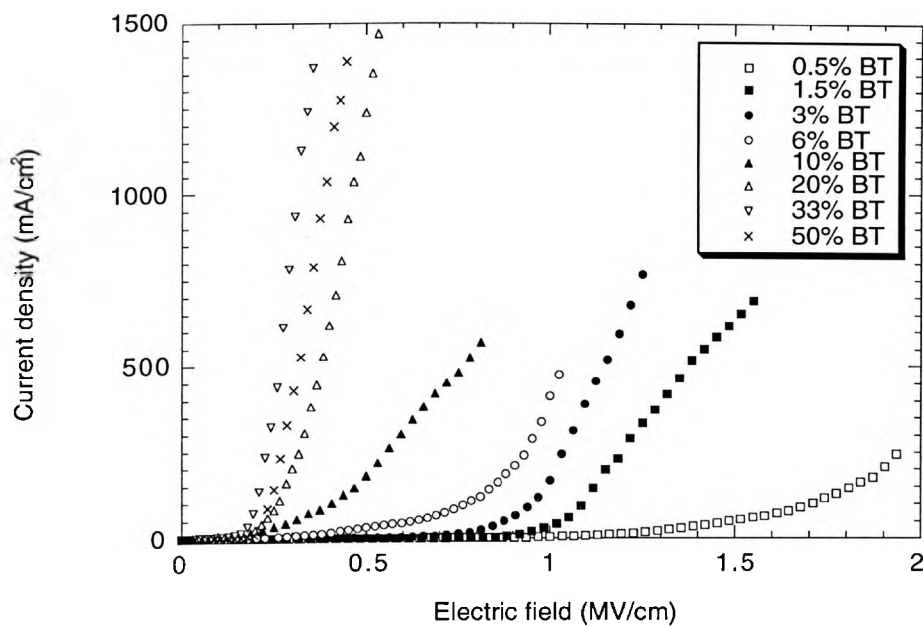


Figure 8.10: Current density versus electric field characteristics of ITO/PEDOT(45nm)/F8P:BT(~150nm)/Ca LEDs with varying BT concentration.

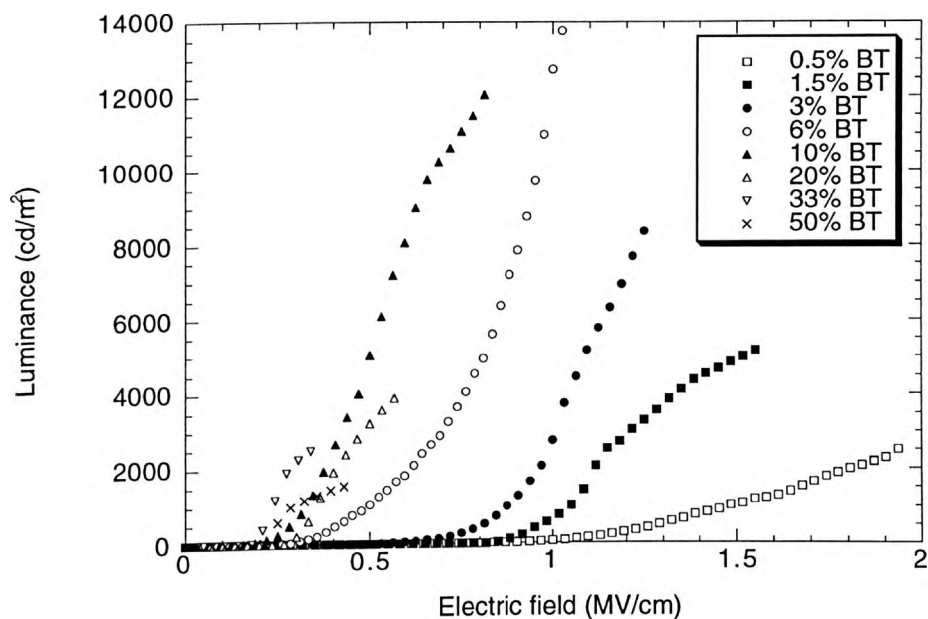


Figure 8.11: Luminance vs. electric field characteristics for the same series of LEDs.

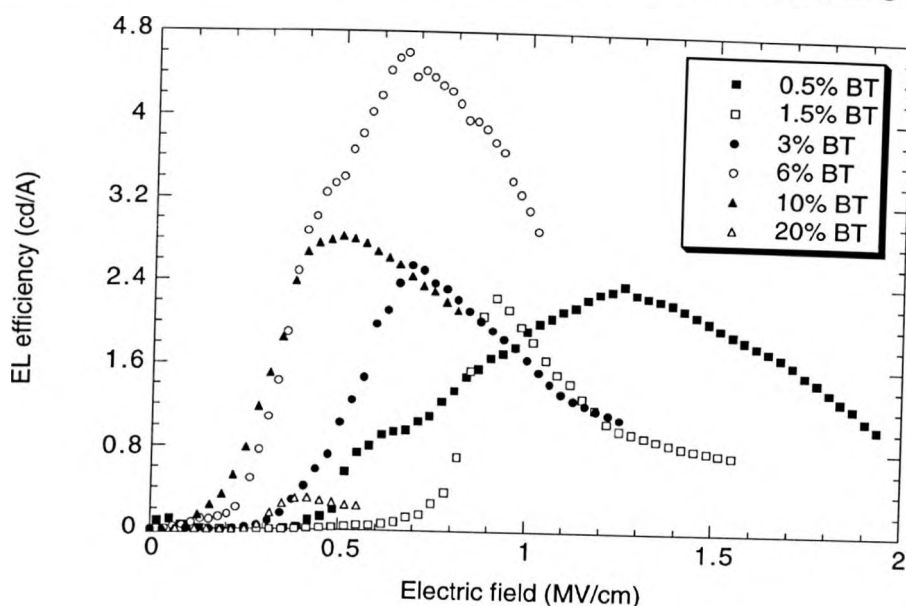


Figure 8.12: EL quantum efficiency vs. electric field characteristics for the same series of LEDs.

In these LEDs, PEDOT acts to improve the hole injection in the bulk of the blends which otherwise would be very difficult due to the high injection barrier height for holes from ITO (~ 4.7 eV) to the HOMOs of either F8P or BT (~ 5.9 eV). It can be noticed that the current density is increased very significantly with increasing BT concentration as a result of the improved electron conduction through the higher population of BT sites. Electrons are expected to be the majority carriers due to the lower injection barrier height for electrons from the Ca cathode to the LUMO of BT (~ 0.6 eV) compared to the 0.8 eV barrier height for holes from the ITO/PEDOT anode to the HOMOs of BT or F8P. However the current density is slightly decreased at high doping concentrations ($> 20\%$) which may be due to phase segregation effects. The brightness also increases with increasing BT concentration until 6wt. % BT and then dramatically decreases due to luminescence quenching as the BT doping level is further increased. The same trend is also observed for the quantum efficiency that reaches its maximum value at the optimal doping level of 6-wt. % indicating that the charge balance factor and the recombination efficiency is optimum at this concentration. This also implies that at higher BT concentrations the percolation threshold for current conduction is reached

and the dopant molecules are very likely to have then formed a continuous conduction channel for electrons that travel through the device and discharge at the anode without recombination thus reducing the efficiency. The efficiency also increases at first then flats out and gradually drops with increasing luminance while the reduction of the PL efficiency above 6-wt. % BT also contributes to the reduction of EL efficiency. A BT concentration of 6-wt. % appears to be the optimum concentration for efficient recombination. At this concentration, the device turns on at 6.5 V (for a luminance of 100 cd/m²), sustains a current density of 475 mA/cm² and reaches a peak brightness of 13750 cd/m² at 20 V. The maximum EL quantum and power efficiencies are 4.65 cd/A (1.4 %) and 1.1 lm/W, respectively. It should be noted that both the brightness and the EL efficiency decrease more rapidly for increasing BT concentration than the PL efficiency although a similar level of doping appears as optimum for both EL and PL. Table 2 summarizes the performance of these LEDs.

% of BT in F8P host	Turn-on voltage (V) (100 cd/m ²)*	Max L (cd/m ²)	Max J (mA/cm ²)	Voltage at max L (V)	Max EL efficiency (cd/A)	Max power efficiency (lm/W)	L at max efficiency (cd/m ²)
0.5	16	2620	265	30.5	2.4	0.4	425
1.5	13	5150	690	23.5	2.25	0.5	230
3	10.5	8350	765	21	2.6	0.75	130
6	6.5	13750	475	20	4.65	1.1	2585
10	4.5	12225	580	14	2.85	1.3	5065
20	4	3950	1650	8.5	0.4	0.2	1930
33	3	2570	1370	6.5	0.35	0.3	1175
50	3	1590	1385	6	0.4	0.35	600

Table 2: Performance of ITO/PEDOT(45nm)/F8P:BT(~150nm)/Ca LEDs with varying BT concentration.

Chapter 8: Energy transfer from blue to green in benzothiadiazole-doped polyfluorene based light-emitting diodes

Figures 8.13, 8.14 and 8.15 compare current density, luminance and EL efficiency versus voltage characteristics of ITO/PEDOT/F8P:BT(6%)/Ca LEDs with varying blend thickness.

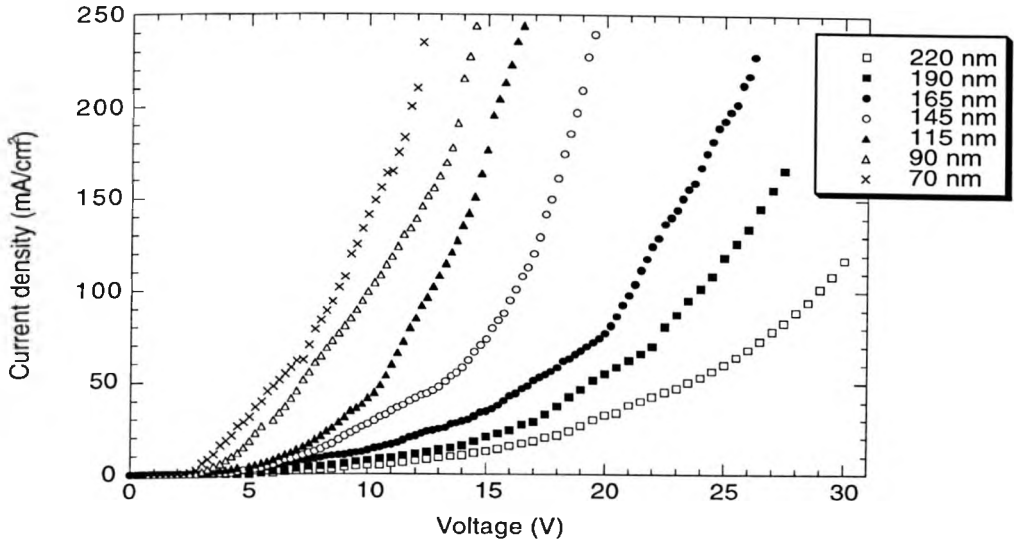


Figure 8.13: Current density vs. voltage of ITO/PEDOT(45nm)/F8P:BT(6%)(varying thickness)/Ca LEDs.

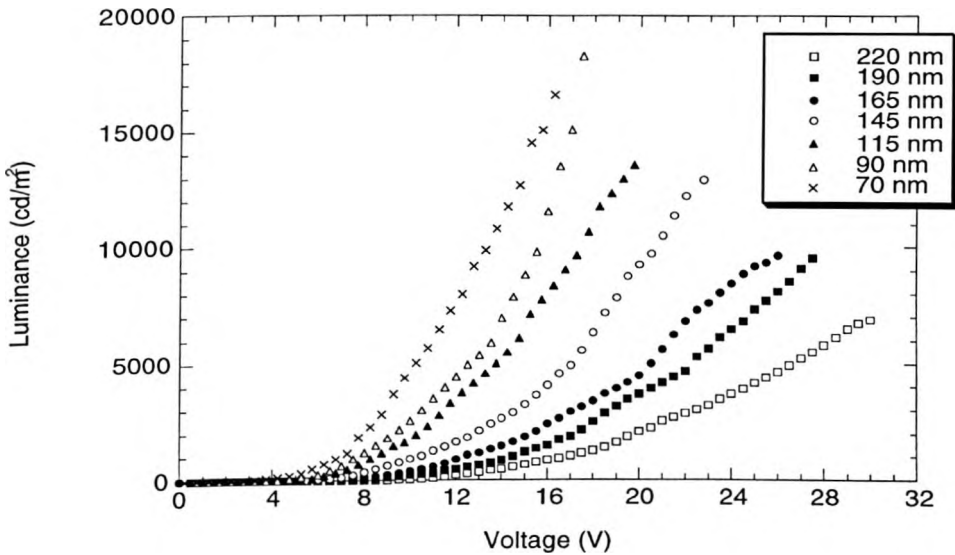


Figure 8.14: Luminance vs. voltage characteristics of the same series of LEDs.

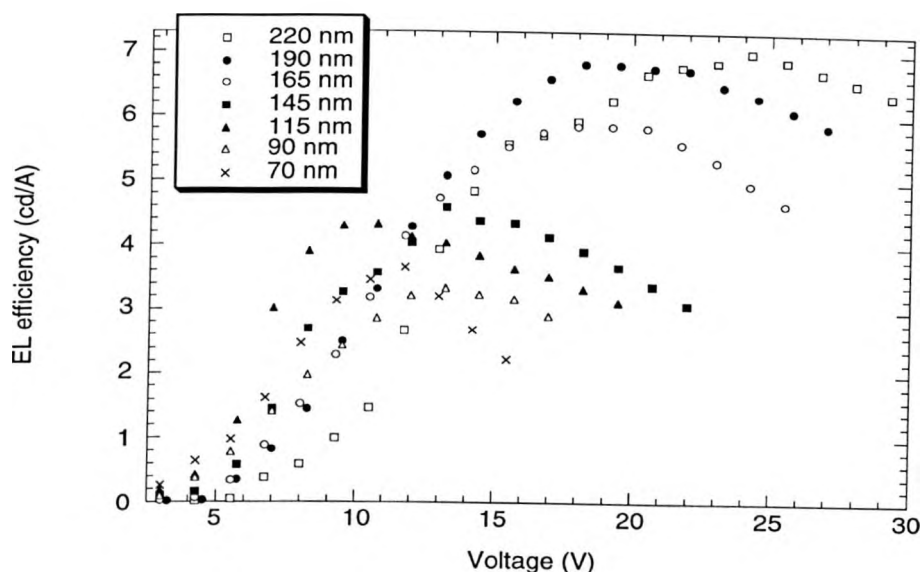


Figure 8.15: EL quantum efficiency vs. voltage characteristics of the same series of LEDs.

A strong variation of the device current density, luminance and efficiency was observed with varying blend emissive layer thickness. The device current was monotonically increased with decreasing device thickness as a result of the space (electron) charge limited conduction from Ca ($J \sim d^{-3}$). The device brightness also increased from 6900 cd/m^2 for a 220 nm thick emissive layer to 19000 cd/m^2 for a 90 nm thick layer. This is a direct result of the increased charge carrier recombination probability that increases the exciton formation rate as the device thickness decreases. However, further reduction of the device thickness resulted in a decrease of the brightness as a result of both the increased luminescence quenching due to the proximity of the recombination/emission zone closer to the cathode and the increased amount of electrons that travels in the bulk of the device with a low recombination probability before discharging at the anode. In contrast, a continuous increase of the device efficiency was observed with increasing thickness. A 220 nm thick emissive layer is needed to achieve the highest EL efficiency of 7 cd/A while a 90 nm thick layer shows a maximum efficiency of 3.35 cd/A , a factor of 2 lower than the maximum efficiency. This is attributed to the increase

of the charge balance factor and the recombination probability with increasing thickness. Therefore, a trade off appears to exist between achieving the highest quantum efficiency and reaching the highest brightness. Thicker devices show higher quantum efficiencies while thinner devices reach higher brightnesses.

Finally, in an effort to improve the device performance further, we attempted the incorporation of 20-wt. % BFB as a hole transport material (more details about this polymer are given in Chapter 5) in a F8P:BT blend with 6-wt. % BT concentration. An enhancement of the device performance was indeed found to occur. An LED with a 90 nm thick emissive layer exhibited a maximum brightness of 30000 cd/m^2 , an increase by a factor of 1.6 compared to an identical LED without BFB. It also showed a very low turn-on voltage of 2.8 V relative to a turn-on of 4 V without BFB. However, these improvements were also at the expense of a reduced quantum efficiency. The maximum EL efficiency was 2.2 cd/A compared to 3.35 cd/A without BFB. The lower operating voltage is attributed to the lower injection barrier height for holes from the ITO/PEDOT anode to the HOMO level of BFB ($\sim 5.26 \text{ eV}$) that facilitates hole injection in the bulk. The higher luminance is due to the increased charge carrier (hole) density in the bulk which increases the exciton recombination probability while the lower EL efficiency is presumably due to the reduced charge balance factor associated with the increased amount of holes present in the device. It should be emphasized that the concentration of the dopant hole transport material in the F8P:BT(6%) blend host is not optimized and therefore a further improvement of the device performance can be expected.

Finally, Table 3 gives a summary of the data related to the performance of the blend LEDs with varying blend emission layer thickness.

Thickness of F8P:(6%)BT (nm)	Turn-on voltage (V) (100 cd/m ²)*	Max L (cd/m ²)	Max J (mA/cm ²)	Voltage at max L (V)	Max EL efficiency (cd/A)	Max power efficiency (lm/W)	L at max efficiency (cd/m ²)
220	11	6900	120	30	7	1.15	3700
190	9	9550	170	27.5	6.85	1.25	3100
165	7.5	9750	230	26	5.85	1.15	3700
145	6.5	13000	450	23	4.65	1.05	2550
115	6	13800	465	20	4.35	1.5	1950
90	5	19000	680	18	3.35	0.85	5100
70	4	17000	850	16.5	3.8	1.1	6500

Table 3: Performance of ITO/PEDOT(45nm)/F8P:BT(6%)/Ca LEDs with varying F8P:BT(6%) thickness.

8.5 Conclusions

This chapter is concerned with energy transfer in a host-guest system where the host is a blue-emitting copolymer of poly (9,9-dioctylfluorene) with 1,4-phenylene, F8P, and the guest is poly (9,9-dioctylfluorene-co-benzothiadiazole), BT. A combined study of absorption, PL, PL efficiency and time resolved PL measurements for varying BT concentration blends showed that the large overlap of the PL spectrum of F8P with the absorption spectrum of BT guest gives rise to an efficient energy transfer from F8P to BT via a Förster-type mechanism which dominates the emission under photoexcitation. Single layer LEDs based on the F8P:BT blend with PEDOT/PSS exhibited bright and efficient green EL emission from BT peaking at 535 nm for BT concentrations as low as 0.5%. This was considered to be the result of the almost complete energy transfer from F8P to BT and the

charge trapping that is followed by recombination on BT. The latter was found to play a significant role under electrical operation and contribute to the enhancement of the device performance. Optimized devices reached a brightness of $15,000 \text{ cd/m}^2$ and an efficiency of 7 cd/A while the incorporation of a BFB HTL in an optimized F8P:BT (6%) LED increased the maximum brightness by a factor of 1.6 and reduced the turn-on voltage to below 3V.

References

1. Tasch, S., List, E.J.W., Hochfilzer, C., Leising, G., Schlichting, P., Rohr, U., Geerts, Y., Scherf, U. & Mullen, K. *Physical Review B* **56**, 4479 (1997).
2. Shoustikov, A., You, Y. & Thompson, M.E. *IEEE Journal of Selected Topics in Quantum Electronics* **4**, 3 (1998).
3. Tao, Y.T., Balasubramaniam, Danel, A. & Tomasik, P. *Applied Physics Letters* **77**, 933 (2000).
4. Shaheen, S.E., Kippelen, B., Peyghambarian, N., Wang, J.-F., Anderson, J.D., Mash, E.A., Lee, P.A., Armstrong, N.R. & Kawabe, Y. *Journal of Applied Physics* **85**, 11 (1999).
5. Tao, Y.T., Balasubramaniam, Danel, A., Jarosz, B. & Tomasik, P. *Applied Physics Letters* **77**, 1575 (2000).
6. List, E.J.W., Holzer, L., Tasch, S., Leising, G., Scherf, U., Mullen, K., Catellani, M. & Luzzati, S. *Solid State Communications* **109**, 455 (1999).
7. Murata, H., Merritt, C.D. & Kafafi, Z.H. *IEEE Journal of Selected Topics in Quantum Electronics* **4**, 119 (1998).
8. Bulovic, V., Shoustikov, A., Baldo, M.A., Bose, E., Kozlov, V.G., Thompson, M.E. & Forrest, S.R. *Chemical Physics Letters* **287**, 455 (1998).
9. Ruhstaller, B., Scott, J.C., Brock, P.J., Scherf, U. & Carter, S.A. *Chemical Physics Letters* **317**, 238 (2000).

10. Uchida, M., Adachi, C., Koyama, T. & Taniguchi, Y. *Journal of Applied Physics* **86**, 1680 (1999).
11. Jin, Y.D., Yang, J.P., Heremans, P.L., Van der Auweraer, M., Rousseau, E., Geise, H.J. & Borghs, G. *Chemical Physics Letters* **320**, 387 (2000).
12. McGehee, M.D., Bergstedt, T., Zhang, C., Saab, A.P., O'Regan, M.B., Bazan, G.C., Srdanov, V. & Heeger, A.J. *Advanced Materials* **11**, 1349 (1999).
13. Virgili, T., Lidzey, D.G. & Bradley, D.D.C. *Advanced Materials*, **12**, 58 (2000).
14. Liang, C.J., Zhao, D., Hong, Z.R., Zhao, D.X., Liu, X.Y., Li, W.L., Peng, J.B., Yu, J.Q., Lee, C.S. & Lee, S.T. *Applied Physics Letters* **76**, 67 (2000).
15. Dogariu, A., Gupta, R., Heeger, A.J. & Wang, H. *Synthetic Metals* **100**, 95 (1999).
16. Shoustikov, A., You, Y., Burrows, P.E., Thompson, M.E. & Forrest, S.R. *Synthetic Metals* **91**, 217 (1997).
17. Mitsuya, M., Suzuki, T., Koyama, T., Shirai, H., Taniguchi, Y., Satsuki, M. & Suga, S. *Applied Physics Letters* **77**, 3272 (2000).
18. Anni, M., Gigli, G., Paladini, V., Cingolani, R., Barbarella, G., Favaretto, L., Sotgiu, G. & Zambianchi, M. *Applied Physics Letters* **77**, 2458 (2000).
19. Hu, B., Zhang, N. & Karasz, F.E. *Journal of Applied Physics* **83**, 6002 (1998).
20. Sakakibara, Y., Okutsu, S., Enokida, T. & Tani, T. *Applied Physics Letters* **74**, 2587 (1999).
21. Bernius, M., Inbasekaran, M., Woo, E., Wu, W. & Wujkowski, L. *Journal of Materials Science: Materials In ElectronicsII*, 116 (2000).
22. Buckley, A.R., Rahn, M.D., Hill, J., Cabanillas-Gonzalez, J., Fox, A.M. & Bradley, D.D.C. submitted to *Chemical Physics Letters* (2000).
23. List, E.J.W, Creely, C., Leising, G., Schulte, N., Schluter, A.D., Scherf, U., Mullen, K. & Graupner, W. *Chemical Physics Letters* **325**, 132 (2000).

CHAPTER 9

CONCLUSIONS AND SUGGESTIONS FOR FUTURE WORK

9.1 Conclusions

This thesis has examined in detail the optical and electrical properties of a series of fluorene-based conjugated polymers and light-emitting devices with the aim to demonstrate high performance polymer LEDs and gain insight into the microscopic physics essential to understand the device operation.

In Chapter 3 the issue of emission from an exciplex state in bilayer light-emitting diodes based on hole transport fluorene-triarylamine copolymers and electron-transport starburst phenylquinoxalines was addressed in detail. An exciplex state is a state formed between a hole on a donor molecule and an electron on an acceptor molecule.¹ Light emission occurs when relaxation to the ground state takes place. Different triarylamine copolymers with low ionization potentials were examined as HTLs in a bilayer configuration with starburst phenylquinoxalines with high electron affinities as ETLs. Two thiophene copolymers with higher ionization potentials were also employed as HTLs. Emission from an exciplex state was only found to occur in the case of the lower ionization potential HTLs. The emission wavelength and color was

determined by the energy difference between the ionization potential of the hole transport material and the electron affinity of the electron transport material. Because the exciplex formation takes place only at the heterojunction interface, the emission color can be tuned by variation of the ionization potential of the hole transporter. Differences between the experimental values of the peak emission wavelength and the theoretically calculated values (based on the difference between the E_{HOMO} of the HTL and the E_{LUMO} of the ETL) were attributed to either systematic overestimation of the energy of the LUMO level of the ETL (due to polarization energy effects) or to the formation of an excited singlet state of the hole transporter prior to the formation of the exciplex state. However, the character of the exciplex state as a new excited state is predominant in these LEDs and offers a simple way of tuning the emission color.

Chapter 4 addresses the concept of blending an emissive polymer with a hole transport material as a means of improving device performance and thus achieving high brightness and efficiency and low operating voltage PLEDs in a single layer configuration.² Applying this concept, bright and efficient blue LEDs were realized, based on a host-guest system with a blue poly(9,9-dioctylfluorene) (PFO) as host and a hole-transport triarylamine copolymer, poly(9,9-dioctylfluorene-co-bis-N,N'-(4-methylphenyl)-bis-N,N'-phenyl-1,4 phenylenediamine) (PFM), as guest. Doped LEDs (with an optimum guest concentration of 20% by weight) show significantly improved performance compared to undoped ones due to the significantly improved charge carrier balance factor as a result of the improved hole injection and transport achieved by blending with PFM. This occurs despite the fact that the PL quantum efficiency is lower in the blend. A much higher brightness and a lower turn on and operating voltage is also achieved for the blend LEDs. The incorporation of an appropriate polymeric hole-transporting material in PFO in a blend configuration results in a marked improvement of the device performance. Optimised LEDs showed bright blue emission with a peak wavelength at 455 nm, a maximum external quantum efficiency of 2.2 cd/A or 1%, a

maximum power efficiency of 1.25 lm/W and a maximum luminance of 8500 cd/m² at 13 V. Hole trapping is evidenced by time resolved electroabsorption measurements as well as from the dispersive shape of the time of flight current signal in the blend. Weak Förster energy transfer is demonstrated to occur from the host to the guest and this is supported by time resolved PL measurements which show a significant reduction of the host lifetime emission in the blend with increasing guest concentration. The emission wavelength as well as the shape of the emission spectrum changes with the doped layer thickness particularly when a Dow metal cathode is used and this is mainly attributed to interference effects. Resemblance of the EL spectra of the doped LEDs with the PL spectrum of PFM indicates that charge transport via hopping between adjacent sites followed by carrier recombination preferentially occurs on the PFM molecules.

In chapter 5 the same concept was applied to demonstrate high brightness, efficiency and low operating voltage green single layer PLEDs. The host polymer termed 5BTF8 is a blend of the green electron transporter, poly(9,9-dioctylfluorene-co-benzothiadiazole) (BT) and the blue poly(9,9-dioctylfluorene) (PFO) in a 5:95 ratio.³ The guest is a triarylamine hole transport copolymer, poly(9,9-dioctylfluorene-co-bis-N,N'-(4-butylphenyl)-bis-N,N'-phenylbenzidine) (BFB). Förster transfer occurs from PFO to BT and the improvement of the charge carrier balance factor by blending 5BTF8 with BFB increases the device brightness by more than two orders of magnitude (from ~ 400 cd/m² to ~ 36500 cd/m²) and the efficiency by a factor of 12 (from ~ 0.4 cd/A to ~ 5 cd/A) compared with the 5BTF8 device. The improvement of the device performance in the blend is mainly due to improved hole injection and transport in the presence of the BFB guest. Single layer devices with a peak emission wavelength at 535 nm that exhibit brightnesses up to 36500 cd/m² at 10 V were realized. The effect of a bilayer LiF/Al cathode on the device performance was also examined and the improvement of the device performance was attributed to enhanced electron injection due to a lowering of the “effective” electron injection barrier as evidenced by

electroabsorption measurements.⁴ A similar decrease of the hole injection barrier was also found on devices where a PEDOT:PSS hole injection layer had been spin coated between the ITO and the polymer resulting in a significant reduction of the operating voltage. Exposure of Ca to oxygen to form a CaO layer was also found to improve significantly the performance of a single layer 5BTF8 LED due to the combined action of CaO to improve the charge balance by acting as a hole blocking layer and to remove the exciton quenching gap states formed at the Ca or Al/polymer interface.

Chapter 6 addresses the mechanism of electrophosphorescence in PLEDs aiming to utilize both singlet and triplet states in order to produce high efficiency PLEDs. In an electroluminescent LED it is expected from single spin statistics that only 1/4 of the injected charge forms emissive singlet excitons. Thus the device performance is limited by the fact that triplet excitons do not contribute to the emission and the maximum internal quantum efficiency is 25%.⁵ However, in some phosphor molecules the incorporation of a heavy metal atom makes the transition from the triplet to the ground state weakly allowed. Thus emission from both singlet and triplet states can be utilized and it should ultimately be possible to achieve near 100% internal quantum efficiency.⁶ Phosphorescent PLEDs with a red phosphorescent emitter, 2,3,7,8,12,13,17,18-octaethyl-21H,23H-porphyrin platinum (II) (PtOEP), as a dopant guest in a blue PFO host were investigated. A triarylamine copolymer, N,N-di (3-hydroxycarbonyl-phenyl)-N,N-diphenylbenzidine (BFA), was used as a separate hole transport layer in bilayer LEDs. By varying the concentration of the PtOEP a spectral range of bluish-red to pure red emission was obtained. Blue emission from PFO could be observed even at 8% dopant concentration under optical excitation of a PFO:PtOEP blend film, while at 1% dopant concentration only red emission from PtOEP could be observed from the corresponding LEDs. From analysis of the absorption, PL and EL spectra together with time resolved PL and electroabsorption measurements, we conclude that direct carrier trapping and subsequent exciton recombination on the dopant molecules is the dominant

EL emission mechanism whereas Förster energy transfer from the host to the dopant dominates the PL emission. Singlets formed on the PtOEP molecules are converted to triplets via efficient intersystem crossing and result in phosphorescence. Any singlets formed directly on PFO by recombination of untrapped charges can subsequently transfer their energy by Förster transfer to the PtOEP singlets and also contribute to the emission. Saturated red emission centred at 645 nm with a FWHM of 17 nm and doped LEDs with external EL efficiencies of 1% at low brightness were realized. By decreasing the workfunction of ITO, efficiencies up to 3% were obtained due to the improved balance of the injected carriers. These high efficiencies were also attributed to the direct trapping of holes and electrons and the subsequent formation of excitons on the dopant molecules. PFO was also doped with PFM and this blend was then used as a host with a PtOEP guest. The efficiency of these devices increased by a factor of 3 and reached 3.2% at low brightness for a high workfunction ITO. For a low workfunction ITO, an external efficiency of 5.8% was obtained at low brightness. The improved performance of the blend LEDs is attributed to more efficient energy transfer from the host to the guest as well as to improved charge balance due to hole trapping on PFM.

Chapter 7 shows how small area device structures can result in very high brightness LEDs that can sustain significantly higher current densities than normal structures. Small area device structures (with an active area with diameter down to 50 μm) were fabricated and characterized. A photolithographically patterned silicon nitride layer was deposited on top of ITO in order to define active areas with diameters of 500, 100 and 50 μm , respectively. A significant improvement of the maximum brightness and the maximum current density is achieved in the small area devices. By reducing the diameter of the device from the standard size (4.5 mm^2) to 50 μm , the current density that can be sustained increases by a factor of 9 in DC mode and by a factor of 60 in pulsed mode. This increase in current density is accompanied by a similar increase in the maximum brightness. The brightness of the 50 μm LED increases by a factor of 6 in

DC mode and by a factor of 35 in pulsed mode. An improvement by a factor of 6 is obtained for both the maxima current density and luminance sustained by the small area LEDs in pulsed mode compared to DC mode which indicates that low duty cycle pulses can significantly reduce the average power dissipation in a device and thus increase its operating lifetime. Optimized 5BTF8 devices emit light with a brightness of $155,000 \text{ cd/m}^2$ in DC mode. In pulsed mode the same devices reached a brightness of $6,500,000 \text{ cd/m}^2$ and sustained current densities up to $5,000,000 \text{ A/m}^2$. These improvements are attributed to the improved thermal management of the small area devices due to reduced Joule heating. Both the Si_xN_y medium and the Ca cathode are proposed to act as efficient heat sinks that enable significant heat dissipation from the device as a result of the heat exchange between the active medium and the surrounding media. However, full color displays require materials with narrow emission spectra. Polymers usually have broad bandwidth EL spectra due to inhomogeneous broadening and coupling to vibronic modes. Microcavities overcome this problem as they narrow the emission linewidth significantly.⁷ The incorporation of the small area structure in a microcavity and the use of highly reflective DBR mirrors and a composite Ca/Al cathode allows for the fabrication of novel small area cavity LEDs. Electrically pumped 5BTF8 cavity LEDs exhibit a light output of 10000 cd/m^2 and a narrow linewidth of 18 nm with an emission peak at 590 nm. Similarly, PFO cavity LEDs reach a luminance of 2500 cd/m^2 with a peak emission wavelength at 449 nm and a narrow linewidth of 11 nm. Spectral redistribution was observed to occur under intense electrical excitation in PFO cavity LEDs. This is evidenced by an increased relative weight of the emission peak at 520 nm relative to the peak at 449 nm above a “threshold” current density of $\sim 155,000 \text{ A/m}^2$. Both the fact that the enhancement occurs on the secondary mode rather than the main cavity mode and that no spectral narrowing was observed led us to attribute the spectral emission redistribution to either changes in the refractive index or electrical-induced degradation of PFO under intense excitation.

Finally, Chapter 8 addresses the issue of energy transfer in a host-guest system where the host is a blue copolymer of PFO with 1,4-phenylene, F8P, and the guest is the green copolymer BT. A combined study of absorption, PL, PL quantum efficiency and time resolved PL measurements of varying BT concentration blends showed that the large overlap of the emission spectrum of the F8P host with the absorption spectrum of the BT guest gives rise to an efficient energy transfer from F8P to BT via a Förster-type mechanism which dominates the emission under photoexcitation. Single layer LEDs based on the F8P:BT blend exhibited bright and efficient green emission peaking at 535 nm for BT concentrations as low as 0.5%. This was a result of almost complete excitation energy transfer from F8P to BT as well as charge trapping followed by efficient recombination on BT sites. The charge trapping process was found to play a significant role under electrical operation and contributes to the enhancement of the device performance. Optimized devices reached a brightness of 15000 cd/m² and an efficiency of 7 cd/A while the incorporation of a BFB HTL in a F8P:BT (6% BT) LED increased the brightness by a factor of 1.6 and reduced the turn-on voltage to below 3V.

9.2 Suggestions for future work

LEDs based on conjugated polymers are under development for commercialization as a new display technology. To obtain a better understanding of the device operation and design more efficient device structures it is essential to gain some insight and determine the microscopic processes occurring in a device. In this thesis we have discussed numerous PLEDs and microcavities and by employing a whole range of different optical and electrical characterization measurements we have been able to characterise different polymers and demonstrate high brightness and efficiency LEDs.

Our findings demonstrate that by using an appropriate blend composition both charge carrier injection and transport in a single-layer LED can be significantly

enhanced to the same level as in a bilayer device. They also illustrate the importance of the cathode/polymer interface in achieving high performance and the advantages of single-layer PLEDs with bipolar charge-carrying properties compared to, more complicated to fabricate, multilayer PLEDs. Charge trapping was also found to play a significant role in the enhancement of a LED's efficiency based on host-guest schemes and the selection of appropriate materials will be crucial to achieve high performance.

Charge trapping was also found to play an important role in achieving high efficiency electrophosphorescent PLEDs from host-guest systems with weak energy transfer coupling. Other approaches that could result in highly efficient phosphorescent PLEDs could be either doping other phosphorescent materials that possess shorter exciton lifetimes into an appropriate combination of an emissive and a hole transporting material used as a host or selecting guest-host combinations with a stronger energy transfer coupling and thus a higher probability for efficient energy transfer.

Passive matrix displays formed from arrays of small area LEDs will require LEDs that emit light with very high peak luminance. Our results confirm that efficient thermal management can be achieved by reducing the device emissive area and this process will be of particular importance in determining the operational stability and lifetime of future PLED displays. By reducing the active device area very high brightnesses could be achieved and a future aspect of this work could be to further reduce the active device area. If LEDs with a 5-20 μm diameter could be fabricated, luminances up to $50,000,000 \text{ cd/m}^2$ in pulsed mode should be possible to achieve and current densities up to $20,000,000 \text{ A/m}^2$ should in principle be sustained before device failure. Such high brightnesses and current densities (which are one order of magnitude higher than the estimated threshold excitation current density from photopumped polymer films) will bring closer the realization of an electrically pumped polymer laser. Efforts should also be focused on reducing the two additional loss mechanisms

associated with electrical diode structures, namely the metal electrode absorption and the charge-induced absorption of the emissive material. Useful approaches could be the use of metal electrodes that do not induce excessive waveguide losses and materials that have reduced charge-induced absorption or higher mobilities. Improved device design and new novel structures should also aim at reducing temperature effects that can prove detrimental in the operation of PLEDs. Future work could also concentrate on to improving the spectral properties of the small area cavity LEDs so that there is only one cavity mode within the EL spectra. This can be achieved by optimizing the thickness of the anode electrode and the polymer layers, respectively. Optimization of the pulsed scheme applied should also be investigated as a means to improve the electrical characteristics of the cavity LEDs.

References

1. Gebler, D.D., Wang, Y.Z., Blatchford, J.W., Jessen, S.W., Fu, D.K., Swager, T.M., MacDiarmid, A.G. & Epstein, A.J. *Applied Physics Letters* **70**, 1644 (1997).
2. Sainova, D., Miteva, T., Nothofer, H.G., Scherf, U., Glowacki, I., Ulanski, J., Fujikawa, H. & Neher, D. *Applied Physics Letters* **76**, 1810 (2000).
3. He, Y., Gong, S., Hattori, R. & Kanicki, J. *Applied Physics Letters* **74**, 2265 (1999).
4. Brown, T.M., Friend, R.H., Millard, I.S., Lacey, D.J., Burroughes, J.H. & Cacialli, F. *Applied Physics Letters* **77**, 3096 (2000).
5. Pope, M. & Swenberg, C.E. *Electronic Processes in Organic Crystals and Polymers*, 2nd Edition, Oxford University Press, Oxford (1999).
6. Baldo, M.A., O'Brien, D.F., You, Y., Shoustikov, A., Sibley, S., Thompson, M.E. & Forrest, S.R. *Nature (London)* **395**, 151 (1998).
7. Lidzey, D.G., Bradley, D.D.C., Martin, S.J. & Pate, M.A. *IEEE Journal of Selected Topics in Quantum Electronics* **4**, 113 (1998).

Appendix A

Additional data related to Chapter 4

The following are additional figures related to Chapter 4 (Blue LEDs) which were excluded from the main body of text for clarity.

A.1 Current and luminance vs. electric field

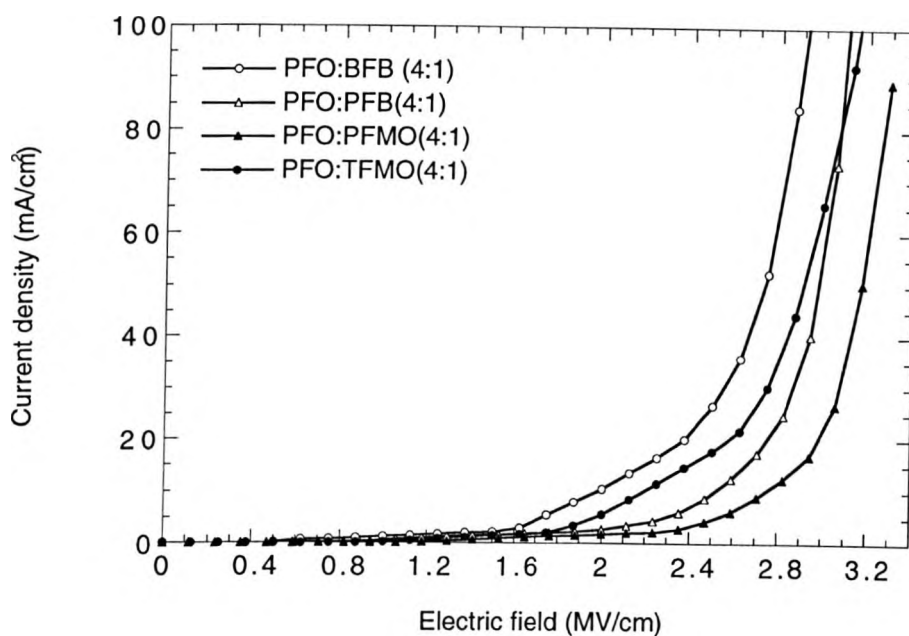


Figure A.1: Current density versus electric field characteristics of ITO/PFO:HTL(20 wt/% HTL)/Al blend LEDs with an 80 nm thick emissive layer.

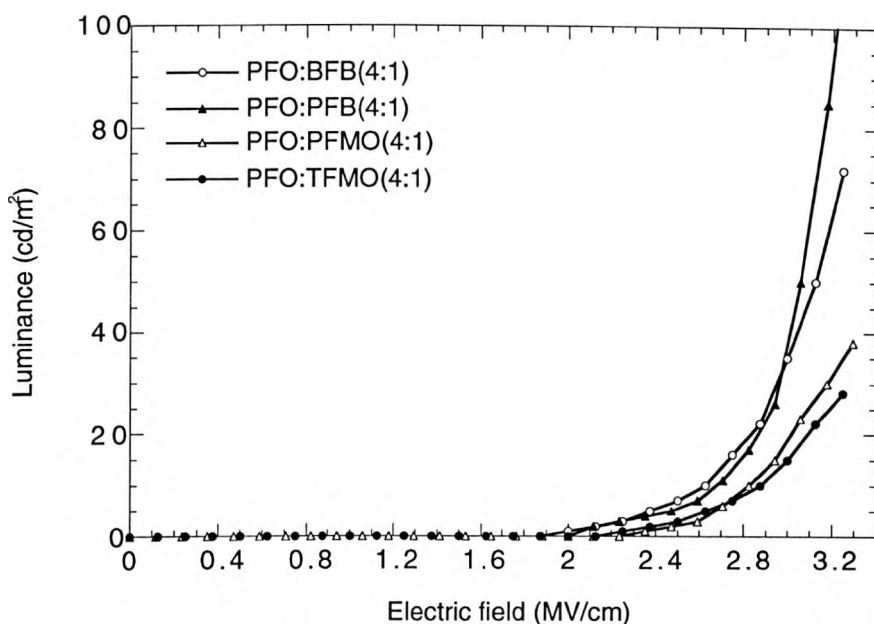


Figure A.2: Luminance vs. electric field characteristics of the same series of blend LEDs.

A.2 Electroluminescence spectra

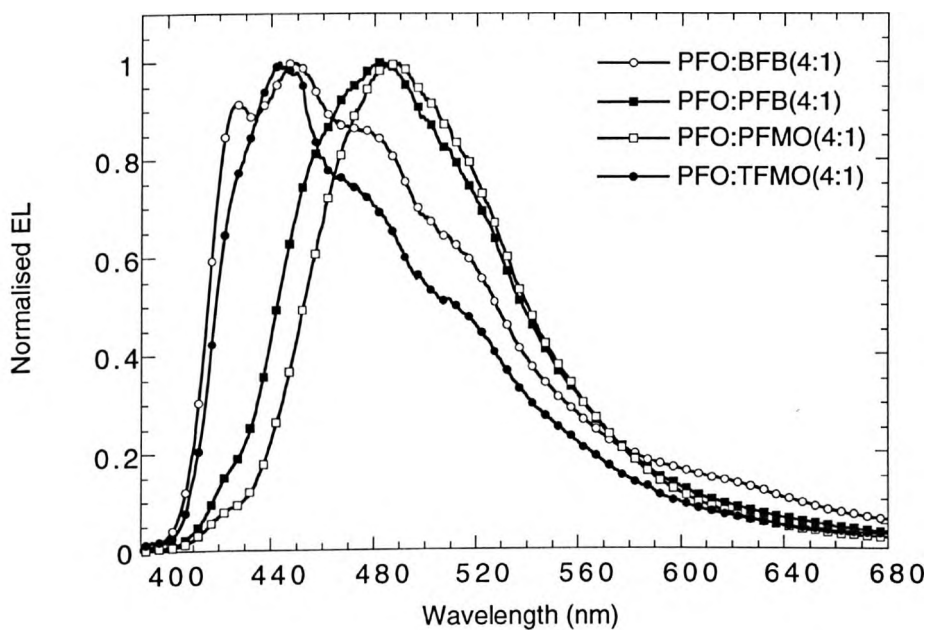


Figure A.3: Electroluminescence spectra of the same series of blend LEDs ($J = 50 \text{ mA/cm}^2$).

Appendix B

Additional data related to Chapter 5

The following are additional figures related to Chapter 5 (Green LEDs) which were excluded from the main body of text for clarity.

B.1 Current and luminance vs. electric field

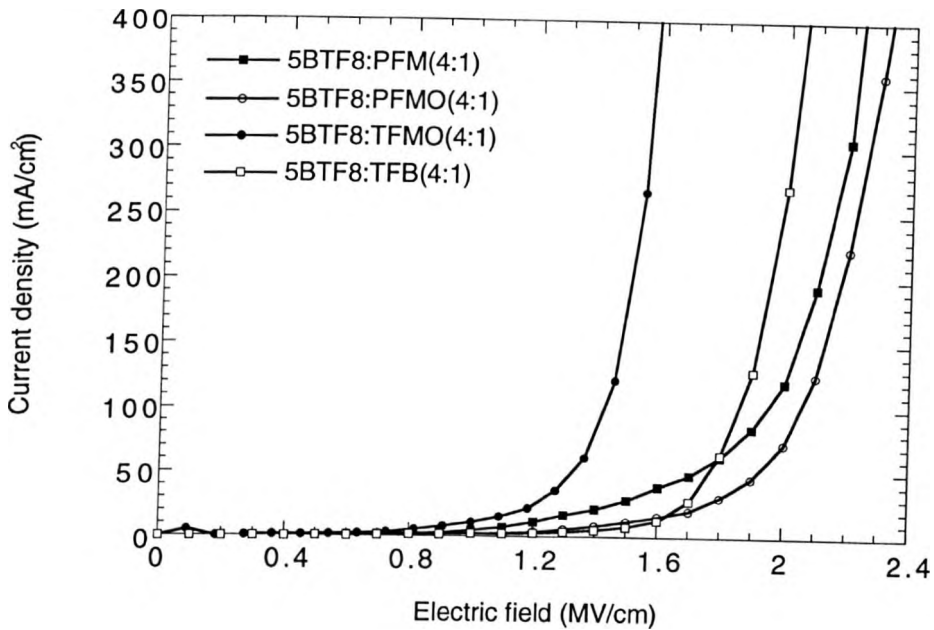


Figure B.1: Current density versus electric field characteristics of ITO/5BTF8:HTL(20 wt.% HTL)/Al blend LEDs with an emissive layer thickness of 100 nm.

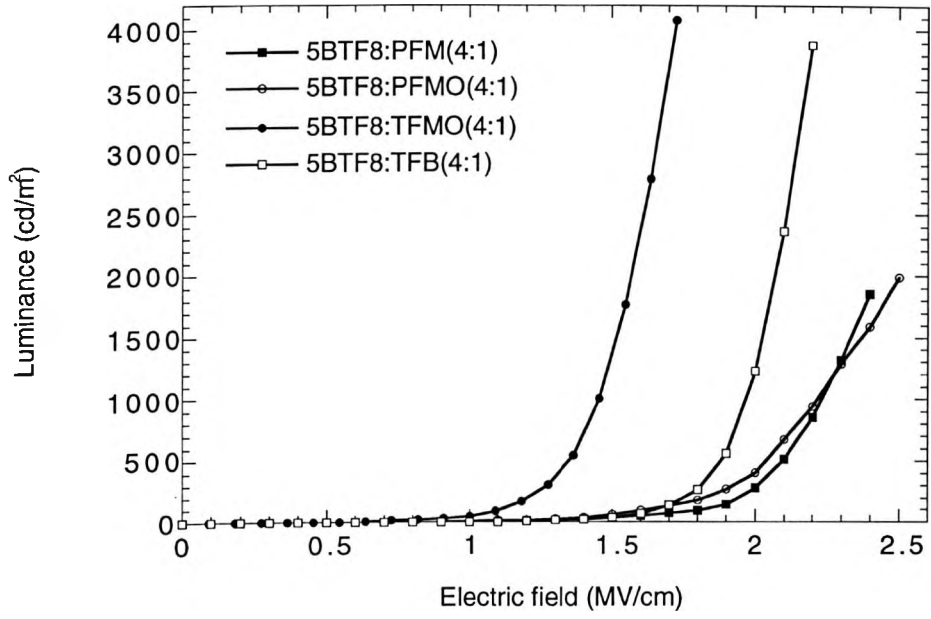


Figure B.2: Luminance vs. electric field characteristics of the same series of blend LEDs.

Appendix C

Publication List

C.1 List of publications on work prior to this thesis

1. Electrical transport and EPR properties of the alpha, beta, and gamma phases of Fe_2WO_6 . N.Guskos, V.Likodimos, S.Glenis, S.K.Patapis, L.C.Palilis, J.Typek, M.Wabia, I.Rychlowska-Himmel, Physical Review B, 60, 11, 7687-7690, (1999).

C.2 List of publications on work discussed in this thesis

1. Bright and efficient blue and green light-emitting diodes based on conjugated polymer blends. L.C.Palilis, D.G.Lidzey, M.Redecker, D.D.C.Bradley, M.Inbasekaran, E.P.Woo, W.W.Wu, Proceedings of ICCEL2, Synthetic Metals, 111, 7172, 159-163, (2000).

2. Bright and efficient blue light-emitting diodes based on conjugated polymer blends. L.C.Palilis, D.G.Lidzey, M.Redecker, D.D.C.Bradley, M.Inbasekaran, E.P.Woo, W.W.Wu, SPIE'99 Proceedings, 3797, 383 (1999).

3. Origin of electrophosphorescence from a doped polymer light emitting diode. P.A.Lane, L.C.Palilis, D.F.O'Brien, C.Giebeler, A.J.Cadby, D.G.Lidzey, A.J.Campbell, W.Blau, D.D.C.Bradley, Physical Review B (in press).

4. Very bright and efficient green polymer light-emitting diodes based on conjugated polymers and associated blends. L.C.Palilis, D.G.Lidzey, C.I.Wilkinson, D.D.C.Bradley, M.Inbasekaran, W.W.Wu, SPIE'00 Proceedings (in press).
5. Electrophosphorescence from a doped polymer light emitting diode. D.F.O'Brien, C.Giebeler, A.J.Cadby, L.C.Palilis, D.G.Lidzey, P.A.Lane, D.D.C.Bradley, W.Blau, Proceedings of the 4th International Topical Conference on Optical Probes of Conjugated Polymers and Photonic Crystals, Synthetic Metals (in press).
6. High efficiency and brightness red polymer light-emitting diodes based on electrophosphorescence. L.C.Palilis, P.A.Lane, D.G.Lidzey, D.D.C.Bradley, In preparation for submission to Applied Physics Letters.
7. Exciplex emission in light emitting diodes based on fluorene-triarylamine copolymers. L.C.Palilis, M.Redecker, D.D.C.Bradley, P.Strohriegl, M.Jandke, M.Inbasekaran, W.W.Wu, In preparation for submission to Advanced Materials.
8. High performance single layer blue polymer light-emitting diodes based on fluorene-triarylamine copolymers. L.C.Palilis, D.G.Lidzey, M.Redecker, D.D.C.Bradley, M.Inbasekaran, W.W.Wu, In preparation for submission to Applied Physics Letters.
9. Enhanced performance of pulse driven small area polyfluorene light emitting diodes. C.I.Wilkinson, D.G.Lidzey, L.C.Palilis, R.B.Fletcher, S.J.Martin, X.Wang, D.D.C.Bradley, Applied Physics Letters (in press).
10. High brightness and efficiency blue light-emitting diodes based on conjugated polymers. L.C.Palilis, D.G.Lidzey, M.Redecker, D.D.C.Bradley, M.Inbasekaran, W.W.Wu,

Proceedings of the International Conference on Science and Technology of Synthetic Metals (ICSM00), Synthetic Metals (in press).

11. Bright and efficient single layer green light-emitting diodes utilizing conjugated polymers and associated blends. L.C.Palilis, D.G.Lidzey, D.D.C.Bradley, M.Inbasekaran, W.W.Wu, In preparation for submission to Advanced Materials.

12. Improved efficiency red phosphorescent light-emitting diodes utilizing a polymer blend host. L.C.Palilis, P.A.Lane, D.G.Lidzey, D.D.C.Bradley, In preparation for submission to Advanced Materials.

13. Improved efficiency polymer light-emitting diodes by employing CaO as a hole-blocking layer. C.I.Wilkinson, D.G.Lidzey, L.C.Palilis, R.B.Fletcher, D.D.C.Bradley, In preparation for submission to Applied Physics Letters.

14. Optimization of the performance of green polymer light-emitting diodes based on fluorene-triarylamine copolymers. L.C.Palilis, D.G.Lidzey, D.D.C.Bradley, M.Inbasekaran, W.W.Wu, In preparation for submission to Journal of Applied Physics.

15. Efficient green electroluminescence from benzothiadiazole-based doped polyfluorene light-emitting diodes. L.C.Palilis, D.G.Lidzey, D.D.C.Bradley, M.Inbasekaran, W.W.Wu In preparation for submission to Applied Physics Letters.

16. Bright and efficient blue polymer light-emitting diodes based on conjugated polymer blends. L.C.Palilis, D.G.Lidzey, M.Redecker, D.D.C.Bradley, M.Inbasekaran, W.W.Wu, In preparation for submission to Physical Review B.

17. Efficient energy transfer from blue to green in benzothiadiazole-doped polyfluorene based light-emitting diodes. L.C.Palilis, D.G.Lidzey, D.D.C.Bradley, M.Inbasekaran, W.W.Wu, In preparation for submission to *Advanced Materials*.

18. High performance small area microcavity, polyfluorene light-emitting diodes. D.G.Lidzey, L.C.Palilis, C.I.Wilkinson, D.D.C.Bradley, M.Bernius, S.Walker, In preparation for submission to *Journal of Applied Physics*.